VIP Insulated Box

Brandon Liu*

Phillips Exeter Academy, 20 Main Street, Exeter, NH 03832, USA

Abstract

The goal is to design and assemble a prototype insulated container using VIP technology. The wood is selected as the wall of the box and VIP is selected as the insulation of the box. The box shows excellent heat－resistance efficiency for the ice relative a traditional refrigerator.

Keywords insulated container, VIP technology, heat-resistance

1. Introduction

The objective of this project was to design and assemble a prototype insulated container using VIP technology in the period of 10 days. Multiple materials were considered for the external enclosure including plastics, wood, and cardboards, and given the time and funding restraints, wood was selected. A single layer of VIP was used in the box. After analysis, the container is an acceptable first draft but fails in several key areas.

2. Materials and design

The box consists of two main parts: a three layer lid and a three layer bottom portion. The lid consists of a 35mm wooden exterior shell, 10mm of VIP, and a 20mm wooden interior shell. The bottom portion is essentially the same design except the outer shell is 25mm. Each layer was secured to each other using a wood glue and also a silicone based sealant. The lid is secured onto the container tightly using draw latches, two latches on two of the sides to make four in total.

Fig. 1. Final cross section schematic of the container; red represents wood, white represents VIP, and black portions are latches.

Originally, the design consisted of two layers of VIP also with a wood shell using a sliding fit design. The lid portion would be similar to the bottom with 5 sides, but slightly smaller to slide directly into the bottom part, creating a socket-plug type of arrangement. This would have created a longer path for the heat to escape, but the plan was ultimately abandoned due to time and budget constraints of custom making the VIP.

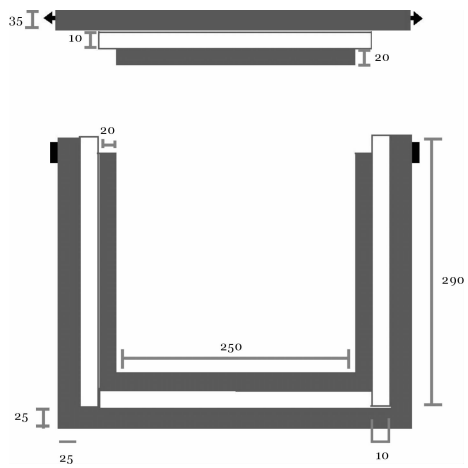

Fig. 1 Final cross section schematic of the container

The second revision was largely identical to the final design, but instead of one VIP layer there were

* corresponding anthor, E-mail: bylin88@gmarl.com

two. One VIP layer was decided in order to first see the insulation effectiveness of one layer versus two or more and to account the cost discrepancies between them. The product produced is shown below.

Fig. 2 The picture of theinsulated box

3. Analysis and procedure

To test the effectiveness of the enclosure, 300mL of ice was placed into a beaker within the insulation box, already chilled to temperature. After two hours, then every one hour after that, the excess water was poured into another beaker to measure the amount of ice melted during that time period until the ice had melted completely. A control of 300mL of ice at room temperature was used as well, recording change in volume in identical periods. The data is listed below.

Tab. 1 Total ice volume melted and change in volume per hour in the box.

Time Elapsed /hours	2	3	4	5	6	7	8	9	10	11
Totalvolume melted /mL	75	122	149	175	202	224	249	285	296	300
Change in volume /mL	−75	−47	−27	−26	−27	−22	−25	−36	−11	−4
Volume of ice left /mg	225	178	151	125	98	76	51	15	4	0

Tab. 2 Total ice volume melted and change in volume per hour at room temperature (outside the box)

Time Elapsed /hours	2	3	4
Total volume melted /mL	140	222	300
Change in volume /mL	−140	−82	−78
Volume of ice left /mg	160	78	0

Fig. 3 shows the volume of ice remaining over time outside and inside the box. The values for 1 hour were not taken; the mean between 0 and 2 hours were used as placeholders

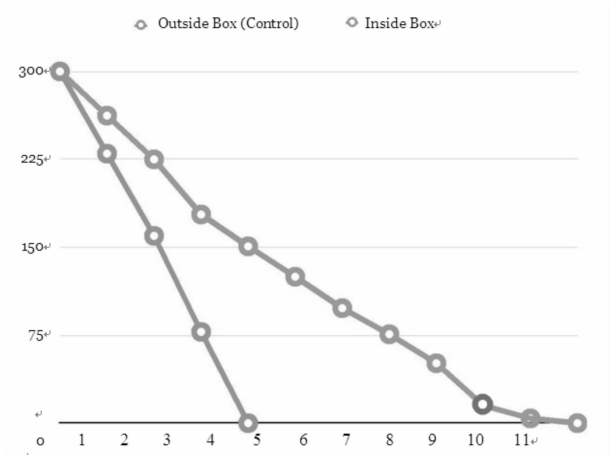

Fig. 3 Volume of ice remaining over time outside and inside the box

4. Sources of error and limitations

With the two largest limitations being time and funding, multiple compromises were made to produce an end product.

First, wood was selected because it could be quickly produced to the specifications without the need of a process akin to injection molding for plastic. However, the disadvantages of wood, its heavy weight, absorption of moisture, and biodegradability, make it a relatively poor choice compared to a hollow plastic or foam.

During the analysis, the opening of the container to measure the melted ice allowed for warmer air to enter the enclosure likely speeding up the thawing time, which could account for some discrepancies between these test and actual performance. One other source of error worth mentioning is the accuracy of the beaker used to measure ice melted. The beaker used only

allowed for relatively crude measurements of water, allowing for human error to affect values by a few milliliters.

5. Conclusion and commentary

After design, construction, testing, and analysis, this box has been shown to perform decently but is flawed. The values found are respectable for a first draft, but the

materials used and the overall design will need revision for better performance and practicality.

The wood is prone to damage through moisture which ultimately decreases the service life of the VIP, and it also makes the container too heavy. Regarding weight, the interior wooden board on the lid creates unneeded strain on the board from the pull of gravity. The interior wood also is especially susceptible to water absorption due to the expected cold temperatures which allow for condensation, so in the future synthetic materials such as foam or plastic should be considered. The wood on the exterior would also best be replaced with the one of the aforementioned materials to reduce weight and strain on the box.

Regarding design, the heat transfer would need to be optimized. The path of travel through the opening between the lid and bottom is open enough for heat to easily pass through, so a cleaner fit is necessary to optimize insulation. Also, the addition of stands on the bottom of the exterior would reduce contact with the bottom surface effectively lowering heat conduction through that plane. Incorporating more layers of VIP would also improve insulation, but further testing is needed.

In conclusion, this first box gives a promising start to the research and design of a possibly commercially marketable insulation container. Through testing and analysis of the prototype, key areas for improvement have been identified and future possibilities noted. The possible uses for a super-insulation VIP box could encompass fields not considered at this moment; thus, further research and development is necessary.

Acknowledgement

The author will like to thank Professor Chen Zhaofeng for the support to work in his research Laboratory and Suzhou V. I. P. New Materials Ltd for their support to do experiments in their laboratory.

Modelling of Mass Transfer Through the Barrier Envelopes of Vacuum Insulation Panels

Antoine Batard[a,b*], Thierry Duforestel[a], Lionel Flandin[b], Bernard Yrieix[c]

a. EDF R&D, - ENERBAT, - EDF Lab Les Renardières, - 77818 Moret—sur—Loing, France
b. LEPMI - LMOPS — Université de Savoie — Campus Savoie Technolac — Hélios — 73376 Le Bourget—du—Lac, France
c. EDF R&D - MMC - EDF Lab Les Renardières - 77818 Moret—sur—Loing, France

Abstract

The long-term thermal performance of Vacuum Insulation Panels (VIPs) is based on the capacity of the envelope to maintain the core material under vacuum. In this study, the aim is to focus on the detailed modelling of mass transfer through the defects of aluminium coated polymer films used for VIPs' envelopes. The 3D simulations were performed with monolayer and multilayer metal—coated polymer films. They have been realized in dynamic conditions with the SYRTHES® software developed by EDF R&D. The results show that the water vapour and air permeations of a monolayer film slightly depend on the polymer substrate thickness, diffusivity and solubility, but primarily, on the defects geometry and arrangement. Regarding multilayer films, the permeation depends on the presence/absence of glue in defects, the alignment of defects and the orientation of layers. We are now able to provide and operate an analytical model which can calculate with a good accuracy, the permeance of monolayer or multilayer metallized polymer films as a function of the coating quality and the geometry of the layers. This study improves the understanding of gas transports through VIPs' films and allows to manage more efficiently the relations between the films microstructures and their overall permeability.

Keywords vacuum insulation panels, barrier envelope, mass transfer modelling, gas permeation.

1. Introduction

The main purpose of this modelling study of atmospheric gas (water vapour and dry air) transfer through the VIPs films is to get a better understanding of the influence of geometric and physical parameters on the measured permeances. It can be split into 4 parts: monolayer modelling, multilayer modelling, experimental approach and, comparison between simulation and experimental results. In this version, only the simulation results on monolayer will be shown and analysed.

2. Presentation of studied cases

The monolayer configuration consists in a polymer substrate metalized on one of its faces. It is usually called PETM1F when a polyethylene terephthalate substrate is used. Geometry and mesh examples of this configuration are represented on Fig. 1. Only one representative piece of film is represented integrating one defect which consists in one circular hole in the aluminium coating [1]. Using biaxial symmetry, only a quarter of this part of film is modelled.

The coating is considered as impermeable to gas.

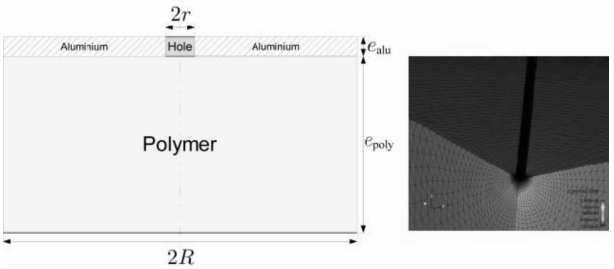

Fig. 1 Monolayer PETM1F modelized

* Corresponding author, Tel:33 - 6 - 31 - 65 - 44 - 49, E-mail:antoine.batard@edf.fr

For all the simulations presented in this paper, a fixed differential gas pressure (ΔP = 2000 Pa) is maintained between both sides of the film.

The aim is to analyse the apparent permeance variations of the component when 3 geometrical parameters are modified: the Surface Fraction of Defects (SFD) in the coating, the numbers of defects (for a constant SFD, an increasing of the number of defects means a decreasing of each defect diameter ϕ) and the polymer thickness (e_{poly}). The influence of the polymer diffusion (D) and solubility (S) coefficients have also been studied.

3. Modelling tools and methods

In the first phase of the work geometries and meshes of the studied components were created with SIMAIL® and SALOME®. Then calculations were carried out with SYRTHES®, a finite element software. Results can be analysed using to a specific post-treatment procedure which calculates the apparent permeance of a film made of a combination of defects with homogeneous size.

In order to simplify calculations, an analogy between heat equation (Fourier's law) and mass transfer equation (Fick's laws of diffusion [2]) has been used. For low pressures and ideal gas,

Henry's law of solubility can be considered [3, 4] to connect the external gas pressure and the corresponding concentration at the surface of the polymer. Because of the small size of the considered elements, geometries have been expanded and materials characteristics have been changed accordingly.

4. Results and discussions

The Fig. 2 indicates that, below a certain value of diffusion coefficient, the apparent permeance of monolayer films is proportional to D. Similar evolutions were obtained for a varying solubility. Above this critical value, which was much higher than the D and S values for polymer used in VIP barriers, the permeance became constant.

The Fig. 3 shows that the permeance gradually decreases with the thickness of the polymer substrate. But this effect tends to diminish with lower SFD. This result confirms a conclusion of HANIKA [5], who

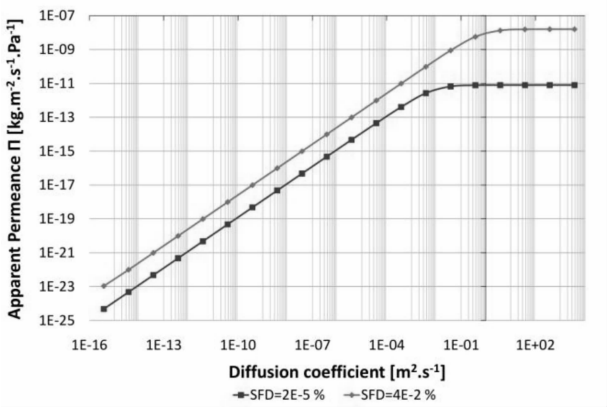

Fig. 2 Theoretical apparent permeance

as function of diffusion coefficient for 2 different surface fractions of defects on PETM1F(e_{poly} = 12 μm - $\phi_{2E-5\,\%} \approx$ 50 nm - $\phi_{4E-2\,\%} \approx$ 2,257 μm)

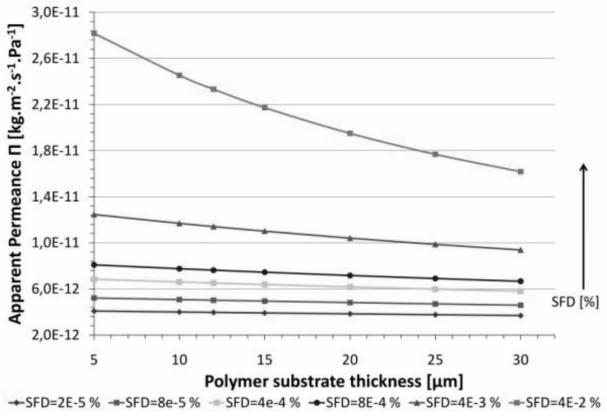

Fig. 3 Theoretical apparent permeance as function of polymer thickness for different surface fractions of defects on PETM1F

($\phi_{2E-5\,\%} \approx$ 0.39 nm - $\phi_{8E-5\,\%} \approx$ 0.79 nm
$\phi_{4E-4\,\%} \approx$ 1.76 nm - $\phi_{8E-4\,\%} \approx$ 2.49 nm
$\phi_{4E-3\,\%} \approx$ 5.58 nm - $\phi_{4E-2\,\%} \approx$ 17.63 nm)

proposed to determine a critical thickness value over which the permeance dependance on the polymer thickness can be neglected.

Fig. 4 reveals also the effect of the number of defects (i. e.: the defects size) for different surface fractions of defects. In the simulation, the number of defects stopped at 262144. Beyond this value, the defect size became smaller than the water vapour molecular size.

The red curve, which represents the lowest surface fraction of defects, shows that when the number of

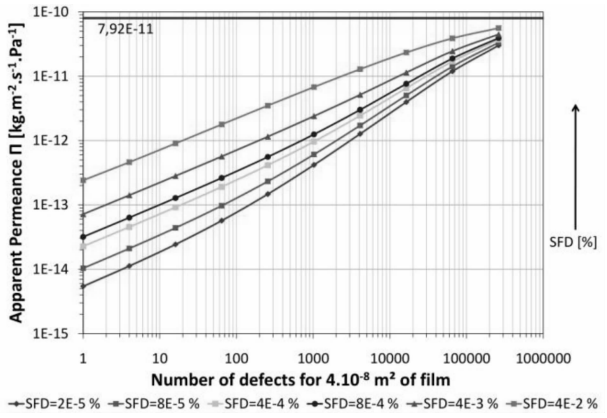

Fig. 4 Theoretical apparent permeance as function of number of defects for different surface fractions of defects on PETM1F (e_{poly} = 12 μm)

defects increases (the defects size decreases), the permeance increases sharply. The same tendency was observed for all values of surface fraction. Higher surface fractions of defects reduces, however, the consequences of the defects size on the permeance. For all surface fractions of defects, a large number of small defects increases the permeance to that of the uncoated polymer. This value (7.92E−11 kg • m^{-2} • s^{-1} • Pa^{-1}) is represented by the straight blue line. This results from a low tortuosity in the diffusion of moieties.

5. Conclusions and outlook

This analysis shows that it is possible to get a better understanding of the relationships between the VIP barrier constitution and its overall permeance to gas. In this specific paper on monolayer films, simulations indicate that having few large defects on the coating is less degrading than a large number of small ones. This is in agreement with the result presented in [6, 7] in which the experimental approaches show that the defects size is more influential on the permeance than the surface fraction of defects which in turn is more influential than the polymer thickness.

In the complete paper that will be produced if this proposal is selected for publication, other parts of the study will be developed, especially: multilayer modelling, experimental approach and comparison between simulation and experimental results in order to develop analytical models of apparent permeance.

Acknowledgements

The authors gratefully acknowledge the collaborators of the project EMMA - PIV (n° ANR - 12 -VBDU - 0004 - 01) that includes this research, and also the National Research Agency (ANR) for their financial support.

References

[1] GARNIER G., YRIEIX B., BRECHET Y., FLANDIN L., Influence of structural feature of aluminum coatings on mechanical and water barrier properties of metallized PET films, J. Appl. Polym. Sci., 115: 3110 - 3119. doi: 10.1002/app.31372, (2010).

[2] FICK A. E., über Diffusion. Pogg. Ann. Phys. Chem. 170 (4. Reihe 94), pp. 59 - 86, (1855).

[3] STANNETT V., Simple Gases, in Diffusion in Polymers, Crank, J. and Park, G. S. (eds.), Academic Press, London and New York, pp. 41 - 73, (1968).

[4] KLOPFFER M. H. and FLACONNECH B., Article, Transport properties of gases in polymers: Bibliographic review, OIL GAS SCI, 56(3), pp. 223 - 244, (2001).

[5] HANIKA M., LANGOWSKI H. −C., MOOSHEIMER U., PEUKERT W., Inorganic layers on polymeric films: Influence of defects and morphology on barrier properties, Chem. Eng. Technol., 26: 605 - 614. doi: 10.1002/ceat.200390093, (2003).

[6] ROCHAT G., LETERRIER Y., FAYET P. and MÅNSON J−A. E., Influence of substrate additives on the mechanical properties of ultrathin oxide coatings on poly (ethylene terephta−late), Surface & Coatings Technology, 200, pp. 2236 - 2242, (2005).

[7] SUGIYAMA A., TADA H. and YOSHIMOTO M., Gas permeation through the pinholes of plastic film laminated with aluminium foil, Vuoto, XXVIII(1 - 2), pp. 51 - 54, (1999).

Modelling of Long-term Hygro-thermal Behaviour of Vacuum Insulation Panels

Antoine Batard[a,b*], Thierry Duforestel[a], Lionel Flandin[b], Bernard Yrieix[c]

a. EDF R&D - ENERBAT - EDF Lab Les Renardières - 77818 Moret-sur-Loing, France
b. LEPMI-LMOPS-Université de Savoie-Campus Savoie Technolac-Hélios-73376 Le Bourget-du-Lac, France
c. EDF R&D-MMC-EDF Lab Les Renardières-77818 Moret-sur-Loing, France

Abstract

The low thermal conductivity of Vacuum Insulation Panels (VIPs) is not stable but increases with time due to gas permeation through VIPs barriers and the ageing of their envelope and core material. Accelerated experiments are carried out in order to better understand this ageing process but they are not sufficient to predict the long term performance of panels. Models have to be used to connect the short term evaluation and the long term behaviours in order to improve the prediction of the thermal conductivity evolution. This paper describes the development of a VIP model in the Dymola® software. This model takes into account the envelope and core material hydro-thermal characteristics and behaviours, and integrates the actual solicitations of the panels on site. The thermo-activation of the envelope permeance is integrated. Many properties of the core material are modelized: type of silica, sorption isotherm, hygro-thermal ageing, pore size distribution, etc.. Simulations in constant and variable conditions in temperature and moisture have been carried out. The results show first at all the unexpectable real behaviour of the VIPs conductivity, not accessible by simple short term linear evolution, and then the important impact of the core material characterization on the estimated long term performance of VIPs.

Keywords vacuum insulation panels, core material behaviour, mass and heat transport modelling.

1. Introduction

The aim of the development of this VIP model is to simulate, over a 50-year period and as accurately as possible, its hygro-thermal behaviour in order to analyse its performance when it is subjected to different real conditions in temperature and humidity. First, this paper describes the different equations for the envelope and the core material on which the model is based. Then, the modelling tools will be presented. Finally, simulation results in constant conditions for VIPs made with core materials more or less hydrophilic are shown and analysed.

2. Behaviour of the envelope

The aim of the VIP barrier is to maintain the core material under vacuum thanks to his low permeance to atmospheric gases. In this paper, only these barrier envelopes composed of metalized multilayer film are studied. The model used for mass transfer though the barrier is the sorption-diffusion model detailed by Crank and Park [1] for polymers. Dissolution on each side of the membrane using Henry's law (Eq. 1), and diffusion though each polymer using Fick's laws (Eq. 2 and 3) are considered. These equations are expressed using the potential c/S (Pa):

$$p = \frac{c}{S} \tag{1}$$

$$\varphi = -\overrightarrow{DS\,\mathrm{grad}}\left(\frac{c}{S}\right) \tag{2}$$

* Corresponding author, Tel: 33-6-31-65-44-49, E-mail: antoine.batard@edf.fr

$$\frac{\partial}{\partial t}\left(\frac{c}{S}\right) = D\nabla^2\left(\frac{c}{S}\right) \quad (3)$$

Wherep p: partial pressure (Pa),

c: mass concentration (kg. m^{-3}),

S: apparent solubility coefficient (kg. m^{-3}. Pa^{-1}),

υ: mass flow density (kg. m^{-2}. s^{-1}),

D: apparent diffusion coefficient (m^2. s^{-1})

t: time (s).

The apparent permeance Π (kg. m^{-2}. s^{-1}. Pa^{-1}) is given by eq. 4, taking into account the thermal activation of diffusion and dissolution represented by the Arrhenius's law.

$$\Pi = \frac{D_0 e^{-\frac{Q_D}{RT}} \cdot S_0 e^{-\frac{Q_S}{RT}}}{d} \quad (4)$$

Where Q: activation energy(J. mol^{-1}),

R: ideal gas constant(J. K^{-1}. mol^{-1}),

T: temperature(K),

d: total film thickness(m).

The equivalent thermal conductivity of the envelope is calculated using the combining rules of layers in series (eq. 5):

$$\lambda_f = \frac{1}{\sum_i \frac{d_i}{\lambda_i}} \quad (5)$$

Where λ_f: film's themal conductivity (W • m^{-1} • K^{-1}),

d_i: thickness of the layer i (m),

λ_i: thermal conductivity of the layer i (W • m^{-1} • K^{-1}).

3. Behaviour of the core material

The core materials studied in this modelling are pyrogenic and fumed silica. The pressure equilibrium in the core material is considered as instantaneous.

Heat transfer in the silica is commonly represented by the parallel flux model. The total core material thermal conductivity λ_c can be split into 3 contributions (Eq. 6): radiative contribution λ_r, solid conduction λ_s and gaseous conduction λ_g:

$$\lambda_c = \lambda_r + \lambda_S + \lambda_g \quad (6)$$

The gaseous conduction is represented using Knudsen's relation developed by Kaganer [2]. It depends on the porosity, the temperature, the pressure, and the pore mean size. The model can integrate the influence of a pore size distribution.

$$\lambda_r = \frac{16}{3}\frac{\sigma n^2 T^3}{E(T)} \quad (7)$$

Where σ: Stefan-Boltzmann's constant (W • m^{-2} • K^{-4}),

n: refractive index,

E: extinction coefficient(m^{-1}).

The solid conduction is determined by the initial thermal conductivity and the mass of water adsorbed (Eq. 8)

$$\lambda_S = \lambda_{cS0} + B\tau_w \quad (8)$$

where λ_{cS0}: initial thermal conductivity (W • m^{-1} • K^{-1}),

B: experimental coefficient(W • m^{-1} • K^{-1}),

τ_w: mass content of water(%).

The relation between the mass content of absorbed water and the relative humidity RH in the pores is fixed by the sorption isotherms models of the silica:

$$\tau_w = f(RH) \quad (9)$$

The gaseous conduction is represented using Knudsen's relation developed by Kaganer [2]. It depends on the porosity, the temperature, the pressure, and the pore mean size. The model can integrate the influence of a pore size distribution.

$$\lambda_g = \varepsilon \frac{\lambda_{g0}(T)}{1 + \frac{CT}{\phi \cdot p_t}} \quad (10)$$

Where λ_{g0}: gaseous thermal conductivity at atmospheric pressure(W • m^{-1} • K^{-1}),

C: various constant,

ϕ: pore mean size,

p_t: total internal pressure.

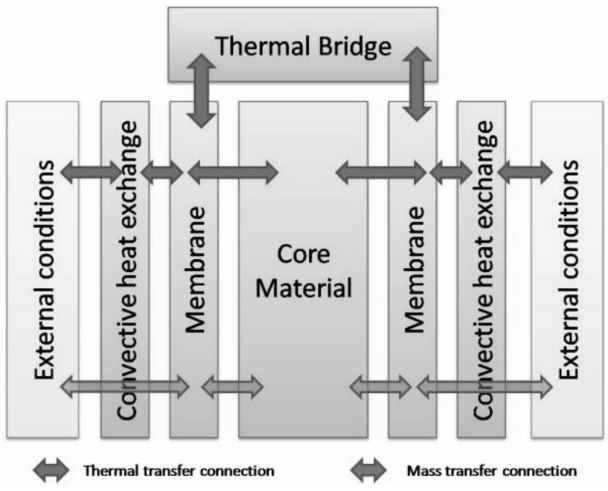

Fig. 1 Schematic illustration of the VIP model

4. Behaviour of the panel

A schematic illustration of the model is represented on the Fig. 1. This model takes into account the envelope and the core material thermal behaviour and mass transfer. In addition, convective heat exchanges and thermal bridge are modelled.

5. Modelling tools and methods

Dymola platform has been used to develop the model in the Modelica language. All components of the model (envelope, core material, thermal bridge etc.) are connected by ports. One port carries six information: temperature, water vapour partial pressure, total gas pressure and the flux.

6. Results and discussions

The Fig. 3, 4 and 5 show the thermal conductivity evolutions over 50 years for 5 VIPs including different core materials: silica A200 new and aged for 24 hours at 70 ℃ and 90 %RH, silica R974 new and aged for 24 hours at 70 ℃ and 90 % RH, and new silica Rodhia T43.

For each of these materials, sorption isotherm was measured at EDF. The fitting curve suggested in the Annex 65 [3] was used. In order to make the silica more hydrophilic, they were treated. The obtained sorption isotherms at 25 ℃ are presented on fig. 2.

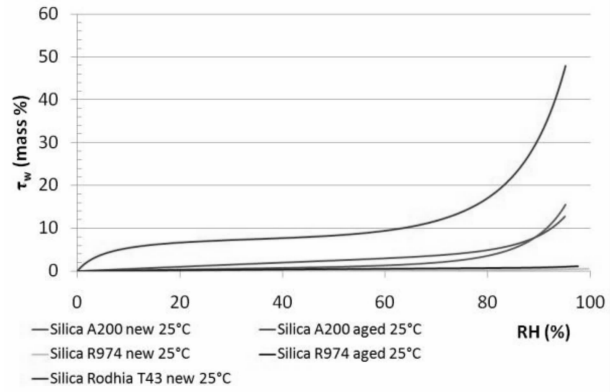

Fig. 2 Sorption isotherms of the 5 silicas studied at 25 ℃

At 20 ℃ and 40 % RH, all VIPs show a similar behaviour with a very weak thermal conductivity variation. The silica Rodhia T43, which is more hydrophilic than the other ones, had a greater conductivity.

The Fig. 4 and 5 show that the thermal behaviour

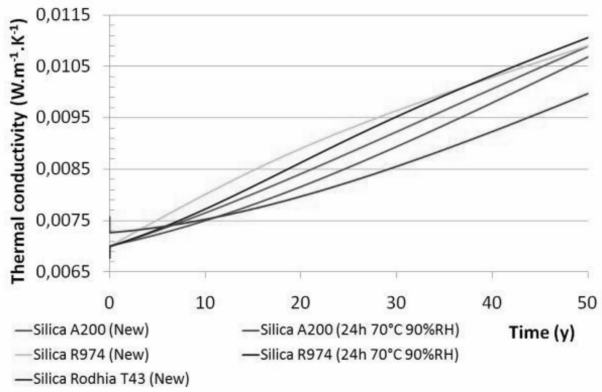

Fig. 3 Thermal conductivities evolution over 50 years at 20 ℃ and 40 % RH

of VIPs, at 40 ℃ and 70 % RH and at 70 ℃ and 90 % RH, differs greatly depending on their core material. The conductivity variations are very different compared to those of the VIPs at 20 ℃ and 40 % RH.

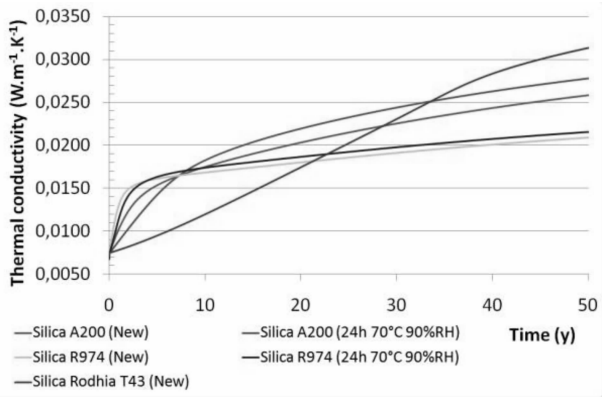

Fig. 4 Thermal conductivities evolution over 50 years at 40 ℃ and 70 % RH

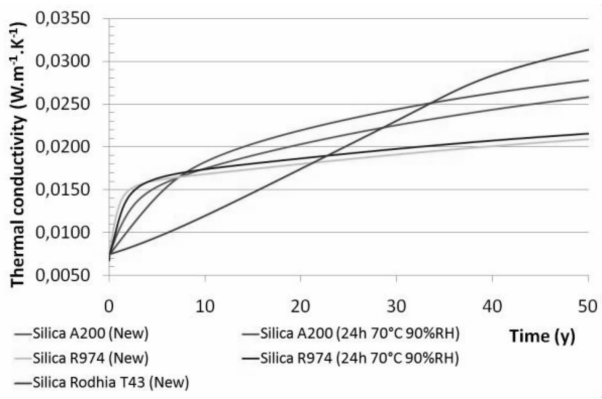

Fig. 5 Thermal conductivities evolution over 50 years at 70 ℃ and 90 % RH

At 40 ℃ and 70 % RH, in the first years the VIPs with silica treated had the lowest thermal conductivity than those with silica untreated. For silica R974 new

and treated, a crossover occurs around 35 years. The VIP made with silica Rodhia T43 had the higher thermal conductivity in the first years but after 10 years, it had the lowest one.

At 70 ℃ and 90 % RH, the same comments can be made about the thermal conductivity evolutions. In short term, the thermal conductivity of VIPs manufactured with more hydrophilic silica was higher than the other ones, however in long term it was the opposite.

7. Conclusions and outlook

The simulations presented in this paper show that the thermal behaviour of VIPs is very dependent on the core material sorption isotherm. Hydrophobic silicas seem more advantageous regarding the short term performance. But in longer term, hydrophilic silicas seem more efficient.

Our complete study includes many other simulations carried out in various conditions with variable temperatures and humidities. Different VIP characteristics can be accommodated in order to optimize the panels thanks to the model. This model which involves taking account of ageing will be integrated in wall models. This final scale will allow to conclude on the performance of VIPs and know how they can be improved.

Acknowledgements

The authors grateful acknowledge the collaborators of the project EMMA - PIV (n° ANR - 12 - VBDU - 0004 - 01) that includes this research, and also the National Research Agency (ANR) for financial support.

References

[1] CRANK J. and PARK G. S., (eds.) Diffusion in Polymers, Academic Press, London and New York, (1968).

[2] KAGANER M. G., Thermal insulation in cryogenic engineering, Israel program for scientific translations, Jerusalem, (1969).

[3] IEA/ECBOS Annex 39, High Performance Thermal Insulation (Subtask A), (2005).

Effect of Contact Resistance on the Effective Thermal Conductivity of Vacuum Insulation Panels with Radiation Shields

Jaehyug Lee, Tae-Ho Song*

School of Mechanical, Aerospace and System Engineering,
Korea Advanced Institute of Science and Technology, Guseong-dong 373-1, Yuseong-gu, Daejeon, Korea

Abstract

Heat transfer in the core materials of highly-evacuated vacuum insulation panel (VIP) occurs by conduction through the solid structure and radiation through the pore. Radiation shields are inserted in the core structure of VIPs to reduce the radiation. In this study, a model for the heat transfer in VIPs with radiation shields incorporating conduction, radiation and contact resistance is suggested and analyzed. Combined conduction and radiation heat transfer in VIPs is analyzed with the discrete ordinates interpolation method (DOIM). Analysis shows an increase of the effective thermal conductivity compared to a conventional separate model for highly reflective boundaries. This result indicates that the capability of radiation shields to reduce the effective thermal conductivity may be smaller than anticipated by the separate model. When contact resistance is added to the analysis, the interaction of conduction and radiation near the wall weakens significantly. These results show that suggested combined heat transfer model in the core materials of VIPs can give an insight in the optimization of insulation performance of VIPs with radiation shields.

Keywords vacuum insulation panels, radiation shields, combined conduction and radiation, contact resistance

1. Introduction

Demand for a high-performance thermal insulation material is increasing to save the energy in buildings and home appliances. Vacuum insulation panel (VIP) arises as a promising solution for such purposes with its very low thermal conductivity.

In high vacuum, heat transfer in the core materials of VIP occurs by conduction through the solid structure and radiation through the pore [1]. Interaction between conduction and radiation may exist in VIPs, as the amounts of heat transfer by two heat transfer modes are in a similar range. While there are some studies on combined heat transfer problem for multilayer insulations [2], this problem has not been studied extensively yet for VIPs.

Lately, a new type of VIP utilizing artificial core structures to support the atmospheric pressure has been suggested [3] (Fig. 1). For this type of VIP, porosity and density of the filling materials is adjustable and radiation shields are employed to reduce the radiation. So an improved analysis to encounter the eff + ect of combined conduction and radiation is needed.

In this study, the coupled effect of conduction and radiation is analyzed. As a special emphasis is placed, the effect of contact resistance to the wall or the shields is scrutinized.

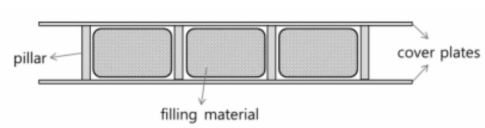

Fig. 1 Structure of pillar-supported VIP [3]

2. Modeling and Numerical Scheme

The core material in VIPs is modeled as a 1D plane-parallel medium. For the sake of simplicity, only

* Corresponding author, Tel: 82-42-350-3072, E-mail: thsong@kaist.ac.kr

the heat transfer through the core material is considered. The core material is assumed to be gray with constant properties. Two walls are isothermal, each at temperatures T_{B0} and T_{U0}. They are diffuse and have an emissivity ε_w. Contact resistance between radiation shields and porous medium is modeled as a conductive resistance between the wall and the medium, so contact resistance R_C may be added at both sides. The physical model of VIP is described in Fig. 2.

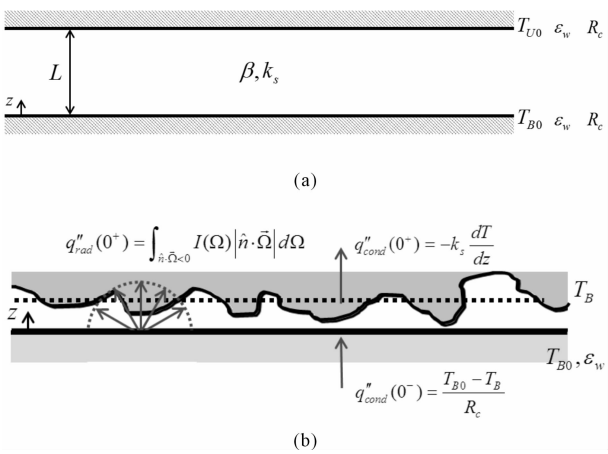

Fig. 2 (a) Physical model of VIP used in this study
(b) Contact resistance at the boundary

The energy equation with constant thermal conductivity k_s can be expressed as

$$k_s \nabla^2 T - \nabla \cdot \vec{q_R} = 0 \tag{1}$$

Here, the radiative heat source term $\nabla \cdot \boldsymbol{q}_R$ is given by [4]

$$\nabla \cdot \vec{q_R} = 4\kappa\left(\sigma T^4 - \frac{1}{4}\int_{4\pi} I \mathrm{d}\Omega\right) \tag{2}$$

Where κ is the absorption coefficient and $\sigma = 5.67 \times 10^{-8}$ W/(m^2 · K^4) is the Stefan-Boltzmann constant.

Contact resistance is modeled in a way that the temperature at a point infinitesimally away from the wall is determined by conduction boundary conditions;

$$\frac{T_{B0} - T_B}{R_c} = -k_s \frac{\mathrm{d}T}{\mathrm{d}z}, \text{ and } \frac{T_U - T_{U0}}{R_c} = -k_s \frac{\mathrm{d}T}{\mathrm{d}z} \tag{3}$$

Where T_B and T_U are the temperatures at the points infinitesimally away from the walls, respectively.

The radiative transfer equation (RTE) and its boundary condition for gray plane-parallel medium with diffuse walls is expressed as [4]

$$\frac{1}{\mu}\frac{\mathrm{d}I}{\beta \mathrm{d}z} = (1-\omega) I_b - I + \frac{\omega}{4\pi}\int_{4\pi} I(\Omega')\Phi(\Omega', \Omega)\mathrm{d}\Omega' \tag{4}$$

$$I_W^+(\Omega) = \varepsilon_w I_{bw} + \frac{1-\varepsilon_w}{\pi}\int_{\hat{n}\cdot s'<0} I(\Omega') \mid \hat{n} \cdot s' \mid \mathrm{d}\Omega' \tag{5}$$

Where μ is the directional cosine, $\omega = \sigma_s/\beta$ is scattering albedo and $\Phi(\Omega', \Omega)$ is the scattering phase function of the medium.

Equations (1) and (4) are nonlinear integro-differential equations and should be solved numerically. The total heat flux q''_{tot} at the centerline is used to determine the effective thermal conductivity of the medium using the relation

$$k_{eff} = q''_{tot} L/(T_{B0} - t_{U0}) \tag{6}$$

To solve the problem, the DOIM incorporated with the conduction solver is used. The DOIM is a modified version of the discrete ordinates method (DOM) using an interpolation scheme to analyze radiative transfer problems [5].

Conduction and radiation are often considered separately in the analysis of insulation materials. The effective thermal conductivity for an additive solution including the contact resistance is represented as [6]

$$k_{eff} = \frac{k_s}{1+N_2} + \frac{4\sigma T_m^3 L}{3\tau_L/4 + (2/\varepsilon_w - 1)} \tag{7}$$

Where $\tau_L = \beta L$ is the optical thickness of the medium and $N_2 \equiv \frac{2R_c}{L/k_s}$ is the ratio of contact resistance to the medium conduction resistance.

3. Results and Discussions

Fundamental Calculations:

The effective thermal conductivity is calculated for various cases with a fixed solid conductivity. Solid conductivity of VIP is usually 1 to 3 mW/(m · K) [7]; however, 1 mW/(m · K) is taken here for computational example. The mean temperature is 300 K and the thickness is 0.01 m.

Fig. 3 shows k_{eff} of the medium for various optical thicknesses and wall emissivities without contact resistance. The results are compared with the additive solution calculated from equation (7). When the medium is nearly transparent ($\tau_L \ll 1$), the total amount of heat flux does not depart much from those of additive solution. In the intermediate optical thickness

range, however, k_{eff} computed by combined analysis is significantly larger than that predicted by the additive approximation for a low emissivity limit. After that, k_{eff} for combined analysis when $\tau_L > 10$ converges to the values for the "black" boundary.

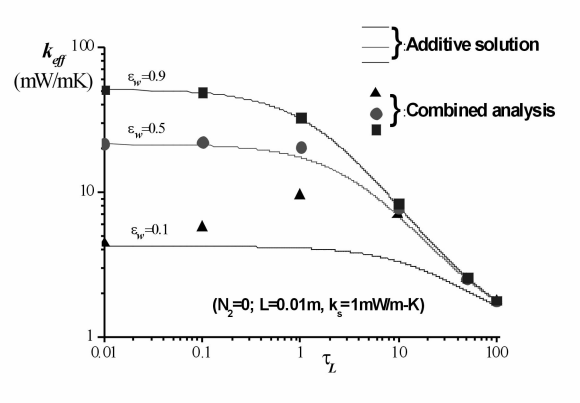

Fig. 3 The effective thermal conductivities at 300K by combined analysis and additive solution without contact resistance

Radiation shields having low emissivity seem to lower the effective thermal conductivity significantly in the additive solution. However, when combined heat transfer is considered, the effect of radiation shields is weaker than expected. For most VIP, porous medium with β larger than 3000 m^{-1} is used without radiation shields [7]. The optical thickness of common VIPs is larger than 50 and additive solution can be safely used. However, when optically thin medium such as aerogel is considered or many radiation shields are used, combined mode of heat transfer considering the effect of wall emissivity should be taken in the analysis.

The effective thermal conductivity of the medium with contact resistance on its boundary is shown in Fig. 4 for N_2 = 0.1 and 1.0. For all cases, k_{eff} decreases compared to the value calculated without contact resistance.

Equation (7) indicates that only the conduction heat transfer decreases by addition of contact resistance in the additive solution. On the other hand, combined analysis results show that decrease in k_{eff} with contact resistance is larger than that of the additive solution. Also, when the results for N_2 =0.1 and those for N_2 = 1.0 are compared, the reduction in k_{eff} in the low emissivity boundary is more pronounced when the contact resistance is large. It can be deduced that not

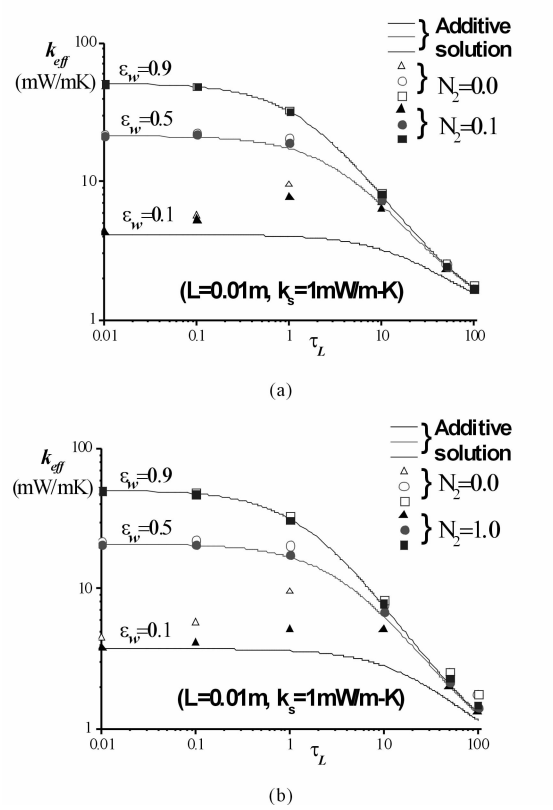

Fig. 4 The effective thermal conductivities when ratio of contact resistance to medium conduction resistance N_2 is (a) 0.1 and (b) 1.0

only conduction, but also radiative heat transfer decreases when contact resistance exists between the porous medium and radiation shields. Because packing density and pressure load on the core material for a new type of VIP are adjustable, the optimization of the core materials of VIP concerning these factor is desirable.

Practical Applications:

Combined analysis for layer with smaller height, which can be expressed by equivalent number of shields per thickness, are further made to see how k_{eff} of actual VIP changes when radiation shields are inserted. Realistic values of ε_w (0.11 for Al and 0.038 for Ag) are used. Assuming loosely spaced glass fiber core [8], optical thickness τ_L =86 and solid conductivity k_s =0.25 mW/(m·K) are used.

Fig. 5 shows k_{eff} of 1 cm VIP without contact resistance. It is clearly seen that much more shields are needed to get the same k_{eff} in combined analysis than predicted by the additive solution. Also, it can be found that difference in the wall emissivity is not influential in the k_{eff} through the combined analyses.

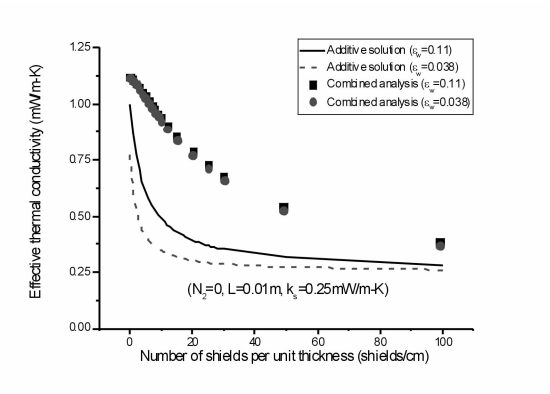

Fig. 5 The effective thermal conductivities of 1cm VIP layer with radiation shields inserted

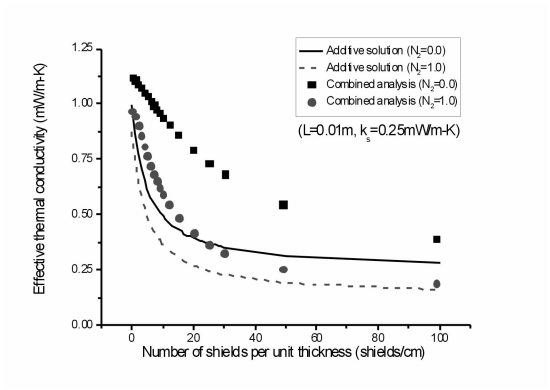

Fig. 6 The effective thermal conductivities of 1cm VIP layer with contact resistance applied

The effect of contact resistance can be found in Fig. 6. When contact resistance between filler material and radiation shields is applied, k_{eff} can be decreased drastically with the addition of radiation shields. This again implies that contact resistance can be the key in the improving performance of VIPs with radiation shields.

4. Conclusions and outlook

In this study, analyses on combined conduction and radiation in the core materials of VIP are conducted with the emphasis on the contact resistance. The reduction of heat transfer by radiation shields is lowered in the combined analysis for the optical thickness larger than 0.1, so the effective thermal conductivity may be much larger than that predicted through an additive solution. Introduction of contact resistance is found to be effective in reducing heat transfer for low emissivity walls, by weakening the effect of enhanced heat transfer near the wall.

Combined analysis developed in this study need to be used in optimization of a new type of VIP with various radiative and conductive properties of porous materials and radiation shields. More detailed study on the contact resistance is also recommended.

Acknowledgements

This work was supported by the National Research Foundation of Korea (NRF) grant funded by the Korea government (MSIP) (No. 2013R1A2A2A07068924) and the second stage of the Brain Korea 21 project in 2015.

References

[1] R. Baetens, B. P. Jelle, J. V. Thue, M. J. Tenpierik, S. Grynning, S. Uvslϕkk, and A. Gustavsen, Vacuum insulation panels for building application: A review and beyond, Energy and Buildings 42:2 (2010) 147 - 172.

[2] M. Spinnler, E. R. F. Winter, and R. Viskanta, Studies on high-temperature multilayer thermal insulations, Int. J. Heat Mass Transfer 47 (2004) 1305 - 1312.

[3] J. Kim, T. H. Song, I. Yeo, B. Choi, The 2nd Generationvacuum insulation panel, The 4th International Conference on Applied Energy (2012).

[4] M. F. Modest, Radiativeheat transfer, 2nd edn, Academic Press (2003).

[5] K. B. Cheong, T. H. Song, Analternative discrete ordinates method with interpolation and source differencing for two-dimensional radiative transfer problems, Numerical Heat Transfer Part B 32 (1997) 107 - 125.

[6] C. L. Tien and G. R. Cunnington, Cryogenic insulation heat transfer, Adv Heat Transfer, vol. 9, Academic Press, New York (1973) 349 - 417.

[7] J. S. Kwon, C. H. Jang, H. Jung, and T. H. Song, Effective thermal conductivity of various filling materials for vacuum insulation panels, Int J Heat and Mass Transfer 52 (2009) 5525 - 5532.

[8] J. Kim, T. H. Song, Vacuum insulation properties of glass wool and opacified fumed silica under variable pressing load and vacuum level, Int J Heat and Mass Transfer 64 (2013) 783 - 791.

The Comparison of Sound Absorption Performance and Thermal Conductivity of Glass Fiber Felt Produced by Centrifugal-Spinneret-Blow System and Fire-Spinneret-Blow System

Wu Cao , Chen Zhaofeng* , Yang Yong,
Chen Zhou, Xu Tengzhou , Li Yanming, Wang Weiwei, Bao Shuting

College of Material Science and Technology, Nanjing University of Aeronautics and Astronautics, Nanjing, 210016, P. R. China

Abstract

In this paper, experiments to investigate fibrous insulating materials have been performed. Glass wool felt made of centrifugal-spinneret-blow method and fire-spinneret-blow method were studied. Scanning electron microscopy (SEM) , impedance tube apparatus and heat flow meter (NETZSCH HFM 436) were used to assess the mechanism of the effect of fiber diameter on the thermal conductivity and absorption performance of materials. It has been found from the experiments that the coefficient of thermal conductivity of all analyzed materials is strongly dependent on the Fiber diameter : the thinner the fiber diameter, the lower the thermal conductivity. The sound absorption ability of FSBGF can reach the III rating requirement of sound absorption material according to national standard.

Keywords acoustic, heat transfer, centrifugal-spinneret-blow, fire-spinneret-blow, glass fiber felt

1. Introduction

Centrifugal-spinneret-blow method and fire-spinneret-blow method are the most commonly used preparation methods of the glass fiber felt, by far. there are a lot of researches on mechanical properties, service life, corrosion resistance of glass fiber felt . However, the comparison of the two methods of the preparation of glass fiber felt on the sound absorption and insulation performance is less. This paper analyzed the sound absorption performance and thermal conductivity of glass fiber felt produced by centrifugal-spinneret-blow system and fire-spinneret-blow system, and discusses the reasons.

2. Theory background

Sound absorption ability of a material is usually describedby sound absorption coefficient (α), which represents the absorption energy rate of the material against the overall incidence energy. Sound absorption coefficient is influenced by physical parameters such as porosity, flow resistivity, fiber diameter, tortuosity, density, and thickness. In general, these parameters can synthetically be characterized by acoustic impedance (Z_S), expressed by the following equation [1]:

$$\alpha = \frac{4Z_r}{(1+Z_r)^2 + Z_i^2} \quad (1)$$

where Z_r and Z_i are the real and imaginary parts of acoustic impedance Z_S . They represent the acoustic resistance and reactance feature of material, which indicates sound energy attenuation and energy reflection, respectively [2]. If the acoustic impedance Z_S of the material is a pure imaginary number ($Z_r = 0$), the material can absorb no energy. On the other hand, if it is a pure real number, the material dissipates sound energy and the absorption coefficient is no more than 1. As shown in Eq. (1), the more the resistance Z_r

* Corresponding author, Tel: 86 - 25 - 52112909, Fax: 86 - 25 - 52112626, E-mail: zhaofeng_chen@163.com

approaches to a constant 1 and Z_i verges on zero, the higher the sound absorption coefficient is.

3. Experimental

3.1 Preparation of materials

Centrifugal-spinneret-blow glass fiber felt (CSBGF) and fire-spinneret-blow glass fiber felt (FSBGF) used in this study were provided by Chengdu Hanjiang New-type building Material Als Co., ltd and Shenyang Longclear glass products Co., ltd, respectively. Composition of the samples consisted of pure glass fiber with phenolic resin adhesive. glass fiber felt with dimensions of 300 mm × 300 mm × 20 mm were fabricated. Fig. 1 (a) shows the manufacturing process of fire-spinneret-blow method and Fig. 1 (b) shows the manufacturing process of Centrifugal-spinneret-blow method. Both of the two methods included the following steps: melting glass raw material (see stage 1 in Fig. 1); forming fiber process (see stage 2 in Fig. 1); spraying glue adhesion agent (see stage 3 in Fig. 1); and drying the glass fiber felt (see stage 4 in Fig. 1)[3,4].

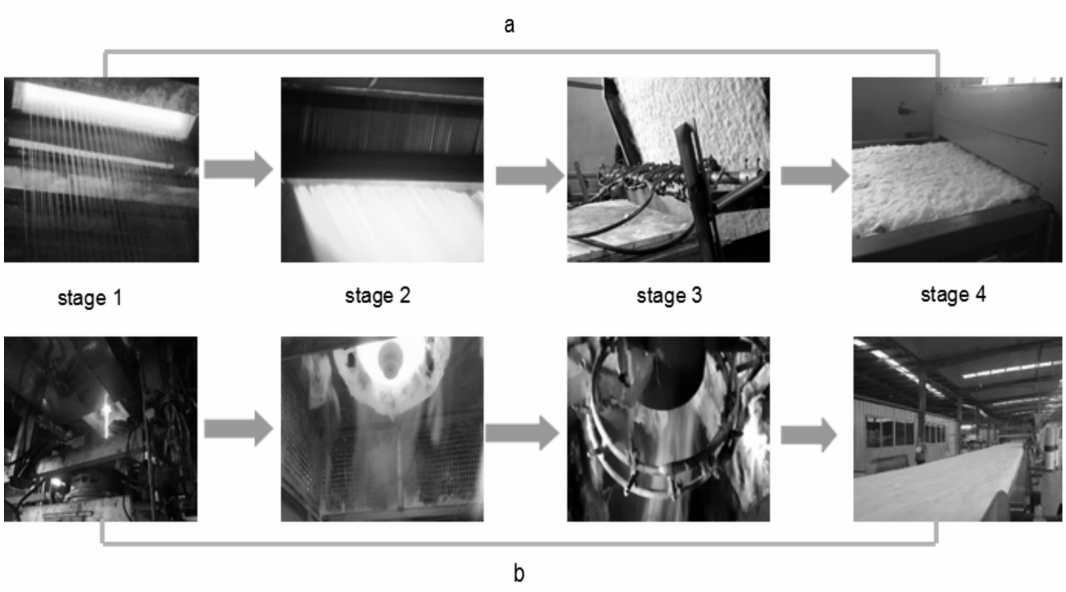

Fig. 1 Manufacturing process of glass fiber felt

(a) fire-spinneret-blow method; (b) Centrifugal-spinneret-blow method

3.2 Measurement apparatus

The diameters of composite fibers were investigated using a scanning electron microscope (SEM).

The impedance tube method was used for measuring the absorption coefficient and acoustic impedance of materials. The measurement apparatus consists of two impedance tubes with diameters of 100 and 29 mm. The large tube was used for the frequency range of 100～1600 Hz and the small tube was prepared for the 250～5000 Hz measurement. The impedance tube apparatus is shown in Fig. 2. In this study, the acoustic impedance of materials was characterized by normalized specific acoustic impedance, which is a ratio of specific acoustic impedance to the characteristic impedance of air.

Fig. 2 The impedance tube apparatus

Experimental samples with a thickness of 20 mm were prepared for the acoustic measurement. Samples were fixed in the impedance tube with the inner surface against a rigid wall and the outer surface covered with covering layers, if necessary. In order to diminish the

experimental deviation during the sampling process, the mass of each sample was rationed before measurement. Sound absorption measurement was carried out at least five times for each sample to insure the experimental accuracy.

The thermal insulation property of glass fiber felt was measured through the steady-state bi-plate technique according to ISO 8301 and ASTM C518 standards. The basic principle of operation is to create one-dimensional axial heat flux through the sample and calculate the thermal property using the Fourier equation of heat transfer:

$$q = -\kappa A \frac{\mathrm{d}T}{\mathrm{d}x} \tag{2}$$

where κ is the thermal conductivity, q is the steady-state heat flow, A is the cross-sectional area of the sample, and $-\mathrm{d}T/\mathrm{d}x$ is the temperature difference gradient.

A heat flow meter (NETZSCH HFM 436) was used in this study for thermal measurement. Sample with cross section of 300 × 300 mm^2 and thickness of 20 mm was sandwiched between a pair of "hot" plate and "cold" plate. Temperature range from 10℃ to 50℃ was adapted to analyze the influence of temperature on the thermal property. Each thermal conductivity value was an average result of five measurements.

3. Results and discussion

4.1 Characterization

Morphological analysis of theglass fiber was carried out through scanning electron microscope (SEM) photomicrograph as shown in Fig. 3. It can be seen that the diameter of the centrifugal-spinneret-blow glass fiber were more diffuse, the diference of fiber diameter were very large, and finer fibers showed bending state. However, the diameter of fire-spinneret-blow glass fiber didn't show much difference, and the fiber were more straight. A rough determination of the fiber size was carried out by counting fiber size SEM images. The results show that the average diameter of centrifugal-spinneret-blow glass fiber is 4.39 μm and the average diameter of fire-spinneret-blow glass fiber is 3.16. Besides, more than 90% of the fire-spinneret-blow glass fiber fibers are between 1～4μm (Fig. 4).

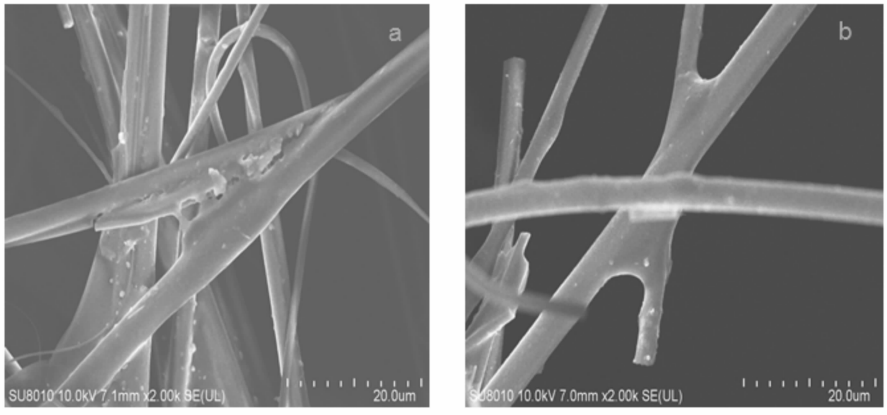

Fig. 3 SEM photomicrograph of the glass fiber felt

(a) Centrifugal-spinneret-blow glass fiber; (b) fire-spinneret-blow glass fiber

4.2 Sound absorption ability

Sound absorption coefficients of CSBGF and FSBGF were measured at the frequency range from 250～5000 Hz and the results were shown in Fig. 5. First, it was found that two kinds of glass fiber felt exhibited a typical absorption spectrum of porous absorbing material, which rapidly increases to its first absorption peak and then gradually flattens with the increasing of incident frequency. CSBGF have very good low-frequency absorption ability. The average absorption coefficient of CSBGF (0.24) is even higher than that of centrifugal-spinneret-blow glass fiber felt FSBGF(0.21) in the range of 250～1500 Hz. Therefore, CSBGF can provide excellent noise absorption in low-frequency band

which is closely associated with road traffic and other mechanical noise[5].

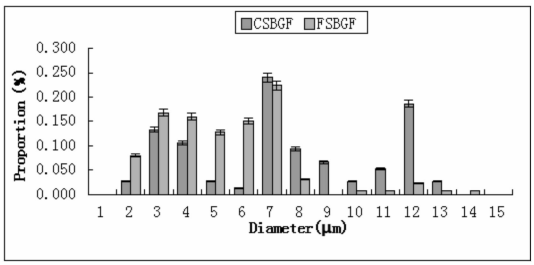

Fig. 4 The diameter of two glass fiber felt

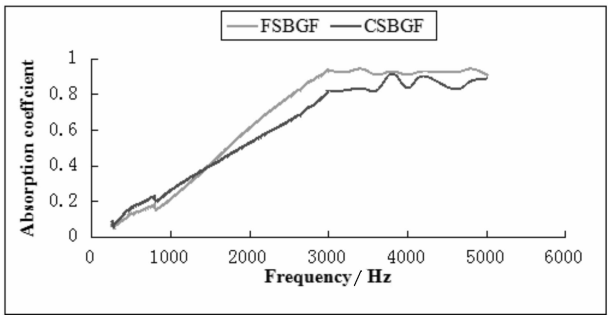

Fig. 5 Acoustic impedance of FSBGF and CSBGF

Besides, the sound absorption ability of FSBGF (0.43) is distinctly better than those of CSBGF(0.41) in a large frequency range. the average absorption coefficient of FSBGF is obviously higher than those of FSBGF in middle frequency ranges. The reason for the absorption difference among these materials can be ascribed to their respective diameter and structure characters. Although the overall porosity of FSBGF is higher than CSBGF (Tab.1), the dimeter of CSBGF is larger than FSBGF[6 - 8]. However, only open pores interconnected with each other are the key factor for sound absorption [9]. As for FSBGF, the pores in the material are formed due to the overlapping of fibers [10, 11]. So, the pores of FSBGF are open ones interconnected with each other which are contributable to the good absorption . When compared with FSBGF, the absorption coefficient of the CSBGF is relatively lower in most frequency range except for the peak region. This is mainly due to the relatively large dimeter of CSBGF, which makes it easy for sound waves to transmit inside the material. In general, the indication of sound absorption ability by absorption coefficient is complex since it differs in different sound frequencies. To solve this problem, a single value for evaluating the sound absorption, which called noise reduction coefficient (*NRC*), was calculated in this study. The *NRC* can be expressed by the following equation[12]:

$$NRC = \frac{\alpha_{250} + \alpha_{500} + \alpha_{1000} + \alpha_{2000}}{4} \quad (3)$$

According to the national standard (GB/T 16731—1997), materials having NCR exceeds 0.2 can be called sound absorbent material. And sound absorbers can be gradated into four levels according to *NRC* value: I, $NRC \geqslant 0.8$; II, $0.8 > NRC \geqslant 0.6$; III, $0.6 > NRC \geqslant 0.4$; IV, $0.4 > NRC \geqslant 0.2$. So, both of the two kinds of glass fiber felt are a high efficient sound absorbing material by meeting III rating requirement.

Tab.1 Physical properties ofglass fiber felt used in experiments

Glass fiber felt	Bulk density kg/m³	Porosity/(%)
CSBGF	135	92.4
FSBGF	127	95.3

4.3 Thermal insulation ability

Thermal conductivity is a measure of the effectiveness of a material in conducting heat. Tab.2 compares the thermal conductivity of FSBGF with those of CSBGF at room temperature (25 ℃). It is evident that the thermal conductivity of FSBGF is lower than those of CSBGF.

Tab.2 Thermal conductivity comparison of FSBGF and CSBGF

Glass fiber felt	Bulk density kg/m³	Thermal insulation W/(m·K)
GSBGF	135	0.044
FSBGF	127	0.036

High porosity has been proved in the FSBGF due to the overlapping of fibers. Pores filled by air serve as scattering centers for phonons. Heat flow transfers through solid fibers and internal pores, while the thermal conductivity of air within the pores is much lower than that of solid substance. So, the high porous structure of FSBGF leads to a low thermal conductivity of the material.

5. Conclusions

This study demonstrates that FSBGF have good sound and thermal insulation properties. The sound absorption coefficient of FSBGF is superior to those of CSBGF. The sound absorption ability of FSBGF can reach the III rating requirement of sound absorption

material according to national standard.

The thermal conductivity of FSBGF was fairly low (0. 036 W/(m • K) at 25 ℃) and the thermal conductivity of FSBGF was lower than those of CSBGF .

Acknowledgement

The duthors would like to thank the financial support from Jiangsu Project BA2013097 and National Project 2015DFI53000.

References

[1] H. Zhou, B. Li, and G. Huang, Sound Absorption Characteristics of Polymer Microparticles, J. Appl. Polym. Sci., 2006, 101, p 2675 - 2679

[2] C. Zwikker and C. W. Kosten, Sound Absorbing Materials, Elsevier, New York, 1949

[3] Takeuchi N, Okada K, Konishi T. Wet process for manufacturing nonwovenfabric and apparatus therefor. United States Patent, US006058583A; 1999.

[4] Helwig, GS, Hendrik J, Paul G. Wet-laid nonwoven mat and a process for making same. United States Patent, US006267843B1; 1998.

[5] M. J. Swift, P. Bris, and K. V. Horoshenkov, Acoustic Absorption in Re-cycled Rubber Granulate, Appl. Acoust., 1999, 57, 203 - 212

[6] M. Dogan and M. Alkan, Some Physicochemical Properties of Perlite as an Adsorbent, Fresenius Environ. Bull., 2004, 13, 251 - 257

[7] P. W. Harben and R. L. Bates, Industrial Minerals Geology and World Deposits, Metal Bulletin, London, 1990, p 184

[8] S. A. Suvorov and V. V. Skurikhin, Vermiculite—A Promising Material for High-Temperature Heat Insulators, Refract. Ind. Ceram., 2003, 44, 186 - 193

[9] C. N. Wang and J. H. Torng, Experimental Study of the Absorption Characteristics of Some Porous Fibrous Materials, Appl. Acoust., 2001,62, 447 - 459

[10] H. Benkreira, A. Khan, and K. V. Horoshenkov, Sustainable Acoustic and Thermal Insulation Materials from Elastomeric Waste Residues, Chem. Eng. Sci., 2011, 66, 4157 - 4171

[11] J. P. Arenas and M. J. Crocker, Recent Trends in Porous SoundAbsorbing Materials, Sound Vib., 2010, 44, p 12 - 18

[12] GB/T 16731—1997, The Gradation of Sound Absorption Property for Absorbent Products, 1997

Long-term Thermal Resistance of Vacuum Insulation Panel (VIP) — Experimental Observations & Predictions

Phalguni Mukhopadhyaya[a*], Caroline St-Onge[b], Bruno Di Lenardo[b], Larry Carbary[c], William Gregg[d], Anil Parekh[e]

a. Associate Professor, University of Victoria, Department of Mechanical Engineering, Victoria, BC, Canada
b. Evaluation Officer, Canadian Construction Materials Centre, National Research Council Canada, Ottawa, ON, Canada
c. Construction Industry Scientist, Dow Corning, Midland, MI, USA
d. General Manager, Promat Inc., Knoxville, TN, USA
e. Senior Research Manager, CanmetENERGY, Natural Resources Canada, Ottawa, ON, Canada

Abstract

Vacuum insulation panels (VIPs), like any other building materials, age with time due to degradation effects from the environmental conditions. The long term thermal resistance (LTTR) of VIP is a very important design consideration, particularly for the exterior building envelope applications. However, determination of LTTR of VIP is one of the biggest challenges faced by the researchers and designers. Limited field performance data, typically lacking for any innovative construction materials or applications, variable VIP constituent compositions, various sizes, varied in-service installation techniques, different climatic conditions and lack of globally accepted performance criteria make it a truly daunting task for manufacturers, researchers or designers to establish a reasonable and reliable LTTR value for a VIP integrated building envelope construction during its anticipated service life. This paper presents and critically analyzes results from laboratory, accelerated and field aging (in Canada) tests conducted on VIP products of different sizes and geographical origins (Asia, Europe and North America) collected over a period of more than 10 years. Furthermore, the paper also proposes appropriate laboratory based comprehensive accelerated aging test conditions, supported by field performance test data, to determine the LTTR of VIPs to be used in building envelope constructions.

Keywords vacuum insulation panels, long-term performance, aging, durability, accelerated aging

1. Introduction

Introduction of new building energy codes across theworld, including Canada [1], has created a huge opportunity for the application of nonconventional high performance thermal insulation in building construction industry. Undoubtedly, vacuum insulation panel (VIP), with 5 to 10 times higher thermal resistance than traditional foam or fibrous insulations, has a tremendous and unique application potential in energy-efficient built environment construction. However, absence of long-term performance data is the biggest impediment keeping VIPs away from building envelope constructions. In order to address this issue, authors present observations from laboratory, accelerated and field aging tests conducted on VIPs of different sizes and geographical origins (Asia, Europe and North America) collected over a period of more than 10 years. Furthermore, based on these observations, this paper also proposes laboratory based accelerated aging test conditions, supported by available field performance test data, to determine the LTTR of VIPs to be used in building envelope constructions.

* Corresponding author, Tel: 1 - 250 - 472 - 4546, E-mail: phalguni@uvic.ca

2. Background

The impact of time and environment on the performance of construction materials (i. e. aging phenomenon) is an undeniable reality. VIP is no exception either. However, due to its unique vacuum fabrication process that leads to an exceptionally high thermal performance characteristics, the performance of VIP can change significantly over the time. Therefore, integrity of the VIP is of supreme importance for its short- and long-term performance. As shown in Fig. 1, in this study, the aging and durability of VIP, both related to its long-term thermal performance, are identified as two different but interrelated phenomena. Aging of VIP is primarily due to very slow but continuous increase of gas/vapour pressure inside the VIP (Fig. 2). Durability is considered as a relatively sudden or rapid failure of the VIP, due to loss of vacuum, caused by mechanical failure of the facer or the seam joint, and can be prevented through appropriate design and stringent quality control during manufacturing and on-site construction. In essence, to a great extent, failure due durability issues can be prevented but aging of VIP is a certainty. The aging of thermal insulation is not a new issue to the construction industry professionals who have dealt with the long-term thermal resistance (LTTR) of closed-cell foam insulation with a captive blowing agent and who are familiar with laboratory-based accelerated aging test procedure (i. e. thin-slicing) [2]. However, establishing an appropriate laboratory-based accelerated aging test method for the VIP is still a job in progress. Without a credible aging test protocol, the mass application of VIPs in building envelope construction will remain a distant pipe dream. Following sections outline a comprehensive accelerated aging test protocol and laboratory test observations.

3. Experimental program

Four different accelerated aging test conditions (E1, E2, E3 and E4) were considered in this study (see Table 1). These conditions together represent extremes of all known building envelope exposure conditions during its service life.

Five different types of VIPs (A, B1, B2, C, D, E) were considered in this study. These VIPs came from different manufacturers and made with different core and facer materials. Three specimens of the same VIP were tested in each test condition. The physical dimensions of the VIPs varied between 300 mm to 600 mm (length)× 300 mm to 600 mm (width) × 8 mm to 40 mm (thickness).

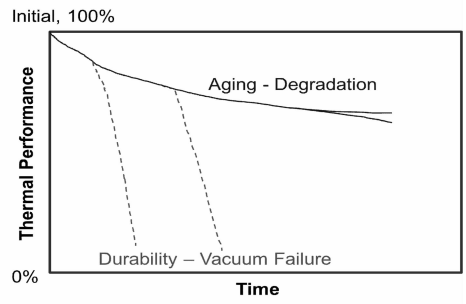

Fig. 1 Aging and durability of VIP

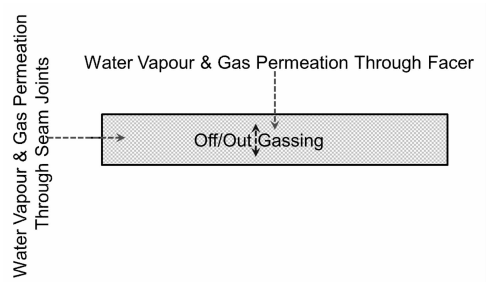

Fig. 2 Aging and durability of VIP

All VIPs were not subjected to all exposure conditions due to time and space limitations.

Tab. 1 Accelerated aging test conditions

Conditions	Temperature-T/℃	Relative Humidity -RH/(%)	Duration
E1	90	Ambient	90 days
E2	23	95	90 days
E3	−30	Ambient	90 days
E4	70	95	90 days

4. Experimental observations

Thermal resistances of the VIPs were measured before and after accelerated aging exposure using a heat flow meter and following ASTM C518 − 10 Standard Test Method for Steady-State Thermal Transmission Properties by Means of the Heat Flow Meter Apparatus. Typical observations on three B1 type VIP specimens with E1 (90 °C, ambient periods RH) aging condition after 30 and 90 days exposure are shown in

Tab. 2. The average aging values after 30 and 90 days are found to be 5% and 8%, respectively.

Tab. 2 Typical aging of VIP specimens B1 due to accelerated high temperature exposure

Specimen	Aging-Reduction of Thermal Resistance/(%)		
	Initial	30 days	90 days
1	0	5.52	10.43
2	0	4.73	8.28
3	0	3.61	6.63
Average Aging/ (%)		≈ 5	≈ 8

The overall average (3 specimens) changes in thermal resistance of VIPs in different accelerated aging environments after 30 and 90 days are shown in Tab. 3 and Tab. 4, respectively. These results clearly identify (1) high temperature, and combination of high temperature and humidity cause the maximum thermal resistance degradation of VIPs, (2) very cold temperature seems to have least or negligible impact on the degradation of thermal performance of VIPs, and (3) consistent degradation performances in 30 and 90 days observations.

Tab. 3 Aging of VIPs due to different accelerated aging conditions after 30 days

↓VIP Type	Average 30 days Accelerated Aging of 3 Specimens-Reduction of Thermal Resistance/(%)			
Conditions →	E1	E2	E3	E4
A	6		0	
B1	5		0	
B2	37		1	
C	16	3		15
D			0	
E	7			

Tab. 4 Aging of VIPs due to different accelerated aging conditions after 90 days

↓VIP Type	Average90 days Accelerated Aging of 3 Specimens-Reduction of Thermal Resistance/(%)			
Conditions →	E1	E2	E3	E4
A	10		0	
B1	8		0	
B2	56		1	
C	30	4		69
D			0	
E	9			

5. LTTR of VIP

The inherent challenge of establishing durability credentials of a new building material through laboratory-based accelerated aging tests is to develop a correlation between laboratory test results and field performance expectations. A definite solution to this issue is an impossible task but a rational conclusion is possible and can be very useful to the stakeholders. In the light of the aforementioned paradigm, authors have critically analyzed and compared the accelerated aging test results from this study to the field observations and other published results on the long term thermal resistance (LTTR) of VIPs.

The laboratory aged (ambient temperature and RH) 10 years performance data (Fig. 3) of VIPs from the published literature [3] show less than 1.5%/year average aging.

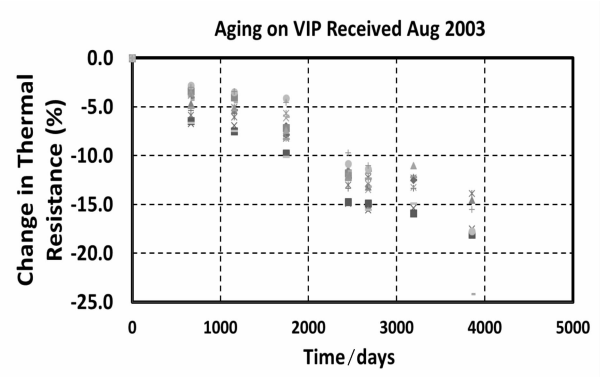

Fig. 3 Laboratory aging of VIPs for 10 years

The same panels became part of an accelerated aging study consisting of high temperature (70℃) and high humidity (95% RH) exposure, not simultaneously, and showed insignificant change in thermal resistance [3].

Results from three Canadian field investigations [4 - 6] with VIPs in exterior walls and roof also showed about 1.5% or less aging over a period of up to five years (Figs. 4 and 5).

Based on the field performance data, published VIP aging test results and the results obtained from this study, it is obvious that thermal degradation response of VIPs exposed to extreme temperature and humidity conditions can be captured, without any exception,

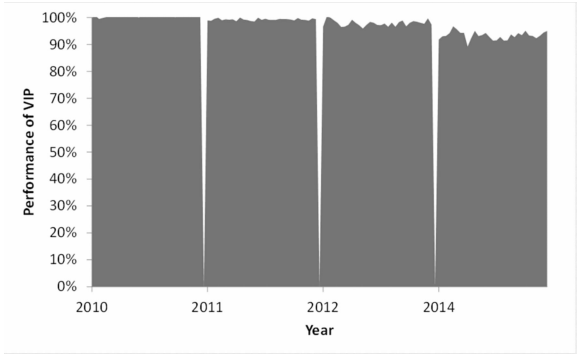

Fig. 4 Field aging of VIPs in wall (Ottawa, Canada)

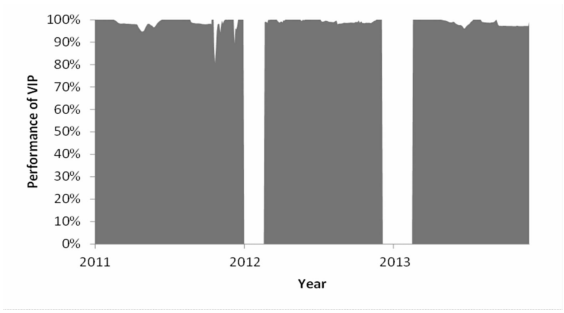

Fig 5 Field aging of VIPs in roof (Ottawa, Canada)

within about 30 to 90 days of accelerated aging tests conducted in the laboratory, and the best performing VIPs identified through accelerated aging laboratory tests can age as much as about 1.5% per year in Canadian cold climate environment.

With the help of the aforementioned observations an accelerated aging test protocol with performance requirements is proposed, as shown in Tab. 5. Furthermore, the VIPs satisfying thermal performance requirements outlined in Tab. 5 would be expected to have an aging rate of 2% per year and minimum estimated thermal resistance retention after 15 years equals to about 70% of the initial thermal resistance value (Fig. 6). For estimating the thermal resistance value of VIPs beyond 15 years of aging, further investigation will be needed (Fig. 6).

It is to be noted that the proposed accelerated aging test protocol and prediction of the long term thermal performance of VIPs are based on the available information and authors' experience with VIPs and other insulating materials. It is expected that the proposed test protocol and the performance requirements would be reviewed when more research and application outputs will be available in the coming years.

Tab. 5 Accelerated aging test protocol and thermal performance requirements for VIPs

No.	Aging Conditions	Total Duration /(days)	% R-value Reduction Requirement
1	70℃, 95%RH	30	⩽ 20
2	95%RH, 22℃	90	⩽ 10
3	90℃, ambient RH	90	⩽ 10
4	−30℃, ambient RH	90	⩽ 5
5	70℃ (ambient RH), 95%RH (22℃) - Alternate	98 (1 week @ 70℃, followed by 1 week @ 95%RH (22℃) − 7 Cycles)	⩽ 10
6	−30℃ (ambient RH), 50% RH (22℃) - Alternate	98 (1 week@ −30℃, followed by 1 week @ 50%RH − 7 Cycles)	⩽ 5

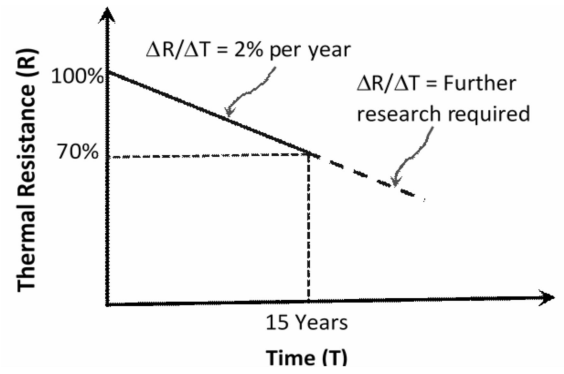

Fig. 6 Prediction of long term performance of VIPs

6. Conclusions and outlook

Based on the laboratory observations and field performance data this paper has proposed an accelerated aging test protocol and thermal performance requirements for VIPs for non-load bearing exterior building envelope applications not exposed directly to weathering elements such as sunlight, UV radiation, rain and wind. Furthermore, a long term thermal resistance (LTTR) prediction model, for a period of 15 years, is also proposed for the VIPs that go through

accelerated aging test protocol and meet the proposed thermal performance requirements. It is to be noted for specific applications that the proposed accelerated aging thermal performance requirements and LTTR prediction model should be carefully reviewed by an experienced building envelope design professional.

Acknowledgements

The authors would like to thank David van Reenen and Sladana Bundalo-Perc of NRC Construction for excellent support and commitment to carry out experimental investigations reported in this paper.

References

[1] National Energy Code of Canada for Buildings (NECB), 2011, National Research Council Canada, 1200 Montreal Road. Building M－58. Ottawa. Ontario. K1A 0R6. Canada.

[2] Mukhopadhyaya, P., Drouin, M., Normandin, N., van Reenen D., Lackey, J. Long-Term Thermal Performance of Impermeably Faced Polyiso Foam Boards—Field and Laboratory Observations, J. Cold Reg. Eng. 28(4), 2014.

[3] Mukhopadhyaya, P., Kumaran M. K., Sherrer G., van Reenen, D., An Investigation on Long-Term Thermal Performance of Vacuum Insulation Panels (VIPs)", Proc. of 10 th International Vacuum Insulation Symposium (IVIS－X), pp. 10, 2011, Ottawa, ON, Canada.

[4] Mukhopadhyaya, P., Molleti, S., van Reenen, D., Vacuum Insulation Panel (VIP): An Historic Opportunity for the Building Construction Industry, RCI Interface, August 2014.

[5] Mukhopadhyaya, P., MacLean, D., Korn, J., van Reenen, D., Molleti. S., Building application and thermal performance of vacuum insulation panels (VIPs) in Canadian subarctic climate, Energy and Buildings, Volume 85, Dec 2014, pp. 672－680.

[6] Mukhopadhyaya, P., MacLean, D., Korn, J., van Reenen, D., Molleti, S., Field Application and Long-term Thermal Performance of Vacuum Insulation Panels (VIPs) in Canadian Arctic Climate, Proc. of 11th International Vacuum Insulation Symposium (IVIS－XI), Switzerland, September 2013, pp. 97－98.

.

Shallow Hollow Core Vacuum Panels Based on Tied Arch Skins

Raymond Glenn Ogden[a], Shahaboddin Resalati[b], Martin Heywood[c], Christopher Charles Kendrick[d*]

a. Faculty of Technology, Design & Environment, Oxford Brookes University, Oxford, UK
b. School of Architecture, Oxford Brookes University, Oxford, UK
c. School of Architecture, Oxford Brookes University, Oxford, UK
d. School of Architecture, Oxford Brookes University, Oxford, UK

Abstract

Modern vacuum insulation systems area potentially effective way of producing highly insulated building cladding systems but the fragility of systems can be problematic. Durable forms of vacuum insulation with resistance to damage, both during construction and in use, will potentially increase market penetration. Thus far however there have been relatively few viable commercial offerings.

Oxford Brookes University has developed the concept of shallow hollow core vacuum panels based on a novel system of tied arch skins. These panels comprise two independent and minimally connected faces that resist atmospheric pressures by transferring the spreading action of the arches into stainless steel foils that act as ties. These foils, which are in tension due to the tying action, form continuous surfaces within the panel and are the primary devices for controlling radiative heat transfer. The surfaces of the two foils have extremely low emissivity therefore minimising radiative heat transfer through the panels.

The panels benefit from low conductivity edge details such that U values of 0.1 W/(m^2 · K) can be achieved.

Keywords vacuum insulation, insulation standards, cladding systems, hollow panels

1. Introduction

Environmental imperatives suggest that demand for highly performing building cladding systems is likely to grow considerably. The high levels of thermal performance achievable using vacuum insulation systems are therefore attractive, although the market for these systems, whilst growing, is still relatively small. A major concern on the part of potential specifiers is perceived fragility of systems both in terms of susceptibility to damage and life expectancy relative to the normal construction sector expectancies (often 40～60 years).

These concerns have generated interest in more durable technologies including the encapsulation of conventional vacuum insulation in insulating foams, and incorporation of evacuated spheres or other elements into insulation. Whilst the appeal of such systems is obvious their actual performance can be compromised by adverse thermal bridging effects. Conventional foams around vacuum bags act as heat transfer paths significantly reducing performance, whilst evacuated elements such as spheres are characterised by high levels of conduction through the enclosure that offset the beneficial effects of the vacuum.

This paper details work carried out at Oxford Brookes University to develop a light weight hollow core vacuum panel based on tied arch principles. The system combines high levels of thermal performance with robustness and material efficiency, and is an alternative to conventional cladding systems, including main stream

* S. Resalati, Tel: 44－1865－484190, E-mail: sresalati@brookes.ac.uk

composite and built-up solutions.

In the system two tied arches are arranged in opposing orientation and separated by low conductivity edge details. Panels may be incorporated between internal and external flat metal facings with the regions between the facings and arches filled with polymeric foam (such as polyurethane). The effect of this is to produce an architecturally flat panel and to provide additional insulation, particularly around the panel joints and over the edge detail where heat loss paths are otherwise most direct.

Resolution of the concept has required an optimisation process involving both complex thermal modelling and confirmatory testing. This has been combined with structural analysis of the novel arch form using appropriate second order elastic analysis methods.

From a thermal perspective, the performance of any hollow panel will largely be determined by radiative heat transfer through the vacuum, combined with conductive heat flows through the edge details and any other points of physical connection of the inner and outer skins. Heat losses due to convection are eliminated by the vacuum. The ratio of panel area to edge detail therefore is an important factor. Small panels have a high ratio whilst larger panels have a far smaller ratio, for example, a 0.4×0.2 rectangular panel has a ratio of edge to face of 15∶1, whilst a 2.0m×4.0m rectangular panel has a ratio of 3∶2, thus reducing edge losses by an order of magnitude. Even a 1.0m×2.0m panel will have double the edge loss per m^2 of panel than a 2.0m×4.0m panel. Inevitably therefore larger panels with the maximum practical arch spans are desirable. However, at wide spans the physical weight of the arches becomes excessive, as does the distance from the crest of the arch to the tie which determines the panel thickness.

Larger panel can however be made using multiple arched sections, thus maintaining the thinness of the panel without compromising the strength through using one shallow arch.

As outgassing is a major consideration in the design of any hollow panel system, materials selection will tend to favour stainless steel on the basis of its low outgassing characteristics, good mechanical properties and the lower thermal conduction of the material in comparison to alternatives such as carbon steel and aluminium.

The adopted design criteria are therefore to achieve:

(1) A stainless steel structure based on sheet material not exceeding 0.7mm thickness on grounds of manufacture (ease of forming), economy and weight.

(2) A maximum nominal panel thickness in the range 115～140mm to accommodate two opposing tied arches each 50mm deep, thereby ensuring thinner envelope solutions than are possible using conventional insulation materials.

(3) The maximum practical panel width within the prescribed height limit and in accordance with the material limits, in order to optimise the general panel area to edge detail ratio.

(4) U－values in the range 1.1～0.9 W/(m^2 · K).

Key aspects of the development process have included:

i) Analysis of the maximum spanning capability of the necessary forms of tied arch. This is a crucial determinant of the panel area to edge detail ratio and therefore a major factor in the levels of thermal performance that it is possible to achieve.

ii) Minimising heat conduction and any radiative heat transfer that may occur at edge details, and control of heat flows though the panel elements toward and away from the edge detail.

2. VIP initial structural assessment

Panels are required to reliably resist atmospheric pressure. This represents an applied force of approximately 10tonnes/m^2. Such a force is in excess of the bending resistance of flat light gauge stainless steel sheet at spans approximating typical cladding panel dimensions, even if advantage is taken of the stiffening effects that can be facilitated by shallow profiles. By taking advantage of the arching action however (Fig. 1) similar weights of material can resist far greater forces and it becomes realistic to consider light gauge elements in this context.

In assessing the structural performance of the proposed panel and its ability to withstand atmospheric pressure, two key design issues were considered:

(1) Geometry of the arch.

(2) Gauge and profile of the stainless steel skins.

3. Arch geometry

The ability of an arch to support an applied load depends onits geometry and the stiffness of the supports, or in this case the tie. The height-to-width ratio needs to be sufficient to permit force to be carried by arching action (compression) rather than bending. If the height-to-width ratio is too low, the panel skins behave like curved (pre-cambered) plates and load transfer is dominated by bending and shear. Furthermore, as the arches are loaded the crown will deflect inwards while the supports spread outwards, resulting in a reduction in the height-to-width ratio and the possibility of failure through elastic instability (known as snap-through failure). In the proposed panel, the spread of the arches is resisted by the stainless steel ties that run across the centre of the panel.

A series of second order elastic analyses were undertaken to assess the potential panel geometries and corresponding tie requirements. As the design intent was to achieve a thin solution (115～140mm depth) a limit of 50mm was placed on the depth of the arch. Analyses therefore determined the maximum arch width corresponding to this height.

The results of the arch analysis arepresented in Tab. 1. It is apparent that widths up to 600mm are possible provided that the tie can be made sufficiently stiff to prevent excessive spread, and strong enough to resist tensile failure. The tie thicknesses given in Tab. 1 assume that the tie is fabricated from stainless steel with a yield strength of 220 N/mm^2 and suggest 0.43 mm thickness for a panel width of 600mm. In theory, thicker ties would permit larger panel widths, however risk of instability due to the flatness of the arch would increase. The adopted height-to-width ratio of 1/12 is close to the practical limit for any arch.

Tab. 1 Arch analysis results

Width	Tie thickness /mm	Skin thickness /mm	$\frac{\text{Inertia}}{mm^4/m^*}$
600	0.43	3.73	4325
500	0.30	2.92	2075
400	0.19	2.2	887
300	0.11	1.54	304
200	0.05	0.95	71
150	0.03	0.71	30
100	0.02	0.50	10

* Second moment of area of flat sheet of stated skin thickness and 1m width.

4. Outer skin gauge and profile

Assessment was made of the feasibility of producing skins using flat (unprofiled) stainless steel sheet to simplify manufacture. Analysis however revealed that the thickness of steel required to withstand the compressive force would be excessive and the solution was discounted. Analyses of ribbed skins however demonstrated good structural performance, and significantly reduced gauge requirements.

Four rib pitches were considered: 200mm, 100mm, 50mm and 20mm. In all cases the ribs were symmetrical (e. g. 200mm pitch was 100mm crest followed by 100mm trough) and assumed to be square in profile with a 1mm bend radius. The analysis revealed that the 200mm and 100mm pitch profiles were susceptible to local buckling, while the 50mm and 20mm profiles were fully effective even at the thinnest gauges. The 100mm and 200mm pitches were, therefore, rejected. Elastic analyses to EN 1993－1－3 were undertaken on the 50mm and 20mm pitch profiles for a range of rib heights and a steadily decreasing steel gauge. In each case, the inertia per metre width was noted and compared against the values tabulated in Tab. 1 to determine the maximum permissible panel width for the combination of rib height and gauge. The results are shown in Tab. 2.

Tab. 2 Suitable arch width for 20mm pitch profile

Rib height /mm	Suitable arch width /mm			
	0.7mm skin	0.6mm skin	0.5mm skin	0.4mm skin
1	200	200	200	200
2	300	300	300	300
3	400	400	400	400
4	500	500	500	400
5	600	500	500	500
6	—	600	600	500
7	—	—	—	600

For the desired arch width of 600mm, suitable solutions range from 0.7mm gauge with a 5mm rib down to 0.4mm gauge with a 7mm rib. These solutions have therefore been taken forward to thermal analysis to determine whether the design requirement of 1.1～0.9 W/(m·K) can be met based on the panel area to edge ratios that this span implies.

5. Heat transfer through the panel

In conventional insulation materials, such as mineral wool and polyurethane (PUR), a large proportion of the total heat transfer is due to conduction across the core material (HiPTI IEA/ECBCS Annex 39, 2005). In this hollow core solution, conductive heat transfer is prohibited across the vacuum, as is convective heat transfer, with the dominant heat flow mechanisms being radiative (across the vacuum cavity) and conductive (through the arches, ties and edge details).

Of these heat flow mechanisms, radiative transfer is minimised by the presence of very low emissivity surfaces on the ties and inside surfaces to the arches (6 surfaces in total). These surfaces allow very low radiative heat transmission between them, effectively forming a barrier to radiative heat transfer across the vacuum cavity (Fig. 1).

To quantify the effect of theselow emissivity surfaces, a finite difference analysis was carried out using BISCO software from Physibel. This demonstrated that the surfaces reduce total heat transmission through the centre of the panel by a factor of approximately 3. Analyses also suggested that these losses account for only 15%～20% of total heat flow,

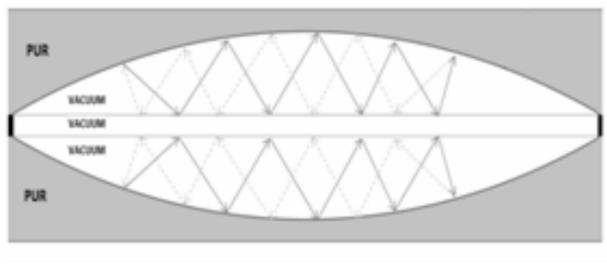

Fig. 1 Radiative heat transfer in the vacuum

the remaining being due to conductive heat transfer through the edge detail (Fig. 2).

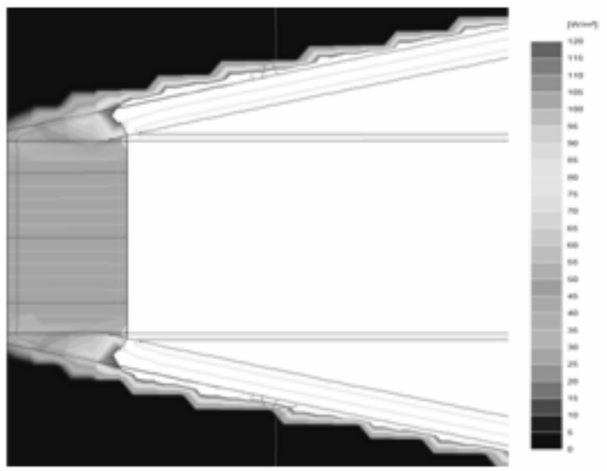

Fig. 2 Typical heat flow through the edge

6. Engineered edge detail

Edge details are a major consideration in the design of any vacuum panel system. Currently available vacuum insulation panels can achieve thermal conductivities of approximately 0.005 W/(m·K). The associated U-values therefore are typically 4～7 times better than conventional insulation materials. These low thermal conductivities however are centre panel values and do not consider thermal bridging. Barrier films used around conventional vacuum insulation act as a thermal bridge and as a consequence the effective thermal conductivity (λ_{eff}) of panels is higher than the centre panel conductivity.

Whilst hollow core insulation panels are also susceptible to this issue, thermal bridging effects can be mitigated (to a point where they fall within acceptable bounds) by considered thermal engineering of the edge detail. A variety of strategies are possible, all of which incorporate thin stainless steel foils as the primary vacuum containing edge element. These are supported

by low conductivity materials which avoid surface-to-surface thermal bridging (which otherwise negates the low thermal conductivity of foil) (Fig. 3).

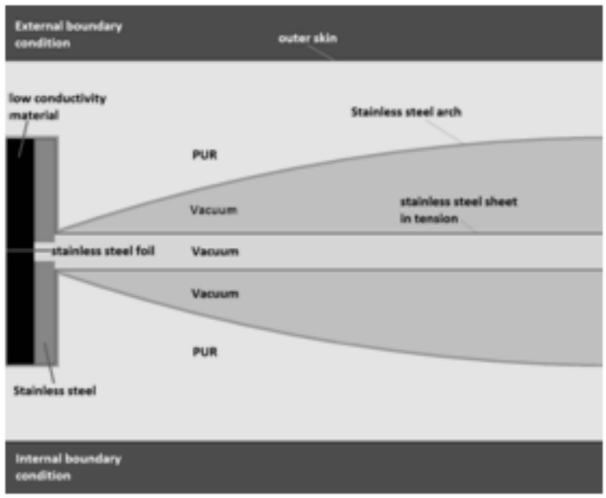

Fig. 3 Hollow core panel

Conduction is the primary heat flow mechanism. In each side of the panel (upper and lower tied arches) this essentially comprises:

(1) External panel face to foam fill.

(2) Foam to arch and arch edge detail.

(3) Edge detail to foil through the stainless steel portion and through the support material.

(4) Edge detail to edge detail through the nominal load carrying contact.

A variety of edge detail designs have been analysed on the basis that the length and thickness of the foil at the edge detail directly affects the amount of heat loss through the panel. Some of these details are presented in Fig. 4.

As a result of the analysesthe optimised edge detail presented in Fig. 5 has been developed. Tab. 3 presents the effect of increasing the conduction path through edge foils incorporated into this detail (where conduction path is defined as length d). A 60mm conduction path (0.1mm thick stainless steel foil) is required to achieve the target U-value. The approach gives an overall conductivity of 0.01 W/(m·K) for 1500mm wide panels based on 5 tied arches at 300mm centres (Fig. 6).

Structural connection and load transfer between the upper and lower tied arches relies on small diameter nominal pin connections acting into countersunk receiver points. As all three parts of the internally evacuated portion of the panel are contiguous (connected), the vacuum provides the dominant clamping action holding the panel together.

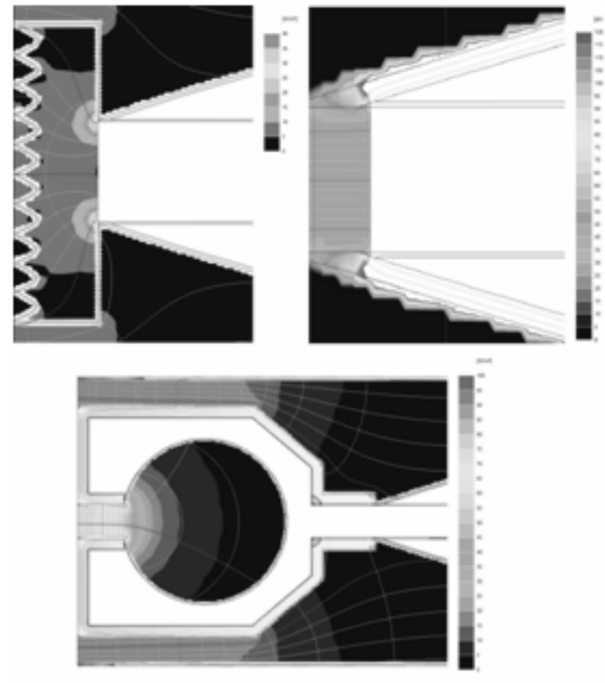

Fig. 4 A variety of edge details investigated

Tab. 3 The effective U-value relative to the foil length at the edge

Foil length (d) /mm	U-Value without considering the heat loss through the structural elements between arches $\frac{W}{(m^2 \cdot K)}$	Additional heat transfer through the structural elements $\frac{W}{(m^2 \cdot K)}$	Effective U-value $\frac{W}{(m^2 \cdot K)}$
20	0.101	0.006	0.107
30	0.098	0.006	0.104
40	0.096	0.006	0.102
50	0.095	0.006	0.101
60	0.094	0.006	0.1
70	0.094	0.006	0.1

7. Conclusions

A fully evacuated coreless stainless steel-based vacuum panel solution has been developed and modelled for both structural and thermal performance. A U-value of 0.1 W/(m²·K) can be achieved for a panel of 100mm thickness, between 40% and 25% the thickness of conventionally insulated panels.

The next stage of development will involve further

prototyping to evidence the predicted structural and thermal performances.

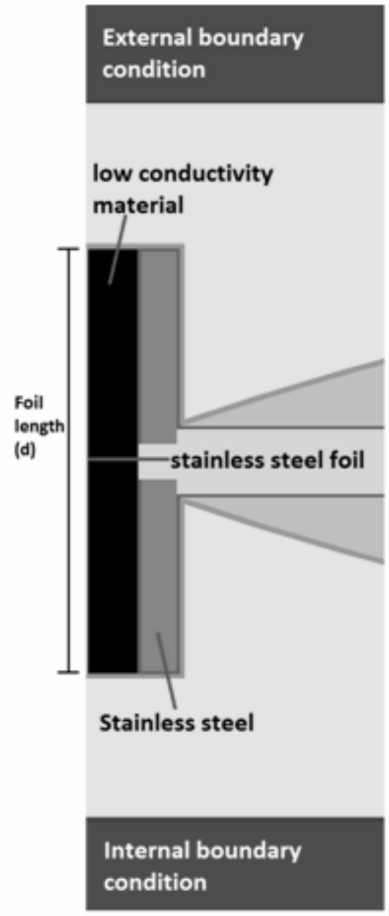

Fig. 5 Engineered edge detail

Fig. 6 Exemplar combination of arches at 300mm centres

It is envisaged that the resulting panel will provide a high performance solution for commercial and multi-residential buildings, where the higher cost can be offset against increased rental income due to increased floor area.

If future building codes regulate for low embodied carbon, these vacuum panels could provide a possible solution, combining extremely high insulation values with very low embodied energy.

References

[1] HiPTI IEA/ECBCS Annex 39 (2005) Vacuum Insulation Panels-Study on VIP-components and Panels for Service Life Prediction of VIP in Building Applications (Subtask A) (1st edition)

[2] Caps R, Heinemann U, Ehrmanntraut M, et al. (2001). Evacuated insulation panels filled with pyrogenic silica powders – properties and applications. High Temperatures-High Pressures 33(2) 151—156.

[3] Erb M and Symons W (ed.) (2010). Vacuum insulation panel properties and building applications. ECBCS Annex 39 Project Summary Report. Published by AECOM Ltd, St Albans, UK.

[4] Frick J, Schwab H and Heinemann U (2006). Vacuum insulation panels-exciting thermal properties and most challenging applications. International Journal of Thermophysics 27(4) 1123 – 1139.

[5] Ogden R (2007) Thin Wall Technology Building Cladding Using Vacuum Insulation. In: 8th International Vacuum Insulation Symposium (IVIS'07). Würzburg: IVIS.

[6] Ogden R and Kendrick C (2005) VIP cladding panels for buildings: applications and conceptual solutions. In: 7th International Vacuum Insulation Symposium (IVIS'05). Dübendorf.

[7] Ogden R, Kendrick C and Wang X (2009). Economic case for vacuum insulation in mainstream new build construction applications. In: Proceedings of 9th International Vacuum Insulation Symposium (IVIS'09), 17 – 18 September, 2009. London, UK.

[8] Ogden R, Wang X and Kendrick C (2011) High performance steel cladding systems using vacuum technology. In: 10th International Vacuum Insulation Symposium. Ottawa.

The Properties Study of New Ultra-temperature Vacuum Insulation Composites

Wang Yang[a,b], Chen Zhaofeng[b,*], Yu Shengjie[a,b]

a. Suzhou Superlong Aeronautical Heat-resistance Materials Co. Ltd., Taicang, 215400, P. R. China
b. Super Insulation Composite Laboratory, College of Materials Science and Technology, Nanjing University of Aeronautics and Astronautics, Nanjing, 210016, P. R. China

Abstract

With regards to the adiabatic principle for insulation, a new ultra-temperature vacuum insulation composites (UT - VIC) is put forward, which can be used in high temperature environment. Carbon fiber reinforced carbon composites have excellent high temperature resistance, high toughness, corrosion resistance and good thermal stability, etc. SiO_2 can be used to fill the microcrack and protect the carbon matrix from oxidizing. This material consist of a core material which is SiC foam ceramic and a flawless outer shell layer of carbon fiber reinforced composites by the methods of CVI (Chemical Vapor Infiltration) and silica sol vacuum impregnation, while maintaining a vacuum state inside. So the new ultra-temperature vacuum insulation composites with novel structure not only can be used at high temperature, but also has a very low coefficient of thermal conductivity compared with C/C and C/SiC composites. Material density is 0.81g/cm^3, the effective thermal conductivity of UT - VIC ranged from 0.193W/(m · K) to 0.721W/(m · K) in 303K to 724K temperature , and the compression strength is 1.5 MPa. The aim of this paper is to investigate and analyze the effect of material structures and presents a possible future high temperature resistance vacuum insulation material.

Keywords vacuum insulation; thermal conductivity; thermal conductivity

1. Introduction

During the last several decades, developments in heat transfer and use of thermal insulations in emerging technologies have extended the range of applications from cryogenic temperatures to high temperatures under reentry conditions into planetary atmospheres [1]. Investigations of thermo-physical properties of ceramic and refractory materials are important in various fields of science, industry, and engineering [2 - 4].

Generally, high temperature insulation materials are multihole materials, considering their net structure [5 - 8]. And the conventional insulation materials considered for high temperature can be subdivided into three groups: fibers, microporous materials, and refractories (or fire clays), which is shown in Fig. 1. Fibrous materials combine a low density of about 100 kg/m^3 with a moderate thermal conductivity of 0.10 W m^{-1} · K^{-1} (20℃) to 0.35 W · m^{-1} · K^{-1} (1000℃), respectively. Microporous materials available are of moderate density of less than 300 kg/m^3 together with a low thermal conductivity of 0.02 W · m^{-1} · K^{-1} (20℃) to 0.04 W · m^{-1} · K^{-1} (1000℃), respectively, whereas fire clays are both of high density (more than 500 kg/m^3) and have high thermal conductivity of up to 0.5 W · m^{-1} · K^{-1} at 1000℃ [9, 10]. Note that the fibers and microporous materials have very low thermal conductivity.

In this paper, the aim was to put forward a new ultra-temperature vacuum insulation composites (UT - VIC). This composite design was used considering an

* Corresponding author, Tel: 86 - 189 - 520 - 189 - 69, E-mail: zhaofeng_chen@163.com

adiabatic structure and the principle of vacuum insulation panel (VIP) for reference [11, 12]. Fig. 2 shown the physical diagram and schematic diagram of UT - VIC section. With regards to the adiabatic principle for insulation, the inside of this composite was vacuum state which is responsible for the reduction of the gaseous convection and conduction. Open cell SiC ceramic foam is used as effective thermal insulation for high-temperature applications, which consists of a highly porous solid material. On the outside, carbon fiber reinforced ceramic matrix composites is used as a sealing layer, which had good thermal stability, oxidation resistance and excellent ablation resistance. This new composites with lighter and lower thermal conductivity have advanced innovation in high temperature insulation field and will have a great potential to substitute for conventional ceramic tiles to protect heat vulnerable regions of a launch vehicle such a space shuttle.

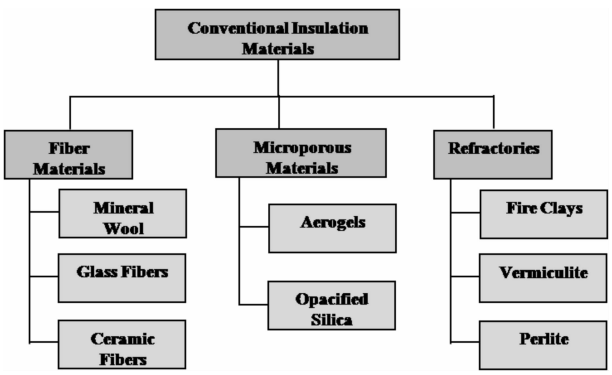

Fig. 1 Conventional insulation materials classification

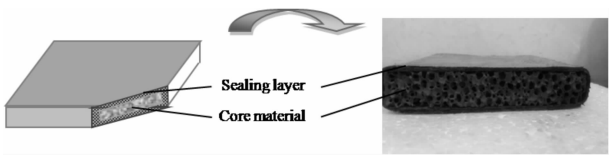

Fig. 2 Physical diagram and schematic diagram of MCSC section

2. Experimental details

Raw materials, including core materials and carbon fiber sheet (CFS) (prepared in Changsha, PR China) were used in this study. More details about CFS can be seen in Tab. 1. SiC - matrix foam ceramics used as core materials with dimensions of 150 mm × 150 mm × 22 mm were provided by Suzhou DeXin Advanced Ceramics Co., LTD (Suzhou, PR China), which the porosity was 85%. Fig. 3 describes the main manufacturing steps of MCSC. First step, core materials were wrapped by multilayer CFS which were about three to five layers, using the setting agent to fix each sheet to avoid the gaps between layers. After that, the pyrolytic carbon (PyC) was deposited in initial carbon fiber fabrication by a method of CVI (Chemical Vapor Infiltration) for 400h to obtain a relative dense sealing layer. In order to prevent the PyC permeating the core material, carbon paper with 0.03mm thick was used as blocked layer attaching to the innermost carbon fiber sheet. Third step, as shown in Fig. 4, in order to get outside layer densification fully, deposited samples were vacuum impregnated (10^{-1} Pa) using colloidal silica solution precursor (35 vol.% silica) for 2 min. The container pressure was increased to 1 atm and maintained for only 1 min at first 5 times cycle, which was to prevent the core material being impregnated by colloidal silica solution. After 5 times cycle, vacuum impregnated time and pressure maintain time increased to 10 min and 5 min, respectively. After each cycle, the samples were dried at 80℃ for 1h and 110℃ for 1h, respectively. Then the dried samples were heated in an vacuum oven (10^{-1} Pa) at 450℃ for 2 h in order to remove the coupling agent and bound water. The whole processes were repeated 15 times to enhance the density of the composites.

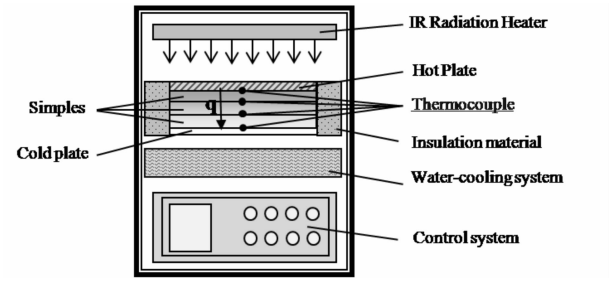

Fig. 3 Schematic diagram of the water flow plate method apparatue

After deposition, Effective thermal conductivity measurement was used water flow plate method, according to ASTM E422 - 05 standard [13]. Fig. 3 shows aschematic diagram of the experimental set-up used forthe measurements. Around the sample, it was stuffed with insulation material. The sample was put into the apparatus, heated up to the test temperature in accordance with the rules. After reaching the steady

state, measuring sample hot and cold surface temperature, water flow and the water temperature difference can calculate the effective thermal conductivity of material according to the following formula.

$$\lambda = Q\delta/(A\Delta T) \quad (1)$$

Where λ is the effective thermal conductivity of material (W/(m • K)), Q is heat of water absorption per unit time (W), δ is the sample thickness (m), A is the sample area (m^2), ΔT is the hot and cold surface temperature difference. The heat of water absorption is proportional to the specific heat of water, water flow and water temperature rise.

$$Q = C m \Delta t \quad (2)$$

Where C is the specific heat of water (J/(g • K)), m is the water flow (g/s), Δt is water temperature rise (K).

3. Results and discussion

3.1 Compressive loading

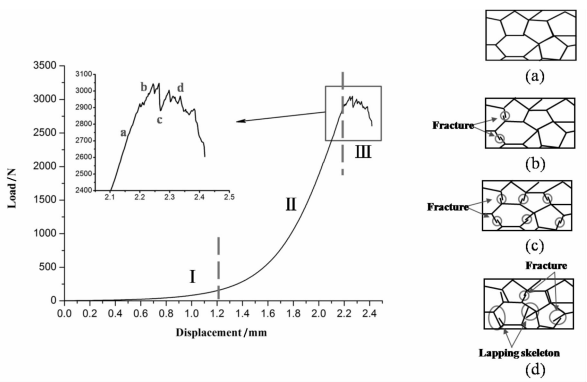

Fig. 4 Compressive loading-displacement curve

Fig. 4 shows the compressive loading-displacement curve of samples, while the SiC core materials play the main role to compressive strength of samples that was determined by the porosity and thickness of SiC skeleton. The average value of compressive strength of the samples was 7.5 MPa at room temperature. The load-displacement curve (see Fig. 4) can be divided into three stages. At Ⅰ stage, there was little load. Due to the initial load worked on the outer layer and certain gaps that existed between the outer and core material. As the increase of displacement, gap disappeared gradually, then the load increased fast. At Ⅱ stage, the mechanical behavior of the samples was nonlinearly elastic. With increasing Load, the initial microcracks grew and expanded in the SiC skeleton (Fig. 4(a)). When the microcracks reach the surface of skeleton, fracture behavior occurs. At Ⅲ stage, the load presented a zigzag curve. It meant the SiC skeleton started to fracture with the increase in displacement. In aero b, a few of skeleton had fractured, while the other were intact (seen in Fig. 4(b)), so the load could continue to increase. In aero c, the material showed a distinct and sudden stress drops with the increase in displacement. In this case, the most SiC skeleton underwent significant fracturing, it can be seen in Fig. 4(c). In aero d, with the displacement increase, fractured skeleton lapped joint together, as shown in Fig. 4(d), which leaded to the load increase again. However, with the displacement increased further, SiC skeleton fractured completely, the load decreased finally.

3.2 Effective thermal conductivity analysis

For the porous material, the heat transfer is mainly composed of gas heat convection λ_c and heat conduction λ_g, solid skeleton heat conduction λ_s as well as the thermal radiation λ_r of four parts, which can be exhibited by the expression [14-16].

$$\lambda_e = \lambda_c + \lambda_g + \lambda_s + \lambda_r \quad (3)$$

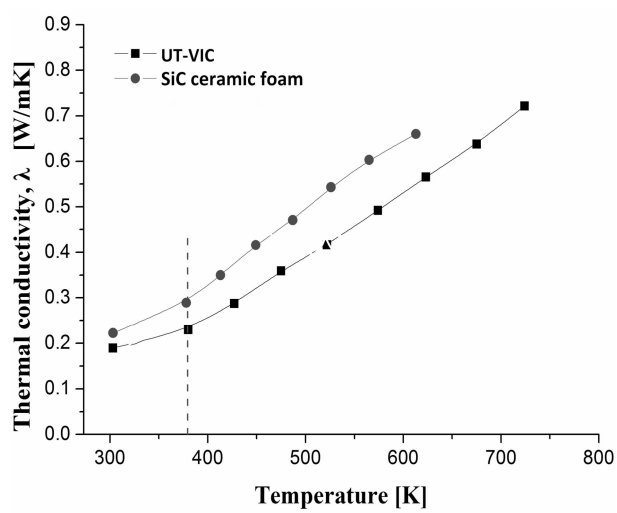

Fig. 5 Temperature dependence of the effective thermal conductivity of UT-VIC, compared to SiC ceramic foam

Fig. 5 illustrates representative results of was measured, with the ordinate showing the effective thermal conductivity in [W/(m • K)] for UT-VIC, compared to SiC ceramic foam. The abscissa is the temperatures T_R in [K]. It can be seen that both of them increased with the temperature, especially when the temperature was above 373K, the curve of effective

thermal conductivity slope was greater. It was because the radiation became the dominant mode of heat transfer in the high temperature [9], when the temperature was below 373K, solid SiC skeleton heat conduction played the main role. Actually, the radiation contribution to the thermal conductivity in porous materials is a relation of the radiation temperature T_R to the third power which can be estimated by the expression [17]

$$\lambda_r = 4\sigma_B \varepsilon n^2 d T_R^3 \quad (4)$$

In which σ_B is the Stefan - Boltzmann constant, ε is the emissivity, n is the refraction index and d is the pore diameter.

Considering the thermal conductivity measurement in a static environment, gas diffusion velocity in pores is zero, Reynolds number Re is below 22, which can clearly ignored the effect of gas heat convection λ_c on the effective thermal conductivity [18]. The gas conductivity λ_g is related to the conductivity at ambient pressure (λ_0) in the bulk and the Knudsen number which is defined by the expression $K_n = l_m / d$ where l_m is the mean free path of the gas and d is the pore diameter by [10]:

$$\lambda_g = \frac{\lambda_n}{1 + 2\beta K_n} \quad (5)$$

Where β is a coefficient equal to 1.5 for air. λ_0 is a function of temperature. According to Handbook of Chemistry Physical Properties (2002) [19], at atmospheric pressure, the coefficient of thermal conductivity of dry air (λ_0) from 273 to 1373K has been given. Since there is no exact formula to calculate λ_0, all these thermal conductivity datum of dry air were well fitted by MATLAB software to be a nonlinear expression of temperature (T):

$$\lambda_0(T) = aT^b \quad (6)$$

Where a about 3.93559×10^{-4}, b about 0.74588, T is in degrees Kelvin. In the experiments shown in Fig. 10, the effective thermal conductivity of UT - VIC ranged from 0.193W/(m • K) to 0.721W/(m • K) in 303K to 724K temperature, compared to that of SiC ceramic foam ranged from 0.223W/(m • K) to 0.664W/(m • K) in 303K to 613K, which is 13.5%～23.3% lower than that of SiC ceramic foam core materials. It should be emphasized that in the internal vacuum in composite, gas heat convection and heat conduction do not exist, resulting in some decline of effective thermal conductivity. However, owing to the intrinsic high thermal conductivity of SiC material (42.5W/(m • K) at 400K for 21.7% porosity) [19], the heat was mainly passed through the SiC foam skeleton, coupled with thermal bridge effect of sealing layer, leading to the thermal conductivity of composites decreased unconspicuously after vacuum inside. Based on this, the relationship between vacuum degree and solid skeleton heat conduction will be researched in the next work.

4. Conclusion

In this work, new ultra-temperature vacuum insulation composites with vacuum inside were successfully fabricated by CVI PyC + silicasol-infiltration-sintering method.

The effective thermal conductivity of SiC ceramic foam and UT - VIC were investigated experimentally. First, both of them increased with the temperature due to the radiation mechanism. Considering vacuum inside, gas heat convection and heat conduction did not exist, hence the effective thermal conductivity of UT - VIC ranged from 0.193W/(m • K) to 0.721W/(m • K) in 303K to 724K temperature, compared to that of SiC ceramic foam ranged from 0.223W/(m • K) to 0.664 W/(m • K) in 303K to 613K, which is 13.5%～23.3% lower than that of SiC ceramic foam core materials.

Acknowledgements

The present work was supported by the Funding of Jiangsu Innovation Program for Graduate Education (the Fundamental Research Funds for the Central Universities), KYLX15_0308.

References

[1] Spinnler M, Winter ERF, Viskanta R. Studies on high - temperature multilayer thermal insulations. Int J Heat Mass Transfer 2004, 47: 1305 - 1312.

[2] Lencoe EN, Katz RN, and Burke JJ. Ceramics for High Performance Application. New York: Plenum Press, 1983.

[3] Cheremisinoff NP. Handbook of Ceramics and Composites. Vols. 1 - 3. New York: Marcel Dekker, 1990.

[4] Hocking HG and Sidky PS. Metallic and Ceramic Coating, Production. High Temperature Properties and Application. New York: Wiley, 1984.

[5] Colombo P, Conventional and novel processing methods for cellular ceramics. Phil Trans R Soc A 2006, 364: 109 -124.

[6] KhedariJ, Suttisonk B, Partinthong N, Hirunlabh J. New lightweight composite construction materials with low thermal conductivity. Cem Concr Compos 2001, 23：65-70.

[7] Litovsky E, Shapiro M, Shavit A. Gas pressure and temperature dependences of thermal conductivity of porous ceramic materials：Part 2, Refractories and ceramics with porosity exceeding 30%. J Am Ceram Soc 1996, 79：1366-1376.

[8] Živcová Z, Gregorová E, Pabst W, Smith DS. Thermal conductivity of porous alumina ceramics prepared using starch as a pore-forming agent. J Eur Ceram Soc 2009, 29：347-353.

[9] Spinnler M, Winter ERF, Viskanta R. Studies on high-temperature multilayer thermal insulations. Int J Heat Mass Transfer 2004, 47：1305-1312.

[10] Nait-Ali B, Haberko K, Vesteghem H, et al. Thermal conductivity of highly porous zirconia. J Eur Ceram Soc 2006, 26：3567-3574.

[11] FrickeJ, Heinemann U, Ebert HP. Vacuum insulation panels：From research to market. Vacuum 2008, 82：680-690.

[12] Li CD, Duan ZC, Chen Q, et al. The effect of drying condition of glassfibre core material on the thermal conductivity of vacuum insulation panel. Mater Des 2013, 50：1030-1037.

[13] ASTM International. ASTM E422-05. Standard test method for measuring heat flux using a water-cooled calorimeter. American Society for Testing and Materials, 2011.

[14] Simmle H, Heinemann U, Kumaran K. Vacuum Insulation Panels：Study on VIP—components and Panels for Service Life Prediction of VIP in Building Applications, HiPTI—High performance Thermal Insulation, 2005, IEA/ECBCS Annex 39.

[15] Kuhn J, Ebert HP, Arduini-Chuster MC et al. Thermal Transport in Polystyrene and Polyurethane Foam Insulations, Int J Heat Mass Transfer 1992, 35：1795-1801.

[16] Doermann D and Sacadura JF. Heat Transfer in Open Cell Foam Insulation, J Heat Transfer, 1996, 118：88-93.

[17] Barea R, Osendi MI, Ferreiri JMF, Miranzo P. Thermal conductivity of highly porous mullite material. Acta Mater, 2005, 53：3313-3318.

[18] Lin. RT, Heat and mass transfer in porous media introduction. Beijing：Science Press, 1995.

[19] Liu GQ, Ma LX, Liu J, Handbook of Chemistry Physical Properties. Beijing：Chemical Industry Press, 2002.

Influence of Sintering Silica on Thermal Conductivity of Ultra-temperature Vacuum Insulation Panel

Yu Shengjie[a,b], Chen Zhaofeng[b,*], Wang Yang[a,b]

a. Suzhou Superlong Aeronautical Heat-resistance Materials Co. ltd., Taicang, 215400, P. R. China
b. Super Insulation Composite Laboratory, College of Materials Science and Technology, Nanjing University of Aeronautics and Astronautics, Nanjing 210016, P. R. China

Abstract

C/SiC layered composite was used as sealing material for ultra-temperature vacuum insulation panel (UT - VIP) due to its thermal stability and oxidation resistance. In order to minimize the thermal conductivity of the panel, a vacuum condition is required inside the panel. Chemical vapor infiltration (CVI) is usually used to fabricate C/SiC composite. However, it is very difficult to infiltrate the pores completely in CVI process. As a consequence, the emergence of these flaws incapacitates C/SiC layered composite to create a vacuum condition inside the panel. In this paper, SiO_2 high temperature vacuum sintering was introduced in filling the inevitable pores and cracks that remained in the composite after the CVI process. Experimental result shows that pores between fiber bundles and cracks in the SiC matrix were filled with sintered silica. The thermal conductivity of ultra-temperature vacuum insulation panel was significantly decreased owing to its low inside pressure created by the fully dense sealing material.

Keywords C/SiC composite, thermal conductivity, silica, vacuum sintering

1. Introduction

Continuous carbon fiber-reinforced silicon carbide matrix composites (C/SiC) have received considerable attention for high-temperature structural applications because of their superior strength and fracture toughness [1 - 3]. Chemical vapor infiltration (CVI) is usually used to fabricate C/SiC composite, however, the infiltration of the pores is mainly dependent on the diffusion of the gaseous reactant species transport [4 - 6]. The diffusion resistance is increased with the decrease of pores size. As a result, it is very difficult to infiltrate the pores completely. And also the voids and cracks would emerge due to thermo-physical property mismatch of the main constituents of C/SiC layered composite during the CVI process.

Thus, in order to create a vacuum condition inside the ultra-temperature vacuum insulation panel, sealed by C/SiC composite layers using chemical vapor infiltration, it is necessary to acquire high densification of sealing materials. SiO_2 high temperature vacuum sintering has been introduced in filling the inevitable pores and cracks that remain in the composite after the CVI process.

The aim of current work is to develop an improved technique to reduce the porosity of C/SiC composite layers and make the materials practical for many more industrial applications, chemical vapor infiltration and high temperature vacuum sintering was proposed for fabricating composites. The pore healing in chemical vapor infiltrated silicon carbide (CVI - SiC) was observed. A comparison was then made between the observed pore healing behaviour with that of infiltrated silicon carbide prepared previously.

* Corresponding author, Tel: 86 - 189 - 5201 - 8969, E-mail: zhaofeng_chen@163.com

2. Experimental

PAN-based carbon fiber cloth was employed and each yarn contained 3000 filaments, and was supplied by the Nanjing Institute of Glass Fiber, People's Republic of China. The fiber volume fraction was 40%. The fabric perform was prepared using the two-dimensional braided method.

In the present experiment, low pressure chemical vapor deposition (LPCVI) was employed to deposit pyrolytic carbon layer and silicon carbide barrier layer, which had been described elsewhere in detail [7-9]. A thin pyrolytic carbon layer was deposited on the surface of the carbon fiber as the interfacial layer with methane at 950℃. Methyltrichlorosilane (MTS, CH_3SiCl_3) was used for the deposition of Si and C, and thus then can produce stoichiometrical SiC. MTS vapor was carried by bubbling hydrogen. Typical conditions for deposition were 1100℃, a hydrogen/MTS ratio of 10, and a pressure of 100 Pa. Argon was employed as the dilute gas to slow down the chemical reaction rate of deposition. The flow rates of H_2 and Ar were 300 ml·min^{-1} and 400 ml·min^{-1}, respectively. A schematic of the chemical vapor infiltration system is shown in Fig. 1. After pre-coating with the pyrolytic carbon layer and the silicon carbide barrier layer, the preform was vacuum infiltrated with silica solution, then sintered at 1200℃ at an argon atmosphere of 0.1 MPa to form a dense silica matrix in the pores between deposited carbon fibers, as well as between bundles, to obtain materials.

After deposition, the morphologies of the C/SiC layer composites before and after infiltrated with silicasol were observed by scanning electron microscopy (SEM, SU8010 Semi-In-Lens). Effective thermal conductivity was measured using water flow plate method, according to ASTM E422—05 standard [10]. Fig. 2 shows a schematic diagram of the experimental set-up used for the measurements. Around the sample was stuffed with insulation material. The sample was put into the apparatus, heated up to the test temperature in accordance with the rules. After reaching the steady state, measuring sample hot and cold surface temperature, water flow

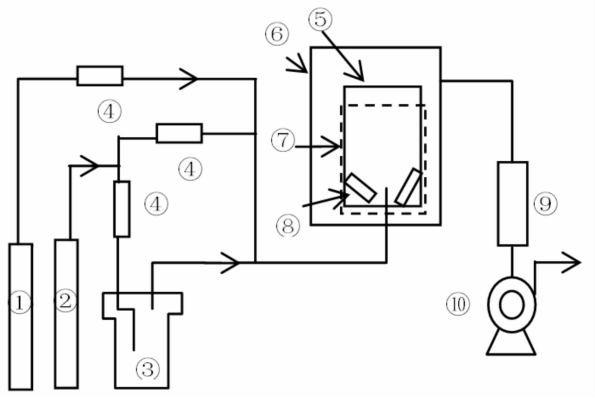

Fig. 1 Schematic representation of the LPCVI apparatus

1—Hydrogen (H_2) gas, 2—Argon (Ar) gas, 3—MTS, 4—Mass flow meter, 5—LPCVI Chamber, 6—Stainless-steel jacket, 7—Graphite heating element, 8—Sample, 9—Trap, 10—Vacuum pump

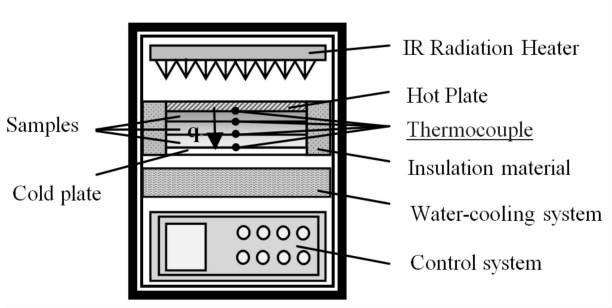

Fig. 2 Schematic diagram of the water flow plate method apparatus

and the water temperature difference can calculate the effective thermal conductivity of material according to the following formula.

$$\lambda = Q\delta/(A\Delta T) \quad (1)$$

Where λ is the effective thermal conductivity of material (W/(m·K)), Q is heat of water absorption per unit time (W), δ is the sample thickness (m), A is the sample area (m^2), ΔT is the hot and cold surface temperature difference. The heat of water absorption is proportional to the specific heat of water, water flow and water temperature rise.

$$Q = Cm\Delta t \quad (2)$$

Where C is the specific heat of water (J/(g·K)), m is the water flow (g/s), Δt is water temperature rise (K).

3. Results and discussion

3.1 Microstructure characteristics of the composites

The pore morphology, size, distribution and content have significant effects on the thermal properties

and heat conduct behavior. The shape of the pores is dominated by the fiber architecture at the inter yarn levels. Within each yarn, the progressive coating of the fibers creates longitudinal pores extending along the fibers. In LPCVI process, the infiltration of the pores is mainly dependent on the diffusion of the gaseous reactant species transport.

The C/SiC layer composites samples are mainly combine of two basic pores types: inter-fiber pores, between fibers in a bundle; inter-bundle pores, between fiber bundles in a fabric layer; In the LPCVI process, the smaller inter-fiber pores can be easily filled by silicon carbide (CVI - SiC), but the larger inter-bundle is difficult to be completely densified because of both the slow deposition and the surface crust. Fig. 3 (a) shows the microstructure of CVI C/SiC composites before infiltrated with silica. From this micrograph, it is easy to find out that only the inter-fiber pores, between fibers in a bundle, within the CVI composites was infiltrated with CVI SiC. However, the inter-bundle pores, between fiber bundles in a fabric layer still remained.

Fig. 3 (b) shows the microstructure of CVI C/SiC composites after infiltrated with silica. The nanoscale particle was observed between fiber bundles in a fabric layer, which revealed the silica particles filled the larger inter-bundle pores after infiltrated with silica solution.

Fig . 3 (c) shows the morphology of CVI C/SiC composites after SiO_2 high temperature vacuum sintering. From the Fig. 2 (c), it is easy to find out that both the inter-fiber pores and inter-bundle pores within the CVI composites were infiltrated with sintered SiO_2.

As it is known, the silica nanoparticles would melt gradually as the temperature increasing. When the sintering temperature up to 1200℃, the silica crystal occurs obvious melting phenomenon as well as grain boundary is fuzzy. Two kinds of the residual pores within the CVI composites tend to gather together, which result in a substantial reduction in porosity of the CVI composites. Thus, the density of the CVI composites greatly improved than before.

3.2 Thermal conductivity analysis

For the porous material, the heat transfer is mainly composed of gas heat convection λ_c and heat conduction λ_g, solid skeleton heat conduction λ_s as well as the thermal radiation λ_r of four parts, which can be exhibited by the expression [11 - 13].

$$\lambda_e = \lambda_c + \lambda_g + \lambda_s + \lambda_r \quad (3)$$

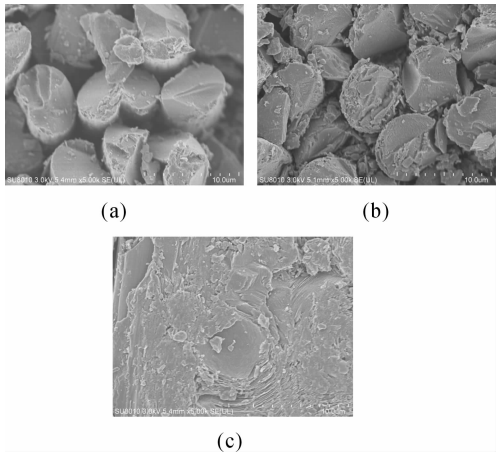

Fig. 3 Microstructure of composites in different processing period

(a) before infiltrated with silica; (b) after infiltrated with silica; (c) after HT—vacuum sintering

Fig. 4 illustrates representative results of measurements with the ordinate showing the effective thermal conductivity (ETC) in [W/(m • K)] for UT - VIP without infiltrated with silica solution, compared to UT - VIP with sintering silica fill. The abscissa is the temperatures T_R in [K]. It indicated that the effective thermal conductivity continuously decreased with the temperature increasing for both two kinds of samples. However, the UT - VIP without infiltrated with silicasol possessed higher effective thermal conductivity than the UT - VIP with sintering silica fills in the whole temperature range.

Inspection of the representative results of effective thermal conductivity revealed that the UT - VIP with sintering silica fill possessed a lower ETC because of the density of the sealing materials covered the porous core material was greatly increased by the sintering silica fill. It is also interesting to note that there exist a significant correlation between the inside pressure of UT - VIP sample and its performance in the thermal conductivity test. A considerable decrease of gas content inside of UT - VIP occurred after sintering infiltrated silica, which led to a significant decrease of heat conduction λ_g inside the panel. Therefore, it was the density of sealing material that had a marked effect on the inside pressure

of UT - VIP composites, and the vacuum inside had a great influence on effect thermal conductivity indeed.

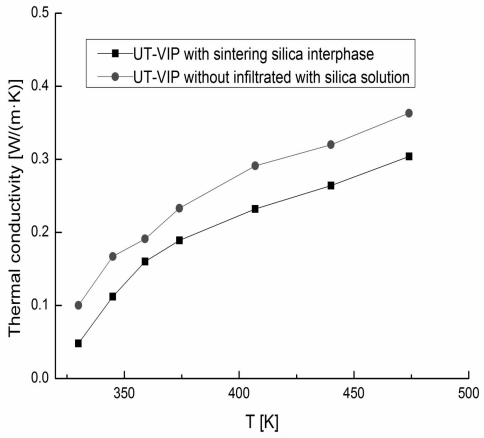

Fig. 4 Representative results of effective thermal conductivity of samples under different temperature

4. Conclusions

It has been shown that detection of the effect thermal conductivity of UT - VIP can be improved significantly by using sealing materials achieved in CVI SiC + silicasol-infiltration-sintering. In this experiment, it was found that both the inter-fiber pores and inter-bundle pores within the CVI composites were infiltrated with sintered SiO_2, which resulted in the density of the CVI composites greatly improving than before. And the UT - VIP without infiltrated with silicasol possessed higher effective thermal conductivity than the UT - VIP with sintering silica in the whole temperature range. A considerable decrease of gas content inside of UT - VIP occurred after sintering infiltrated silica, which led to a significant decrease of heat conduction λ_g inside the panel. Therefore, it was the density of sealing material that had a marked effect on the inside pressure of UT - VIP composites, and the vacuum inside had a great influence on effect thermal conductivity indeed.

Acknowledgements

The present work was supported by the NUAA Fundamental Research Funds, No. NS2015060.

References

[1] Kodama H, Sakamoto H, Miyoshi T. J Am Ceram Soc. 1989; 72:551.

[2] Nakano K, Kamiya A, Ogawa H, Nishino Y. JJp Ceram Soc. 1992; 100:472.

[3] Jamet JF, Lamicq PJ. In: Naslain R (Ed.), High-temperature Ceramic Matrix Composites, London: Woodhead Publications, 1993; 735.

[4] Clarke DR. J Am Ceram Soc. 1992; 75:739.

[5] Cornie JA, Chiang YM, Uhlmann DD, Mortensen A, Collins JM. Am Ceram Soc. Bull 1986; 65:293.

[6] Shappard LM. Am Ceram Soc. Bull 1990; 69:666.

[7] Hillig WB. J Am Ceram Soc. 1988; 71: C - 96.

[8] Besmann TM, Sheldon BW, Lowden RA. Science. 1991; 253:1104.

[9] Naslain R. In: Warren R (Ed.), Ceramic Matrix Composites, London: Chapman and Hall, 1992; 199.

[10] ASTM International. ASTM E422 - 05. American Society for Testing and Materials. 2011.

[11] Simmle H, Heinemann U, Kumaran K, HiPTI — High performance Thermal Insulation, 2005; IEA/ECBCS Annex 39.

[12] Kuhn J, Ebert HP, Arduini-Chuster MC et al, Int J Heat Mass Transfer 1992; 35: 1795 - 1801.

[13] Doermann D and Sacadura JF, J Heat Transfer, 1996; 118: 88 - 93.

Electromagnetic Interference Shielding Effectiveness of Multilayer Envelope Materials of Vacuum Insulation Panels Used in Building

Liu Weilan, Chen Zhaofeng*, Chen Xianhui

Super Insulation Composite Laboratory, College of Material Science and Technology, Nanjing University of Aeronautics and Astronautics, Nanjing, 210016, P. R. China

Abstract

The shielding characteristic of multilayer envelope materials of vacuum insulation panels (VIPs) was analyzed based on the electromagnetic interference shielding theory of Schelkunoff. The kind of multilayer envelope materials were designed and investigated with observation of microstructure by SEM and testing of shielding effectiveness (SE). Results show that the envelope materials of VIPs can be used to achieve effective shielding, and the SE of envelope materials with aluminum foil plays an important role in shielding performance. In addition, the absolute value of SE is relatively higher in the high frequency and the SE increases almost linearly with the increase of Al foil thickness in the envelopes under the condition of higher frequency.

Keywords electromagnetic interference, multilayer envelope materials, shielding effectiveness, vacuum insulation panels

1. Introduction

In the buildings with no electromagnetic shielding effect, the problems of electromagnetic disturbance and electromagnetic compatibility caused by electromagetic waves seriously harm the patients, pregnancies and children [1]. It not only has interference and damage to electronic instruments and equipments, seriously affecting its regular work and restricting the international competitiveness of China's electronic products and equipments, but also pollutes the environment and endangers human health. Also, leakage of electromagnetic waves would endanger national safety in information security and military core secrets. In particular, electromagnetic pulse, as a new concept weapon, has made substantial breakthroughs and directly impact electronic equipments and power systems [2]. It can cause temporary failure or permanent damage to information systems with multitudinous deliveries. The powerful electromagnetic pulse can also cause damage to human body, resulting in neuro disorder and behavior in a mess [3].

Shielding material hinders or attenuates electromagnetic energy propagation between shielded area and surrounding region. This is known as electromagnetic shielding. The principle of electromagnetic shielding takes advantage of the effect of shielding on electromagetic energy flow with reflection, absorption and guidance, which is closely related to the charge, current and polarization induced by the surface of the shield structure and the inside shield [4]. Shielding includes field shielding (static shielding and alternating electric field shielding), magnetic shielding (low frenquency fields and high frequency magnetic field shielding), and electromagnetic shielding (electromagetic shielding). The common electromagnetic shielding has shield effect on electric and magnetic fields simultaneously.

Shielding effectiveness (*SE*) was used to evaluate

* Corresponding author, Tel: 025—52112909, E-mail zhaofeng_chen@163.com

the shielding effect, showing the degree of attenuation of the shields on electromagnetic waves [5]. *SE* is defined as the ratio of the before and after shield electromagnetic field strength at one point, namely:

$$SE = 20\lg(E_0/E_s) \text{ or } SH = 20\lg(H_0/H_s) \quad (1)$$

Where E_0 and H_0 are respectively the electric and magnetic field strengths before shield at one point, and E_s and H_s are respectively the electric and magnetic field strengths after shield at one point. The related evaluation of *SE* is listed in Tab. 1.

Tab. 1 Evaluation of *SE*

	<10	10～30	30～60	60～90	>90
SE	Poor	Slightly poor	Medium	Well	Excellent

2. Experimental

All materials, including centrifugal glass fiber core material, Al foil envelope material and glass fiber VIPs investigated in this work are commercial grade, supplied by Suzhou V. I. P. New Material Co. Ltd. The general manufacturing process of glass fibre VIP core material has been reported elsewhere [6,7]. Most VIP producers in China use the wet processing method [8]. The dried core materials were bagged in multilayer envelope, simultaneously evacuated and sealed in a vacuum chamber to inner pressure of about 0.1 Pa, to form glass fibre VIP. The envelope material was prepared by heat lamination of the various single films using a roller hot-welding processing method under varied heat and pressure loads. Prior to Scanning electron microscopy (SEM) analysis, the specimens were coated with gold using a sputter coater (model: BALTEC SCD 5). The surface morphology of the envelop material was observed by scanning electron microscopy (SEM model: JOEL JSM-6360). Four samples were used to test the shielding performance. All of the four samples of VIPs contain Aluminum (Al) foil, which is devoted to enhance folding endurance, toughness, and reducing heat radiation, also provide the ability of shielding effect [9]. All materials, including centrifugal glass fibre core material, Al foil envelope material and glass fibre VIPs investigated in this work are commercial grade, supplied by Suzhou V. I. P. New Material Co. Ltd. The general manufacturing process of glass fibre VIP core material has been reported elsewhere [6,7]. Most VIP producers in China use the wet processing method [8]. The dried core materials were bagged in multilayer envelope, simultaneously evacuated and sealed in a vacuum chamber to innerpressure of about 0.1 Pa, to form glass fibre VIP. The envelope material was prepared by heat lamination of the various single films using a roller hot-welding processing method under varied heat and pressure loads. Prior to Scanning electron microscopy (SEM) analysis, the specimens were coated with gold using a sputter coater (model: BALTEC SCD 5). The surface morphology of the envelop material was observed by scanning electron microscopy (SEM model: JOEL JSM—6360). Four samples were used to test the shielding performance. All of the four samples of VIPs contain Aluminum (Al) foil, which is devoted to enhance folding endurance, toughness, and reducing heat radiation, also provide the ability of shielding effect [9].

In order to determine the diffusion-induced intermetallic compound phases, X - ray diffraction, using monochromatic Cu - Kα radiation and operated at 40 kV and 100 mA, was conducted. SEM in backscattered electron mode with energy-dispersive spectrometry (EDS) and Electron Backscatter Diffraction (EBSD) were performed using Quanta 200F (FEI) equipped with Jeol field emission gun, EDAX system and a TSL EBSD system, operating at 20 kV.

3. Microstructure analysis of multilayer envelope materials of VIPs

Figs. 1～4 show the microstructural images of the multilayer envelope materials of VIPs and the corresponding energy spectrum diagrams. As can be seen in Fig. 1～4(a), no delamination could be visibly detected from the magnification and testing apparatus used. The blue curve in Fig. 1～4(b) represent the element material of Al. Therefore, the thickness of Al foil from Fig. 1～4(b) by the energy spectrum diagrams are 0.36 μm, 0.48 μm, 0.24 μm, and 0.10 μm, respectively. Homogeneous conductive material with high surface smoothness, its electron can transfer easily with stronger eddy and better shielding effectiveness. However, Heterogenous conductive material with low surface smoothness (such as electrically conductive paint consisting of conductive filler particles and binder), its

electron transfers hard with weaker eddy and lower shielding effectiveness [10].

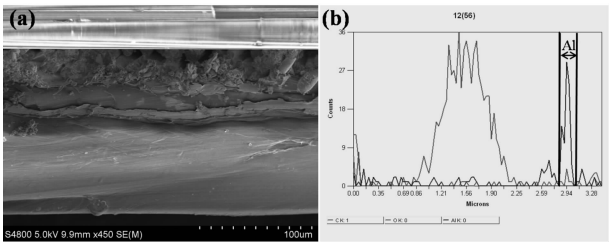

Fig. 1 SEM image of multilayer envelope materials of VIP in sample 1

(a) SEM picture and (b) energy spectrum diagram

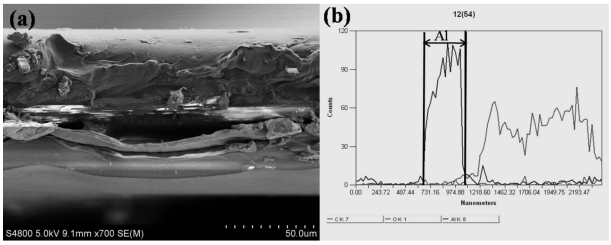

Fig. 2 SEM image of multilayer envelope materials of VIP in sample 2

(a) SEM picture and (b) energy spectrum diagram

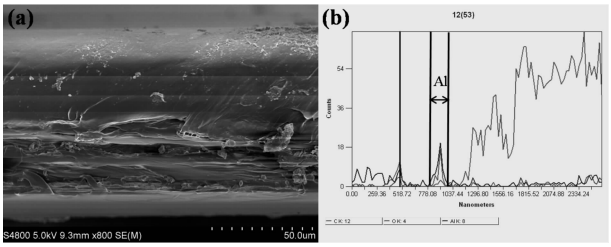

Fig. 3 SEM image of multilayer envelope materials of VIP in sample 3

(a) SEM picture and (b) energy spectrum diagram

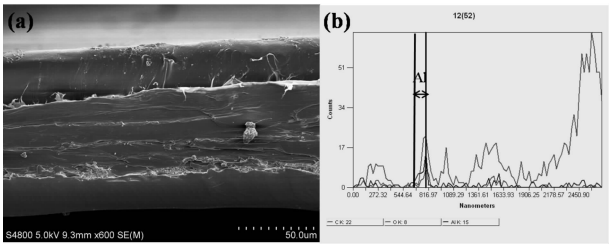

Fig. 4 SEM image of multilayer envelope materials of VIP in sample 4

(a) SEM picture and (b) energy spectrum diagram

4. Electromagnetic interference shielding performance of multilayer envelope materials of VIPs

Fig. 5(a) shows the relationship between the shielding effectiveness and etectromagnetic wave frequency in sample 1, and the range of frequency was from 30MHz～1.5GHz. Firstly, it can be seen in Fig. 5a that the value of the SE is negative. Also, the absolute value of SE was relatively lower in the lower frequency range of 30 MHz ～ 700 MHz while the average absolutely value was about 45 dB in the higher frequency range of 700 MHz～1.5 GHz. In a similar way, the other three samples were tested to evaluate the shielding effectiveness performances, which can be seen in Fig. 5(b)～(d), the average absolutely values were respectively about 55 dB, 40 dB, and 32dB in the in the higher frequency range of 700 MHz～1.5 GHz.

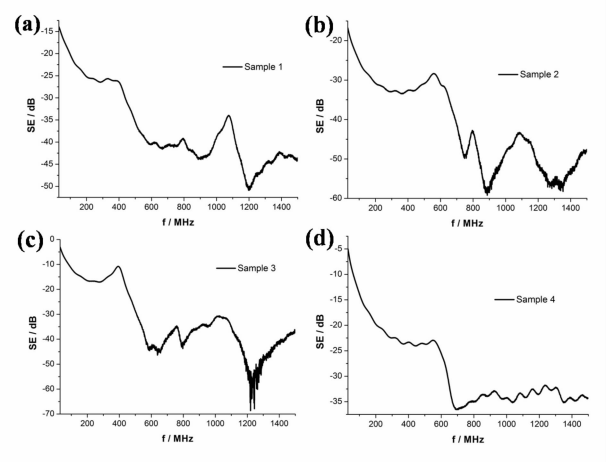

Fig. 5 Variation between shielding effectiveness and etectromagnetic wave frequency

(a) sample 1, (b) sample 2, (c) sample 3 and (d) sample 4

Compared to ordinary material, multilayer envelope materials of VIPs include the special material of Al foil improving the electromagnetic interference shielding performance. The relationship between the thickness of Al foil and the absolute value of *SE* is shown in Fig. 6. Under the condition of higher frequency, it can be seen that the *SE* increased almost linearly with the increase of Al foil thickness in the envelope. When the electromagnetic wave entered the multilayer envelope materials of VIP, reflection of electromagnetic waves occurred encountering the Al foil material, thus providing the opportunity to absorb attenuation and reflect attenuation. It also indicates that thicker thickness of Al foil in VIPs contributed to the better shielding effectiveness performance.

5. Conclusion

In this paper, multilayer envelope materials of

vacuum insulation panels were designed and investigated with observation of microstructure by SEM and testing of shielding effectiveness. Results show that the *SE* of envelopes with Al foil is of great importance, so that the envelopes of VIPs can be used to achieve effective shielding. In addition, the absolute value of *SE* was relatively lower in the lower frequency range of 30 MHz～700 MHz while the absolute value is higher in the higher frequency range of 700 MHz～1.5 GHz. The SE increased almost linearly with the increase of Al foil thickness in the envelopes under the condition of higher frequency. Therefore, VIP with Al foil on film is efficient as the insulation in building.

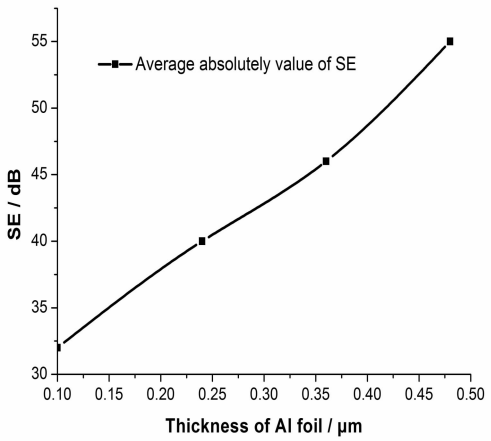

Fig. 6 The relationship between the thickness of Al foil and the absolute value of SE

References

[1] O'Shea P. How to meet the shielding needs of a 500—MHz PC. Eval. Eng. 1998; 37: 40, 43, 45 - 46.

[2] Hempelmann S. Surface engineering for EMI compliance. Process and practical examples. Galvanotechnik 1997; 88 (2): 418 - 424.

[3] Tenforde T S, Kaune WT. Interaction of extremely low frequency electric and magnetic fields with humans. Health Phys. 1987; 53(6): 585 - 606.

[4] Wang Y, Jing X. Intrinsically conducting polymers for electromagnetic interference shielding. Polym. Adv. Technol. 2005;16: 344 - 351.

[5] Robinson MP, Benson TM, Christopoulos C, Dawson JF. Analytical formulation for the shielding effectiveness of enclosures with apertures. Ieee T. Electromagn. C. 1998; 40(3): 240 - 248.

[6] Li CD, Duan ZC, Chen Q, Chen ZF, Boafo FE, Wu WP, Zhou JM. The effect of drying condition of glassfibre core material on the thermal conductivity of vacuum insulation panel. Mater. Design 2013; 50: 1030 - 1037.

[7] Baetens R, Jelle BP, Thue JV, Tenpierik MJ, Grynning S, Uvslokk S, Gustavsen A. Vacuum insulation panels for building applications: A review and beyond. Energy Buildings 2010; 42(2): 147 - 172.

[8] Di X, Gao Y, Bao C, Hu Y, Xie Z. Optimization of glass fiber based core materials for vacuum insulation panels with laminated aluminum foils as envelopes. Vacuum 2013; 97: 55 - 59.

[9] Huebener RP, Kampwirth RT, Clem JR. Meissner shielding currents and magnetic flux penetration in thin-film superconductors. J. Low Temp. Phys. 1972; 6(3 - 4): 275 -285.

[10] Schelkunoff S A. The impedance concept and its application to problems of reflection, refraction, shielding and power absorption. Bell System Technical Journal 1938; 17(1):17 - 48.

Selective Optimisation of a Compound Insulating Material as Interior Insulation—Capillary-active Materials Combined with High-performance Insulation Using the Example of Calcium Silicate in Combination with Vacuum Insulation Panels (VIP)

Holger Simon*

Forschong sinstitut für Wärmeschutz e. V. München, Flw München, Lochhamer Schlag 4, D-82166 Gräfelfing, Germany

Abstract

In order to be able to satisfy the continually changing challenges in the building industry, the planning of a building or a single construction project requires a high level of expertise with respect to the building materials to be used. At the same time, it is important that the materials used function over the long term in the intended application and display tolerant behaviour if the internal or external boundary conditions vary within a certain range.

It is only natural that there cannot be a material which is suitable for all requirements, but for all requirements there is a suitable material. In the case of insulation, it may be necessary, for example—depending on the field of application—for the insulation to provide particularly high stability to pressure or to behave favourably in terms of sound insulation. With internal insulation it is usually desirable to achieve the maximum insulating effect with an insulating material which is as thin as possible. The aim here is to maintain valuable living space, especially in conurbations. For this partial aspect of interior insulation, vacuum insulation panels (VIP) would be ideal. However, it is often desirable in the case of interior insulation materials for these to be capillary-active and for condensation water that occurs in the boundary layer between the outer wall and insulating material to be transported back into the room. This function can be taken over, for example, by calcium silicate boards (CaSi), which can be connected to the wall by means of a suitable adhesive.

The two insulation systems behave completely differently to one another. While VIP demonstrates its strength as a high-performance insulating material but is not capillary-active, the situation is the reverse in the case of CaSi—the insulating material displays good capillary-active properties, but its thermal conduction is significantly higher than that of VIP. In this investigation the aim is now to work out a way of ideally combining the advantages of the two materials. The idea pursues the approach of integrating the vacuum insulation panels into the calcium silicate boards in such a way that maximum thermal insulation is achieved while simultaneously ensuring sufficient capillary activity.

For this purpose, numerous hygrothermal simulations and parameter studies will be performed. Geometrical aspects in particular will be varied, such as the differences between the VIP (joints) and the thickness of the covering with CaSi. Furthermore, the simulations for various material properties and boundary conditions will be carried out in order to ensure a sufficient range of applications.

The evaluation of the simulations is performed with the focus on an internal insulation system with permanent hygrothermal functions and optimised performance with respect to its thermal insulation effect and capillary activity.

* Corresponcling Author, Tel: 49-(0)89-85800-20, Fax: 49-(0)89-85800-40, E-mail: simon@fiw-muenchen.de

Vacuum Glazing with Stainless Steel Edge Seal

Won Kyeong Kang, Tae-Ho Song*

Korea Advanced Institute of Science and Technology, Daejeon, Korea

Abstract

Vacuum glazing (VG) can greatly improve the energy efficiency of building by employing a vacuum gap between two glass panes. Usually, fused edge seal is made at the periphery of the gap to retain vacuum. Support pillars are positioned to maintain the gap against the atmospheric compression. In VG, there are four heat transfer paths, i. e., through pillars, residual gas, radiation and edge of VG. A significant amount of heat loss occurs through the edge of conventional VG. Therefore, the edge of VG should be improved for further application and commercialization. For this purpose, VG with stainless steel edge seal is conceived. By replacing the fused edge with a very thin stainless steel cover, conduction through edge of VG is tremendously reduced. Poly-urethane(PU) adhesive is used to glue the stainless steel and the glass. However, gas permeation occurs from the atmosphere to inside of VG through the adhesvie. For this reason, feasibility of VG using PU adhesive is verified by estimating the service lifetime. Further improvement by employing lateral bumps on the surface of stainless steel is also studied numerically, which is found to substantially reduce gas permeation through the edge seal.

Keywords vacuum glazing, polyurethane adhesive, service lifetime

1. Introduction

Considerable amount of heat is lost through windows in buildings, and it occupies a large portion of energy consumption in the building energy. Therefore, insulation performance of glass in the window should be enhanced. VG is a super insulator which can greatly improve the energy efficiency of building. VG has a vacuum gap between two glass panes. Usually, fused edge seal is made at the periphery of the gap to retain vacuum. Support pillars are positioned to maintain the gap against the atmospheric compression. It has a superior thermal insulation performance. In addition, it is thinner than the existing glazing systems, providing additional space.

However, existing VG has a few serious drawbacks. One of them is the heatloss through the edge seal. It is called the heat bridge effect or the edge conduction. The amount of heat loss through the edge is substantial, sometimes even fatal. Another problem is that of fixed edge seal. VG is usually manufactured by welding edge of two glass panes using low melting glass solder. When installed in building with a large temperature difference between interior and exterior panes, it inducess significant thermal stress in the VG, and it may result in a failure of VG.

For furtherutilization of VG, these problems must be solved. Griffith et al. fabricated VG adding adiabatic frame to the edge seal [1]. It is effective in reducing the edge conduction, but it didn't resolve the problem fundamentally. Lee et al. tried to make VG with rubber gasket and urethane edge packing [2]. However, it has not been used practically yet due to the problem of service lifetime. The Ulster team manufactured VG with indium alloy edge [3, 4]. They considered edge

* Corresponding author, Tel: 821048075413, E-mail: thsong@kaist.ac.kr

conduction of VG with window frame, their VG still has a significant heat loss through the edge when VG is used alone.

VG with metal edge seal is proposed to solve these problems. The edge of VG is made of metal with a very small thickness and low thermal conductivity. Stainless steel 304 is taken as the choice with its thermal conductivity of about 14.9 W/(m • K). With less-than-1mm thickness, heat loss through the edge can be minimized. In addition, since metals have better mechanical flexibility than glass, the VG can be free from bending stress cause by the temperature difference. For the joining, Kang tried to join glass and stainless steel with low melting temperature solder glass [5]. However, glass pane is apt to fail due to thermal expansion difference between glass and stainless steel in the cooling process.

The purpose of this study is to try a joining methodusing adhesive for manufacturing of the new concept VG (Fig. 1). Feasibility is varified by estimating service lifetime theoretically and numerically. Then, the issue whether the joining method is suitable for manufacturing of VG.

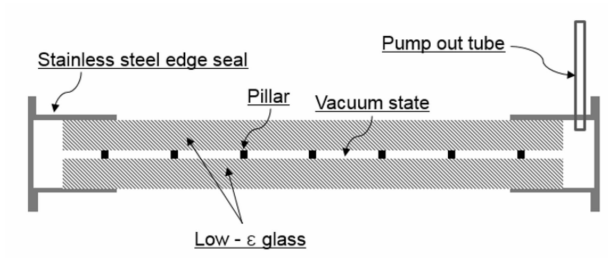

Fig. 1 Scheme of new edge concept VG

2. Method using adhesive

In this study,joining stainless steel and glass pane using adhesive is tried. Use of adhesive has many advantages compared to the low melting temperature solder glass [5]. Because the process using adhesive does not need high temperature, it protects low emissivity coating on glass from oxidizing and prevents breaking of glass due to thermal stress between glass and stainless steel [1]. However, the method using adhesive has a shortcoming; gas permeation from the atmosphere to the inner gap through adhesive layer occurs and it degrades vacuum in VG. Therefore, gas permeation characteristics through the adhesive layer should be identified. After a search for a low permeability adhesive, PU adhesive is taken as the candidate as its gas permeability is shown Tab. 1.

Tab. 1 Gas permeability of poly-urethane adhesive

	N_2	O_2	CO_2	H_2O
$K \times 10^{17}$ m^2/−s−Pa	0.035	0.082	0.300	9.313

3. Gas permeation and service lifetime estimation

3.1 Gas permeation in VG

Pressure increase inside VG due tothe permeation of gas species i across the adhesive layer can be estimated by the following equation [6].

$$P_{i,\mathrm{VG}} = P_{i,\mathrm{atm}}\left[1-\exp\left(-\frac{K_i}{\nu_o}\frac{A_s}{\delta}\frac{R_U T}{V}t\right)\right] \quad (1)$$

Where

$P_{i,\mathrm{atm}}$ = partial pressure of gas species i in the atmostphere,

K_i = gas permeability for gas species i ,

A_s = area normal to the direction of permeation,

R_u = universal gas constant,

T = temperature,

ν_o = standard state molar volume,

δ = length of the adhesive layer to the direction of permeation,

V = volume inside VG,

t = Time.

Total pressure increase can be estimated by summing overall i,

$$P_{\mathrm{VG}} = \sum_{i}^{\mathrm{gases}} P_{i,\mathrm{VG}}(t) \quad (2)$$

3.2 Service lifetime estimation

Service lifetime of VG is defined here as the time when the distance d (m) between vacuum gap and mean free path λ (m) of gas inside the VG becomes the same. This criterion is taken since the heat transfer in VG gap is dependent on d/λ as relation in Fig. 2, although other definitions are possible.

Mean free path ofair inside VG may be written as follows [8]:

$$\lambda = \frac{6.65\times10^{-3}}{P_{\mathrm{VG}}} \quad (3)$$

Where P_{VG} is expressed in Pa.

Using the criterion and equation (3), crictical pressure at which the service lifetime is defined is

obtained as follows：

$$P_{cr} = \frac{6.65 \times 10^{-3}}{d} \text{ (Pa)} \quad (4)$$

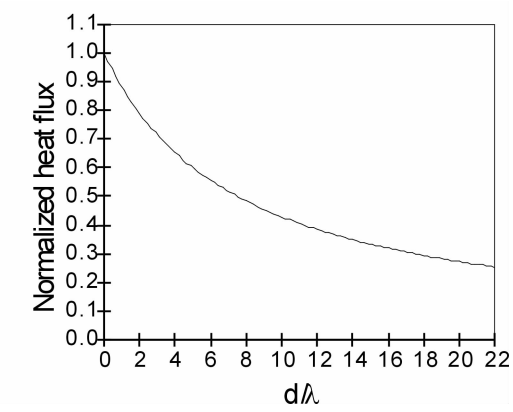

Fig. 2 Heat flux dependency across the VG gap (normalized to the air-filled gap case). Qualitatively re-drawn from Fig. 1 of Ref. [7]

Equation (4) is plotted as Fig. 3. Critical pressure change with the gap between the glass panes. It is better to reduce the gap to have greater service lifetime. Generally, gap of about 0.2 mm is employed in the manufacturing process.

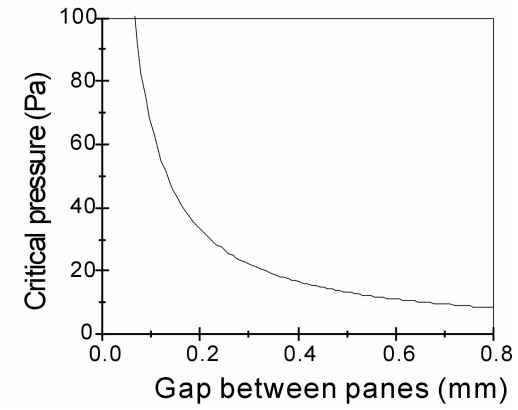

Fig. 3 Critical pressure depending on gap between glass panes

For 270 mm×270 mm VG, service lifetime can be calculated from equations (2) and (4). In this case, area normal to direction of gas permeation is 0.84×10^{-4} m^2 with a bonding thickness of 5 μm. The length δ along the permeation direction is taken as 2 cm and volume inside VG is 108.25 cm^3 and 114.5 cm^3 for two gap sizes $d = 0.1$ mm and $d = 0.2$ mm. Note that the side volume made by stainless steel structure is about 102 cm^3 (see Fig. 1). This side volume functions as the buffer of pressure increase in VG. The computed lifetimes are 28.4 and 15.3 years for $d = 0.1$ and 0.2 mm, respectively.

The VG at hand is estimated to have service lifetime of more than 10 years due to the side volume. Though long, it is not perfectly satisfactory yet. Therefore, methods to improve the service lifetime of VG is needed.

4. A Method to improve the service lifetime

Gas permeation can be controlledby reducing the area. Reducing the area locally causes a bottleneck phenomenon and it can suppress the gas permeation. By making impermeable bumps on the stainless steel at the surface adjacent to adhesive (see Fig. 4), lifetiem can be improved substantially.

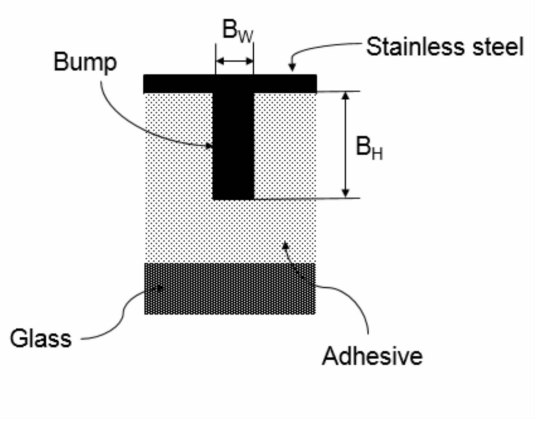

Fig. 4 Boding unit with bump

Assuming a steady state permeation in the cross sectional area parallel to the gas permeation in the Fig. 4, the conservation equation for gas species is

$$\frac{\partial J_x}{\partial x} + \frac{\partial J_y}{\partial y} = 0 \quad (5)$$

where J_x and J_x are the mass flux in x and y directions expressed from Fick's law as,

$$J_x = -D\frac{\partial C}{\partial x}, J_y = -D\frac{\partial C}{\partial y} \quad (6)$$

where D =diffusion coefficient (m^2/s),

C =gas concentration (mole/m^3).

From Henry's law, the gas concentration at the surface of adhesive is related to the solubility of the gas to adhesive as,

$$C = SP_i \quad (7)$$

where S =solubility (mole/m^3−Pa).

Gas permeability K_i is expressed as product of

diffusion coefficient and solubility as,

$$K_i = D_i S \quad (8)$$

Equation (7) can be extended to define an equilibriumpressure P_i anywhere in the adhesive. Then using equation (6), (7) and (8), equation (5) is re-written as follows :

$$\frac{\partial}{\partial x}\left(K_i \frac{\partial P_i}{\partial x}\right) + \frac{\partial}{\partial y}\left(K_i \frac{\partial P_i}{\partial y}\right) = 0 \quad (9)$$

This equation is solved using a finite volume method-based house code.

The reduction of gas permeation by the bump is expressed as the ratio of permeation with bump to that without it. This ratio is denoted K_{eff}/K. K is subtituted into equation (1) with K_{eff} to find the permeation rate in the bump-installed adhesive layer. The ratio K_{eff}/K is calculated changing the ratio width of bump to bonding thickness and ratio height of bump to bonding to thickness (Fig. 4).

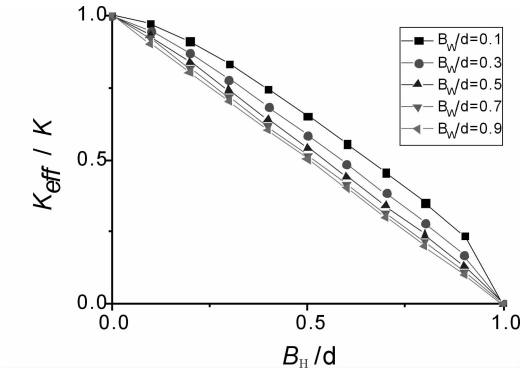

Fig. 5 Effective gas permeability depending on ratio width of bump to bonding thickness and ratio height of bump to bonding thickness

Fig. 5 shows that increasing B_H has a significant effect while increasing B_W has a minor effect. If a bump with 2.5 μm height and 0.5 μm width is made, service lifetime of VG with 0.2 mm gap improves to 23.5 years (increase of 8.2 year). Thus, it is found to be a promising way to increase the service lifetime.

5. Conclusions

Feasibility of manufacturing VG with stainless steel is verified by estimating service lifetime theoretically and numerically. The method using adhesive is suitable for the joining of VG. because of the low gas permeability. Side volume functions as a buffer of pressure increase in the VG. VG with PU adhesive can have service lifetime of more than 10 years. Additionally, by making bump on the stainless steel at the surface adjacent to adhesive, service lifetime can be improved substantially.

Acknowledgements

This work was supported by the National Research Foundation of Korea (NRF) grant funded by theKorea government (MSIP) (No. 2013R1A2A2A07068924) and the third stage of the Brain Korea 21 Project in 2015.

References

[1] P. W. Griffiths, M. D. Leo, P. Cartwright, P. C. Eames, P. Yianoulis, G. Leftheriotis and B. Norton, (1998), Fabrication of evacuated glazing at low temperature, Solar Energy, 63(4), pp. 243 - 249.

[2] B. H. Lee, I. S. Yoon, T. H. Song, H. S. Kwak, (2006), Experimental study on manufacturing of insulation vacuum glazing and measurement of the thermal conductance, KSME, 30(8), pp. 772 - 779.

[3] T. J. Hyde, P. W. Griffiths, P. C. Eames, B. Norton, (2000), Development of a novel low temperature edge seal for evacuated glazing, In: Proceeding of world renewable energy congress VI, pp. 271 - 274.

[4] J. F Zhao, P. C. Eames, T. J. Hyde, Y. Fang, J. Wang, (2007), A modified pump-out technique used for fabrication of low temperature metal sealed vacuum glazing, Solar Energy, 81(9), pp. 1072 - 1077.

[5] W. K. Kang, (2015), Study on development of Vacuum glazing with stainless steel edge seal, MS Dissertation, Korea Advanced Institute of Science and Technology, Daejeon, Republic of Korea, pp. 7 - 31.

[6] H. Jung, C. Jang, I. Yeo, T. H. Song, (2013), Investigation of gas permeation through Al-metallized film for vacuum insulaltion panels, International Journal of Heat and Mass Transfer, 56, pp. 436 - 446.

[7] G. S. Springer, (1971), Heat transfer in rarefied gases, Advanced in Heat Transfer edited by T. F. Irvine, Jr. and J. P. Hartnett, Academic press, 7, pp. 163—218,

[8] A. Roth, (1990), Vacuum Technology 3rd ed., Elsevier, Amsterdam, pp. 17 - 61.

Hollow Silica Nanospheres as a Stepping-stone Toward Thermal Super Insulation Materials

Bjørn Petter Jelle[a,b*], Gao Tao[b], Sohrab Alex Mofid[b]
Serina Ng[a], Bente Gilbu Tilset[c], Mathieu Grandcolas[c]

a. SINTEF Building and Infrastructure, Department of Materials and Structures, NO-7465 Trondheim, Norway
b. Norwegian University of Science and Technology (NTNU), Department of Civil and Transport Engineering, NO-7491 Trondheim, Norway
c. SINTEF Materials and Chemistry, Department of Nano and Hybrid Materials, NO-0314 Oslo, Norway

Abstract

The development of high performance thermal insulation materials and solutions is regarded as one of the key strategies in order to obtain energy-efficient buildings with low embodied energy and low carbon dioxide footprint. These insulation materials are targeted with thermal conductivities below 20 mW/(m·K) and are often called super insulation materials (SIM). A possible and promising way to manufacture a SIM is to utilize the Knudsen effect by making nano insulation materials (NIM), where the gas thermal conductivity is reduced as the pore diameter in a material is decreased below the mean free path of the gas molecules, i.e. in the nanometer range. As to avoid any leakage and degradation issues, air at atmospheric pressure is assumed to be used in the pores of a NIM. A possible pathway or stepping-stone toward achieving a SIM is to make hollow silica nanospheres (HSNS) by selected sacrificial template methods. This work summarizes our current experimental investigations of making a SIM from NIM and HSNS, among the results presenting manufacturing procedures and characterizations by scanning and transmission electron microscopy and thermal conductivity measurements.

Keywords hollow silica nanosphere, super insulation material, nano insulation material, thermal conductivity

1. Introduction

As the world's focus is drawn stronger toward minimizing energy usage, the construction of energy-efficient buildings is becoming more widespread. In this respect, the development of high performance thermal insulation materials and solutions targeting thermal conductivities below 20 mW/(m·K) isof great importance. These are often called super insulation materials (SIM). A promising way to make a SIM is by utilizing the Knudsen effect by producing nano insulation materials (NIM), where the gas thermal conductivity is reduced as the pore diameter in a material is decreased below the mean free path of the gas molecules, i.e. in the nanometer range [1-5]. The pores in a NIM are assumed to contain air at atmospheric pressure in order to avoid any leakage and degradation issues, in contrast to e.g. vacuum insulation panels (VIP) [1,3,6-9]. This work summarizes our ongoing research activities attempting to manufacture a SIM through NIM by the possible pathway or stepping-stone by making hollow silica nanospheres (HSNS) by selected sacrificial template methods.

2. Experimental

Various experimental procedures for synthesizing HSNS are described in our earlier work [4,5,10-12]. However, the work is still ongoing with many experimental pathways and parameters to be explored. The HSNS synthesis is based on a sacrificial template

* Corresponding author, Tel: 47-73593377, Fax: 47-73593380, E-mail: bjorn.petter.jelle@sintef.no

approach (Fig. 1), where e. g. polyacrylic acid (PAA) and polystyrene (PS) have been used as template materials. Initially, our starting point was based on the work by Du et al. [13], who used the method to prepare antireflection coatings, and the study by Wan and Yu [14].

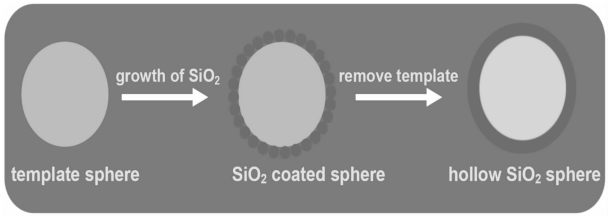

Fig. 1 Illustration of the HSNS synthesis by the sacrificial template approach

3. Results and discussion

PS templates coated with silica from tetraethyl orthosilicate (TEOS) and water glass (Na_2SiO_3) are shown in Fig. 2 and Fig. 3, respectively. The scanning electron microscope (SEM) images show that the PS template sphere is covered by a silica shell, made up of silica nanoparticles 10～20 nm in diameter when coated with silica from TEOS (Fig. 2), and appearing as a large, wrinkled silica sheet when coated with silica from water glass (Fig. 3). TEOS as the silica precursor for HSNS provides a high success rate when coating the PS templates, however, TEOS and ethanol are expensive and energy intensive chemicals. Utilizing water glass as the silica precursor is more economical as it is inexpensive compared to TEOS and since distilled water is used as reaction medium. An example of an unsuccessful silica coating process from water glass is shown by the PS spheres and silica rods depicted in the SEM image in Fig. 4. The HSNS powder samples have thermal conductivity values typically in the range 20～90 mW/(m · K), though some uncertainties in the Hot Disk apparatus measurement method have to be further clarified.

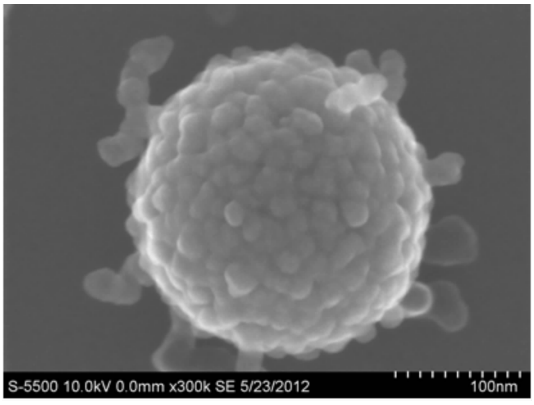

Fig. 2 PS template coated with silica from TEOS where the appearance of the silica shell is as silica nanoparticles covering the PS sphere (magnification 300000× and scale-bar 100 nm)

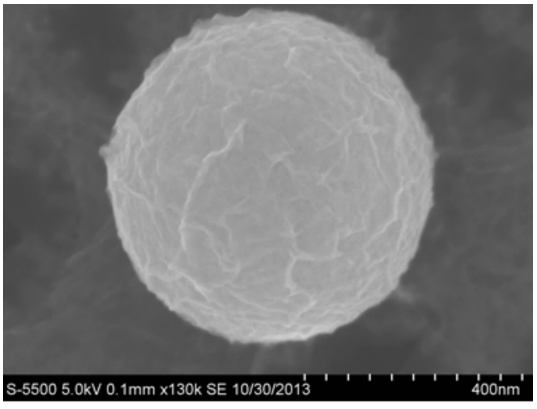

Fig. 3 PS template coated with silica from water glass where the appearance of the silica shell is as a large, wrinkled silica sheet covering the PS sphere (magnification 130000× and scale-bar 400 nm)

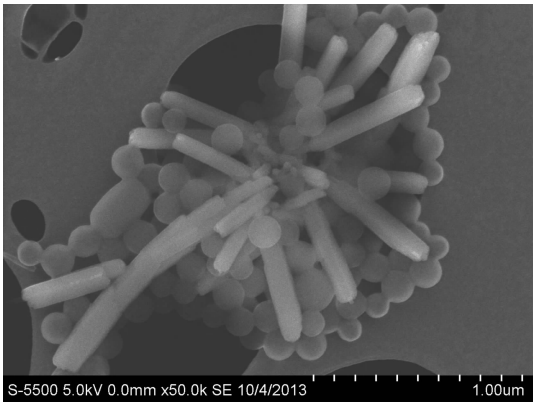

Fig. 4 Example of unsuccessful silica coating process (from water glass) depicting PS spheres and silica rods (magnification 50000× and scale-bar 1 μm)

4. Conclusions

Utilizing sacrificial template methods, nano insulation materials as hollow silica nanospheres have been synthesized, which represent a possible stepping-stone toward thermal super insulation materials.

Acknowledgements

This work has been supported by the Research Council of Norway and several partners through "The Research Centre on Zero Emission Buildings" (ZEB).

References

[1] R. Baetens, B. P. Jelle, J. V. Thue, M. J. Tenpierik, S. Grynning, S. Uvslokk and A. Gustavsen, Vacuum insulation panels for building applications: A review and beyond, Energy and Buildings, 42, 147 - 172, 2010.

[2] B. P. Jelle, A. Gustavsen and R. Baetens, The path to the high performance thermal building insulation materials and solutions of tomorrow, Journal of Building Physics, 34, 99 -123, 2010.

[3] B. P. Jelle, Traditional, state-of-the-art and future thermal building insulation materials and solutions—Properties, requirements and possibilities, Energy and Buildings, 43, 2549 - 2563, 2011.

[4] B. P. Jelle, B. G. Tilset, S. Jahren, T. Gao and A. Gustavsen, Vacuum and nanotechnologies for the thermal insulation materials of beyond tomorrow—From concept to experimental investigations, Proceedings of the 10th International Vacuum Insulation Symposium (IVIS－X), pp. 171 - 178, Ottawa, Canada, 15 - 16 September, 2011.

[5] B. P. Jelle, T. Gao, L. I. C. Sandberg, B. G. Tilset, M. Grandcolas and A. Gustavsen, Thermal superinsulation for building applications—From concepts to experimental investigations, International Journal of Structural Analysis and Design, 1, 43 - 50, 2014.

[6] S. Brunner and H. Simmler, In situ performance assessment of vacuum insulation panels in a flat roof construction, Vacuum, 82, 700 - 707, 2008.

[7] M. J. Tenpierik, Vacuum insulation panels applied in building constructions (VIP ABC), Ph. D. Thesis, Delft University of Technology, Delft, The Netherlands, 2009.

[8] S. E. Kalnæs and B. P. Jelle, Vacuum insulation panel products: A state-of-the-art review and future research pathways, Applied Energy, 116, 355 - 375, 2014.

[9] S. Brunner, K. G. Wakili, T. Stahl and B. Binder, Vacuum insulation panels for building applications—Continuous challenges and developments, Energy and Buildings, 85, 592 - 596, 2014.

[10] T. Gao, B. P. Jelle, L. I. C. Sandberg and A. Gustavsen, Monodisperse hollow silica nanospheres for nano insulation materials: Synthesis, characterization, and life cycle assessment, ACS Applied Materials and Interfaces, 5, 761 - 767, 2013.

[11] L. I. C. Sandberg, T. Gao, B. P. Jelle and A. Gustavsen, Synthesis of hollow silica nanospheres by sacrificial polystyrene templates for thermal insulation applications, Advances in Materials Science and Engineering, 2013, 6 pages, Article ID 483651, 2013.

[12] T. Gao, L. I. C. Sandberg and B. P. Jelle, Nano insulation materials: Synthesis and life cycle assessment, Procedia CIRP, 15, 490 - 495, 2014.

[13] Y. Du, L. E. Luna, W. S. Tan, M. F. Rubner and R. E. Cohen, Hollow silica nanoparticles in UVvisible antireflection coatings for poly (methyl methacrylate) substrates, ACS Nano, 4, 4308 - 4316, 2010.

[14] Y. Wan and S. H. Yu, Polyelectrolyte controlled large-scale synthesis of hollow silica spheres with tunable sizes and wall thicknesses, Journal of Physical Chemistry C, 112, 3641 - 3647, 2008.

Methods for Evaluation of Thermal Conductivity Increase of VIPs

Roland Caps[a*], Ines Wallaschek[a], Ismail Abu-Shawriyeh[a], Samuel Brunner[b]

a. va-Q-tec AG, Karl-Ferdinand-Braun-Str. 7, 97080 Würzburg, Germany

b. EMPA, Ueberlandstr. 129, CH—8610 Duebendorf, Switzerland

Abstract

In order to determine the mean thermal conductivity of VIPs during service life time a common procedure is accelerated aging by storing VIPs at elevated temperatures with and without humidity. Increase of thermal conductivity, water intake and gas pressure is measured during storage. For evaluation of the results data on the relation between thermal conductivity and gas pressure, the influence of water content on thermal conductivity (for silica), the adsorption isotherm of core material (silica) or dryer and getter capacities have to be known. As usually only small variations of thermal conductivity can be detected, a detailed evaluation of the measurement methods and their potential accuracy is necessary. The paper reports on results of measurements on various barrier films and core materials. Advantages and disadvantages of different methods including fast measurement procedures are discussed.

Keywords vacuum insulation panels, accelerated aging, air permeation, vapor permeation, service life time

1. Introduction

Currently a draft for the standardization of VIPs applied in buildings is drawn up by the European standardization organization in CEN TC 88/WG11 in coordination with the related ISO working group. A critical issue is the definition and measurement of a declared value of thermal conductivity. A common understanding is that it should be the mean value of thermal conductivity during 25 years of service life time and including the thermal bridge effect of the envelope.

Ten years ago the German organization for building technology (DIBT) based its designation of a declared value of thermal conductivity (Bemessungswert) on accelerated aging of VIP at a dry climate of 80 ℃. From subsequent measurements of thermal conductivity increase every three months an ageing surcharge to the initial thermal conductivity is derived. Additionally, thermal bridges due to the envelope and possible gaps along the edges are taken into account. Disadvantage of this procedure is that influence of water vapor permeation through the envelope is neglected and that the acceleration factor in regard to an ambient climate is not established.

At Empa in Switzerland accurate measurements of gas pressure increase and humidity content of VIP have been developed during the same time. Aim was to measure the small changes of these properties at room temperature and calculating the change of thermal conductivity from these parameters. So, the extrapolation of results obtained at high temperatures to room temperature is avoided. Disadvantage of Empa's procedure is, that the necessarily very accurate measurements of small changes of gas pressure and humidity content are not available everywhere and that, for control, a direct measurement of thermal conductivity change of silica VIPs at room temperature is very hard to perform (possible changes are in the range of 0.1 mW/(m · K) and lower per year).

* Corresponding author, Tel: 49-931 35942-0, E-mail: caps@va-q-tec.com

Further, with the in meantime developed improved laminated, even smaller differences have to be measured.

In the following, the author report on results of accelerated aging of VIPs, which have been stored in a climate of 50℃/70 % humidity for half a year. Additionally, some methods are presented, which allow the investigation of basic properties of the VIP envelope like air and water vapor permeation within a short time.

2. Parameters influencing long term thermal Conductivity Increase

The thermal conductivity of silica based vacuum insulation panels depends on the gas pressure of air p_{air} and water vapor p_{H2O} within the panel and also on the moisture content X [1]. Therefore, permeation of air and water vapor through the envelope are mainly responsible for the aging of vacuum panels. At higher temperatures, especially beyond 70 ℃ and in combination with high relative humidity, also destruction of the barrier film is possible.

For simplicity, we assume that the relations between thermal conductivity change $\Delta\lambda$ and gas pressure change Δp and water content change ΔX are linear, as well as the relation between rel. humidity φ and water content X. This is similar to [1, 2], except the additional simplification, that saturation effects of water vapor, when reaching an equilibrium of adsorption, are neglected [3]:

$$\Delta\lambda = \partial\lambda/\partial p \cdot \Delta p + \partial\lambda/\partial X \cdot \Delta X \qquad (1)$$

with $\partial\lambda/\partial p = 0.04$ mW/(m • K mbar)
(for air and approximately also for water vapor) and $\partial\lambda/\partial X = 0.5$mW/(m • K %) [1]

$$\Delta p = \Delta p_{air} + \Delta p_{H_2O} = \Delta p_{air} + p_s(T) \cdot \partial\varphi/\partial X \cdot \Delta X \qquad (2)$$

with $\partial\varphi/\partial X = 14\%/\%$
and $p_s(T)$: vapor saturation pressure at temperature T.

In order to calculate the mean thermal conductivity during service life time, we need to know the yearly increase of thermal conductivity under real climate conditions, or the yearly increase of both gas pressure and humidity content during the same conditions.

3. Long term oObservations

Data on long-term observations of vacuum panels have been provided by Empa [4]. One part of the panels were stored for ten years at a constant climate of 23 ℃ under dry conditions (33 % r. h.), the others under wet conditions (80% r. h.). After ten years the thermal conductivity has risen by 0.6 mW/(m • K) and 2.2 mW/(m • K), respectively. The gas pressures changes Δp were 5mbar and 17.5mbar, respectively (starting both from around 1 mbar) and the moisture increase ΔX was 0.6% and 3.1%, respectively. Applying eq. (1), we get a theoretical thermal conductivity increase after ten years of $\Delta\lambda_{th} = 0.5$ mW/(m • K) for the dry case and $\Delta\lambda_{th} = 2.3$ mW/(m • K) for the wet case, which is close to the measured values. The results give confidence that the simple linear relationship (1) is usable to calculate thermal conductivity change $\Delta\lambda$ from the increase of gas pressure Δp and water content ΔX.

4. Storage at accelerated aging conditions

As the thermal conductivity changes at room temperature are very small to get reliable information in shorter times, accelerated aging conditions are used. The higher the temperature, according to Arrhenius law, the faster will be the permeation of air and water vapor through the envelope. Fig. 1 shows the results of gas pressure and Fig. 2 of thermal conductivity measurements with Al foil vacuum panels, which have been stored at a temperature of 80 ℃ under dry conditions. Here, the influence of humidity on change of thermal conductivity is very small. After conditioning effects in the first month, it was noticed that small steady yearly increase of thermal conductivity of 0.25 mW/(m • K • a) and a corresponding gas pressure increase of 6 mbar/a.

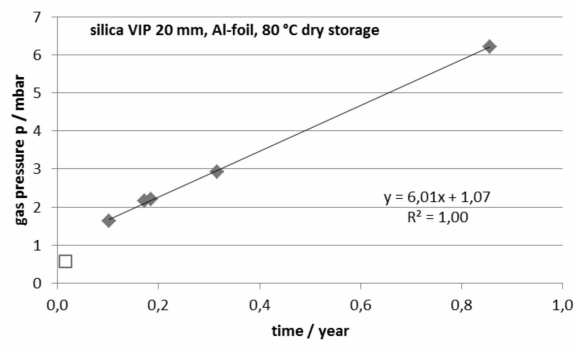

Fig. 1 Increase of gas pressure, Al-foil VIP @ 80 ℃

However, silica VIPs with Al-foil are not used in

practice, as the heat bridges around the edges are too high. In contrast to Al foils, metallized films additionally transmit moisture, which may have a considerable influence on thermal conductivity increase (compare Empa long-term results in chapter 3 on a va-Q-tec VIP produced in 2004 with laminate quality as a decade ago available).

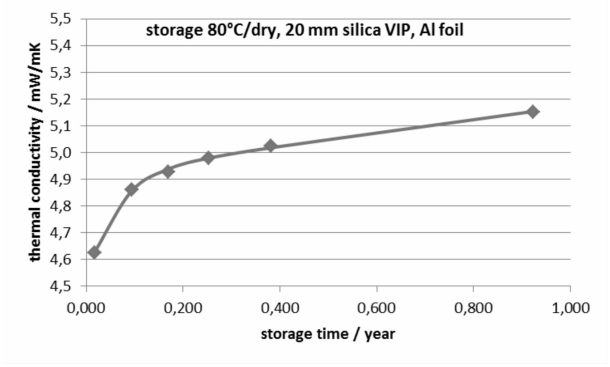

Fig. 2 Increase of thermal conductivity, Al foil VIP @80 ℃

Tests under wet conditions and at high temperatures like 80 ℃ show, that many barrier films don't survive these conditions for more than a few weeks. Therefore, the working group CEN TC 88/WG11 decided to perform storage tests at a more moderate climate of 50℃ /70% r. h. In Fig. 3 the results of the conductivity increase of VIP samples from va-Q-tec are depicted. The silica panels were equipped with a triple metallized high barrier film. The increase of thermal conductivity λ here is 0.79 mW/(m • K • a).

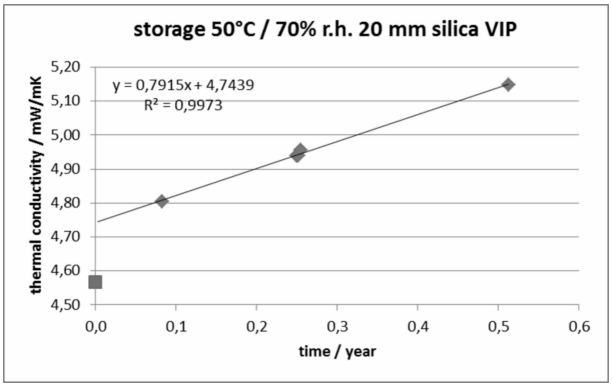

Fig. 3 Thermal conductivity increase of VIP with triple metallized film @50℃/70%r. h

Furthermore, the increase of humidity content and total gas pressurewas measured, yielding $\Delta X/\Delta t$ = 0.7%/a and $\Delta p/\Delta t$ = 9.5 mbar/a. Using relation Eq. (1), we obtain a calculated increase of conductivity λ_{th} = 0.73 mW/(m • K), which is close to the measured one.

In Fig. 4 the different mechanisms of thermal conductivity increase derived from gas pressure and water uptake measurements and applying eqs. (1) and (2) are shown. Under these climate conditions permeation of water vapor through the envelope has the highest impact on the thermal conductivity increase.

Finally, the thermal conductivity changes derived by the accelerated conditions are to be extrapolated to other, more moderate climates like room temperature.

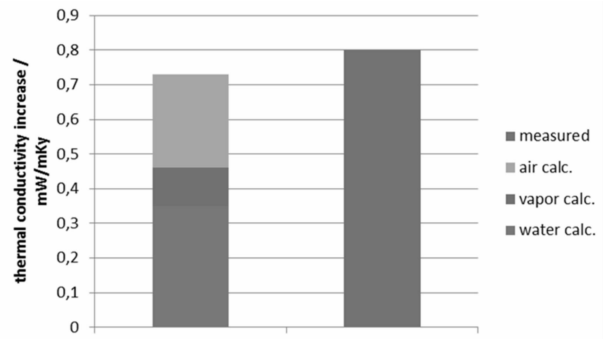

Fig. 4 Comparison of thermal conductivity increase obtained by water uptake and pressure increase with tested thermal conductivity increase @50℃/70%r. h

Here more data on the temperature dependent air and water vapor permeation through high barrier films is needed.

For metallized films a doubling of air permeation about every 15 K increase of temperature is common. In comparison to room temperature for the climate 50℃/70% r. h. an acceleration of air permeation of about 4 is to be expected. The vapor pressure difference also is a factor of about 4 lower at room temperature. If an overall acceleration of 4 is assumed, an extrapolated value of 0.2 mW/(m • K) per year is gained (compare Empa results @ 80% r. h. in ch. 3). For the environmental conditions of 23℃ /80%r. h. a 2.5 mW/(m • K) mean increase during a life time of 25 years under humid conditions then is to be expected. Real application conditions may be more severe for some shorter period [3], but also longer times dominate with colder temperatures than considered here.

5. Fast methods for testing permeation

Thermal conductivity increases faster, if coarser core materials than silica, e. g. glass fibers, are used

[5]. Air and water vapor permeation are separated by performing the tests under dry conditions. Measurements at different mean temperatures are possible to obtain the Arrhenius relations for a specific kind of film.

Fig. 5 depicts the U - value increase of an Al foil laminate sample with glass fibers. Within a few days of measurement a straight line of U - value increase is obtained. From the slope of the increase the amount of air permeation can be derived, which here amounts to 0.85 mbar liter/(m^2 of panel and year). This corresponds to a permeation of air through the film of around 0.001 $cm^3/(m^2 \cdot d)$. The increase of thermal conductivity of the fiber core VIP with Al foil envelope here amounts to 60% per year.

The above method relies on very accurate measurements of thermal conductivity increase. To demonstrate the potential of this procedure, a 30 mm silica vacuum panel was continuously measured during four days at a mean temperature of 28 ℃ and dry conditions. According to Fig. 6 an increase not higher than 0.07 mW/(m • K) per year can be detected. This corresponds to a mean thermal conductivity change of 1mW/(m • K) within 25 years for this dry condition.

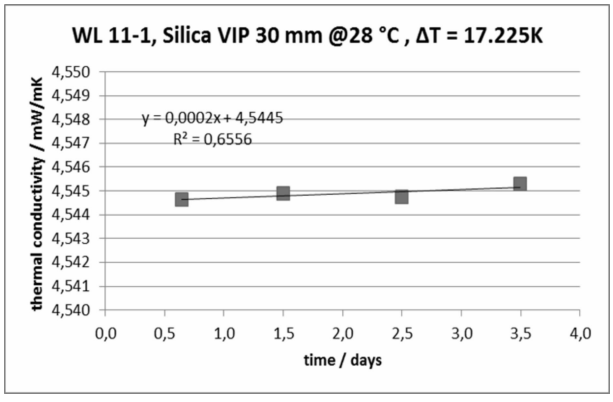

Fig. 5 Increase of U - value of 5 mm VIP with glass fiber core and Al foil at a mean temperature of 28 ℃

For fast tests of weight increase due to water vapor permeation, thin, plain sample bags with barrier film are favorable, which are filled with dryer, sealed and stored for three weeks at 50℃/70% r. h. Here the water intake of a triple metallized film amounts to 10 $g/(m^2 \cdot a)$, which is less than half of the result obtained during the half year storage of the real silica VIP samples. The higher value may be due to pin holes

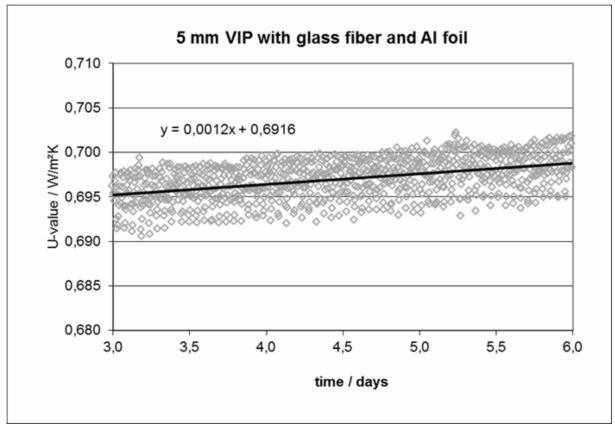

Fig. 6 Thermal conductivity change ofa silica VIP

at the corners and envelope folds. For Al foil laminates water vapor intake was measured lower than 1 $g/(m^2 \cdot a)$.

6. Conclusions and outlook

It has been shown that with moderate climate conditions of 50 ℃ and 70% humidity relevant aging properties of silica VIPs can be obtained after 6 months of storage. In combination with Arrhenius relations for the air and water vapor permeation the derived values can in principle be extrapolated to other climate conditions. The mean thermal conductivity during service life of e. g. 25 years thus can be calculated in a convincing way.

Thermal conductivity increase of VIPs with glass fiber core material and weight increase of thin laminate bag samples with dryer inside allow resolutions of up to 0.001 $cm^3/(m^2 \cdot a)$ for air permeation and 0.001 $g/(m^2 \cdot a)$ for water vapor diffusion.

Acknowledgements

For the financial support the authors acknowledge the European Commission in the frame of the projects NANOINSULATE, ELISSA and RESSEEPE.

References

[1] SchwabH, et al., Journal of Thermal Envelope and Building Science 2005;28 319 - 326.

[2] Simmler H et al. Energ. Buildings 37 (2005) 1122 - 1131.

[3] Brunner S et al. Vacuum 82 (2008), 700 - 707.

[4] Brunner S. IEA EBC Annex 65 Kick-off meeting, Grenoble Sept2014.

[5] Caps R et al. Vacuum 82 (2008) 691 - 699.

Quality Control of Vacuum Insulation Panels: An Instrument for Measuring Internal Pressure

Zheng Qing, Chen Zhaofeng*, Zhu Wanping

Super Insulation Composite Laboratory, College of Materials Science and Technology,
Nanjing University of Aeronautics and Astronautics, Nanjing, 210016, P.R. China.

Abstract

Vacuum insulation panel(VIP)is mainly rely on its internal vacuum degree to improve the thermal insulation performance. Because the internal pressure value is the most important physical parameters of the characterization of vacuum insulation panels' insulation performance, it is therefore very important to measure the internal pressure of vacuum insulation panel accurately. It is helpful to guarantee both quality and quantity of the vacuum insulation panels, and then can be widely used at many situations where heat insulation is needed. In the research of vacuum degree of vacuum insulation panels testing technology, this article devotes to the study of one instrument which can measure the value of internal pressure. The instrument presented here can be used to measure the internal pressure of vacuum insulation panels, which is suitable for hard core materials. It can determine whether the vacuum insulation panels are qualified quickly. The instrument is manufactured by vacuum, CAM drive, sensor measurement and electric control systems. The mechanical part of CAM transmission is used as the core. Vacuum pump, laser distance measuring instrument, vacuum gauge and barcode printer. These functional components are controlled by single chip microcomputer to realize the automation. The presented method is newly-developed, more efficient and has the advantage of green environmental protection. It has been successfully developed to non-destructively evaluate the pressure in the vacuum insulation panels, fabricated on industrial scale, and is essential for reliable quality control of vacuum insulation panels.

Keywords vacuum insulation panels, rapid detection, internal pressure measurement, thermal conductivity

1. Introduction

Vacuum insulation panels (VIPs) is a grade A1 Non-combustible super efficient thermal insulation material. It is based on the vacuum insulation principle, by filling the core layer of porous thermal insulation material. It can improve the vacuum degree within the panels to the maximum extent in order to prevent the thermal conduction and then achieve the purpose of heat preservation and energy saving [1]. VIPs are widely used in refrigerators, freezers, cold storage, building wall insulation, vessels, ships, automobile, electric water heater, etc [2]. Its coefficient of thermal conductivity is about 1～3mW/(m·K). The traditional material includes Foam Concrete, EPS, XPS, PUR, PF, Mineral Wool and theirs' thermal conductivity are far beyond the VIP.

Nowadays, at the VIP inspection area, there are two sets of scientific characterization of vacuum insulation panels insulation performance of the system, measuring the thermal conductivity and inner pressure [3]. Firstly, coefficient of thermal conductivity can be a very accurate characterization of the VIP adiabatic performance, and it is a very important parameter. The heat load is calculated by the coefficient of thermal conductivity and provides the basis for choosing the refrigeration or heating equipment system, then the VIP can be applied to a better heat insulation of various

* Corresponding auther, Tel: 86-25-52112909, E-mail:zhaofeng_chen@163.com

needs. There are many ways of measuring heat conductivity coefficient, but the basic principles are similar, plate heat flow meter method [4]. Secondly, the methods of measuring inner pressure are divided into two parts: Sensor inside and Sensor external. Sensor inside mainly includes thermal infrared imaging method, spining rotor gauge, remote sensing of VIP quality, capacitance-type sensor, thermal detector etc. Sensor external includes denotation method of vacuum gauge and vacuum chamber method [5].

2. Testing principle

This vacuum insulation panel inner pressure measuring instrument adopts the inverse method of vacuum principle. By manufacturing an equal or smaller external pressure than vacuum insulation panel's internal pressure, the envelope of VIP is displaced, and the laser range finder is monitoring this displacement everytime. When this displacement changes suddenly, the external pressure of VIP is equal to internal pressure. In order to prevent the deformation of the core material from affecting the experiment, we use a set of up and down probe and make a balance on the core material. We will use a double serial data program into single chip microcomputer and at the same time record the T time laser rangefinder and vacuum gauge data transmission. In addition to single chip microcomputer and computer connection, then in the computer through serial port data read software to generate Distance-Pressure curve. It captures the moment of membrance summoned visually and records at the time of corresponding pressure value.

3. Design of the measuring instrument

The measuring instrument is composed of Laser distance measuring instrument, ZDR Vacuum gauge, Pirani gauge, Vacuum pump, Barcode printer. The vacuum insulation panel inner pressure measuring instrument, from its side view and front view, the instrument has a set of vacuum probe.

Controlled by single-chip microcomputer, liquid crystal display, display panels, electromagnetic valve, resistance gauge, a laser range finder, electrical automation system composed of bar code reader, it can be connected to the computer data line interface, bar code printer interface and vacuum machine interface.

The device is a side view of a hollowed rectangular trapezoidal control panel oblique angle of 90° from the horizontal; the upper and lower vacuum in each vacuum probe with a probe diameter 50mm, consistent alignment; all vacuum probe and the interface is connected with a vacuum machine, all equal vacuum pressure probe; the resistance gauge, control panel, laser range finders and barcode reader from the data collected through the microcontroller operation, the output to the bar code printers, computers and LCD screens. MCU can control the rise and fall of vacuum probe control, solenoid valve to open and close, the control resistance gauge, a laser range finder, barcode reader and regulation of electricity and power resistors. Vacuum probe is composed of the CAM drive mechanism, the lever mechanism sucker and stop rings. The down vacuum probe is equipped with a resistance gauge, laser range finder, down sucker and 2mm clear glass, wherein the laser range finder distance of 27mm from the test plane. Pressure within the vacuum insulation panels measuring instrument design is shown in 1(a) as shown; Pressure measurement in the vacuum insulation panel meter prototype kind is shown in 1(b) as shown.

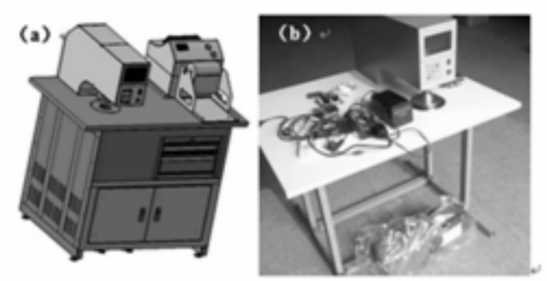

Fig. 1 Within the VIP pressure gauge

(a) Design picture; (b) prototype physical picture

4. Measurement data cure processing

In the measuring instrument commissioning process, Fumed silica core samples are used for testing and debugging the VIP gauge. For the different types core material of VIP, the impact of changes in internal pressure by the thermal conductivity is different. In the high vacuum state, the glass fiber material has the lowest thermal conductivity compared to other insulating materials. However, when the vacuum pressure exceeds

100Pa, the thermal conductivity of the glass fiber increases rapidly. For precipitated silica and pyrogenic silica core material, less vacuum pressure at 1000Pa, the pressure increases and the thermal conductivity is low. The fumed silica VIP is shown in Fig. 2, the fumed silica core VIP sample 1# Distance-Pressure Curved and local curve are showed in Figure 3 and Figure 4 respectively.

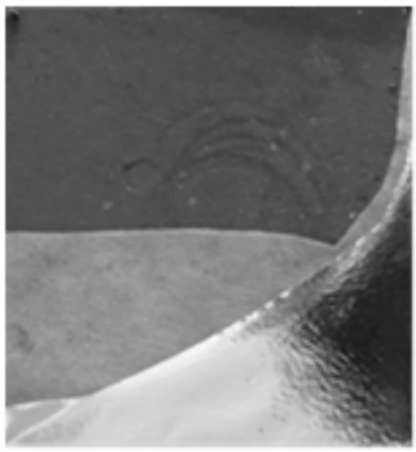

Fig. 2 The fumed silica VIP(1#)

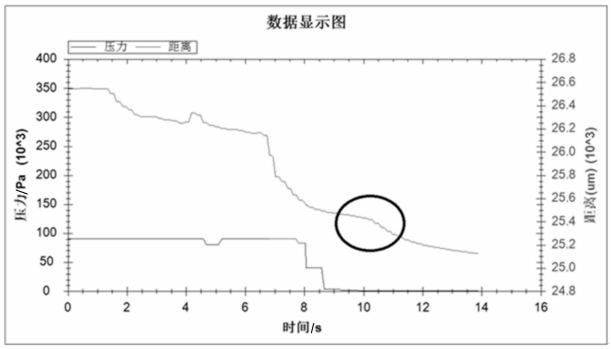

Fig. 3 The fumed silica core VIP sample 1# Distance-Pressure Curved

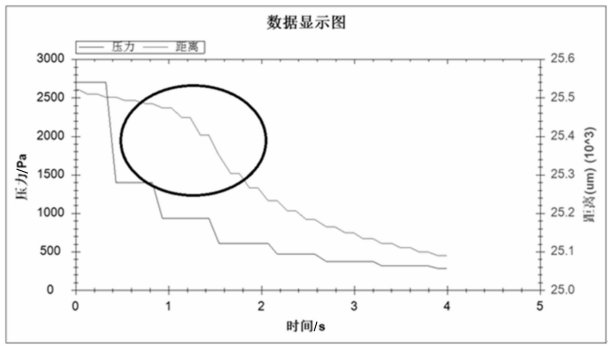

Fig. 4 Sample 1# Distance-Pressure Local curve

From the Fig. 4 distance curve, it can be seen that the turning point doesn't occur, due to the suction cup and VIP weren't pressed firmly and the fluctuations occurred in the first half. Air leaks and manual pressure are caused by the fluctuation, the rear section sucker has sucked the VIP panel firmly, the curve experiences a turning point, not a period of smooth curve. When we enlarge the curve, we can find the inflection point corresponding to the pressure values between 500 ~ 1500Pa easily and corresponds the true value range of the internal pressure. So we can initially determine the inflection point, the film is mustered by the pressure diffence.

In order to obtain a vacuum insulation panel pressure gauge precision index, the subject of using the measuring instrument with a fumed silica VIP(#1) in the pressure test track is done repeatedly[6]. Table 1 is a comparison of the obtained measurements and epitaxial gauge "Super Bee" true value.

Tab. 1 The comparison of the measured value and real value

Number	Measured Value/Pa	Real Value/Pa	Difference/Pa	Relative Error/(%)
1	999	1023	−24	2.34
2	1052	1023	31	3.03
3	1029	1023	6	0.59
4	1001	1023	−22	2.15
5	972	1023	−51	4.99
6	1028	1023	5	0.49
7	1098	1023	76	7.43
Average	1025.57	1023	2.57	

From Tab. 1 we can see this instrument is not high precision, but the testing numbers are all correct. Therefore, description meter has basically eliminated the systematic errors and still produces occasional errors.

5. Conclusions

This topic has successfully developed a prototype within a pressure gauge, detecting a VIP only 8～12s. The gauge is efficient, and the testing process does not damage VIP, belonging to non-destructive testing areas. Principle proof of meter, functional analysis, mechanical design, electrical design, assembly, commissioning, data processing, analysis, measurement error analysis and pyrogenic silica VIP course experiments. The following conclusions can be drawn:

(1) The testing efficiency of VIP pressure gauge is 8 ～ 12s / piece, the range is 50 ～ 10^5 Pa, the detection error is less than 30% of the theoretical equal to the real value, the error of the measured range is 12.42%;

(2) Collecting data from a vacuum gauge and a laser range finder measured, dual serial data reading software to generate Distance－Pressure curve. Distance appears on the curve inflection point the only time recorded on the Pressure curve corresponding pressure value at this time, then this pressure value is the testing result, equal to VIP's internal pressure.

(3) Whentesting fumed silica core VIP, fumed silica powder core material has virtually no resilience. Inflection point occurs near the true value of the pressure during the test curve including distance, this test verifies the inverse vacuum method of scientific principles. This instrument can measure the fumed silica core VIP's interior pressure.

Acknowledgement

The authors would like to thank Mr. Wang Xuhu and Hongtai equipment Co. Ltd. to help us produce the instrument for measuring VIP internal pressure.

References

[1] XiaoBo Di, CongGao Bao, YiMin Gao. Study on the relationship between the degree of vacuum in the vacuum insulation panel thermal conductivity and board [J]. Vacuum. 2011, 48(3):12－15.

[2] Simmler H, Brunner S. Thermal properties and service life of vacuum insulation panels (VIP)[C]//Proc. of the 4th Europ. Conf. on Energy Perform. a. Indoor Climate in Build. (ENTPE), Lyon. 2006: 1－6.

[3] AiChun Li, Steady—state heat flow meter method thermal conductivity coefficient of thermal conductivity meter test based panels[J]. Nanjing Forestry University: Natural Science, 1997, 21(3):99－102

[4] ZhengGuoWang, ZiZhu Dai. Determination of thermal conductivity with the heat flow meter type thermal conductivity meter[J]. Construction Chemicals, 1995, 3.

[5] Caps R. Determination of the gas pressure in an evacuated thermal insulating board (vacuum panel) by using a heat sink and test layer that are intergrated therein: U. S. Patent 7,400,999[P]. 2008－7－15.

[6] Jung H, Jang C H, Yeo I S, et al. Investigation of gas permeation through Al-metallized film for vacuum insulation panels[J]. International Journal of Heat and Mass Transfer, 2013, 56(1): 436－446.

The Impact of Barrier Laminates on Thermal Property and Service Life of Vacuum Insulation Panels

Kan Ankang*, Wang Chong, Cao Dan

Merchant Marine College, Shanghai Maritime University, Shanghai, 201306, P. R. China

Abstract

As a high-performance thermal insulation method for energy conservation purpose, Vacuum insulation panels (VIPs) have been widely applied in various fields. However, the service life, that is, thermal performance versus time, is an interesting focus for researchers, manufacturers and users. Rarefied gas pressure inside the panel represents the vital influence on thermal insulation performance. The barrier laminate is explored to analyze the aging of service life. The primary objective of this work is to theoretically define the service life of VIPs, and the impact factors are respectively analyzed. The effects of gas & moisture permeation through the barrier laminates, on the effective thermal conductivity of VIPs are studied. Three typical barrier laminates, AF, MF1 and MF2 are introduced and the properties parameters are measured. Taking them as the envelopes, the VIPs are analyzed for the tendency of the effective thermal conductivity changes. The service life is numerical analyzed and predicted. Accelerated ageing tests are taken to support theoretical predication model at 70℃ & 80%RH or under 800kPa high exterior air pressure.

The comparison of simulation work and the accelerated aging experiments show that the VIPs are durable and high quality for energy conservation purpose. And the optimization methods according to authors' research are also given to prolong the service life of VIPs.

Keywords VIPs, barrier laminates, effective thermal conductivity, service life, analysis model

1. Introduction

VIPs, as the most effective thermal insulation materials up to now, are already widely used in many fields, for building energy conservation (insulation of building envelopes, trail house), for refrigeration cargo storage and transportation (insulation of the doors and side walls of refrigerators, reefer containers, railway containers, storage tanks and other vehicles), for the insulation of various construction elements, such as air conditioning ducts, heater, furniture and so on [1 - 3]. The thermal efficiency of VIPs is almost ten times better than that of conventional insulating materials and the thermal conductivity can be lower than 0.0030 W/(m • K)[4]. This means that high thermal resistance can be achieved with an extremely small thickness of VIPs. So the building designers can gain much space, especially since the net volume of envelope is much smaller [5]. Generally the vacuum is the key aspect of the thermal property of VIPs, the vacuum creating and keeping is a vital task for the VIPs. Special multilayer films, taken as VIPs barrier envelopes, should guarantee air tightness against almost all atmospheric gases and vapor to prevent the permeation of air and moisture. The properties of the barrier laminates are crucial for the VIPs resistance to ageing [6 - 10].

However, the thermal conductivity is not constant but rises with the time. The atmospheric gases and vapor gently permeate into the VIPs through barrier laminate and lead to the air pressure rising inside the core materials, causing the thermal conductivity going up and thermal property deterioration [6]. Barrier

* Corresponding author, Tel: 86 - 21 - 38282971, E-mail: ankang0537@126.com

laminate is mainly used to prevent the diffusion of atmospheric gases and vapor to keep the vacuum inside VIPs. The quality of the barrier is the important factor for the insider vacuum-keeping and service life [7]. The thin stainless steel was used as gas barrier for early VIPs [8]. But it was gradually replaced by multilayer barriers for its high thermal bridge effect [9]. And high quality foils have recently entered the market. Now, the wide application forms of gas barriers are metal films and metalized polyester films [10].

Theoretical and experimental researches were taken by many researchers [6 - 10]. The development and improvement of the barrier membranes promotes the thermal performance and the durability of VIPs, but the failure of VIPs was not clearly defined by all the literatures mentioned above. The standard service life of VIPs, referred in ASTM C 1484 — 01 [9], can be measured under the condition that, the VIPs surrounding average temperature is 24℃ while the relative humidity 50%. The proceeding time, that is, the value at which the center thermal conductivity reaches to 0.011495 W/(m • K), is the standard service life of VIPs. When the conductivity is higher than that value, the decision can be made that the VIPs fail.

The numerical method that was used in this paper aimed at theoretically evaluating the degradation of VIPs. The ageing mechanism of VIPs was introduced and the accelerated ageing experiments for VIPs samples with three typical barriers were taken to compare the results with the numerical prediction. The understanding on the impact of barrier laminates on the service life of VIPs enhanced in this research.

2. The effective thermal conductivity of VIPs

The thermal conductivity in this research work is collected based on the standards GB/T3399—2009 and ASTMC1484—01. The function of thermal conductivity versus times can be described as [9,10]:

$$\lambda_e(\tau) = \lambda_{ini} + \lambda_g(\tau) + \lambda_{wv}(\tau) \quad (1)$$

Where, $\lambda_e(\tau)$ is the thermal conductivity of VIPs versus time going (W/(m • K)); λ_{ini} is the initial thermal conductibility of VIPs (W/(m • K)); $\lambda_g(\tau)$ is the additional increase value of thermal conductivity caused by permeation of gases with the time going (W/(m • K)); $\lambda_{wv}(\tau)$ is the additional increase value of thermal conductivity caused by permeation of vapor with the time going (W/(m • K)).

2.1 Additional increase value of thermal conductivity caused by permeation of gases

When air pressure inside is achieved at 0, the gas conduction would approach 0. This is the so-called the Knudsen effect. The mean free path length of the gas molecules increases as the pressure decreases. The influence on rarefied gas effective conductivity $\lambda_{e,g}$ from the Knudsen effect can be determined as [5]:

$$\lambda_{e,g} = \frac{\lambda_{g,0}}{1 + 2\beta k_n} \quad (2)$$

Where, $\lambda_{g,0}$ is the free gas thermal conductivity at the normal condition, W/(m • K), here $\lambda_{g,0}$ =0.023 W/(m • K); β is the constant to characterize the energy transfer efficiency when the collision between gas molecules and solid-state pore walls occurs, and the value is always 1.5～2.0 according to the temperature, the gas type and the core materials, here β =1.5; k_n is the Knudsen number, equal to the ratio of mean free path of air l_m (m) to the pore feature size δ (m), as shown in equation(3):

$$k_n = \frac{l_m}{\delta} \text{ and } l_m = \frac{k_B T_m}{\sqrt{2}\pi d_g^2 p_g} \quad (3)$$

Where, T_m is the mean temperature of core materials in Kelvin scale, K; d_g is the mean diameter of air molecule, m, here $d_g = 3.72 \times 10^{10}$ m; k_B is the Boltzmann's constant and $k_B = 1.38 \times 10^{10}$ mJ/K; p_g is the rarefied gas pressure inside the panel, Pa; τ is the time, s. So the gaseous heat conduction in porous media can be written as:

$$\lambda_{e,g} = \frac{\lambda_{g,0}}{1 + \frac{\sqrt{2}\beta k_B T_m}{\pi d_g^2 \delta_g}} \quad (4)$$

Gas transmission

An empirical value is employed in this research work to describe the gas transmission ability. This value is referred to as the gas transmission rate (*GTR*), $cm^3/(m^2 \cdot d)$. And the value is determined by the materials and temperature, humidity and joint heat sealed quality. However, the value offered by the manufacture is Oxygen Transmission Rate (*OTR*), $cm^3/(m^2 \cdot d)$ or $cm^3/(m \cdot d)$. *OTR* specifies how

much of oxygen permeates the area or line of barrier during a given time. Although the oxygen takes only 21% in the air, and its partial pressure is 1/4 of that of nitrogen, the oxygen is a very active gas and its barrier permeating ability is 5 times than that of nitrogen[7]. The total GTR can be defined as[8]

$$GTR_{tot} = GTR_A A_{VIP} + GTR_C C_{VIP} = (OTR_A + OTR_A/5)A_{VIP} + (OTR_C + OTR_C/5)C_{VIP} \quad (5)$$

where, GTR_A is the surface GTR of the barrier cover per VIPs area, $cm^3/(m^2 \cdot d)$; GTR_C is the linear GTR of the barrier per VIPs along the circumference, $cm^3/(m \cdot d)$; OTR_C is the surface OTR of the barrier cover per VIPs area, $cm^3/(m^2 \cdot d)$; A_{VIP} is the linear OTR of the barrier per VIPs along the circumference, $cm^3/(m \cdot d)$; A_{VIP} is the total surface area of VIPs, m^2; C_{VIP} is the length of circumference, m.

However, the air pressure difference plays an important role in the GTR. The Q_g specifies the volume changes with the air pressure difference.

$$Q_g = \frac{GTR_{tot}}{\Delta P} \quad (6)$$

The air pressure increasing rate as the gas permeance is described as

$$\frac{dp_g}{d\tau} = \frac{p_0 Q_g (p_0 - p_g) T_m}{T_0} \frac{T_m}{V_e} = \frac{GTR_{tot,air}}{V_e} \frac{T_m}{T_0} (p_0 - p_g) \quad (7)$$

where, V_e is the volume summation of the micro volume of all pores in the VIPs, m^3, the value depending on the core materials type; T_m is the mean temperature of the core materials under the measurement condition, K; T_0 is the standard normal condition depending on the air pressure p_0, K_0

Eq. (7) can be solved analytically to give an expression for internal pressure as a function of time and external pressure

$$p_g(\tau) = p_0 - (p_0 - p_{ini}) e^{\frac{T_m GTR_{tot,air}(p_0 - p_{ini})}{T_0 V_e}} \quad (8)$$

where p_0 is the applied external pressure , Pa; p_{ini} is the initial internal gas pressure of VIP ,Pa.

Combined with Eqs. (4) and (8), additional increase value of thermal conductivity caused by permeation of gases can be described as:

$$\lambda_g(\tau) = \frac{\lambda_{g,0}}{1 + \frac{\sqrt{2}\beta K_B T_m}{\pi d_g^2 \delta [p_0 - (p_0 - p_{ini}) e^{\frac{T_m GTR_{tot,air}(p_0 - p_{ini})\tau}{T_0 V_e}}]}} \quad (9)$$

2.2 Additional increase value of thermal conductivity caused by permeation of vapor

An empirical value called Moisture Vapor Transmission Rate (MVTR) is employed. The MVTR specifies how much of vapor permeates the unit area or line of barrier cover a unit time, $g/(m^2 \cdot d)$ or $g/(m \cdot d)$. The vapor mass increasing rate can be defined as [10].

$$\frac{dm_{mv}}{d\tau} = MVTR_A \times A_{VIP} + MVTR_C C_{VIP} = \Delta p_{mv} \times Q_{wv,tot} \quad (10)$$

where, m_{mv} is the increased moisture mass, g; $MVTR_A$ is the surface $MVTR$ of the barrier cover per VIPs area, $g/(m^2 \cdot d)$; $MVTR_C$ is the linear $MVTR$ of the barrier per VIPs along the circumference, $g/(m \cdot d)$; Δp_{mv} is the partial vapor pressure difference between internal and external VIPs, Pa; $Q_{wv,tot}$ is the total vapor permeating through the barrier foil, $g/(d \cdot Pa)$.

The partial vapor difference can be calculated by:

$$\Delta p_{mv} = p_{mv,out} - p_{mv,in} = (\varphi_{out} - \varphi_{in}) p_{mv,satu,T_m} \quad (11)$$

where, $p_{mv,out}$, $p_{mv,in}$ are respectively external and internal partial vapor pressures, Pa; $p_{mv,satu,T_m}$ is the vapor saturation pressure depending on the VIPs mean temperature T_m , Pa; here the value is 2980Pa; φ is the relative humidity.

The vapor sorption ability of core materials has a linear relationship as the following:

$$x_{mv} = \frac{m_{mv}}{m_{VIP,dry}} = K\varphi_{in} \quad (12)$$

where, x_{mv} is the mass ratio that the mass of vapor permeating into the core materials to the mass of the dry VIPs; $m_{VIP,dry}$ is the mass of dry VIPs, g; K is a constant to represent the ability of vapor sorption of core materials and here $K = 0.0008$ [10].

As the initial boundary condition, $x_{mv}(\tau = 0) = 0$, the vapor increasing mass ratio to mass of dry VIPs cover a given time can be calculated by:

$$x_{mv}(\tau) = K\varphi_{out}(1 - e^{\frac{(MVTR_A A_{VIP} + MVTR_C C_{VIP}) p_{mv,stam,t_m}}{K m_{VIP,dry}}}) \tau \quad (13)$$

The conclusion can be made from Eq. (13). So the additional increase value of thermal conductivity caused by permeation of vapor can be gotten by:

$$\lambda_{nv}(\tau) = b x_{mv}(\tau) =$$

$$Kb\varphi_{\text{out}}\left(1-\mathrm{e}^{-\frac{(MVTR_{\text{A}}A_{\text{VIP}}+MVTR_{\text{C}}C_{\text{VIP}})p_{\text{mv,stau}}T_{\text{m}}}{Kn_{\text{VIP,dry}}}\tau}\right) \tag{14}$$

where, b is a variable in W/(m · K), gotten from experiment and here $b=0.050$ W/(m · K).

2.3 Effective thermal conductivity prediction model of VIPs

Combined with Eqs. (9) and (14), the Effective thermal conductivity prediction model as a function of time can be gotten as:

$$\lambda_{\text{e}}(\tau)=\lambda_{\text{int}}+\frac{\lambda_{\text{g,0}}}{1+\dfrac{\sqrt{2}\beta K_{\text{B}}T_{\text{m}}}{\pi d_{\text{g}}^{2}\delta\left[p_{0}-(p_{0}-p_{\text{ini}})\mathrm{e}^{\frac{T_{\text{m}}OTR_{\text{tot,air}}(p_{0}-p_{\text{ini}})}{T_{0}V_{\text{e}}}\tau}\right]}}+Kb\varphi_{\text{out}}\left(1-\mathrm{e}^{-\frac{(MVTR_{\text{A}}A_{\text{VIP}}+MVTR_{\text{C}}C_{\text{VIP}})p_{\text{mv,stau}}T_{\text{m}}}{Kn_{\text{VIP,dry}}}\tau}\right) \tag{15}$$

With the time going under a certain boundary condition, while the $\lambda(\tau)\geqslant 0.011495$ W/(m · K), the VIPs can be defined failure and the corresponding time τ is so called service life of VIPs.

3. Composition and property parameters of barrier laminates

3.1 The composition of barrier laminates

For the barrier envelope purpose, the gas-tight layer, thermal resistive layer and heat seal layer should be involved. There are two typical barrier membranes widely used as VIPs envelope. i.e. laminated aluminum foils(AF) and metalized polymer films (MF). The three typical barrier films, widely used as VIP envelopes, are introduced in this research, and the section structures of the barriers, namely as AF, MF1, MF2, are shown in Fig. 1, respectively.

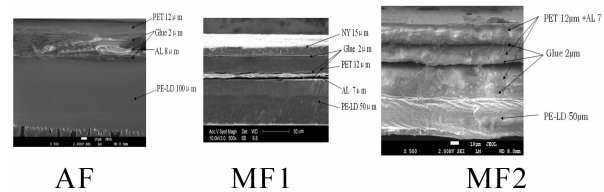

Fig. 1 The SEM pictures for micro section of 3 typical barrier laminates

3.2 The physical parameters of the barrier laminates

The anti gas permeability and the anti moisture permeability of the barrier membrane can be measured by the GTR and MVTR of the surface and sealed joints of the barrier membrane. The physical parameters of the three typical barrier laminates are collected in Tab. 1, including the data source or testing methods.

Table. 1 The parameters of barrier laminates

Properties	Barrier laminate materials			Source or Test Methods
	AF	MF1	MF2	
Thickness /μm	124	90	113	
OTR_A / (cm³/(m² · d))	0.0013	0.0009	0.0004	ASTM D3985 (23℃,50%PH)
OTR_C / (cm³/(m · d))	0.0015	0.0067	0.0033	ASTM D3985 (23℃,50%PH)
$MVTR_A$ / (g/(m² · d))	0.0005	0.0192	0.0048	ASTM F1249—90 (38℃,100%PH)
$MVTR_C$ / (g/(m · d))	0.0012	0.0008	0.0006	ASTM F1249—90 (38℃,100%PH)
Thermal diffusion coefficient /(mm²/s)	0.132	0.119	0.116	NETZSCH LFA(25℃)
Thermal conductivity /(W/(m · K))	0.230	0.221	0.256	NETZSCH LFA(25℃)

The superfine glass fiber was selected as core materials and three VIPs were made, with the three typical barrier membranes as envelopes and the dimensions of the VIPs are all 300×300×20mm³.

4. The results and discussion

4.1 The simulation results and discussion

Assumed that the VIP service environment is standard atmospheric pressure, the mean temperature,

24℃, the relative humidity, 50%. The theoretical prediction of the three VIPs with the different barriers is shown in Fig. 2.

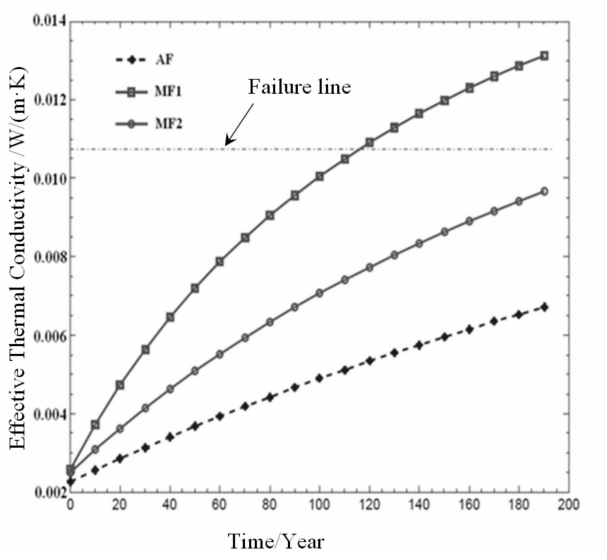

Fig. 2 The theoretical prediction for service life of the three VIPs

The red line in Fig. 2. is the failure limited effective thermal conductivity value, means the value reaches to 0. 011495 W/(m · K). Under the experimental boundary condition according to the testing standard, the VIPs with the barrier laminate AF can maintain the effective adiabatic property for a long time in theoretical prediction model, exceeding 200 years. The next is the VIP with the barrier laminate MF2, a little more than 200 years. The shortest one is the VIP with the barrier MF1, 115 years.

The conclusion also can be made associating with the barrier structure in Fig. 1. , the increasing thickness of aluminum foil layer (s) means the longer service life of VIPs. The aluminum foil is a good gas barrier material and is a vital impact factor for maintenance of VIPs thermal stability and endurance, namely, service life. In fact, the increasing thickness of aluminum foil layer(s) always results in the thermal conductivity rising and the thermal bridge effect increasing [6].

4. 2 The testing results and discussion

The temperature and the air pressure are the main variable values influencing the two rates. In order to prove our theoretical prediction model, the constant temperature and humidity box and pressured box are involved in this research, and the aging testes are taken.

Aging test in high temperature

The three typical VIPs with the different barrier envelopes, namely AF, MF1, MF2, were involved in the constant temperature and constant humidity box. The setting temperature was 70℃ and the relative humidity, 80%. And the setting condition was keeping for 30 days. The data was collected in Tab. 2. The comparison between theoretical results and testing results was also calculated.

Tab. 2 Aging test results in constant temperature & humidity box and the comparison with theoretical results

Specimens	Barrier envelopes	Initial thermal conduction/ (W/(m · K))	Aging condition		Final thermal conductivity/(W/(m · K))	Theoretical thermal conductivity /(W/(m · K))
			T℃	RH /%		
1	AF	0. 00225	70	80	0. 00253	0. 00241
2	MF1	0. 00256	70	80	0. 00277	0. 00267
3	MF2	0. 00249	70	80	0. 00274	0. 00262

Compared with aging test results and theoretical results in Tab. 2, the agreement is ideal even with a little deviation. The reason is that, the gas and vapor released by the barrier itself and core material itself is ignored in Eq. (15). And the gas and vapor released into VIPs will deteriorate its thermal performance, resulting in the increase of thermal conductivity. The glass fiber, as the core material, resolves its water of crystallization under the vacuum condition, causing the main deviation in the comparison.

Aging test in high air pressure

Another 3 VIPs samples with the 3 typical barrier membranes were prepared for the aging test in high air pressure. The initial thermal conductivities λ_i and thicknesses d_i of the VIPs samples were measured before the high air pressure testing. The initial temperature in box was 25℃, and relative humidity 50%. Then the box was pressured to 800kPa, and the condition was kept for

30 days. The finial thermal conductivities λ_f and the finial thicknesses d_f were measured after the high air pressure testing. The theoretical thermal conductivity λ_t calculated by the prediction model were also collected to make comparison with the testing in Tab. 3.

Tab. 3 Comparison with the testing data and theoretical calculation values in high air pressure aging test

Specimen	Barrier envelopes	d_i/mm	λ_i/ (mW/(m·K))	d_f/ mm	λ_f/ (mW/(m·K))	λ_t/(mW/(m·K))
1	AF	19.5	3.14	16.8	4.53	4.52
2	MF1	19.3	3.32	16.6	4.92	4.57
3	MF2	19.0	3.33	16.3	4.43	4.25

As the vapor that transmitted into the VIPs in the pressured air box was ignored, the deviation was present between the measured value and the theoretical calculated value. However, the changes of VIPs thickness always cause the thermal conductivity deviation with that in pressured air box and that in the real standard environment condition. The aging testing in high air pressure box can be used to evaluate the accuracy of our prediction model.

5. The optimization methods to prolong the service life of VIPs

The vital impact factor of the service life is the vacuum degree in VIPs, and the barrier envelope is the key shield for the gas and moisture permeation. So the properties of the barrier membranes are important to prolong the service life. Based on the analysis of barrier laminate above, some optimization methods for the improvement of VIPs thermal performance are given by the authors.

Metallic foils are good for anti gas and moisture permeability but cause big thermal bridge. Plastic films have advantage in low thermal bridge effect but disadvantage in OTR and GTR. Metal and plastic composite films are always taken as the barrier laminates.

The barriers are so thin that they are easy to be mechanically damaged. Once the barriers are damaged, the vacuum in VIPs vanishes instantly. The thermal conductivity will increase 5 times larger than that of the previous, and the VIPs fail. The protection from mechanical damage should be taken in the transporting and installation operation.

The huge air pressure difference between internal and atmospheric promotes permeation of gas and moisture into VIPs. Nesting barriers design was developed by authors and effectively envelopes are innovated to prolong the service life. Core material layers are separated into several independent chambers. The outmost chambers are placed a few getter or not to absorb residual gas, if any. As the tiny air pressure difference between the outmost chamber and the second chamber, the gas permeating from the outmost chamber to the second chamber is slim or negligible. In this manner, the center chamber can be in vacuum state for a very long life.

6. Conclusions

As one of important components of VIPs, the barriers laminate plays an essential role in the adiabatic performance maintenance and endurance keeping of VIPs. The parameters, such as OTR, MVTR, etc. are introduced and the service life prediction model is established. The typical 3 barriers, that is, AF, MF, MF2, are involved in this research to collect the property parameters. 3 VIPs with superfine fiber glass as core materials and 3 barrier laminate as envelopes are made for aging test. The testing results and the theoretical prediction results are compared. The optimization methods for prolong service life are also given by the authors according to the barriers analysis.

(1) Aluminum foils, the good gas barrier materials, are indispensable part for VIPs barrier envelopes. There should be one aluminum layer existing in barrier laminates.

(2) The barrier laminates, can maintain the vacuum degree in VIPs, but also can cause thermal bridge effect to reduce the adiabatic performance. The thickness of the aluminum layer(s) should be decided by the application conditions, the system, and the service

life of the unit.

(3) Taking the theoretical prediction model into consideration, the service life of VIPs is the function of barrier laminates, the core materials, the internal vacuum degree, getter and desiccant, the application condition, and so on. The real temperature, air pressure, relative humidity, imported into the mathematics model, can be used to predict the real service life.

(4) The service life can be prolonged by the raw materials selection, the improvement of manufacturing, transportation and installation craft, nesting design of barrier envelopes, outside protective layer(s), and so on.

Acknowledgements

The work is financially supported by the Natural Sciences Foundation of Shanghai, China (15ZR1419900). The authors would also like to render thankfulness to the Jiangsu Sunkey Package Co., Ltd. and Fujian Super Tech Advanced Material Co., Ltd for the materials supply.

References

[1] Ruben Baetens, Bjϕrn Petter Jelle, Jan Vincent Thue, et al. Vacuum insulation panels for building applications: A review and beyond, Energy and Buildings. 4(2010),147—172.

[2] Roman Kunic, Vacuum Insulation Panels-An Assessment of the Impact of Accelerated Ageing on Service Life, Journal of Mechanical Engineering,58(2012)10. 598 - 606.

[3] Mathias Bouquerel, Thierry Duforestel, Dominique Baillis, Gilles Rusaouenb. Mass transfer modeling in gas barrier envelopes for vacuum insulation panels: A review. Energy and Buildings. 55 (2012) 903 - 920.

[4] H. Simmler, S. Brunner. Vacuum insulation panels for building application: Basic properties, aging mechanisms and service life [J]. Energy and Buildings. 37(2005)1122 - 1131.

[5] Martin Tenpierik, HansCauberg, ClimateDesignGroup. Analytical Models for Calculating Thermal Bridge Effects Caused by Thin High Barrier Envelopes around Vacuum Insulation Panels. Journal of Building Physics. 30(2007)3, 185 - 216.

[6] Haeyong Jung, Choong Hyo Jang, In Seok Yeo, Tae-Ho Song. Investigation of gas permeation through Al-metallized film for vacuum insulation panels. International Journal of Heat and Mass Transfer. 56(2013),436 - 446.

[7] Erlend Wegger, Bjϕrn Petter Jelle, Erland Sveipe1, et al. Aging effects on thermal properties and service life of vacuum insulation panels. Journal of Building Physics. 35 (2010) 2,128 - 167

[8] Hubert Schwab, Ulrich Heinemann, Andreas Beck. Prediction of Service Life for Vacuum Insulation Panels with Fumed Silica Kernel and Foil Cover. Journal of Thermal Envelope and Building Science. 28 (2005) 4, 357 - 374.

[9] ASTM standard: C 1484 — 01. Standard Specification for Vacuum Insulation Panels. West Conshohocken, United States. (2001).

[10] M. Alam, H. Singh, M. C. Limbachiya. Vacuum Insulation Panels (VIPs) for building construction industry-A review of the contemporary developments and future directions. Applied Energy. 88 (2011)3592 - 3602.

Defects in the Envelope Barrier of Vacuum Insulation Panels after Hygrothermal Aging in Severe Conditions

Florence Dubelley[a,b*], Emilie Planès[a,b], Corine Bas[a,b], Bernard Yrieix[c], Lionel Flandin[a,b]

a. Univ. Savoie, LEPMI, F—73000 Chambéry, France

b. CNRS, LEPMI, F—38000 Grenoble, France

c. EDF R&D, Matériaux et Mécanique des Composants, Site des Renardières, 77818 Moret-sur-Loing Cedex, France

Abstract

The use of VIPs for building application is limited by the degradation of the barrier performance of the envelope, especially at high temperature and humidity. The most critical component of a VIP is the envelope. It is responsible for preventing permeation in the core material. This multilayered materials is however sensitive to degradation. The effect of hydrothermal ageing was investigated thoroughly, leading to the identification of series of possible defects. In this paper, the flaws are presented and plausible explanations for their origin were given.

Keywords vacuum insulation panels, multilayer degradation, PET hydrolysis

1. Introduction

Our commercial barriers envelopes are assemblies of metallized PET and polyolefin (PE or PP). After a severe ageing at temperature close to the T_g of PET and at high relative humidity (close to 90 %RH), these multilayers present major defects at the macroscopic scale: delamination of the different interfaces and even breakup within the different polymeric layers (Fig. 1).

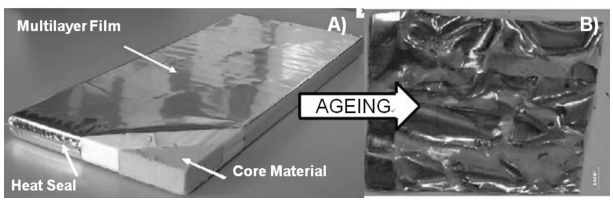

Fig. 1 A) Fresh vacuum insulation panel, B) a multilayer aged 870 days at 70℃, 90% RH

Hydrolysis of ester moieties is the most common degradation mechanisms in PET in these conditions. It usually results in the formation of carboxylic acids [1, 2] and chain scission [3]. Different characterization methods may be used to reveal these degradations [4 - 7]: the titration of the carboxylic acid, viscometry, DSC, or FT - IR spectroscopy.

FT - IR is probably the most versatile technique for this purpose. In addition one can probe the chemistry of each layer individually with a IR microscope. In this paper, we propose to establish a kinetic of the PET degradation based on FTIR analyses.

2. Experimental

Materials

The multilayer films are composed of a polyethylene (PE) or polypropylene (PP) layer assembled with three polyethylene terephthalate (PET) coated with evaporated aluminum. The different layers were glued together with a polyurethane adhesive.

Methods

Film ageing

The multilayers were exposed at 70 ℃ and 90 % RH in climatic chamber for various durations up to 870 days. A temperature close to glass transition

* Corresponding author, E-mail: Florence.dubelley@univ-savoie.fr

temperature T_g of PET was chosen to favor degradation.

Film Characterization

FTIR spectra were performed with a Perkin-Elmer spectrometer, Paragon 1000, equipped by a single reflexion device (PIKE Diamond MIRacle™, Pike Technologies, Madison) for ATR measurements. All scans were obtained in the 600～4000 cm^{-1} spectral region using a resolution of 4 cm^{-1} and 16 scans.

ATR－FTIR maps were collected with a Perkin Elmer Spotlight 400 system with germanium crystal connected to a Spectrum Perkin Elmer One spectrometer. Each spectrum was the average of 16 scans in the 700～4000 cm^{-1} wavelength region with 4 cm^{-1} resolution.

Differential Scanning Calorimetry (DSC)

The measurements were carried out on a DSC－7 instrument (Perkin-Elmer). The instrument was calibrated with an indium standard. The reference was an empty aluminium pan and the average mass of samples was comprised between 5 and 10 mg. The samples were heated from 30 to 300 ℃ at a scan rate of 10 ℃. min^{-1}. The amount of semi-crystalline phase in PET could be determined with the integrated signal of the melting peak. The area of this peak is proportional to the weight fraction χ_m (wt%) of crystalline polymer, as given by:

$$\chi_m = \frac{\Delta H_m}{\Delta H_m^{\infty}}$$

Where H_m is the enthalpy of the polymer specimen and H_m^{∞} is the enthalpy of completely crystalline PET (125 J. g^{-1} [3]). Nevertheless, it is necessary to use the volume crystallinity ratio χ_v (vol%) to perform a correlation between FTIR and DSC analysis:

$$\chi_v = \frac{\rho_{PETa} \times \chi_m}{\rho_{PETa} \times \chi_m + (1-\chi_m)\rho_{PETc}}$$

with ρ_{PETa} (equal to 1.337 [3]) and ρ_{PETc} (equal to 1.476 [3]) the density of the amorphous and totally crystalline PET phases.

3. Results and discussions

Fig. 2 and Fig. 3 represent spectra of outer PET layer of the barrier envelope for different ageing times between 3800～1800 cm^{-1} and 1800～600 cm^{-1} wave number ranges respectively.

Fig. 2 spectra of outer PET layer of the barrier envelope for different ageing times between 3800～1800 cm^{-1} stretching vibration range.

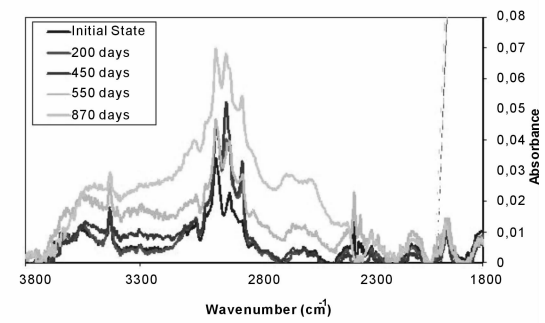

Fig. 2 Spectra of outer PET layer of the barrier envelope for different ageing times between 3800～1800 cm^{-1} stretching vibration range

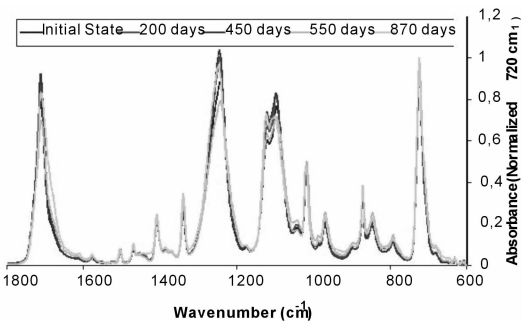

Fig. 3 Spectra of outer PET layer of the barrier envelope for different ageing times between 1800～600 cm^{-1}

FT－IR spectrometer

The infrared spectrometer used in this study is not polarized. Nevertheless, the spectrum was found to significantly depend on the angle of the incident beam with the sample (Fig. 4).

The effect is due to polarization induced by the ATR measurement in BOPET film. The effect of orientation might seem marginal at a first glance (Fig. 5), but the chemical degradation within the PET sample however only concerns a very small fraction of the ester bounds. One should thus start with a precisely defined sample and consider the orientation effect. The analysis were thus be carried out by varying the angle between the main direction of the sample and the incident beam from 0 ° to 360 ° with a step of 22.5°. From the radar chart plotted in Fig. 5, both maximum and minimum values were determined, for fresh and aged samples.

PET hydrolysis

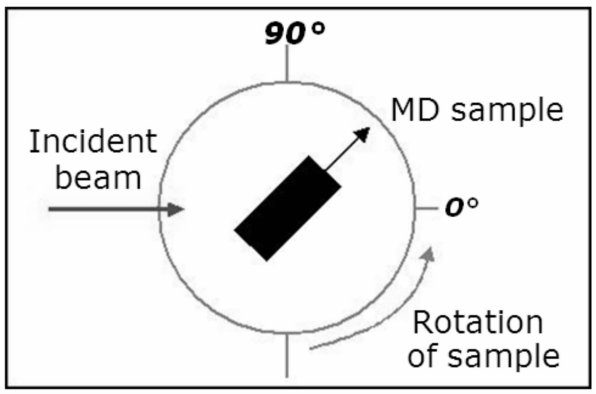

Fig. 4 Angle between the main direction of the sample—MD—and the direction of the incident beam

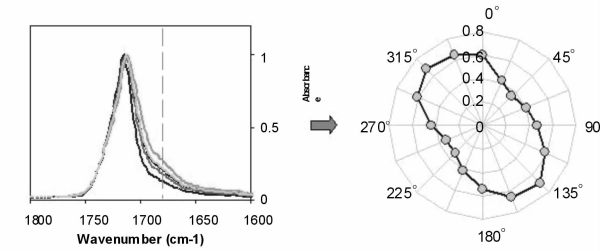

Fig. 5 PET spectra between 1800～1600 cm^{-1} for different angles and Intensity at 1696 cm^{-1} as a function of the incident angle

The absorption band around 1715 cm^{-1} can be assigned to the C＝O stretching vibration of ester group. A band at 1696 cm^{-1} grew in intensity with increasing ageing times. This peak shoulder is commonly assigned to the C=O stretching vibration of carboxylic acid [8]. The carbonyl index, defined as the ratio between the intensity at 1696 cm^{-1} and the intensity at 1715 cm^{-1}, characterized the PET hydrolysis. The results for the outer PET layer of the barrier envelope after different exposure durations are shown in Fig. 6.

The carboxylic acids have a second valence band, related to O—H stretching vibration around 3400～2400 cm^{-1}. The intensity of this band increased after 550 days ageing and indicated the PET hydrolysis. This result is in good agreement with the carbonyl index.

Other changes in the PET infrared spectrum are observed after ageing like theν(C—O—C) stretching vibration assigned to the ester around 1120 cm^{-1} and 1096 cm^{-1}. As can be seen in Figure 7, the intensity of the band with maximum at 1096 cm^{-1} decreased with time. This absorption band have been attributed to the gauche transition of ethylene glycol group, whereas, the band at 1120 cm^{-1} have been attributed to the trans transition [9]. Crystalline regions of PET are associated with the trans glycol conformation of the polymer repeat unit. Amorphous regions are associated with the gauche and the trans conformation [10]. The trans-gauche content of the outer PET layer of the barrier envelope after ageing was compared by examining the ratio of the peak intensities at 1120 cm^{-1} and 1096 cm^{-1}. An increase of this ratio with time indicates a crystallisation of PET. This increase in the crystallinity ratio is also confirmed by DSC experiments. This crystallisation under severe ageing conditions is likely to result from the scission of the PET macromolecules.

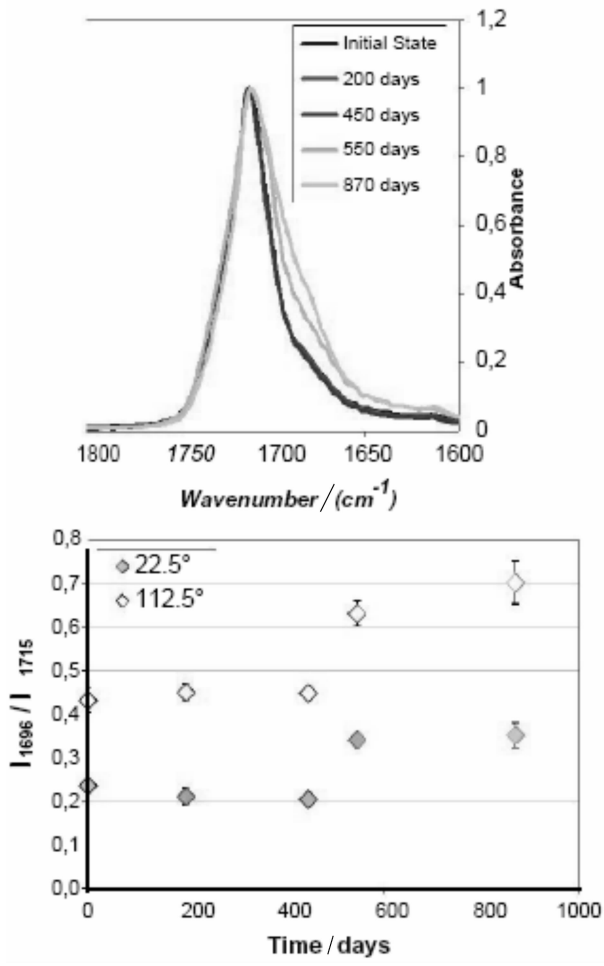

Fig. 6 a) PET spectra of outer layer between 1800～1600cm^{-1} after different ageing time at the 112.5° incident beam, b) carbonyl index for two orientations versus ageing times

In addition, the inner layers of PET was analysed

with a IR-microscope. Their individual degradation was demonstrated using previous markers.

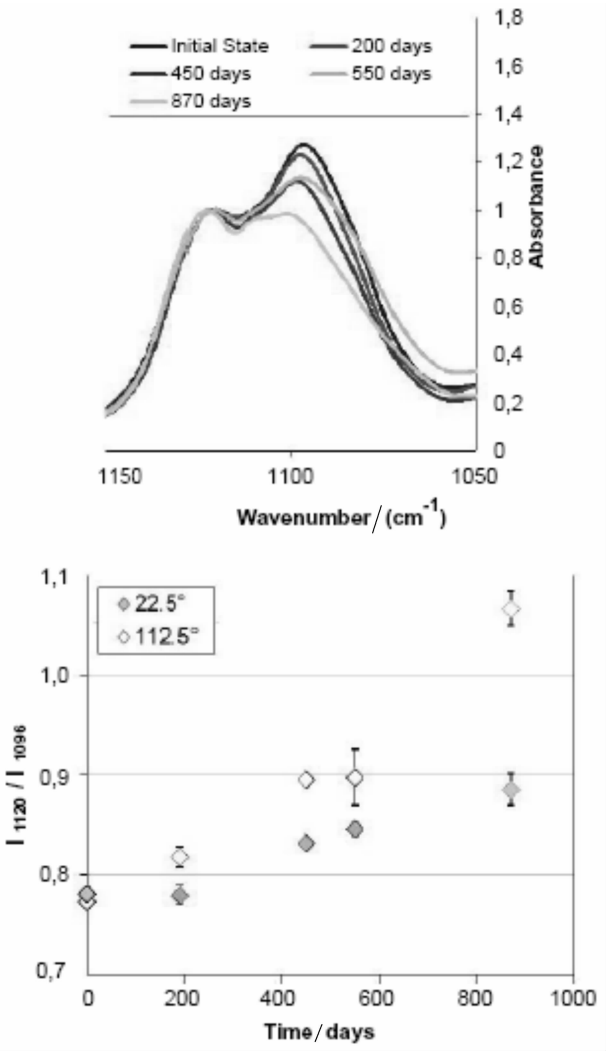

Fig. 7 a) PET spectra of outer layer between 1150 ~ 1050 cm^{-1} after different ageing time at the 112.5° incident beam, b) trans-gauche ratio for two orientations versus ageing times

4. Conclusions and outlook

The developed method allows following accurately the state of degradation of the various PET layers present in the barrier envelope.

The study of PET degradation in outer layer allowed highlighting several chemical markers characteristic of hydrolysis and in turn probes of PET crystallization due to the reduction of the molecular weight. The degradation is detected for the outlet PET layer aged at 70 ℃ under 90 % RH after 400 days ageing. The use of infrared microscopy enables the local characterization of the degradation in the polymer multilayer constituting the PIV envelope.

Acknowledgements

The authors acknowledge the ANR (French National Research Agency) and the ADEME (French Agency for Environment and Energy Management) for their financial support of the EMMA - PIV projects. They thank the industrial partners of project: REXOR and MICROTHERM. This work was performed within the framework of the Centre of Excellence of Multifunctional Architectured Materials (CEMAM) n° AN - 10 - LABX - 44 - 01.

References

[1] T. Wu et al, Polymer Degradation and Stability 86 (2004) 233 - 243.

[2] B. J. Holland et al, Polymer 46 (2002) 1835 - 1847.

[3] G. Garnier, Institut Polytechnique de Grenoble (2009).

[4] E. Pirzadeh et al, Journal of Applied Polymer Science 106 (2007) 1544 - 1549.

[5] A. Launay et al, Polymer Degradation and Stability 63 (1999) 385 - 389.

[6] N. W. Hayes et al, Surface and Interface Analysis 24 (1996) 723 - 728.

[7] C. Sammon et al, Polymer Degradation and Stability 67 (2000) 149 - 158.

[8] J. V. Gulmine et al, Polymer Degradation and Stability 79 (2003) 385 - 397.

[9] Z. Chen et al, European Polymer Journal 48 (2012) 1586 -1610.

[10] N. WHayes et al, Surface and Interface Analysis 24 (1996) 723 - 728.

A New Method to Characterize the Mechanical Resistance to Perforation of Polymeric Films

Florence Dubelley[a,b*], Emilie Planès[a,b], Corine Bas[a,b], Bernard Yrieix[c], Lionel Flandin[a,b]

a. Univ. Savoie, LEPMI, F—73000 Chambéry, France

b. CNRS, LEPMI, F—38000 Grenoble, France

c. EDF R&D, Matériaux et Mécanique des Composants, Site des Renardières, 77818 Moret-sur-Loing Cedex, France

Abstract

The low thermal conductivity of PIV is provided by maintaining the silica core under vacuum with the barrier envelope. A defect on the surface, generated by the manufacture of VIP and its installation, may result in a loss of the vacuum and therefore thermal insulation of the VIP. The essential work of fracture (EWF) is an efficient way to characterize the fracture polymeric films. One can gain valuable information on the resistance to perforation and propagation of flaws. VIP ageing in severe conditions may degrade the morphology of the different layers of the envelope barrier. Various authors brought to light the relationship between physico-chemical properties (crystallinity, chain length) and mechanical properties from the EWF method. The latter however, requires the use of up to 5 samples. A new technique will be presented with which the same amount of information may be obtained with a single sample. It is useful to probe the heterogeneous behavior of the degradation of the envelope.

Keywords essential work of fracture (EWF), polymeric films, photoelasticimetry, birefringence

1. Introduction

Polymer metal multilayers were found useful in buildings, as envelope of vacuum insulation panels (VIPs). These heterogeneous structures provide attractive combinations of properties involving mechanical resistance to perforation, barrier properties to air and water. Tensile properties allow assessing the classical mechanical parameters of the composites, but are not very discriminant as far as their fracture properties are concerned. The essential work fracture (EWF) method has generally used to characterize theses properties [1 - 7].

VIP ageing in severe conditions may degrade the morphology of the different layers of the envelope barrier. Various authors brought to light relationships between the physico-chemical properties of the polymeric film (crystallinity, chain length) and the mechanical properties from the EWF method [8 - 11]. Unfortunately, the EWF method requires the use of at least five samples of the same kind in order to vary the initial length of the filament. Getting a homogeneous series of samples is often not compatible with the study of polymer aging. This is expensive, time consuming, and most of all strong heterogeneities may result from the aging step. A new technique is proposed from which the same amount of information may be obtained with a single sample. The latter method was first obtained by coupling of photoelasticimetry and tensile test on notched specimen. The photoelasticimetry was employed to observe, by birefringence, the rupture propagation and the area altered by the stress at every moment of the test. To implement this method, we use

* Corresponding author, E-mail: Florence.dubelley@univ-savoie.fr

polyethylene (PE).

2. Experimental Material

The base film is a Low Density Polyethylene (LDPE) film of 40 μm in thickness. This is a semi-crystalline polymer with about 34 wt% crystallinity as measured by DSC. The stress optical coefficients in TD (1093 ± 29) Br and MD direction (916 ± 45) Br are sufficient to observe photoelasticimetry in PE even at low stresses.

Methods

Tensile Test

Tensile tests were performed on standard dumb-bell shape specimens with a 12 mm gauge length L_0 and 2 mm width at room temperature on an ADAMEL Lhomargy tensile machine (100 N) with a crosshead speed of 5 mm/min. Tensile tests were carried out in two loading directions: in machine (MD) and transverse (TD) directions. For each direction, five specimens were tested. The data were plotted in a true stress σ_H versus true strain ε_H, which were obtained assuming a constant volume of the specimens during deformation.

Essential Work of Fracture (EWF)

The fundamental concept of the EWF method is based on the energy partition, which separates the total fracture energy (W_f) in to two components: the essential work of fracture (W_e) and the non-essential work of fracture (W_p).

$$W_f = W_e + W_p$$

$$W_f = W_e lt + \beta W_p t l^2 \quad (1)$$

Where W_e, which represents the energy dissipated in the inner fracture process zone (IFPZ), can be interpreted as the work required to create two new surfaces. W_p represents the energy dissipated in the outer plastic deformation zone (OPDZ), where the plastic deformation and heat dissipative process occur. The specific total work of fracture w_f can be expressed as:

$$w_f = \frac{W_f}{Lt} = w_e + \beta w_p L \quad (2)$$

Therefore, there is a linear relationship between w_f and L, where w_e, the specific essential work of fracture, can be obtained from the y-axis intercept and βw_p, the specific non-essential work of fracture, can be obtained from the slope of the curve.

For the measurement, DENT specimens used in the present study were cut from rectangular shape (length: 50 mm, width: 25 mm and 2 mm < Ligament L < 8 mm) in the Machine Direction (MD) and Transverse Direction (TD)]. The specimens were loaded on an ADAMEL Lhomargy tensile machine (100 N) at a crosshead speed of 5 mm/min.

Photoelasticimetry

Photoelasticimetry is a technique based the optical birefringence induced by the application of a stress. Photoelasticimetry bench consist of a circular polariscope. This polariscope includes a light source (white), a polarizer and an analyzer (that is crossed with respect to the polarizer), two quarter - wave - plates inserted between polaroids. A camera was used to record (one photography per second) the birefringence development of the DENT and dumb bell shape specimens, crack propagation (the ligament length at some time) and the size of the plastic zone.

3. Results and discussions

Fig. 1 displays the load - displacement curve of DENT specimens with various ligament lengths in MD direction. The method to determine the specific work of fracture requires calculation of the total energy by the initial ligament area. The specific EWF (w_e = (27±2) kJ/m^2) is obtained by extrapolating the straight line to zero ligament length. The non - essential part, or plastic work term (βw_p = (13.4±0.4) MJ/m^3), was also obtained from the slope of the linear relation of w_f versus ligament length.

New EWF method with one sample

In Equation (2), L is the initial length of the ligament and W_f is the total energy required to break the entire ligament length L. This length may also be viewed as a continuous sum of small ligaments l gradually broken. It is possible to substitute in the previous equation the total length ligament L by l, the change in ligament length at some time τ. As a result, W_f depends on the length l, noted W_f [l], and corresponds to the energy necessary to break the length left on the ligament l:

$$W_f(l) = w_e lt + l^2 \pm \beta W_p$$

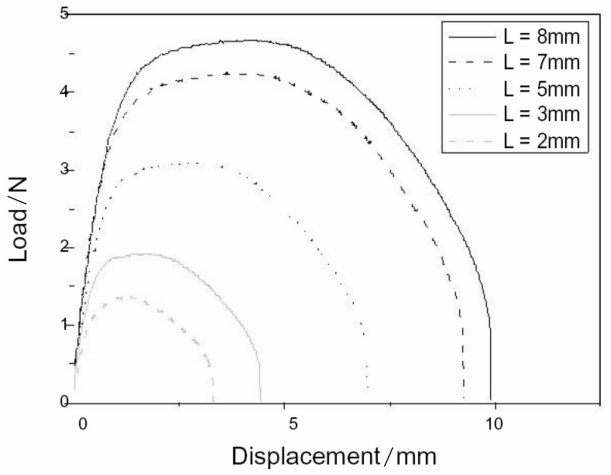

Fig. 1 Load-Displacement curve of DENT specimens of PE in MD direction

With this incremental approach on can directly measure, with a single run, the energy W_f [l] required to gradually break the ligament, is a function of the amount of ruptured film. W_f [l] curve has a parabolic shape(Fig. 2).

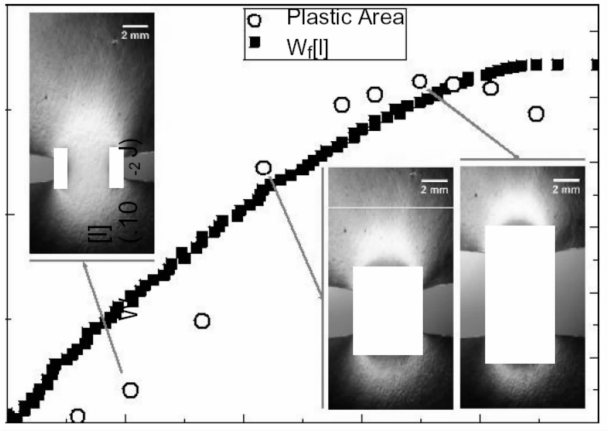

Fig. 2 Energy W_f required to gradually break the ligament l and evolution of the plastic deformation and photoelastic observations

w_e and w_p should be measured in pure plane stress state independently from the energy used to yielding the film. In other words, the EWF parameters are determined when the plastic deformation appears constant, so when the fracture energy W_f only contributes to rupture the filament. Photoelasticimetry characterization may be used to accurately measure the outer plastic deformation zone (OPDZ) (Fig. 2).

The curve $W_f[l]$ presents a linear behaviour in the constant OPDZ area regime (Fig. 2). Following the method commonly used for EWF tests, the intersection of the straight line W_f [l] (in OPDZ area constant) with the y-axis is defined as the fracture energy W_e. The specific fracture energy w_e is then deduced by dividing W_e by the total surface broken (tL). The βw_p parameter may be determined using Equation (3).

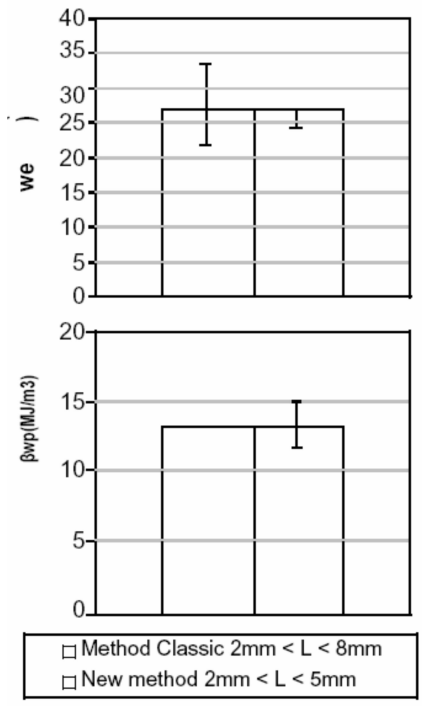

Fig. 3 Comparison of EWF parameters calculated between the two methods in MD direction

The parameters w_e and βw_p values were plotted both from conventional EWF tests and the methods described in the present work (Fig. 3). They are in good agreement.

Note: The same experimentations were performed in Transverse Direction (TD) and the parameters w_e and βw_p determined by the new method are in good agreement with the ones derived from the regular EWF method.

4. Conclusions and outlook

A new technique was developed to better understand the EWF experiments. It revealed a narrow window in ligament length were the method may be applied rigorously, i. e. following the mechanical hypotheses. Experimentally, the estimation of we and βw_p parameters remains satisfactory in a much broader range of filament length. It suggests that the initial hypotheses for the Cotterell test may be too demanding.

The coupled measurements proposed in this study permitted to determine we and βwp with a single sample. The only limitation of this new method is that its rigorous application requires a material that becomes birefringent under constrains. A tensile test coupled to photoelasticimetry may first be used to determine the stress optical coefficient of the materials. The series of measurements shed some new light on the EWF testing method and will now be very useful to determine the resistance to crack propagation with very little amount of material. We believe it will be especially helpful to characterize the heterogeneous behavior of films, for instance after ageing.

Acknowledgements

The authors acknowledge the ANR (French National Research Agency) for his financial support of the EMMA-PIV projects. This work was performed within the framework of the center of Excellence of Multifunctional Architectured Materials (CEMAM) n° AN-10-LABX-44-01. Special thanks are also given to Pauline Ratel and Nicolas Crowin for their assistance and numerous hours to perform experimental work.

References

[1] T. Barany et al. Prog. Polym. Sci., 35(10):1257 - 1287, 2010.

[2] T. Barany et al. Express. Polymer. Lett., 1(3):180 - 187, 2007.

[3] J. Karger-Kocsis et al. Polymer, 37(12): 2433 - 2438, 1996.

[4] Y.W. Mai et al. Int. J. Fract., 32(2):105 - 125, 1986.

[5] Y.W. Mai et al. J. Polym. Sci., Part B: Polym. Phys., 29(7):785 - 793, 1991.

[6] A. S. Saleemi et al. Polym. Eng. Sci., 30(4):211 - 218, 1990.

[7] J. Wu Polym et al. Eng. Sci., 36(18):2275 - 2288, 1996.

[8] T. Barany et al., Polym. Degrad. Stab. 82(2):271 - 278, 2003.

[9] G. Garnier et al. J. Mater. Sci., 44:5537 - 5543, 2009.

[10] E. Moukheiber et al. Int. J. Hydrogen Energy, 39(6): 2717 - 2723, 2014.

[11] H.N. Vu et al. Polym. Int., 61(7):1094 - 1100, 2012.

Accelerated Aging Test of Vacuum Insulation Panels with Different Barrier Films

He Yi*, Zhai Chuanwei, Li Zhuangxian, Liu Ting, Liu Honghai, Liang Hongchao, Ning Qianshuai, Hu Delong

Qingdao Kerui New Environmental Materials Co., Ltd., 30th F, Century Building, 39 Donghai Rd, Qingdao, China

Abstract

Investigation of the permeation of oxygen and water vapor through barrier films of VIPs is crucial for determining the long-term performance of VIPs. In this work, we investigated and simulated the permeation mechanism of oxygen and water vapor through barrier films. Permeation equations for polymer film with single defective layer and polymer film with double defective layers are obtained by numerical simulation and curve fitting. Both equations take into account the characters of the aluminum layers as well as polymers adjacent. With the equation derived, the acceleration ratios of common acceleration strategy with elevated temperature and pressure difference are calculated. Acceleration strategy with volume reduction is introduced and implemented to provide higher acceleration ratios and avoid unequal acceleration for different permeants due to elevated temperature and pressure difference.

Keywords

vacuum insulation panel, numerical simulation, accelerated aging test

1. Introduction

The thermal performance of vacuum insulation panels (VIPs) deteriorate due to the permeation of water vapor and air through the barrier film. Accumulation of these permeant inside VIPs results in the elevation of the internal pressure and thus the increase of the gaseous thermal conductivity. Therefore one of the major concerns about VIPs is their long-term performance, since most VIPs are used in thermal insulation of refrigerators and buildings with target service life more than 10 years. However, estimation of the thermal performance of VIPs over a long period is challenging, as the permeation rate of water vapor and air through the barrier film is extremely low. Without any acceleration strategy, the measurement of the permeation rate is very time-consuming and this will hinder the growth of the VIP industry. In this paper, the permeation mechanism is investigated, followed by the discussion about two acceleration strategies.

2. Numerical simulation of permeation through barrier films

Air and moisture can not permeate through a perfect aluminum layer. Therefore the numerical simulation of permeation of air and moisture through a barrier film in this work is based on the assumption that the defects of aluminum layers are the major permeation channels. In general, there are two types of barrier film according to film composition, namely aluminum foil film and metalized film. During the simulation, they are characterized as polymer film with single defective layer (PFSDL) and polymer film with double defective layers on both sides (PFDDL), as shown in Fig. 1.

For one-dimension (1D) permeation problem, such as permeation through a uniform film, the permeation equation is simplified to

$$Q = \frac{A\Pi(P_2 - P_1)}{L} \tag{1}$$

Where

* Corresponding author, Tel: 86-15901020279, E-mail: heyi@cncreek.net

Q =permeation rate through the film,
A =area of the film,
Π =permeability of the film,
L =thickness of the film,
P_1, P_2 =partial pressure of the permeant on both sides of the film.

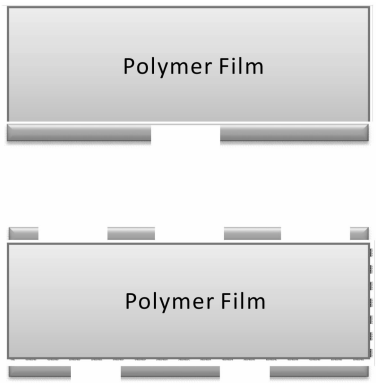

Fig. 1 Schematic picture of the two film models used in this work: (top) polymer film with single defective layer (PFSDL) and (bottom) polymer film with double defective layers on both sides (PFDDL)

However, for more complicated geometries and compositions, the original differential equation should be solved,

$$\Pi\left(\frac{\partial^2 P}{\partial x^2}+\frac{\partial^2 P}{\partial y^2}+\frac{\partial^2 P}{\partial z^2}\right)= S\frac{\partial P}{\partial t} \quad (2)$$

Where

S =solubility of permeant in the film,
x, y, z =coordinates,
t =time.

Note that for steady state permeation, the right-hand-side of the equation vanishes.

Numerical studies for permeation through PFSDLs with different defect sizes were implemented by the finite volume method, which meshes the domain with a fine grid and solves the differential equation above. The distributions of the permeant concentration across the film in different cases are shown in Fig. 2.

According to the results of the numerical simulation, the permeation rate due to a single defect can be expressed as

$$Q_i = A_i f(A_i)\Pi(P_2-P_1) \quad (3)$$

Where

Q_i =permeation rate through the ith defect,
A_i =area of the ith defect,
f =coefficient for the area of the defect.

Here f is a function of the defect area and was determined by curve fitting, as shown in Fig. 3.

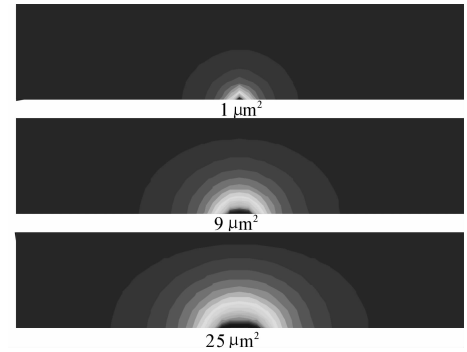

Fig. 2 Numerical simulation of the distributions of the permeant concentration across the film for PFSDLs with different defect sizes

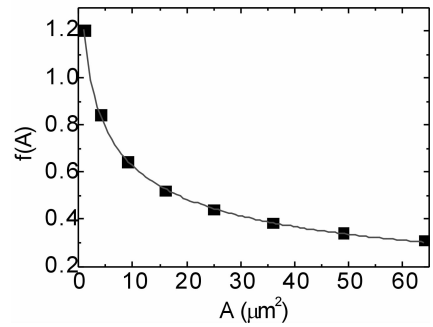

Fig. 3 Coefficient for the area of the defect $f(A)$

As an approximation, the total permeation rate can regarded as the summation of the contribution of each individual defect

$$Q=\sum_i A_i f(A_i)\Pi(P_2-P_1)=\alpha\Pi(P_2-P_1) \quad (4)$$

Here α is an important characteristic number of the aluminum layer and thus it will vary from case to case. The larger the number, the worse the barrier film will perform.

Numerical studies for permeation through PFDDLs with different defect sizes are even more complicated due to the coupling of the defects on both sides. The distributions of the permeant concentration across the film with different defect patterns and sizes are shown in Fig. 4, which illustrates the complexity arising from the change of the relative positions as well as the sizes of the defects on both sides.

In general, the permeation rate in the case of PFDDLs can be expressed as

$$Q=\sum_i\sum_j A_i A_j f'(A_i, A_j, d_{ij})\Pi(P_2-P_1) \quad (5)$$

Where f' is a function of the distance and the defect areas of the two defects associated. Note that PFDDL configuration often exists in barrier films with multiple

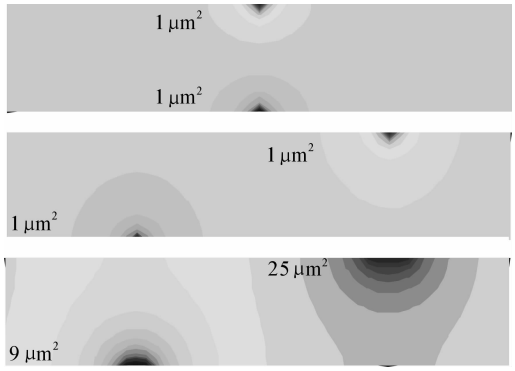

Fig. 4 Numerical simulation of the distributions of the permeant concentration across the film for PFDDLs with different defect patterns and sizes

metalized layers, whose aluminum layers have a high defect density. Therefore, replacing f' by the characteristic numbers of aluminum layers on both sides should be a good approximation with sound physics

$$Q = \left(\frac{1}{\Pi\alpha_1} + \frac{1}{\Pi\alpha_2}\right)^{-1}(P_2 - P_1) \tag{6}$$

According to Eqs. (4) and (6), the permeation rates through a typical Al-foil based barrier film with composition of PET/Al/PE and a typical metalized barrier film with composition of PET/Al/PET/Al/PET/Al/PE can be calculated as Eqs. (7) and (8) respectively,

$$Q_{AF} = \alpha_{AF}\left(\frac{1}{\Pi_{PET}} + \frac{1}{\Pi_{LDPE}}\right)^{-1}(P_2 - P_1) \tag{7}$$

$$Q_{MF} = \alpha_{MF}\left(\frac{1}{\Pi_{LDPE}} + \frac{5}{\Pi_{PET}}\right)^{-1}(P_2 - P_1) \tag{8}$$

3. Accelerated aging test by elevated temperature and pressure difference

In accelerated aging test of vacuum insulation panel, the permeation rate is usually enhanced by elevated temperature and pressure difference. Higher temperature will result in higher permeability and thus permeation rate based on the empirical formula

$$\Pi = \Pi_0 \exp\left(-\frac{E_\Pi}{RT}\right) \tag{9}$$

Where

Π_0 =coefficient,

E_Π =activation energy.

Our research is focused on the permeation rates of oxygen and water vapor through barrier films composed of PET, PE and Al. Therefore the data related to the permeability of oxygen and water through PET and PE are required and collected from Refs. [1]-[4].

For accelerated aging test, the relative permeation rate instead of the absolute one is more interested, so the acceleration ratio is introduced as

$$AR = Q/Q_0 \tag{10}$$

Namely the permeation rate at the test condition over the permeation rate at the reference state. In this work 20 ℃ and 50% R. H. is used as the reference state. AR of oxygen and water calculated with Eqs. (7) and (8) for Al-foil based barrier film and metalized barrier film are plotted in Figs. 5 and 6, respectively. It can be found that the acceleration ratios of two types of film are quite close within the whole temperature range investigated.

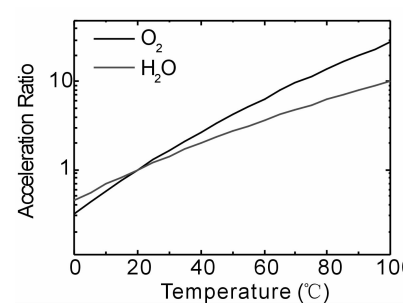

Fig. 5 Acceleration ratio of oxygen and water through Al-foil based barrier film

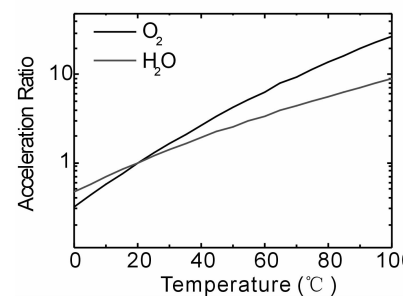

Fig. 6 Acceleration ratio of oxygen and water through metalized barrier film

On the other hand, the *AR*s of water vapor are small for both types of film, even at the 100 ℃. To further enhance the *AR*s for faster aging test, the partial pressure of water vapor has to be increased, which means test conditions with higher relative humidity. *AR*s of water vapor through AF and MF at various test conditions are given Tables 1 and 2.

Tab. 1 *AR*s of water vapor through Al-foil based barrier film at various test conditions

R. H. / T(℃)	50%	70%	90%
40	5.95	8.33	10.71
50	13.63	19.09	24.54
60	30.99	43.39	55.79

Tab. 2 *AR*s **of water vapor through metalized barrier film at various test conditions**

R. H. / *T*(℃)	50%	70%	90%
40	5.76	8.06	10.37
50	13.00	18.20	23.41
60	29.14	40.79	52.45

Again, it is found that the *AR*s of water vapor permeation rates are close for the two types of film studied. For frequently used test condition, namely 50℃ and 70% R. H., the *AR*s for water vapor are 19.09 and 18.20. The *AR*s for oxygen at this condition are 4.22 and 4.21 from Figs. 5 and 6.

4. Accelerated aging test by volume reduction

The advantage of the acceleration strategy based on elevated temperature and pressure difference is its simplicity in terms of experiments. However, as has been demonstrated in the last section, the method suffers from two issues. First, the *AR*s of oxygen and water vapor through two types of film are not very high at the common test condition (50℃ and 70% R. H.), while further increase the temperature may result in potential damage of the barrier films. Second, the permeation of water vapor and oxygen are not equally accelerated, which makes the analysis of the experimental results difficult, even we have known the *AR*s of a given film by its composition. In a more general case where polymers other than PET and PE are used and thus the *AR* of the film is unknown, more tests have to be conducted at various conditions to determine the temperature dependence of the permeability of water vapor and oxygen through these materials. Also, most accelerated aging tests neglect the permeation of nitrogen. But it should be noticed that although nitrogen has lower permeability than oxygen, its partial pressure in air is about 4 times of the oxygen, and thus its contribution to the pressure increase inside a vacuum insulation panel could be comparable to oxygen.

To solve the issues above, we developed a device targeting for large *AR* and equal acceleration based on the strategy of volume reduction. In this method, the *AR* is calculated as

$$AR = V_0/V \tag{11}$$

namely the original vacancy volume over the practical vacancy volume. The practical vacancy volume is minimized by replacing the porous core of vacuum insulation panel with a solid core with a small cavity. The volume of the cavity is about several mL and is just large enough to accommodate the sensors inside. In this case the *AR* can be as large as 450, which may reduce the time for aging test significantly. Since the *AR* is large enough, no elevation of temperature or pressure difference is required, and the aging test can be conducted at the reference condition or the condition where the panels are supposed to be used. In this manner, the permeation is equally accelerated for oxygen and water vapor, which will facilitate the data analysis.

5. Conclusions

Permeation of oxygen and water vapor through barrier films of VIPs were simulated numerically. By taking into account the characters of the aluminum layers and polymers adjacent, we derived the permeation equations for both polymer film with single defective layer and polymer film with double defective layers. Acceleration ratios for water vapor and oxygen through Al-foil based barrier film and metalized barrier film are calculated according to the permeation equations obtained. At condition for common accelerated aging test, namely 50℃ and 70% R. H., the *AR*s for water vapor through Al-foil based and metalized barrier films are 19.09 and 18.20. The ARs for oxygen at this condition are 4.22 and 4.21. Acceleration strategy with volume reduction is introduced and implemented to overcome the limitations of the traditional approach. With the volume reduction method, *AR* can be as large as 450, and the permeation is equally accelerated for oxygen and water vapor.

References

[1] A. S. Michaels, W. R. Vieth, and J. A. Barrie, Diffusion of gases in polyethylene terephthalate, Journal of Applied Physics, 34 (1963), 13 - 20.

[2] A. S. Michaels and H. J. Bixler, Flow of gases through polyethylene, Journal of Polymer Science, 50 (1961), 413 - 439.

[3] H. Eslami and F. Müller-Plathe, Water permeability of poly(ethylene terephthalate): A grand canonical ensemble molecular dynamics simulation study, Journal of Chemical Physics, 131 (2009), 234904.

[4] D. W. McCall, D. C. Douglass, L. L. Blyler, Jr., G. E. Johnson, L. W. Jelinski, and H. E. Bair, Solubility and Diffusion of Water in Low-Density Polyethylene, Macromolecules, 17 (1984), 1644 - 1649.

Thermal Conductivity Measurements of Granular and Powdered Silica Aerogel Super Insulation Materials at Different Temperature and Pressures with THS Method

Wang Lixin, Wei Gaosheng *, Du Xiaoze, Yang Yongping

School of Energy, power and Mechanical Engineering, Key Laboratory of Condition Monitoring and Control for Power Plant Equipment of Ministry of Education, North China Electric Power University, Beijing, 102206, China

Abstract

This paper dedicates to the experimental determination of thermal conductivity of powdered and granular silica aerogels with the transient hot-strip (THS) method. A vacuum furnace is designed for the THS method in order to measure the thermal conductivity at different temperature and pressures. The specific surface area and average mesopore diameter of two samples were also measured by cryogenic nitrogen adsorption method. The results show that the thermal conductivity of the two samples demonstrates similar patterns with variation of pressure, which are generally in agreement with the granular data in literature. There exists a turning point at about 1000 Pa for thermal conductivity with variation of pressure. The thermal conductivity drops slowly when $p > 1000$ Pa, but drops quickly when air pressure is lower than 1000 Pa. The thermal conductivity of measured samples increases distinctly with elevation of temperature. In addition, the thermal conductivity rises with increase of average pore size at a certain temperature range.

Keywords thermophysical properties, thermal conductivity, transient hot-strip method, aerogel, Nanoporous insulation materials

1. Introduction

Aerogel is a super insulation material consisting of a nanostructured SiO_2 network made by sol-gel chemical processing and drying technology (supercritical drying or conventional drying), which has excellent insulation performance with a thermal conductivity lower than of the still air at ambient temperature for its nano-porous structure and very high porosity. Perfect insulation capability makes aerogel have great application potential in aeronautics and astronautics, energy saving in buildings, and transportation of offshore oil and gas [1 - 6]. Thermal conductivity is one of the most important thermophysical properties for aerogel, and experimental measurement is almost the only approach to determine the thermal conductivity of porous media for thermal conductivity since its highly dependent on the composition and microstructure of the materials. Experimental data is also very important for validation of the theoretical heat transfer model.

The heat transfer mechanism and thermal conductivity prediction by theoretical method has been widely studied in recent years [7 - 19]. However, the experimental data related to thermal conductivity of aerogel is relatively scarce. There are mainly three kinds of structure form of aerogel, monolithic, granular, and powdered aerogel. Zeng el al [20] measured the thermal conductivity of monolithic silica aerogel opacified with fine carbon particles (3.25 percent volume) at different pressures using hot-wire method in 1995. Wei et al [2] measured the thermal conductivity of monolithic silica aerogel and xonotlite-aerogel composites at different temperatures and pressures with transient hot-strip method. Reichenauer et al [21] measured the thermal conductivity of granular aerogel at conventional

* Corresponding author, Tel: 86 - 10 - 61773372, E-mail: gaoshengw@126.com

temperature and different pressures when investigating the pressure dependent gaseous thermal conductivity of porous media. Spagnol et al [22] measured the pressure dependent thermal conductivity of both monolithic aerogel and granular aerogel with different diameters by a guarded thin-film-heater method. Bi et al [23] measured the pressure dependent of effective thermal conductivity of six monolithic silica aerogels with different densities at room temperature according to the hot-plate method based on the one-dimensional steady state heat conduction. Gao et al [24, 25] measured the thermal conductivity of granular aerogel with different particle sizes with a Hot-Disk Thermal Constants Analyzer in order to analyze the effect of the particle size on the thermal performance of aerogel glazing units. Neugebauera et al [26] measured the thermal conductivity of granular aerogels with different densities at different pressures using the hot-wire method.

The transient hot-strip (THS) method was used to measure the thermal conductivity of granular and powdered silica aerogels in this study. A vacuum furnace was designed for THS method in order to measure the thermal conductivity at different temperature and pressures. The pressure range of the vacuum furnace is from atmosphere pressure to 1 Pa, and the temperature range is from ambient temperature to 900 K. The thermal conductivity of granular and powdered silica aerogel samples were measured with the THS method at different temperature and pressures, and compared with the data from literatures.

2. Experimental investigations

TheTHS method was used to measure the thermal conductivity of powdered and granular aerogels at different temperature and pressures. The schematic experimental apparatus is shown in Fig. 1. The measurement theory can referred to Gustafsson et al [27]. The temperature of the strip buried in the middle of the measured sample increases when an electric current flows through it. The temperature increasing rate is directly related to the thermal conductivity of the sample. This is the basis for thermal conductivity determination with the THS method. The thermal conductivity of the measured sample is calculated as

$$k = P_0/(4\pi)/[\mathrm{d}T(t)/\mathrm{dln}(t)] \quad (1)$$

Where P_0 = power input to the strip,

t = time,

$\mathrm{d}T(t)/\mathrm{dln}(t)$ = slop of temperature versus ln(t) after enough heating time, and can be easily obtained in actual measurement process.

A 2.0mm (width) × 0.1 mm (thickness) nickel-chrome (Ni80Cr20) strip is used as the heating source. The strip is straightened and buried in the middle of the sample. The powdered or granular sample is packed in a cuboid box made of stainless steel with dimensions of 250 mm (length) × 150 mm (width) × 220 mm (height). The ceramic beads are spread out on the top of the sample to avoid of the escape of the powdered sample at vacuum condition. The PA36 - 3B type stabilized power source is used to heat the strip. The variations of temperature are detected by a type K 0.1 mm diameter thermocouples welded on the center of the strip surface. The signals from the thermocouple together with the voltage signals between two sides of the sample are monitored by a data acquisition system, and then used to calculate the thermal conductivity with Eq. (1).

A vacuum furnace is specially designed for the THS method, which allows the thermal conductivity determination at different temperatures and pressures. Fig. 2 gives a picture of the vacuum furnace and arrangement of the THS apparatus, which can provide any vacuum and high temperature surroundings for thermal conductivity determinations with the THS method in the pressure range of 1 Pa to atmospheric pressure and in temperature range of ambient temperature to 900 K. Five districts are heated independently and controlled respectively in the furnace in order to maintain an uniform temperature in the furnace. The temperature difference between any two points is guaranteed to less than 1 K in the core region of the furnace. The size of the inner room of the vacuum furnace is ϕ 400mm × 500 mm. Three groups all together 12 electrodes are set in the bottom of the furnace, and it is convenient to detect temperature and voltage signals in the furnace. The identical materials with K type thermocouples were adopted as the electrodes. A vent valve was arranged at the side face of

the vacuum furnace for convenient fill different inertia gases in the furnace. So the thermal conductivity of porous media in different filling gases can be also determined by this apparatus.

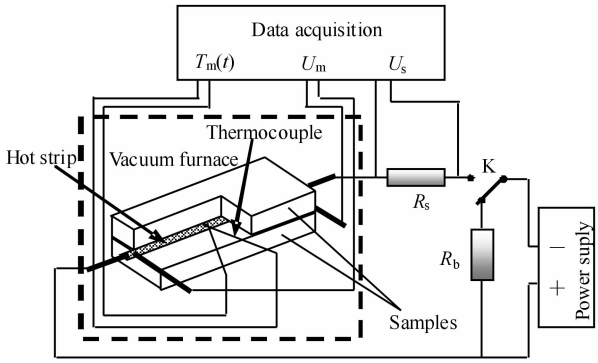

Fig. 1 Schematic illustration of THS method

The THS apparatus are carefully examined by measuring some kinds of conventional materials as shown in Tab. 1. It is shown that both the reproducibility of the measured results and the maximum error between measured and the recommended results in literature are both within 5 percent, which ensures the reliability of the experimental setup.

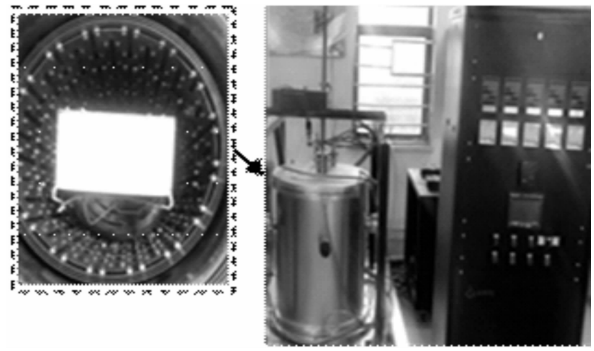

Fig. 2 A picture of the arrangement of THS apparatus in a vacuum furnace

The physical properties of measured powdered and granular aerogels are shown in Tab. 2. The powdered sample was provided by NANO HIGH - TECH Ltd, and the granular sample was provided by Zhongshan Kebang Chemical Materials Technology Ltd. Fig. 3 gives the typical SEM picture of powdered silica aerogel measured with the scanning electron microscope. The scanning result shows that the particle diameter is about 80～120 μm, and the macropore diameter is about 70～100 μm. The particle diameter and the macropore diameter of granular sample are about 2～5 mm and 1～2 mm, respectively as shown in Fig. 4.

Tab. 1 Thermal conductivity of several conventional materials at ambient temperature

Materials	Measured		Reproducibility /(%)	Recommended in literature		Maximum error/ (%)
	Density / (kg · m^{-3})	Thermal conductivity /(W · m^{-1} · K^{-1})		Density / (kg · m^{-3})	Thermal conductivity / (W · m^{-1} · K^{-1})	
Polystyrene	15	0.04103	2.9	15.9	0.042[28]	2.3
calculate silicate	126	0.04135	2.1	124.5	0.0416[2]	2.7
Lightweight insulation brick	503	0.1817	2.8	513	0.174[29]	4.3
Black rubber	1322	0.31548	3.5			
Sand	1376	0.2654	2.6		0.2774[30]	4.3
High aluminum brick	2280	1.4437	4.6	2230	1.51[29]	4.8

Tab. 2 The physical properties of measured powdered and granular aerogels

Samples	Apparent density kg/m^3	Total porosity %	Interpartical porosity %	Pore volume within particles cc/g	Specific surface area m^2/g	Average mesopore diameter / nm	Particle diameter	Macropore diameter
Powdered aerogel	128	93.6	45.8	37.35	528.22	28.29	80～120 μm	70～100 μm
Granular aerogel	190	90.5	40.7	26.21	279.04	37.57	2～5 mm	1～2 mm

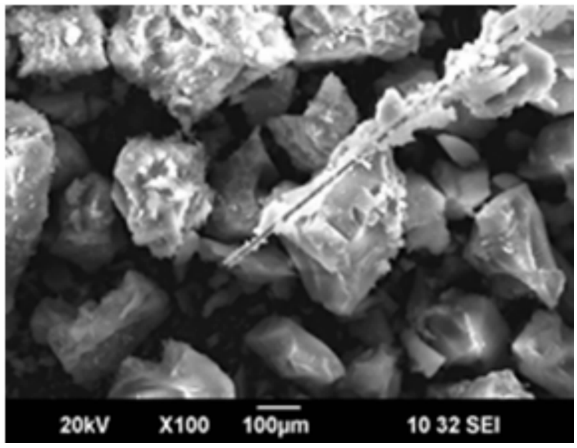

Fig. 3 SEM picture of powdered silica aerogel

The specific surface area, average mesopore diameter and pore volume within the particles were measured by cryogenic nitrogen adsorption method with the automatic surface area and porosity analyzer of model (Quantachrome, Autosorb - iQ2 - MP, America). The nitrogen adsorption/desorption isotherms at 77.35K and mesopore size distribution of measured samples are shown in Fig. 5. According to IUPAC classification, both of the adsorption/desorption isotherms are Ⅳ type which is the typical isotherm type of mesoporous materials as shown in Fig. 5(a). The adsorption amount of nitrogen increases significantly with increase of relative pressure due to the capillary condensation phenomenon. Based on the adsorption/desorption isotherms, the BET theory [31] was applied to calculate the specific surface area of the samples, and the results are also presented in Tab. 2.

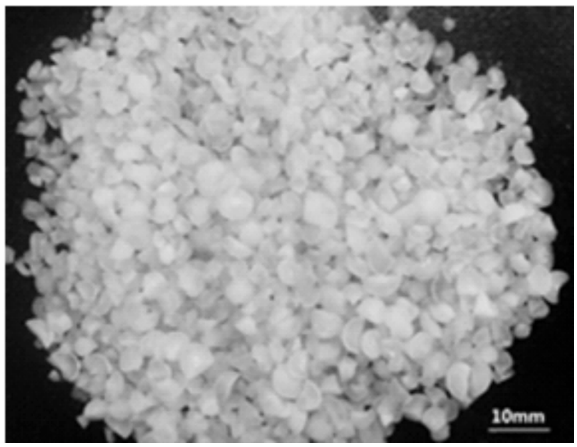

Fig. 4 A picture of granular silica aerogel

As shown in Fig. 5(b), there are two distinct distribution peaks for powdered and granular samples when the pore diameter is about 20nm and 30nm respectively. Therefore, there exit many pores with diameter of 20nm and 30nm for powdered and granular samples separately. The calculation results of average mesopore diameter by BJH model [32] are shown in Tab. 2. The interpartical porosity (ratio between macropore volume and overall volume) can be calculated combined with the apparent density, total porosity and the pore volume within the particles.

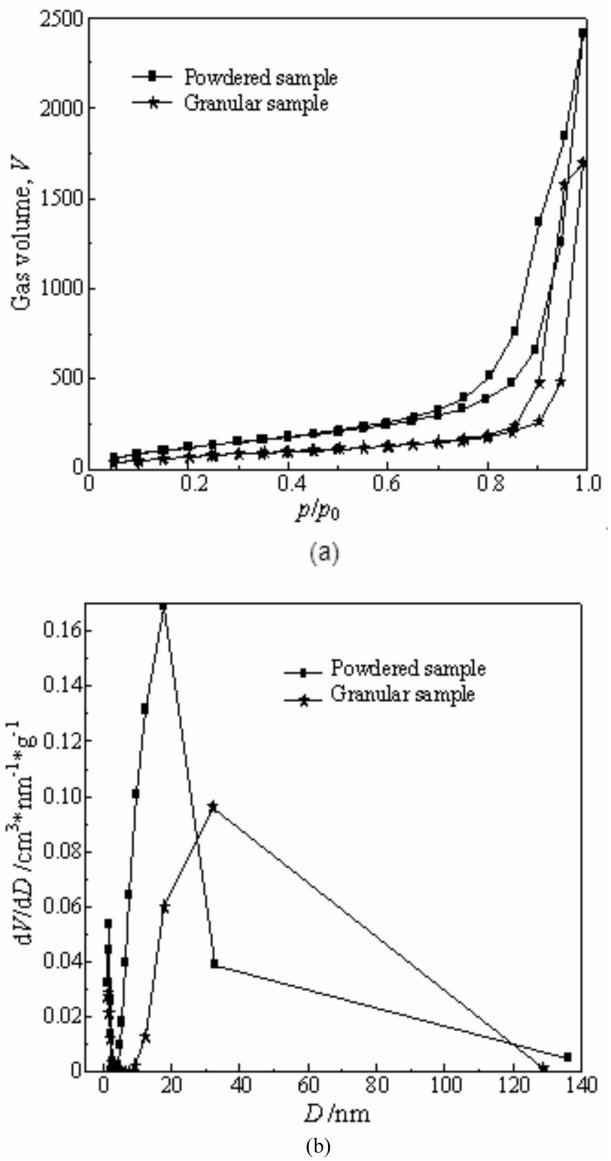

Fig. 5 Nitrogen adsorption/desorption isotherms and mesopore size distribution of powdered and granular silica aerogels

(a) Nitrogen adsorption/desorption isotherms

(b) Mesopore size distribution

3. Results and discussion

Fig. 6 shows the experimental temperature variation of the strip in thermal conductivity measurement with the THS method. It is shown that the temperature of the strip increases linearly with ln (t) when $t > 10$ s. The start-point of the linear relation between temperature variation and ln (t) varies with different measured materials. The experimental results show that a smaller start-point time with a relative larger thermal conductivity of the measured material, and a larger start-point time with a relative smaller thermal conductivity. The start-point time is not larger than 15 s for most of the measured materials, and this is coincided with theory of THS method.

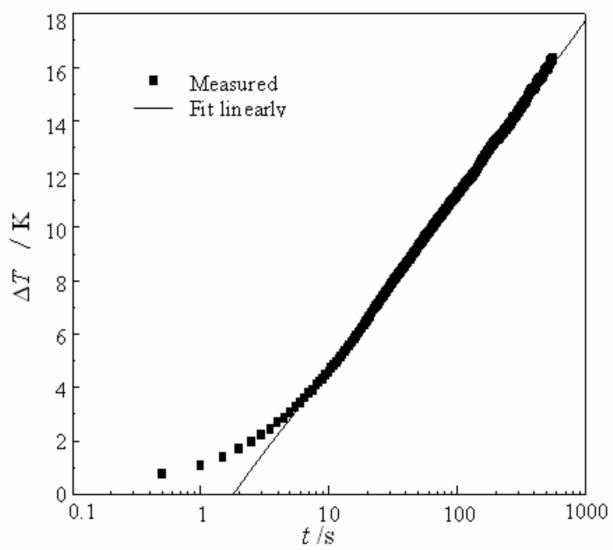

Fig. 6 Measured temperature rise at the strip surface

The thermal conductivity data of measured samples across a range of air pressures at ambient temperature are shown in Fig. 7, and compared with the powdered data from literature [26]. Results from previous testing of a monolithic sample have also been included for comparison [2]. It is noticed that the thermal conductivity of the granular sample is apparently larger than the value of the powdered sample in the whole pressure range except the case when pressure less than 3 Pa. The thermal conductivity of powdered sample reaches to constant when pressure less than 20 Pa, while, the thermal conductivity of granular sample reaches to constant when pressure less than 3 Pa. It is well known that the thermal conductivity is mainly due to solid conduction and radiation when gas pressure reaches to zero. It can be sure that the gaseous thermal conductivity is the main heat transfer contribution to the total thermal conductivity of all the samples, the sum of solid conduction and radiation contribution is not larger than 0.004 $W \cdot m^{-1} \cdot K^{-1}$ at ambient temperature.

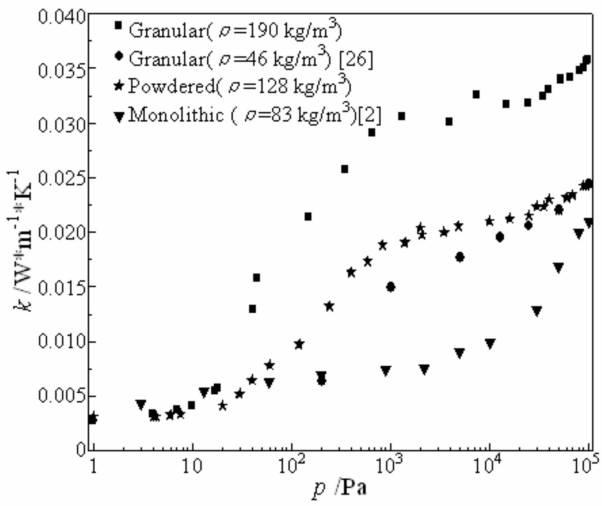

Fig. 7 Pressure dependent effective thermal conductivity of silica aerogel at ambient temperature

It is noticed that the thermal conductivity of granular sample is apparently higher than other samples. We deduce that the gas diffusion occurred in heat transfer process for granular samples. That is to say it contains convection heat transfer contribution in thermal conductivity of granular sample due to it's relative large particle diameter in range of 2～5mm.

The thermal conductivity of the measured samples demonstrated similar patterns in decrease with lower of gas pressure, which are generally in agreement with the data of powdered sample in literature [26]. There exists a turning point at about 1000Pa in decreasing process of thermal conductivity. It drops slowly when $p > 1000$ Pa, but drops quickly when gas pressure is lower than 1000 Pa. We can explain this phenomenon by kinetic theory of gases. The mean free path of gas molecules in free space increases with lower of pressure. Once the free motion of gas molecules is restricted by the nanopores within particles or the macropores between particles, the heat transfer ability of gas molecules will be lowered. Then the gaseous thermal conductivity starts to drop with lower of pressure. For monolithic samples with only nanopores in them, the restriction

effect of nanopores on the free motion of gas molecules is strengthened greatly with pressure decreases, and the gaseous thermal conductivity of the sample decreases apparently and reaches to zero at about 10^4 Pa. For powdered and granular samples with macropores in them in addition to nanopores, although the gaseous conduction contribution to total thermal conductivity in nanopores decreases quickly with lower of pressure, the gaseous conduction contribution in macropores begin to decrease only when pressure less than 1000 Pa, and reach to zero only when pressure less than 20 Pa and 3 Pa, respectively. Above reasons result to the different variation patterns of thermal conductivity between powdered and granular samples and monolithic samples.

Fig. 8 gives the temperature dependent effective thermal conductivities of the measured samples at ambient pressure. Results from previous testing of monolithic samples have also been included for comparison [2]. It is shown that the effective thermal conductivities of all the samples increase distinctly with elevation of temperature, and the thermal conductivity of granular and powdered samples increases faster than monolithic samples. There are very clear understandings up to now that it is almost transparent to the radiation with wavelength between 3 and 8 μm for silica aerogel materials, and the radiative heat transfer is the major heat transfer mechanism at high temperature [1, 2, 33, 34]. So opacifying arrangement is necessary for application of silica aerogel as insulation materials including powdered, granular, and monolithic samples.

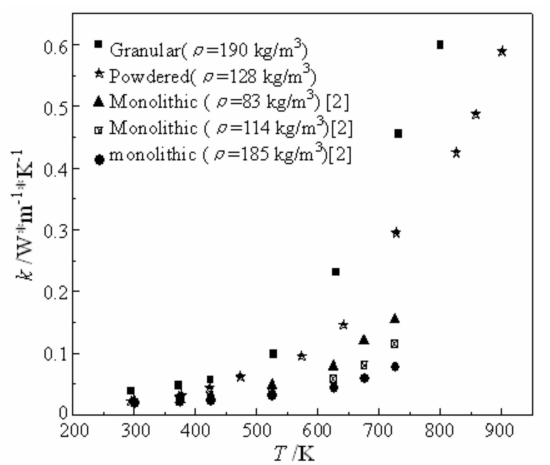

Fig. 8 Temperature dependent effective thermal conductivity of silica aerogel

Conventionally, the thermal conductivity of the samples with large density is lower at high temperature as demonstrated in Fig. 8 for monolithic silica aerogel samples because radiation heat transfer contribution is low for the sample with high density. However, the thermal conductivity of granular sample (with density of 190 kg/m^3) is apparently larger than the thermal conductivity of powdered sample (with density of 128 kg/m^3) at elevated temperatures in this study. This is because of the effect of macropores existed in granular and powdered samples. Big pores can reduce the adsorption, refection and scattering of radiative energy when it transfers through porous material. The macropore size of granular sample is apparently larger than the value of powdered sample. So the thermal conductivity of granular sample is higher than powdered sample at high temperature. For same reasons, the thermal conductivity of monolithic samples is apparently lower than the thermal conductivity of granular and powdered samples at high temperature for there are no macropores exist in them.

4. Uncertainty analysis

According to Eq. (1), many factors may affect the accuracy of thermal conductivity determination with the THS method, including the stability of the power supply, the temperature measurement precision, and the differences between the actual measurement condition and the theoretical model. The latter one may be the largest source of uncertainty in the thermal conductivity determination in THS method, including the effect of thermal resistance between the thermocouple and the strip, and between the strip and the sample, the nonzero thickness and the nonzero heat capacity of the heating strip, the dimensions of measured samples are not infinite.

In order to minimize the measurement errors caused by the temperature measurement precision, the 0.1mm diameter thermocouples are used to detect the temperature signals and the precision spot welding machine was used to weld the thermocouple. The uncertainty caused by the heat losses on the sample surface is governed by the thermal penetration depth $\Delta\tau = 2(at_{\max})^{1/2}$ [35, 36]. It represents the minimum distance from the heating strip to the surface of the

sample. By adopting t_{max} with 300 s and a large cuboid box for packing samples, it can be guaranteed that the uncertainty is less than 1% due to the finite sample dimensions in this study. According to our previous numerical study [37], the nonzero thickness and the nonzero heat capacity of the heating strip is a main measurement error, especially for the materials with relative low thermal diffusivities. The thermal diffusivities of the measured samples are all larger than $4.0\times10^{-7}m^2/s$ in this study. By adopting the minimum time t_{min} of 30 s in thermal conductivity estimation, it can be guaranteed the error caused by the nonzero thickness and the nonzero heat capacity is less than 2%.

All of the above factors have been considered independently to assess the measurement uncertainties, and by uncertainty analysis separately, and using the law of uncertainty propagation, it is sure that the combined uncertainty of the thermal conductivity measurement with the THS method is less than 3 percent at ambient temperature.

5. Conclusions

The physical properties of measured powdered and granular samples were characterized withan automatic surface area and porosity analyzer and SEM picture. The thermal conductivity of the samples was measured with THS method at various temperature and pressures. The results can be concluded as follows:

(1) The thermal conductivity of powdered sample reaches to constant only when pressure less than 20 Pa, and the thermal conductivity of granular sample reaches to constant only when pressure less than 3 Pa due to macropore effect.

(2) The measured samples demonstrated similar patterns in thermal conductivity decreasing process with lower of gas pressure, It drops slowly when $p > 1000$ Pa, but drops quickly when $p < 1000$ Pa.

(3) The thermal conductivityof the measured granular and powdered silica aerogels increases distinctly with elevation of temperature. The bigger of the macropore in the silica aerogel samples, the higher of the thermal conductivity for silica aerogel materials at elevated temperatures.

Acknowledgements

This research was financially supported by the National Natural Science Foundation of China (No. 51376060) and the Fundamental Research Funds for the Central Universities (No. 10MG22).

References

[1] Y. L. He, T. Xie, Advances of thermal conductivity models of nanoscale silica aerogel insulation material, Applied Thermal Engineering 81 (2015) 28 - 50.

[2] G. S. Wei, Y. S. Liu, X. X. Zhang, F. Yu, X. Z. Du, Thermal conductivities study on silica aerogel and its composite insulation materials, Int. J. Heat Mass Transfer 54 (2011) 2355 - 2366.

[3] A. Saboktakin, M. R. Saboktakin, Improvements of reinforced silica aerogel nanocomposites thermal properties for architecture applications, Int. J. Biol. Macromol. 72 (2015) 230 - 234.

[4] Z. D. Shao, Y. Zhang, X. Cheng, Advances in mechanically enhanced silica aerogel monoliths as thermal insulating materials, Progress in Chemistry 26 (8) (2014) 1329 - 1338.

[5] G. Hayase, K. Kugimiya, M. Ogawa, Y. Kodera, K. Kanamori, K. Nakanishi, The thermal conductivity of poly methyl silsesquioxane aerogels and xerogels with varied pore sizes for practical application as thermal superinsulators, J. Mater. Chem. A2 (2014) 6525 - 6531.

[6] H. Zhang, W. Gua, M. J. Li, Z. Y. Li, Z. J. Hu, W. Q. Tao, Experimental study on the kinetics of water vapor sorption on the inner surface of silica nano — porous materials, Int. J. Heat Mass Transfer 78 (2014) 947 - 959.

[7] T. Xie, Y. L. He, Z. J. Hu, Theoretical study on thermal conductivities of silica aerogel composite insulating material, Int. J. Heat Mass Transfer 58 (1) (2013) 540 - 552.

[8] Y. F. Han, X. L. Xia, H. P. Tan, H. D. Liu, Modeling of phonon heat transfer in spherical segment of silica aerogel grains, Phys. B Condens. Matter 420 (2013) 58 - 63.

[9] C. Bi, G. H. Tang, Z. J. Hu, Heat conduction modeling in 3 - D ordered structures for prediction of aerogel thermal conductivity, Int. J. Heat Mass Transfer 73 (2014) 103 - 109.

[10] T. Y. Ng, J. J. Yeo, Z. S. Liu, A molecular dynamics study of the thermal conductivity of nanoporous silica aerogel, obtained through negative pressure rupturing, J. Non-Cryst. Solids 358 (2012) 1350 - 1355.

[11] Z. X. Lu, Z. S. Yuan, Q. Liu, Z. J. Hu, F. Xie, M. Zhu, Multi-scale simulation of the tensile properties of fiber-reinforced silica aerogel composites, Materials Science & Engineering A 625(2015)278 - 287.

[12] Y. Zhao, G. H. Tang, M. Du, Numerical study of radiative properties of nanoporous silica aerogel, Int. J.

Heat Mass Transfer 89 (2015) 110 - 120.

[13] M. S. Jeng, R. Yang, D. Song, G. Chen, Modeling the thermal conductivity and phonon transport in nanoparticle composites using Monte Carlo simulation, J. Heat Transf. 130 (2008) 042410 - 042411.

[14] D. Dan, H. Zhang, W. Q. Tao, Effective structure of aerogels and decomposed contributions of its thermal conductivity, Appl. Therm. Eng. 72 (2014) 2 - 9.

[15] H. T. Yu, D. Liu, Y. Y. Duan, X. D. Wang, Theoretical model of radiative transfer in opacified aerogel based on realistic microstructures, Int. J. Heat Mass Transfer 70 (2014) 478 - 485.

[16] J. J. Zhao, Y. Y. Duan, X. D. Wang, B. X. Wang, Effects of solidegas coupling and pore and particle microstructures on the effective gaseous thermal conductivity in aerogels, J. Nanopart. Res. 14 (2012) 1 - 15.

[17] J. Feng, Q. Gao, J. Feng, Y. Jiang, Preparation and properties of fiber feinforced SiO2 aerogel insulation composites, J. Natl. Univ. Def. Technol. 32 (2010) 40 - 44.

[18] G. S. Wei, Y. S. Liu, X. X. Zhang, X. Z. Du, Radiative heat transfer study on silica aerogel and its composite insulation materials, J. Non-Cryst. Solids 362 (2013) 231 - 236.

[19] H. Zhang, Y. Qiao, X. Zhang, S. Fang, Structural and thermal study of highly porous nanocomposite SiO2—based aerogels, J. Non—Cryst. Solids 356 (2010) 879 - 883.

[20] S. Q. Zeng , A. Hunt, R. Greif,Geometric structure and thermal conductivity of porous medium silica aerogel, ASME Journal of Heat Transfer 117(4) (1995) 1055 -1058.

[21] G. Reichenauer, U. Heinemann, H. P. Ebert, Relationship between pore size and the gas pressure dependence of the gaseous thermal conductivity, Colloids and Surfaces A: Physicochem. Eng. Aspects 300 (2007) 204 - 210.

[22] S. Spagnol, B. Lartigue, A. Trombe, F. Despetis, Experimental investigations on the thermal conductivity of silica aerogels by a guarded thin - film - heater method, ASME Journal of Heat Transfer 131 (2009) 1 - 4.

[23] C. Bi, G. H. Tang, Z. J. Hu, H. L. Yang, J. N. Li, Coupling model for heat transfer between solid and gas phases in aerogel and experimental investigation, Int. J. Heat Mass Transfer 79 (2014) 126 - 136.

[24] T. Gao, B. P. Jelle, T. Ihara, A. Gustavsen,Insulating glazing units with silica aerogel granules: The impact of particle size, Applied Energy 128 (2014) 27 - 34.

[25] T. Gao, B. P. Jelle, A. Gustavsen, S. Jacobsen,Aerogel-incorporated concrete: an experimental study, Constr Build Master 52 (2014) 130 - 136.

[26] A. Neugebauera, K. Chen, A. Tang , A. Allgeierd, L. R. Glicksmana, L. J. Gibsonc, Thermal conductivity and characterization of compacted, granular silica aerogel, Energy and Buildings 79 (2014) 47 - 57.

[27] S. E. Gustafsson, E. Karawack, M. N. Khan, Transient hot-strip method for simultaneously measuring thermal conductivity and thermal diffusivity of solids and fluids, J. Phys. D: Appl. Phys. 12 (9) (1979) 1411 - 1421.

[28] Z. Z. Chen, X. S. Ge, Y. Q. Gu, Calorimetry and Measurement of Thermophysical Properties (in Chinese), University of Science and Technology of China Press, Hefei, 1990.

[29] Y. S. Touloukian , P. E. Livey, S. C. Saxena, Thermal Conductivity: Nonmetallic Solids, IFI/Plenum Press, New York, 1970.

[30] F. Yu, X. X. Zhang, Experimental investigation on the thermal conductivity measurement of materials with hot-strip method, Acta Metrol. Sin. (in Chinese) 26 (1) (2005) 27 - 29.

[31] S. Brunauer, P. H. Emmett, E. Teller , Adsorption of gases in multimolecular layers, J. Am. Chen. Soc. 60 (1938) 309.

[32] K. Ramesh, K. S. Reddy, I. Rashmi, A. K. Biswas, Nanostructured Natural Zeolite: Surface Area, Meso-pore and Volume Distribution, and Morphology, Communications in Soil Science and Plant Analysis 45 (22) (2014) 2878 - 2897.

[33] J. Wang, J. Kuhn, X. Lu, Monolithic silica aerogel insulation doped with TiO2 powder and ceramic fibers, J. Non-Cryst. Solids 186 (1995) 296 - 300.

[34] S. Q. Zeng, A. Hunt, R. Greif, Theoretical modeling of carbon content to minimize heat transfer in silica aerogel, J. Non-Cryst. Solids 186 (1995) 271 - 277.

[35] M. Gustavsson, H. Wang, R. M. Trejo , E. Lara-Curzio, R. B. Dinwiddie, S. E. Gustafsson. Int J Thermophys, 27 (2006) 1816.

[36] M. Gustavsson, H. Nagai, T. Okutani, Solid State Phenom, 124 - 126 (2007) 1641.

[37] G. S. Wei, X. Z. Du, X. X. Zhang, F. Yu, J heat Transf , 132(2010) 1.

Determination of Linear Thermal Transmittance of Vacuum Insulation Panels by Measurement in A Guarded Hot-Plate (GHP) or a Heat-Flow Meter (HFM) Apparatus

Christoph Sprengard*, Andreas H. Holm

Forschungsinstitut für Wärmeschutz e. V. München - FIW München - (Research Institute for Thermal Insulation)
Lochhamer Schlag 4; 82166 Gräfelfing, Germany

Abstract

The determination of the linear thermal transmittance ψ is usually carried out by numerical simulations according to ISO 10211, but it can be carried out by measurement in a guarded hot-plate apparatus (GHP) or in a heat-flow meter apparatus (HFM) as well, if additional measures take the non-uniform temperature distribution within the surfaces of the VIP assembly with joints into account. The paper reports on linear thermal transmittance measurements that have been carried out and on reasonable boundary conditions and hints for exact measurements.

Keywords vacuum insulation panels, linear thermal transmittance, thermal bridging effects, measurement

1. Introduction

Besides the unidirectional heat-flows in the center of panel (COP) area, additional heat flows on the edges of VIPs occur due to thermal bridging effects, caused by the metal and plastic layers of the envelope of the VIP, the folding and welding areas of the envelope on the mere panel edges and by additional sealing layers and adhesive tapes used at these edges. In the joints between the panels in construction assemblies additional materials (e. g. pre-compressed gasket strips) lead to further thermal bridging effects. Even narrow air gaps in between panels arranged next to each other are a significant thermal bridge for highly insulating constructions containing VIP.

Thermal performance of VIP and constructions containing VIP can be determined by calculating the U-value (thermal transmittance) for a single element or component. It depends on the size of the panel or on the size of the construction and the thermal bridging effects. At least all two-dimensional effects have to be taken into account. If mechanical fasteners are used for the constructions which penetrate the insulating layer, also the three-dimensional effects are unneglectable:

$$U_{\text{Element}} = \frac{Q_{\text{Element}}}{A_{\text{Element}} \cdot \Delta\vartheta} \tag{1}$$

$$Q_{\text{Element}} = \Delta\vartheta \cdot (U_0 \cdot A_{\text{Element}} + \sum(\psi_i \cdot l_i) + \sum(\chi_i \cdot n_i))$$

U_{Element}, corrected U - value of whole element in W/(m^2 · K),

Q_{Element}, Heat flux through element in W,

A_{Element}, Area of element in m^2,

$\Delta\vartheta$, Temperature difference in K,

U_0, U - value of element without thermal bridges (center of element - one - dimensional) in W/(m^2 · K),

ψ_i, Linear thermal transmittance (e. g. for edges of panels) in W/(m · K),

χ_i, Point thermal transmittance (e. g. for mechanical fasteners) in W/K,

l, n, Length of the rims in m; number of anchors (dimensionless).

* Corresponding author, Tel: 49 - 89 - 85800 - 58, Fax: 49 - 89 - 85800 - 40, E-mail: sprengard@fiw - muenchen. de

For easier declaration of the thermal performance of VIPs in technical approvals and for similarity to conventional insulating materials, a single thermal performance value for VIPs needs to be determined. Equivalent thermal resistance for the elements or equivalent thermal conductivity for the insulating material is derived backwards from thermal transmittance and the thickness of the panels:

$$\lambda_{\text{eq Element}} = \frac{d_{\text{Element}}}{\frac{1}{U_{\text{Element}}} - R_s} \quad (2)$$

$\lambda_{\text{eq Element}}$, Equivalent thermal conductivity for a VIP including 2 - and 3 - dimensional thermal bridging effects in W/(m·K),

d_{Element}, thickness of the VIP in m,

R_s, Sum of internal and external thermal resistances at the surfaces of the panel in $m^2 \cdot K/W$.

If U_{Element} is determined by measurement of a joint assembly in a GHP or a HFM apparatus from $R_{\text{eq Element}}$ the cold-side and warm-side surface resistances are neglectible. The term R_s in equation can be omitted:

$$\lambda_{\text{eq Element}} = \frac{d_{\text{Element}}}{R_{\text{eq Element}}} \quad (3)$$

$\lambda_{\text{eq Element}}$, Equivalent thermal conductivity for a VIP including 2 - dimensional thermal bridging effects at the panel edges in W/(m·K),

d_{Element}, thickness of the VIP in m,

$R_{\text{eq Element}}$, Thermal resistance of the VIP including thermal bridges - taken from a measurement of a joint assembly in $m^2 \cdot K/W$.

2. Determination of ψ by measurement

The determination of the linear thermal transmittance ψ is usually carried out by numerical simulations according to ISO 10211 but it can be done by measurement in the guarded hot plate (GHP) and guarded heat-flow meter (HFM) as well, if additional measures take the non-uniform temperature distribution within the surfaces of the VIP assembly with joints into account.

Therefore two VIP were assembled within the GHP or HFM apparatuses that their joint is within the metering area (see Fig. 1). Temperature sensors have to be placed directly on the joint (area strongly influenced by thermal bridge), in the area slightly influenced by the edge effect and in the undisturbed area (COP) as well.

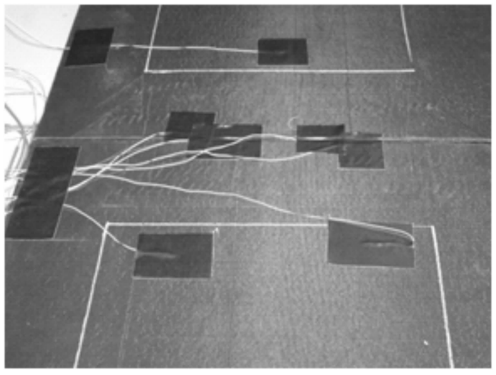

Fig. 1 Picture of a vacuum insulation paneljoint assembly in between two VIPs with two thermocouples attached directly to the joint, two near the joint (the slightly influenced area) and three in the center of panel (COP). The white marks show the metering area for earlier λ_{COP} measurements. The red mark shows the metering area for the edge assembly

The measured temperature differences on the different areas have to be area weighted and averaged before calculating the equivalent thermal conductivity result for the VIP.

$$\Delta\theta_m = \frac{A_{COP}\Delta\theta_{COP} + A_{SA}\Delta\theta_{SA} + A_{joint}\Delta\theta_{joint}}{A_{COP} + A_{SA} + A_{joint}} \quad (4)$$

$\Delta\theta_m$, Area weighted temperature difference for joint assembly in K,

A_{COP}, Center of panel area in m^2,

A_{SA}, Area slightly affected in m^2,

A_{joint}, Joint area (strongly affected) in m^2,

$\Delta\theta_{COP}$, Temperature difference for COP area in K,

$\Delta\theta_{SA}$, Temperature difference for SA area in K,

$\Delta\theta_{joint}$, Temperature difference for Joint area in K.

With the use of this area weighted temperature difference, the equivalent thermal resistance of the VIP including thermal bridges $R_{\text{eq Element}}$ were derived from the GHP or HFM measurement according to the respective standards, considering converging criteria and uncertainty. Equivalent thermal conductivity for a VIP including 2 - dimensional thermal bridging effects at the panel edges $\lambda_{\text{eq Element}}$ can be calculated then. Special precautions have to be taken, if the λ_{COP} of the two VIP is not identical.

The linear thermal transmittance ψ can be

determined by comparison of a GHP or HFM measurement in the center of a panel and the GHP or HFM measurement of the joint assembly by applying the following formulae. The surface resistances can be omitted for this calculation of the GHP and HFM setups, as it is assumed, that the heating and cooling plates are in perfect thermal contact with the specimens:

$$\psi = \frac{A}{d l_{\psi}} (\lambda_{\text{eq ja}} - \lambda_{\text{COP}}) \qquad (5)$$

ψ, linear thermal transmittance for the joints in the metering area in W/(m·K),

A, A metering area of the GHP or HFM apparatus used for the measurement in m^2,

d, thickness of the specimens (equal thickness of joint assembly and COP specimens required for this method) in m,

l_{ψ}, length of the joints within the metering area in m,

$\lambda_{\text{eq ja}}$, equivalent thermal conductivity including edge effects for the specific joint assembly in W/(m·K),

λ_{COP}, thermal conductivity for center of panel in W/(m·K).

In order to avoid congruency of the thermopiles of the heat-flow-meter sensor mat with the significant area of the joint, the heat-flow-meter mat should be arranged under an angle of 20°.

The linear thermal transmittance values for joints of two panels refer to the length of the joint. Linear thermal transmittance values for panel edges refer to the perimeter length of the panel. If a linear thermal transmittance value for a joint is used to calculate the equivalent thermal conductivity of a panel, it is to be divided by 2, before the multiplication with the perimeter length of the panel.

3. Supporting FD - Simulations

The width of the influenced areas depend strongly on the cross conduction within the barrier layers of the envelope and possible cover-layers on the surfaces of the VIPs. The sizes of the VIPs shall be selected big enough to assure a significant undisturbed area (COP) and a significant length of the joint within the metering area. Reasonable values for the influenced areas and the minimum panel sizes can be determined by numerical simulations of the assembly. In addition to the barrier properties, the results are influenced by the same criteria that influence the linear thermal transmittance, e. g. joint filler material and it's dimensions, edge design etc.. Fig. 2 shows the temperature gradient on the edge of an overlapping edge design of a naked VIP (without any cover layers). The calculation has been carried out for the same setup tested in the HFM apparatus with a gasket strip of 4 mm with thin adhesive layers on both sides. The warm-side boundary conditions for the simulation were 20℃ with a thermal surface resistance R_{si} = 0.13 m^2·K/W.

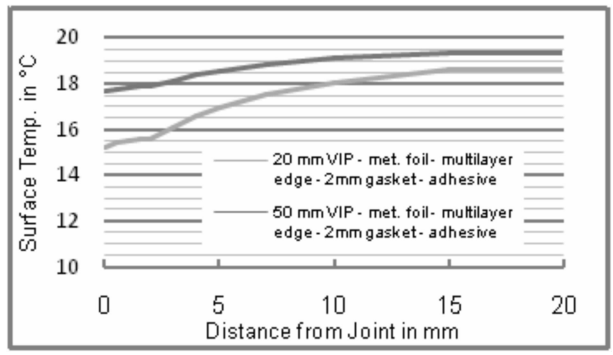

Fig. 2 Simulated temperature gradient on the edge of the tested 20 mm and 50 mm VIP assemblies

From the simulated temperature gradient on the panel edge, the representative areas for the weighted temperature differences are derived. The areas for the assessment of the measurement of the joint assembly are stated in Tab. 1. Only a minor dependency on the thickness of the VIP can be found for the 20 mm and 50 mm panels simulated.

Tab. 1 Areas for weighting the temperature differences for metering area 500 × 500 mm in HFM

Type of area	Representative area A in m^2 for temperature difference	
	20 mm VIP	50 mm VIP
Center of panel (A_{COP})	0.235	0.237
Slightly affected by thermal bridge (A_{SA})	0.013	0.011
Joint area (A_{joint})	0.002	0.002
Total metering Area (A_{tot})	0.250	0.250

4. Results and discussions

The results for the linear thermal transmittance ψ obtained from numerical simulations (FD－method) and from measurements of similar joint assemblies are shown in Tab. 2. For the 20 mm thick VIP assembly, the results from measurement and simulation fit well under consideration of 5 % uncertainty for the measurement. The result of the 50 mm thick VIP from measurement is significantly higher than ψ from numerical simulation－even under consideration of an increased uncertainty of 8 %, due to higher thermal resistance and much lower heat-flux.

Tab. 2 Comparison of results for ψ obtained from simulations and measurements-metallized foil-multilayered edge design-with silicone foam mats as contact layers

VIP Thickness	Linear thermal transmittance ψ in W/(m·K) obtained from...	
	numerical simulation with FDM	measurement in HFM apparatus
10 mm	0.0209	—
20 mm	0.0144	0.0151 ± 0.000755
30 mm	0.0109	—
40 mm	0.0088	—
50 mm	0.0073	0.0127 ± 0.00102

The deviating results for the 50 mm VIP can-partly be traced back to an increased λ_{COP} for one of the VIPs. Additionally, the width of the joint could have been slightly more than 4 mm due to higher force required to compress the gasket strip.

5. Conclusions and outlook

The measurement of linear thermal transmittance ψ is dependent on a large variety of influencing factors that need to be considered for highest level of accuracy. Even small deviations in the measurement setup can lead to big uncertainties for the results. In order to use measurements for the determination of ψ in future, the definition of exact boundary conditions for comparable results is inevitable. More tests are needed in the future to find out about the practicability of measurements on VIP with other edge designs, other barrier materials, thicker barrier layers (e. g. Al-foil) and for VIP with cover layers.

References

[1] EN 12667:2001
[2] EN 12664:2001
[3] EN 1946－2:1999
[4] EN 1946－3:1999

Evaluation of VIPs After Mild Artificial Aging During 10 years: Focus on the Core Behavior

Emmanuelle Pons[a*], Bernard Yrieix[a], Samuel Brunner[b]

a. EDF R&D, Materials and Mechanics of Components, EDF Lab les Renardières, F-77818 Moret-sur-Loing, France

b. Empa, Swiss Federal Laboratories for Materials Science and Technology, Laboratory for Building Energy Materials and Components, Ueberlandstrasse 129, CH-8600 Duebendorf, Switzerland

Abstract

The prediction of the long term performance of VIPs remains challenging. To improve the forecast, the evaluation of VIPs aged for very long periods can help significantly. This study reports the characterization method which was implemented on VIPs after an artificial aging of 10 years in the laboratory, at room temperature and in two different relative humidities (quite low and high). The aim is to evaluate the hygrothermal and structural evolutions of the core material and to interpret them thanks to the detailed study of the aging of the fumed silica core. The permeance of the barrier laminate is also estimated.

Keywords long term aging, characterization, fumed silica core

1. Introduction

The prediction of the long term performance of VIPs remains challenging. It is important that the thermal conductivity of VIPs after a long aging in laboratory or in service is not underestimated. There are many reasons for the deviation towards too low predicted values: e. g. the relevance of the model used or the accuracy of the data. The aging of the core material that is often not taken into consideration can also be responsible for the difference between prediction and measurements, as it has recently been pointed out [1].

To improve the forecast, the evaluation of VIPs aged for very long periods can help significantly. It is the object of this study, which reports the characterization procedure which was developed on VIPs aged during 10 years in the laboratory. The aim is to evaluate the hygrothermal and structural evolutions of the core material, thanks to water sorption measurement, drying tests, and nitrogen sorption measurements (to evaluate the irreversible modifications of the silica core after 10 years of aging). The tests were proceeded on the core as the VIPs were opened but also after an additional aging of the core outside the VIPs during over 1 month at high humidity level. The evolutions can be interpreted thanks to the detailed study of the aging of the fumed silica core. Concerning the barrier laminate, the follow-up on the weight and internal pressure of the VIPs gives an assessment of the water vapor and air permeances.

2. Experimental

2.1 Samples

The VIP samples aged in Empa laboratory at 23℃ and in two different relative humidities, quite low (33%) and high (80%). 6 VIPs were studied: 2 VIPs of 500×500 mm^2 aged at 33% RH (ref. 12/13) and 4 VIPs aged at 80% RH (ref. 3/4 250×500 mm^2 and ref. 6/7 500×500 mm^2). The beginning of the aging was 2003, and it was ended in 2014. The core is made up of fumed silica (Wacker WDS 200 $m^2 \cdot g^{-1}$), fibers and opacifier.

* Corresponding author, E-mail: emmanuelle.pons@edf.fr

Concerning the details of their composition and conditioning, the hypothesis done are:

—fibers: a mass ratio of 2% of PET fibers was supposed but it could be also cellulose fibers;

—opacifier: SiC mass ratio of 5%;

—drying at 140℃.

The measurements during aging are the following (VIPs of 500×500 mm^2):

—Mass and internal pressure at the beginning, after about 200 days and at the end with about 3950 days.

—Conductivity at the beginning and at the end.

The barrier laminate isthe three-fold metalized polymer laminate referenced MF4 in the Annex 39 of the IEA [2] and MF2 in the linked paper [3].

2.2 Evaluation method of the silica core

The evaluation method of the core isas follows:

—Quantification of the water mass content τ_{VIP} by the weight measurements of the VIP.

The VIP is opened to sample the core, and then re-sealed. It was checked that the water content adsorbed in the sample τ_{ads} can be approximated by the water content of the VIP (influence of the mass of water vapor negligible).

—Quantification of thechemi-and physisorbed water by the drying method. The VIP are opened to sample the core, and they are re-sealed. The drying is done thanks to a vacuum pretreatment instrument Belprep (Bel Japan) and an analytical balance model AT261 DeltaRange (Mettler Toledo) as follows:

• First drying during 2h at 140℃, which is the temperature usually employed by the VIP manufacturers,

• Second drying during 2h at 200℃, to besure having dried all the physisorbed water [4, 5]; the dried amount gives τ_{phys}.

• The chemisorbed amount can then be deducted: $\tau_{chem} = \tau_{ads} - \tau_{phys}$.

—Water sorption isotherm at 25℃ after preparation under vacuum at 140℃. The preparation is made with the Belprep and the isotherm is established on a very accurate apparatus (Belsorp Aqua) using the volumetric method (Bel Japan). The main parameters deducted from the isotherms are ā (the slope of the water vapor isotherm $\tau_{ads} = f(p_v)$ of the core in the considered aging states and the value $\tau_{abs@50\%RH}$. The comparison with the classical new silica gives the intensity of the aging of the core.

—Water sorption isotherm at 25 ℃ after a treatment in climatic chamber (23℃, 90% RH, 1month) to age the core to the same level as the one reached in service in intermediate solicitations conditions.

—Nitrogen sorption to determine the specific area (BET method) and the pore size distribution (BJH method) and therefore evaluate aging. The same preparation than for water sorption measurement is made with the Belprep and the isotherm is recorded with a Belsorp Max (Bel Japan).

As the reference state of the silica is no more available, the silica aged at (23℃, 33% RH) is considered to be very little modified.

2.3 Evaluation method of the multilayer barrier laminate

The weight and internal pressure increases of the VIPs were recorded, sothe water vapor and air permeance of the barrier laminate can be estimated. The following equations were used:

$$j = \pi A(p_{ext} - p_{int}) \quad (1)$$

Where

j =mass flux ($kg \cdot s^{-1}$),

π =permeance ($kg.\ m^{-2} \cdot s^{-1} \cdot Pa^{-1}$),

A =barrier laminate area (m^2),

p_{ext}, p_{int} = partial pressures outside, inside the VIP (Pa).

For water vapor, the weight increase during theaging is used and Eq. (2) directly gives the permeance of water vapor:

$$\pi_{wv} = \frac{\Delta m}{\Delta t} \times \frac{1}{A(p_{wv,ext} - p_{wv,int})} \quad (2)$$

For air, two different hypotheses are considered: i) all the pressure increase corresponds to air, or ii) the pressure increase corresponds to a mix of dry air and water vapor. The pressure increase inside the VIP during the aging is used to calculate the mass permeance by Eq. (3)

$$\pi_a = \frac{M_a \times V_{pores}}{R \times T} \times \frac{\Delta p_{a,int}}{\Delta t} \times \frac{1}{A \times (p_{a,ext} - p_{a,int})} \quad (3)$$

Where

M_a = molar mass of air (kg • mol^{-1}),

V_{pores} = porous volume of the VIP core (m^3),

R = universal gas constant (8.314 m^3 • Pa • K^{-1} • mol^{-1}),

T = temperature (K).

3. Results

3.1 Weight, pressure and conductivity increase over 10

The evolutions of the mass, internal pressure and conductivity during over 10 years are listed in Tab.1.

Tab. 1 Weight gain, pressure increase in the VIP and conductivity evolution during aging (for each condition: average over 2 VIPs)

Sample	Aging	Envelope area / m^2	$\frac{\Delta m}{\%}$	$\frac{\Delta p_{int}}{mbar}$	$\frac{\Delta\lambda}{mW \cdot m^{-1} \cdot K^{-1}}$
12/13	3948 days at (23℃, 33% RH)	0.535	0.57	4.9	0.6
6/7	3881 days at (23℃, 80% RH)	0.532	3.13	17.6	2.2

3.2 Drying tests

The weight loss of the core dried 2h at 140 and 200℃ is given in Tab.2 (% of the wet initial mass).

Tab.2 Weight loss of the core by drying (assessment of the physisorbed water)

Sample	Aging	Weight loss by drying /(%)	
		at 140℃	at 200℃
12	10 years at (23℃, 33% RH)	0.85	1.16
3	10 years at (23℃, 80% RH)	2.30	2.47

The amount of physisorption τ_{phys} is about 1.2% for the VIPs aged at 33% RH and 2.5% for the VIPs aged at 80% RH. As a consequence, the amount of chemisorbed water τ_{chem} is respectively no significant (Δm% lower than τ_{phys}) and 0.66% which is a low value typical of fumed silica. It can be noted that at 140℃ some physisorbed water can remain, up to 27% according to the results obtained for the sample 12. The results confirm the need to dry at 200℃ to completely dry the physisorbed amount of water.

3.3 Water vapor sorption

The water sorption isotherm were recorded on the core just as the VIP was opened but also after an additional aging of the core outside the VIP during over 1 month at high humidity level for one VIP aged at 80% RH. This additional aging was performed at 23℃ and 50℃ to evaluate the level of the long-term aging at (23℃, 80% RH) in comparison with the maximum level that the silica core could reach. Table 3 gives the equilibrium water content at 50% RH for the samples tested of the VIP aged at (23℃, 80% RH), just as aged and after short-term additional aging. The water content is relatively moderate in comparison with the levels reached after additional aging (the additional aging was pursued and the reached levels—not given in the table—are higher). The water vapor isotherm allows also to estimate the humidity level reached inside the VIP: 3% of water content corresponds to a humidity level inside the VIP of 88% or 24.7 mbar at 23℃. This value is close to the exposure value, so the water vapor flux through the envelope at the end of the aging must be zero. Correspondingly, during the whole time of aging, the mass increase of the VIP cannot be linear. The hygric aging of the VIP in these stationary conditions has reached a maximum which can only be shifted towards higher equilibrium value of the water content by the aging of the core itself and its increasing hygrophilicity.

Tab. 3 Water content deducted from the adsorption isotherm

Sample	Aging	$\tau_{ads@50\% RH}$
3	10 years at (23℃, 80% RH)	0.9%
3	10 years at (23℃, 80% RH) + 42 days at (23℃, 90% RH)	2.3%
3	10 years at (23℃, 80% RH) + 1 month at (50℃, 90% RH)	3.9%

3.4 Nitrogen sorption: evolution of the BET specific area

Tab.4 gives the BET specific areas(A_{BET}) deducted from the nitrogen adsorption. The hypothesis made on the composition of the real core leads to a correction of 7% for the value on the silica only (only the average value is given for the silica).

In comparison with the A_{BET} of the sample aged at (23℃, 33% RH), the A_{BET} for an aging at 80% RH appears nearly stable with a very small decrease of only 6%. As expected the A_{BET} of the core additionally aged shows a greater decrease.

Tab. 4 BET specific area (nitrogen measurements) of the core / estimation for the silica

Sample	Aging	$A_{BET\ core}$ measured $m^2.g^{-1}$	$A_{BET\ silica}$ calculated $m^2.g^{-1}$
12	10 years at (23℃, 33% RH)	219～220	235
3	10 years at (23℃, 80% RH)	175～205	203
3	10 years at (23℃, 80% RH) + 1 month at (23℃, 90% RH)	168	180

3.5 Evaluation of the laminate

The permeances of air and water vapor calculated from Eq. (2) and Eq. (3) are given in Tab. 5. The values of the water vapor permeance correspond to current high quality metalized laminates (calculated in similar vapor pressures). The ratio between the water vapor and air permeances is about 4 orders of magnitude, that corresponds to bibliographic data [6]. But for the calculation of the air permeance, the internal pressure measurements of the VIP have been used considering it is only air, what completely disagrees with the high water vapor pressure inside the VIP estimated from the weight gain and the sorption isotherm (24.7 mbar). This is to be checked.

Tab. 5 Permeances of water vapor and air assessed from weight and pressure increases over 10 years (mean values over 2 VIPs)

Sample	Aging	Π_{wv} $kg \cdot m^{-2} \cdot s^{-1} \cdot Pa^{-1}$	Π_a $kg \cdot m^{-2} \cdot s^{-1} \cdot Pa^{-1}$
12/13	10 years at (23℃, 33% RH)	3.2E−14	1.5E−18
3/4	10 years at	7.5E−14	–
6/7	(23℃, 80%RH)	7.4E−14	5.2E−18

4. Discussion

4.1 Evaluation of the surface hygrophilicity

The ratio of the water content at equilibrium at 50% RH divided by the specific area $\psi_{ads} = \tau_{ads@50\%HR}/A_{BET}$ is a fine way to express the surface hygrophilicity which can be strongly affected in the case of aging. The results are shown in Tab. 6.

The surface hygrophilicity of the VIP aged at (23℃, 80% RH) during 10 years is very close to the one of standard fumed silica, and far fromthe values obtained on this silica aged 30 days at (23℃, 80% RH). This shows that the core of the VIP aged 10 years at (23℃, 80% RH) is not or only slightly aged. This is consistent with the small decrease of A_{BET} .

Tab. 6 Assessment of the surface hygrophilicity of the VIP core

Sample	Aging	$\frac{\psi_{ads}}{\mu g \cdot m^{-2}}$
3	VIP 10 years at (23℃, 80% RH)	47.6
Reference fumed silica	silica not aged	47.0
	silica, 30 days at (23℃, 80% RH)	170.0

4.2 Prediction of the conductivity evolution

Impact coefficient of water and pressure intakes The models developed in 2005 are expressed in the following equations [3, 4]:

$$\Delta\lambda = B\tau_W + Gp_g \quad (4)$$

$$\Delta\lambda_{(t)} = B\tau_{W\infty}\left(1-\exp\left(\frac{-t\Delta m_{(t)}}{\tau_{W\infty}}\right)\right)+G\Delta p_{g(t)}\,t \quad (5)$$

Where

$\tau_W, \tau_{W\infty}$ = water content of the VIP and at equilibrium,

p_g =pressure inside the VIP (p_{int} in the simplified version or $p_{g} = p_{dry\ air} = p_{int} - p_{wv}$ in the version used in [3] and [7]).

The values of the parameters B and G, which don't consider any aging of the core, are the following [3, 7]:

$B = 0.5\ mW \cdot m^{-1} \cdot K^{-1}\%^{-1}$

$G = 0.035\ mW \cdot m^{-1} \cdot K^{-1} \cdot mbar^{-1}$

This simple model has been applied with the values of the aging of 10 years (Tab. 1). The predicted values of the conductivity are given in Table 7 and compared with the measured values. They in good agreement.

Tab. 7 Calculated values by the model Eq. (4) and measured values of the thermal conductivity increase

Sample	Aging	Δm (%)	Δp_{int} (mbar)	$\Delta\lambda_{calc}$ ($mW \cdot m^{-1} \cdot K^{-1}$)	$\Delta\lambda_{meas}$ ($mW \cdot m^{-1} \cdot K^{-1}$)
12	3948 days (23℃, 33% RH)	0.57	5.1	0.5	0.6
13		0.57	4.8	0.5	0.6
6	3881 days (23℃, 80% RH)	3.16	17.8	2.2	2.2
7		3.11	17.5	2.2	2.2

This shows that the parameters B and G are suitable and accurate for the VIPs aged during 10 years. In other words, this means that the core is not

sufficiently aged to exhibit modified behavior, and thus to modify the parameters B and G. This conclusion is consistent with the one deducted from the surface hygrophilicity and A_{BET}.

4.3 Relevance of short-term determination of the permeances

Another question is the relevance for very long durations of the permeances of water and air determined by short-term tests. The short-term values for these VIPs (previously estimated [3] and deducted from the present work and [9]) are compared in Table 8 to the long-term ones (this publication and presentations of R. Caps at the Annex 65 of the IEA [8]).

The water vapor permeance is calculated from the mass uptake. In Tab.8, the gas permeance is calculated considering the total pressure increase in the VIP as a whole (no distinction between the vapor and dry air because of the discordance of the two pressures mentioned above).

The experimental results reveal no significant dispersion in the couples of samples tested (individual results not given in the Table). The following observations can be made (Tab.8):

—Unlike other works [2, 3, 7], no influence of the geometry is observed. This might be related to the small difference in dimension of samples considered here.

—The water vapor and gas permeances are higher after 10 years than after about 200 days. This is not consistent with the WV pressure inside the VIP deducted from the WV isotherm.

—The water vapor and gas permeances at 80% RH are close to those at 50% RH and slightly higher than those at 33% RH.

Using the short-term tests, we can finally estimate the long-term conductivity increase using Eq. 4 and 5. For this last equation, the parameter $\tau_{W\infty}$ is taken equal to 8%, a value corresponding to the aged core "SIL 2" [2]. The comparison with the measured conductivity increase is done for samples 6 and 7 in Tab.8. The two methods underestimate this increase. This is consistent with already cited work [1] but it is quite surprising in our case, because of the poorly aged core and because of the water uptake which is supposed to be finished. This needs further works; some already in progress and others to be engaged for example on cycling and thermal gradient effects.

5. Conclusions and outlook

The evaluation of VIPs after mild artificial aging during 10 years revealed that the silica core has not been or slightly aged, even at high relative humidity (80% RH). This was highlighted by different results: i) the moisture content at equilibrium, which is far from the moisture content that could be reached by short-term additional aging at higher humidity levels, ii) the evolution of the specific area, and iii) the validity of the parameters B and G for the simplified model.

On the other hand, the water sorption isotherm indicates that the moisture content inside the VIPs, deducted from the weight increase, corresponds to a humidity level over 80%. So the water ingress must have been stopped (driving force for water permeation), if the value is near 80%. And the VIPs can even be dried, if the environmental conditions change, as it was confirmed by the weight loss of the VIPs over the last year, where they were placed at (23℃, 50% RH). In parallel, although the stationary conditions have avoided higher relative humidity periods, the high current water content reached inside the VIP (corresponding to 80% RH at 25 ℃) can now strongly activate the core aging of the silica. Indeed, it is now just in the capillary condensation domain and any temperature decrease will lead to micro condensation and maybe saturation and therefore to a strong aging of the core itself.

As the main lever to age the silica is the humidity, one can deduce that the VIP aging is divided in two steps: the first where no aging of the silica occurs because of too dry conditions inside, and a second one where the silica ages because of the high humidity inside. For the studied samples the results above lead to estimate the duration of the first period at just under ten years. To go further, similar investigations of VIPs from real applications with changing boundary conditions should give clearer answers.

Acknowledgements

The authors acknowledge the ANR (French National Research Agency) for their financial support of

the EMMA - PIV project (ANR - 12 - VBDU - 0004) and the SFOE (Swiss federal office of energy) for the financial support of Empa in the Annex 65 project. Special thanks to Dr. Roland Caps (va - Q - tec) for the fruitful discussion and to Christophe Gourgues (EDF R&D) for the experimental tests.

References

[1] S. Brunner, K. Ghazi Wakili, Vacuum 100 (2014) 4 - 6.

[2] H. Simmler et al, IEA/ECBCS Annex 39 HiPTI-project (High Perfor-mance Thermal Insulation for Buildings and Building Systems), Technical Report on Subtask A (2005).

[3] H. Simmler, S. Brunner, Energy and Buildings, 37, (2005) 1122 - 1131.

[4] B. Yrieix, B. Morel, E. Pons, Energy and Buildings 85 (2014) 617 - 630.

[5] L. T. Zhuravlev, Colloids and Surfaces A: Physicochemical and Engineering Aspects, 173 (2000) 1 - 38.

[6] M. Bouquerel, PhD Thesis, Institut National des Sciences Appliquées de Lyon (2012).

[7] S. Brunner, H. Simmler, Vacuum 82 (2008) 700 - 707.

[8] R. Caps, presentation at the IEA EBC Annex 65 Kick-off Meeting, Grenoble 11&12 Sept. 2015 (followed up by his IVIS2015 paper).

[9] S. Brunner, presentation at the IEA/ECBCS Annex 39, 29 April 2004.

Tab. 8 Mass and pressure increase rates and permeances for different VIP aged at 23 °C; comparison of the calculated and measured conductivity increases

Sample	Aging	Size	$\Delta m/\Delta t$	$\Delta p_{int}/\Delta t$	Π_{WV}	Π_g	$\Delta\lambda$forecasted Eq. 4	$\Delta\lambda$forecasted Eq. 5	$\Delta\lambda$measured
		(cm^3)	($\%.y^{-1}$)	($mbar.y^{-1}$)	($kg.m^{-2}.s^{-1}.Pa^{-1}$)		($mW.m^{-1}.K^{-1}$)		
12/13	3948 days at (23℃, 33% RH)	50×50×2	0.05	0.46	3.2E−14	1.5E−18	—	—	0.60
[3], [9]	180 days at (23℃, 50% RH)	25×25×2	0.16	1.4	6.0E−14	4.0E−18	—	—	—
		25×50×2	0.13	1.3	5.1E−14	3.8E−18			
		50×50×2	0.12	1.0	4.9E−14	3.0E−18	—	—	—
3/4	222 days at (23℃, 80% RH) [9]	25×50×2	0.22	1.1	5.6E−14	3.4E−18	—	—	—
	4115 days at (23℃, 80% RH)		0.30	—	7.5E−14	—	—	—	—
6/7	236 days at (23℃, 80% RH)[9]	50×50×2	0.21	1.3	5.3E−14	5.1E−18			
	3881 days at (23℃, 80% RH)		0.30		7.4E−14	5.2E−18	1.59	1.45	2.20

Experimental Investigations of Vacuum Insulation Panels in an Alkaline Environment

Bjørn Petter Jelle[a,b*], Synne Christina Helgerud[b], Samuel Brunner[c], Gao Tao[b], Egil Rognvik[a]

a. SINTEF Building and Infrastructure, Department of Materials and Structures, NO—7465 Trondheim, Norway
b. Norwegian University of Science and Technology (NTNU), Department of Civil and Transport Engineering, NO—7491 Trondheim, Norway
c. Swiss Federal Laboratories for Materials Science and Technology, Laboratory for Building Energy Materials and Components, CH—8600 Dübendorf, Switzerland

Abstract

The durability and various ageing mechanisms of vacuum insulation panels (VIP) are crucial aspects to be investigated. Loss of vacuum, either partially and gradually or totally and promptly, will increase the thermal conductivity of the VIPs, typically in the range from 4 mW/(m · K) (pristine non-aged condition, centre-of-panel) to 20 mW/(m · K) (total loss of vacuum). In this work, the durability of VIPs in an alkaline environment, i. e. with respect to applications where VIPs are used in contact with or in close proximity to concrete and cementitious materials was studied. The alkaline environment in concrete may lead to reactions with the aluminium in the multi-layered laminate used as the VIP envelope, thus weakening or destroying the barrier function of the laminate. The VIPs were subjected to alkaline solutions at different pH-values and temperatures. The VIPs during exposure ageing were characterized by thermal conductivity measurements and scanning electron microscopy (SEM) studies of the VIP laminate. The results from the VIP experiments showed various degrees of degradation effects. In general, elevated temperatures proved to be the most significant ageing strain.

Keywords vacuum insulation panel, VIP, alkaline, concrete, durability, ageing

1. Introduction

As the world's attention is drawn stronger towards various means of decreasing the energy usage, the application of high performance thermal insulation materials and technologies like e. g. vacuum insulation panels (VIP) [1 - 13] for achieving energy-efficient buildings may represent part of a viable solution. However, long-term durability of the VIPs are crucial [1, 2, 5, 6, 9], and in this respect the resistance in alkaline environment like concrete constructions will be important. Hence, this work investigates the behaviour and durability of VIPs placed in an alkaline environment at different pH-values and temperatures.

2. Experimental

The VIPs used in the experiments were of the type Vacuspeed from the producer Porextherm [14] with dimensions 250 mm × 250 mm × 20 mm (length × width × thickness). The VIP envelope cross-section for the VIPs employed in this study is shown in Fig. 1 as a schematic illustration and a scanning electron microscope (SEM) photo, including the metallized aluminium (Al) polymer layers. The VIPs were subjected to an alkaline environment (aqueous $Ca(OH)_2$ solution) as depicted in Fig. 2, i. e. between two concrete slabs with no

* Corresponding author, Tel: 47 - 73593377, Fax: 47 - 73593380, E-mail: bjorn. petter. jelle@sintef. no

protective plastic films applied (worst-case scenario), at a temperature of 20℃ and pH-values 10.6 (A1) and 12.6 (A2) and a temperature of 70℃ and pH-values 10.6 (B1) and 12.6 (B2). For pH = 10.6 (A1 and A2) the liquid level was 15 mm under the upper edge of the underlying concrete slab, whereas for pH = 12.6 (B1 and B2) the VIP was fully submerged in the alkaline solution. A reference experiment with VIPs submerged in water at 20℃ and pH = 7.0 (C1) was conducted as illustrated in Fig. 3.

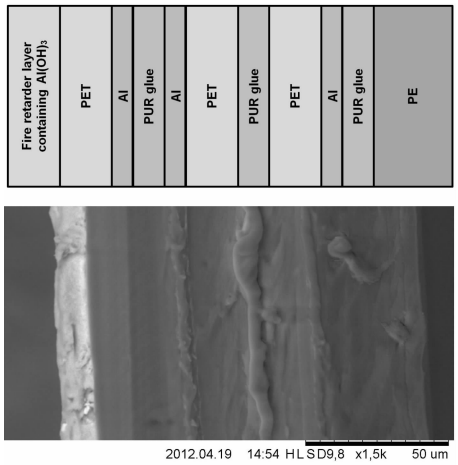

Fig. 1 VIP envelope cross-section (exterior layer to left) for the VIPs employed in this study as a schematic illustration (top) and a SEM photo (bottom) (non-aged VIP) (magnification 1500x and scale-bar 50 μm). Polyethylene (PE), polyurethane (PUR) and polyethylene terephthalate (PET)

The VIP samples were examined by visual observations (digital photos) and measurement of physical dimensions, mass and thermal conductivity, during an ageing period of 12 weeks. A heat flow meter apparatus was used to measure the thermal conductivity.

A VIP envelope was separated from the VIP core, where upon the backside of the envelope was sealed with lacquer and thereafter immersed in a 0.03 M $Ca(OH)_2$ aqueous alkaline solution at 20℃ and pH = 12.6 as depicted in Fig. 4. A Hitachi TM 3000 Tabletop SEM was used to investigate the VIP envelope configuration and any degradations during an ageing period of 9 weeks.

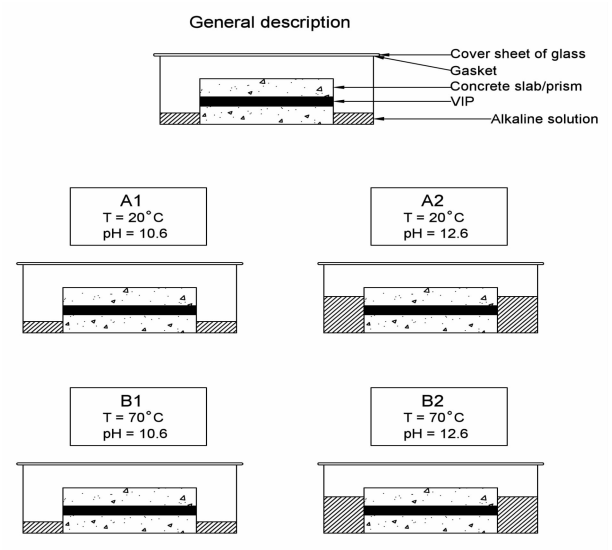

Fig. 2 Schematic setup of VIP alkaline experiments

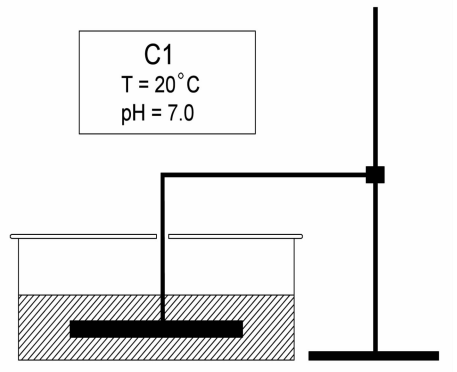

Fig. 3 Schematic setup of VIP reference experiment

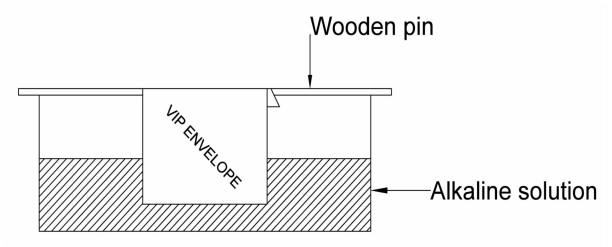

Fig. 4 Schematic setup of VIP envelope experiment

The full details of the experimental conditions will be reported in a complete journal article.

3. Results and discussion

In Figs. 5～7 VIPs are shown for various ageing times at temperatures 20 and 70℃ and pH-values 10.6 and 12.6. No significant visible degradation was observed for ageing at 20℃ (A1 and A2), whereas considerable visible degradation was observed for ageing at 70℃ (B1 and B2) where the top polymer layer and top Al layer were destroyed.

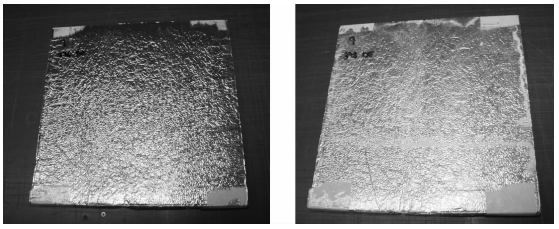

Fig. 5 Two VIPs aged at 20℃ and pH = 10.6 (left, A1) and pH = 12.6 (right, A2) for 9 weeks. No significant visible degradation was observed. Various marks are due to tape glue and $CaCO_3$ residues

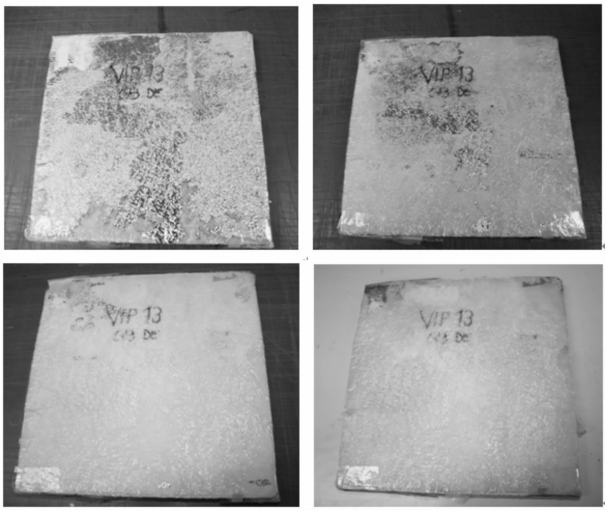

Fig. 6 A VIP aged at 70℃ and pH = 10.6 (B1) for 3, 6, 9 and 12 weeks (from top left to bottom right corner). Considerable visible degradation was observed

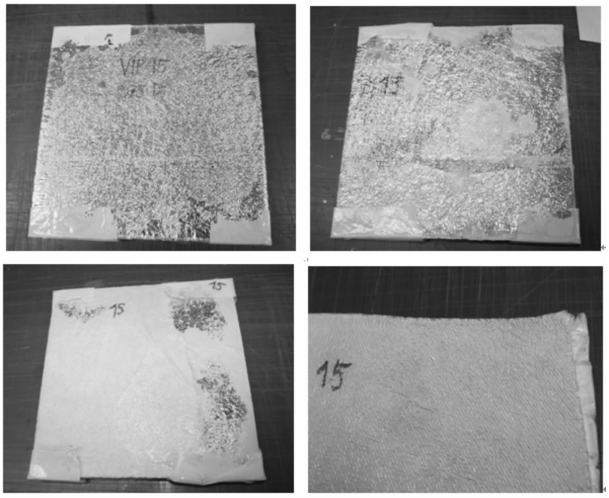

Fig. 7 A VIP aged at 70℃ and pH = 12.6 (B2) for 3, 6, 9 and 12 weeks (from top left to bottom right corner). Considerable visible degradation was observed

Measurement of the VIP thickness during ageing time did not reveal any significant differences between the various ageing experiments as shown in Fig. 8. Note that two VIPs for the B2 experiments ($B2_2$ and $B2_3$) were totally destroyed after only 3 weeks of ageing, and are hence not depicted in Figs. 8～10.

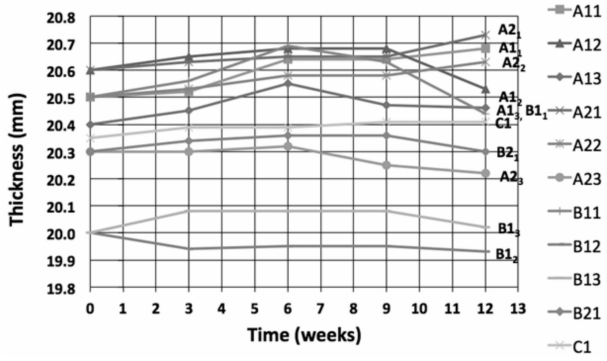

Fig. 8 VIP thickness versus time for various ageing experiments. A1, A2, B1, B2 and C1 experiments with the second numbers denoting parallel samples

Measurement of the VIP mass during ageing time revealed a large difference between the various ageing experiments as shown in Fig. 9, with only a small mass increase for the A1, A2 and C1 experiments (20℃) and a large mass increase for the B1 and B2 experiments (70℃). The large mass increase for the B1 and B2 experiments is explained by ingress from the surrounding alkaline solution (concrete slabs and aqueous $Ca(OH)_2$ solution).

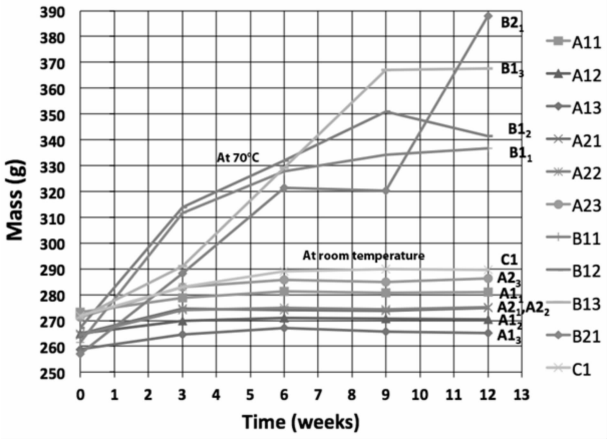

Fig. 9 VIP mass versus time for various ageing experiments. A1, A2, B1, B2 and C1 experiments with the second numbers denoting parallel samples

Measurement of the VIP thermal conductivity during ageing time revealed a large difference between the various ageing experiments as shown in Fig. 10, with only a small thermal conductivity increase formost

of the A1, A2 and C1 experiments (20℃) and a large thermal conductivity increase for the B1 and B2 experiments (70℃). All the VIPs in the B1 and B2 experiments got punctured, i.e. three after (or before) 3 weeks ($B1_1$, $B2_2$ and $B2_3$) and three after 9 weeks ($B1_2$, $B1_3$ and $B2_1$) ageing (Fig. 10). Compare also the mass increase (Fig. 9) with the thermal conductivity increase (Fig. 10). None of the VIPs in the A1, A2 and C1 experiments got punctured, and most of these VIPs experienced only a small or almost no increase in the thermal conductivity as shown in the close-up in Fig. 11.

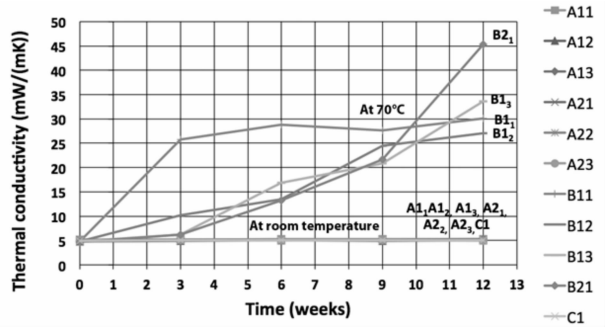

Fig. 10 VIP thermal conductivity versus time for various ageing experiments. A1, A2, B1, B2 and C1 experiments with the second numbers denoting parallel samples

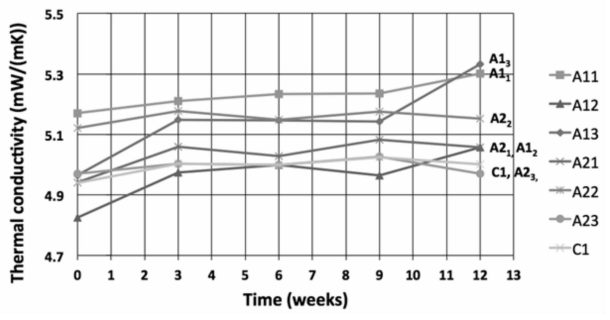

Fig. 11 VIP thermal conductivity versus time for various ageing experiments. Close-up of the A1, A2 and C1 experiments from Fig. 10

The deterioration of the VIP envelope was examined closer by carrying outa VIP envelope ageing experiment (Fig. 4) with SEM and energy dispersive spectroscopy (EDS) elemental analysis results as shown in Fig. 12 and Fig. 13.

The SEM photos and the EDS analysis in Fig. 12 and Fig. 13 (not all details shown here) demonstrate a deterioration of the VIP envelope during the 9 weeks exposure in the VIP envelope experiment (Fig. 4). Note that the temperature was 20℃ in this ageing experiment. The three non-aged thin Al layers of about 0.1 μm may be a bit difficult to spot, while the outer fire retarder layer containing $Al(OH)_3$ is much thicker and hence more visible. The total thickness of the VIP envelope was found to decrease during the 9 weeks exposure in the alkaline environment, including a decrease in the distance between the three Al layers. Evidently, there were changes to the exterior fire retarder layer containing $Al(OH)_3$ and reductions of the various polymer layers.

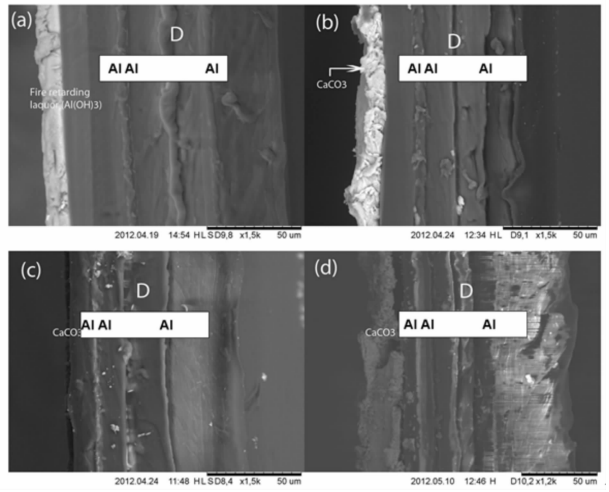

Fig. 12 SEM photos of VIP envelope cross-sections for non-aged (a), aged 3 (b), 6 (c) and 9 weeks (d) samples as depicted in Fig. 4 (scale-bars 50 μm)

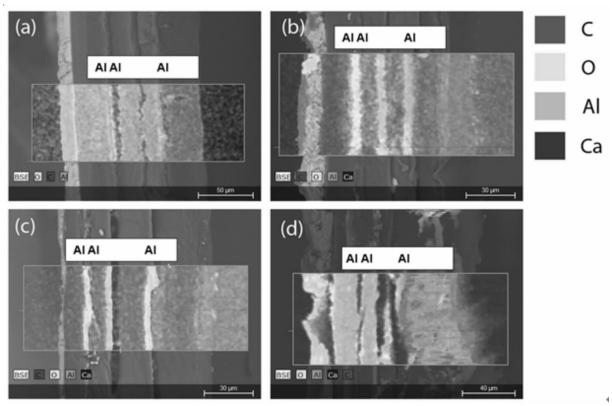

Fig. 13 SEM photos with EDS element area mapping of VIP envelope cross-sections for non-aged (a), aged 3 (b), 6 (c) and 9 weeks (d) samples as depicted in Fig. 4 (scale-bars ranging from 30 to 50 μm)

The full details of theresults and corresponding discussion will be reported in a journal article.

4. Conclusions

The durability of vacuum insulation panels (VIP) in an alkaline environment, i. e. applications where VIPs are used in contact with or in close proximity to concrete and cementitious materials, has been investigated at different pH-values and temperatures with and without direct contact with the liquid alkaline solutions. The VIPs in alkaline solutions at pH-values 10. 6 and 12. 6, showed no significant visible degradation at 20℃ for aging periods up to 12 weeks, whereas at 70℃ considerable visible degradation was observed with all VIPs becoming punctured after or before 3 to 9 weeks ageing. Thus, the elevated temperatures proved to be the most significant exposure strain for degradation of the VIPs.

Acknowledgements

This work has been supported by the Research Council of Norway and several partners through "The Research Centre on Zero Emission Buildings" (ZEB). Franco Blɸchlinger from Metallplan AS and the manufacturer Porextherm are acknowledged for supplying the vacuum insulation panel test samples.

References

[1] H. Schwab, U. Heinemann, A. Beck, H.-P. Ebert and J. Fricke, Prediction of service life for vacuum insulation panels with fumed silica kernel and foil cover, Journal of Thermal Envelope & Building Science, 28, 357—374, 2005.

[2] H. Simmler and S. Brunner, Vacuum insulation panels for building application—Basic properties, ageing mechanisms and service life, Energy and Buildings, 37, 1122 - 1131, 2005.

[3] J. Fricke, H. Schwab and U. Heinemann, Vacuum insulation panels—Exciting thermal properties and most challenging applications, International Journal of Thermophysics, 27, 1123 - 1139, 2006.

[4] S. Brunner and H. Simmler, In situ performance assessment of vacuum insulation panels in a flat roof construction, Vacuum, 82, 700 - 707, 2008.

[5] M. J. Tenpierik, Vacuum insulation panels applied in building constructions (VIP ABC), Ph. D. Thesis, Delft University of Technology, Delft, The Netherlands, 2009.

[6] R. Baetens, B. P. Jelle, J. V. Thue, M. J. Tenpierik, S. Grynning, S. Uvslɸkk and A. Gustavsen, Vacuum insulation panels for building applications: A review and beyond, Energy and Buildings, 42, 147 - 172, 2010.

[7] B. P. Jelle, A. Gustavsen and R. Baetens, The path to the high performance thermal building insulation materials and solutions of tomorrow, Journal of Building Physics, 34, 99 -123, 2010.

[8] B. P. Jelle, Traditional, state-of-the-art and future thermal building insulation materials and solutions—Properties, requirements and possibilities, Energy and Buildings, 43, 2549 - 2563, 2011.

[9] E. Wegger, B. P. Jelle, E. Sveipe, S. Grynning, A. Gustavsen, R. Baetens and J. V. Thue, Aging effects on thermal properties and service life of vacuum insulation panels, Journal of Building Physics, 35, 128 - 167, 2011.

[10] E. Sveipe, B. P. Jelle, E. Wegger, S. Uvslɸkk, S. Grynning, J. V. Thue, B. Time and A. Gustavsen, Improving thermal insulation of timber frame walls by retrofitting with vacuum insulation panels—Experimental and theoretical investigations, Journal of Building Physics, 35, 168 - 188, 2011.

[11] M. Alam, H. Singh and M. C. Limbachiya, Vacuum insulation panels (VIPs) for building construction industry—A review of the contemporary developments and future directions, Applied Energy, 88, 3592 - 3602, 2011.

[12] P. Johansson, S. Geving, C. - E. Hagentoft, B. P. Jelle, E. Rognvik, A. S. Kalagasidis and B. Time, Interior insulation retrofit of a historical brick wall using vacuum insulation panels: Hygrothermal numerical simulations and laboratory investigations, Building and Environment, 79, 31 -45, 2014.

[13] S. E. Kalnæs and B. P. Jelle, Vacuum insulation panel products: A state-of-the-art review and future research pathways, Applied Energy, 116, 355 - 375, 2014.

[14] Porextherm, Vacuspeed, data sheet, http://www.porextherm.de//images/downloads/doc_289_en.pdf (accessed 19. 10. 2011), 2011.

Thermal Insulation Performance of Nanoporous Alumina Compact

Li Junning[a*], Fan Yu[b], Yang Hailong[a], Yang Jingxing[a], Hu Zijun[a]

a. National Key Laboratory of Advanced Functional Composite Materials, Aerospace Research Institute of Materials & Processing Technology, Beijing, 100076, P. R. China

b. China Academy of Launch Vehicle Technology, Beijing, 100076, P. R. China

Abstract

High performance thermal insulation materials are highly demanded for the ever-increasing requirement for reducing energy consumption over the world. Nanoporous insulators with ultra-low thermal conductivity have drawn significant attention in the last decade. The article presents the synthesis of the nanoporous alumina compact and its thermal insulation properties. SEM was adopted to characterize the nanostructure of the porous alumina compact. Thermal conductivity of the synthesized material under different temperature and pressure was measured by the transit hot plane method. It was found that the nanoporous alumina compact had high porosity and the pore size was in the nano range, which greatly reduced the gaseous heat transfer. The thermal conductivity of the synthesized material was 0.029 W/(m·K) at ambient temperature and 10^5 Pa, and decreased to 0.005 W/(m·K) with the gas pressure reducing to 10 Pa. The nanoporous alumina compact exhibits good thermal insulation performance and may have a future as a good thermal insulation material.

Keywords thermal conductivity, nanoporous, alumina, insulator

1. Introduction

The past several decades have witnessed an exponential growth of energy consumption all over the world. Energy conservation is recognized as one of the most important measures to keep a sustainable development of the human society. High performance thermal insulation materials have drawn increasing attention in the world because of the effectiveness in reducing the energy loss in building, steel, furnace industries [1, 2]. Recently, nanoporous thermal insulation materials such as silica aerogel and fumed silica pressed boards with ultra-low thermal conductivity of 10^{-2} W/(m·K) are the focus of many research. Though silica aerogel with a high porosity of more than 95% shows the lowest thermal conductivity in almost of all the solid materials under atmosphere, the practical application of the silica aerogel has always been restricted by due to their fragility and costly supercritical procedure [3-5].

It is well-known that microporous thermal insulation prepared by pressing a mixture of fumed silica and opacifier particles together also has low thermal conductivity. Fumed silica is an aggregate of nanoparticles and characterized by its porous structure, which brings low thermal conductivity for the fumed silica pressed boards usually used as core materials in vacuum insulation panels (VIPs) [6,7]. So far, most of the researchers have chosen fumed silica as raw material to prepare nanoporous thermal insulation and investigate the thermal transfer behavior in the nanopores and nano solid netwoks. However, little attention has been paid to fumed alumina in nanoporous thermal insulation material area. In this paper, nanoporous alumina compact was fabricated by pressing the mixture fumed

* Corresponding author, Tel: 86-10-88521241, E-mail: ljn1212@163.com

alumina，opacifier and fibers into monolith and the thermal conductivity of the synthesized material was measured under different pressures. Thermal conductivity of the pressed fumed silica board was also analyzed to compare with the nanoporous alumina compact. In addition，the thermal transfer mechanism of the nanoporous alumina compact was analyzed based on the established theory.

2. Materials and methods

Nanoporous alumina compact was prepared by compressing the mixture of $\gamma-Al_2O_3$ nanoparticle (Alu C，Aeroxide®，Evonic，Germany)，ZrO_2 opacifier (particle size，1～3μm，Oriental Zirconic Corporation，China) and silica fiber (diameter 1～3μm，Feilihua Silica Fiber Corporation，China) together in mould made of steel on pressure former. Briefly，the powders were mixed by mechanical attrition for 5 min，then the powder mixture was transferred into a mould and uniaxially pressed on a pressure former at pressure of 2.5MPa to obtain the nanoporous alumina compact. The amount of the powder mixture was decided by the size and the density of the pressed board.

Nanoporous silica compact was also prepared by the same method except that the fumed alumina is used instead of fumed silica (A380，Aerosil®，Evonic，Germany) and the ZrO_2 was instead used of SiC (Beijing Weina Materials Corporation).

Microstructure of the nanoporous compact was characterized by scanning electron microscopy (SEM，JEOL，Japan). Thermal conductivity was measured by the laboratory developed equipment on the basis of transient hot-plane method [8，9]. Fig. 1 shows the scheme of the transient hot-plane setup. The mechanism of the measurement was reported in the previous document. The whole equipment is sealed in a vacuum system and can measure thermal conductivity of the sample under different pressures ($10\sim10^5$ Pa).

3. Results anddiscussion

Fig. 2 shows the microstructure of the nanoporous alumina compact. It is found that the alumina nanoparticles agglomerated together due to the high surface energy and the size of the agglomeration are in the range of dozens of nanometers to several hundred nanometers. Macropores were formed between the agglomerated alumina nanoparticles，which endow the compact with a high porosity of more than 80%. Moreover，there are large quantities of pores in the micro and meso range between the primary alumina particles. These pores reduce the collision of the gas molecular and decrease the gaseous thermal transfer effectively.

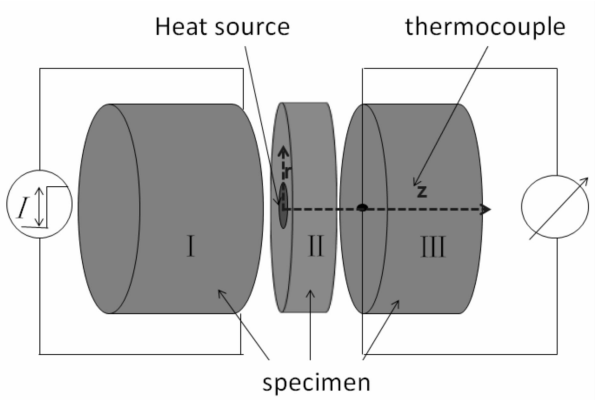

Fig. 1 Scheme of thetransient hot-plane equipment

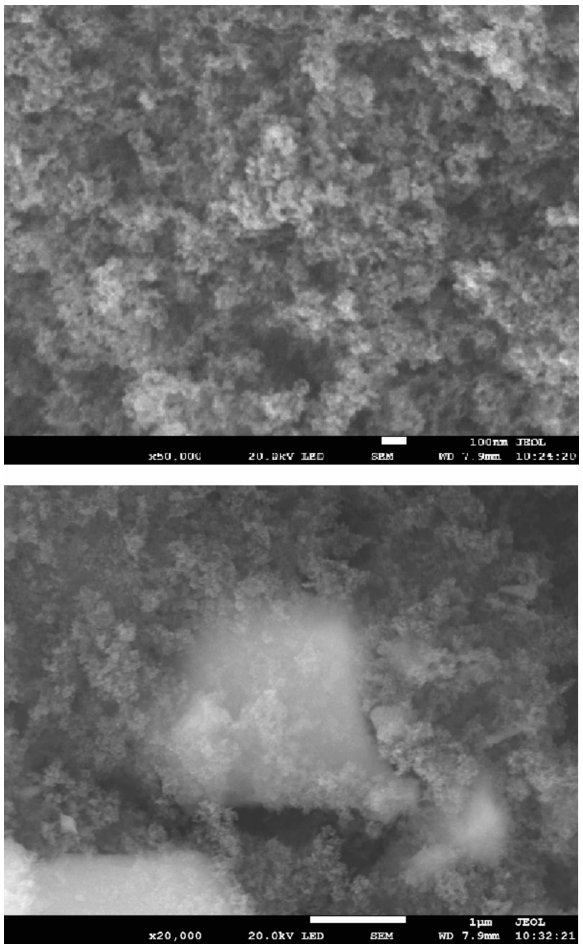

Fig. 2 SEM image of the nanoporous alumina compact

It is observed in Fig. 2 that the ZrO_2 particles with size of about 2 μm are imbedded into the fine alumina powder matrix. Opacifiers can scatter or absorb infrared radiation and are often used to reduce the radiative heat transfer especially at high temperature. Nanoporous alumina compact used ZrO_2 as opacifier to improve the thermal insulation performance of the nanoprous alumina compact. On the other hand, the addition resulted in the formation of macropores due to the fine alumina powder being unable to fill the surrounding space of the ZrO_2 particle. The size of the macropores were as large as to several micrometers and will enhanced the gaseous thermal transfer, which resulted in the increasing of the thermal conductivity of the alumina insulator. Nevertheless, if the nanoporous alumina compacts were to be used as an insulator under elevated temperature, the increase the gaseous thermal conductivity due to macropores could be ignored compared to the considerably improvement of the radiation thermal conductivity by ZrO_2. Therefore, it is necessary to add opacifier to the nanoporous alumina compact though some macropores may be formed.

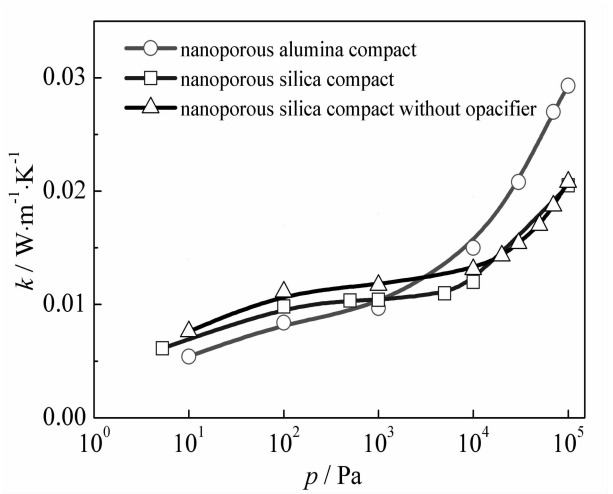

Fig. 3 Thermal conductivity of the nanoporous compact under different pressures

Fig. 3 demonstrates the thermal conductivity of the nanoporous alumina compact. The nanoporous silica compacts with and without SiC opacifier were also shown to compare with the alumina counterpart. It was found that the thermal conductivity of the nanoporous alumina compact is 0.029 W/(m • K) under ambient temperature and 10^5 Pa. The thermal conductivity reduces to 0.005W/(m • K) when the pressure fell to 10Pa. Thermal conductivity values of the synthesized alumina-based insulator decrease sharply at pressure higher than 10^4 Pa. However, the drop trend becomes smooth with the pressure falls from 10^4 Pa to 10 Pa. The phenomenon was consistent with other research, though the thermal conductivity drop of this work is larger than the reported data about silica-based materials. The difference may be due to the existence of lots of macropores between alumina agglomerations [10].

As shown in Fig. 3, the thermal conductivity of the nanoporous silica compact was 0.02 W/(m • K) and 0.005W/(m • K) at pressure of 10^5 Pa and 10 Pa, respectively, under ambient temperature. However, the thermal conductivity and pressure relationship curve of the nanoporous silica compact exhibits a s-shape which was unlike to the trend of fumed silica core materials used in VIPs. Between the pressure of 10 Pa and 100 Pa, the thermal conductivity showed a gradually decrease, whereas the change was not found for fumed silica panels [11]. As the case of the nanoporous alumina compact, intergranular voids were responsible for the drop of the thermal conductivity in the lower pressure. Because there are micro-sized opacifier and silica fibers in the nanoporous silica compact, these additives cause the formation of the macropores during the powder mixing process. Moreover, the exclusion of SiC results in a higher thermal conductivity value of 0.007 W/(m • K) and 0.021 W/(m • K) at 10Pa and 10^5 Pa than the SiC incorporated nanoporous silica compact, which was because the absence of the SiC opacifier increasing the thermal conductivity contributed by radiation. It is noteworthy that the pressure dependence of the thermal conductivity is similar to the opacified nanoporous silica compact, which indicated the existence of the macropores.

The microstructure feature of the fumed alumina and fumed silica agglomerations led to the different thermal insulation performance of thenonporous compact. It was impressive that the thermal insulation property of the nanoporous alumina compact was superior to its silica counterpart when pressure lower than 10^3 Pa. Though the thermal conductivity of the

alumina-based insulator was higher than silica-base insulator at pressure above 10^3 Pa. This indicated that the nanoporous alumina compact may be a candidate for thermal insulation materials in a vacuum or low pressure. Furthermore, alumina is more heat-resistant than silica, which makes this insulator find application in high temperature thermal insulation field. Thermal conductivity values at elevated temperatures of the nanoprous alumina compact are necessary to further evaluate the insulation performance under high temperature environment.

It is well-known that the heat transfer within nanoporous materials is through the gas molecule in the nanopores, solid network and radiation [12]. Therefore, the thermal conductivity of the nanoporous alumina compact was contributed by the gaseous, solid phase and radiative thermal transfer. The gaseous and solid thermal conductivity are main contributions at ambient temperature and 10^5 Pa for the radiative heat transfer being extremely low. To improve the thermal insulation performance of the nanoporous alumina compact, the influence of the connectivity of the alumina particles and porous structure including size and distribution is of importance to obtain insulator with excellent properties.

4. Conclusions and outlook

Nanoporous alumina compact with extremely low thermal conductivity has been successfully prepared by a convenient dry-pressing method. Though the thermal conductivity of the nanoporous alumina compact was higher than the silica-based compact under 10^5 Pa, the nanoporous alumina compact showed advantages when evacuated to 10^3 Pa or lower. The results have shown that the nanoporous alumina compact is potential for thermal insulation applications in various fields.

Acknowledgements

This work was supported by The National Basic Research Program of China (No. 2015CB655200).

References

[1] E. T. Afriyie, P. Karami, P. Norbery, K. Gudmundsson, Textural and thermal conductivity properties of a low density mesoporous silica materials, Energy and Buildings 75 (2014) 201 - 215.

[2] S. Akamine, M. Fujia, Controlling heat radiation for development of high-temperature materials, Journal of the European Ceramic Society 34 (2014) 4031 - 4036.

[3] H. Abe, I. Abe, K. Sato, M. Naito, Dry powder processing of fibrous fumed silica compacts for thermal insulation, Journal of the American Ceramic Society 88 (2005) 1359 - 1361.

[4] G. Hayase, K. Kugimiya, M. Ogawa, Y. Kodera, K. Kanamori, K. Nakamishi, The thermal conductivity of polymethylsilsesquioxane aerogels and xerogels with varied pore size for pretical application as thermal superinsulators, Journal of Materials Chemistry A 2 (2014) 6525 - 6531.

[5] Y. - G. Kwon, S. - Y. Choi, E. - S. Kang, S. - S. Beak, Ambient-dried silica aerogel doped with TiO_2 powder for thermal insulation, Journal of Material Science 35 (2000) 6075 - 6079.

[6] M. Alam, H. Singh, M. C. Limbachiya, Vacuum Insulation Panels (VIPs) for building construction industry-A review of the contemporary developments and future directions, Applied Energy 88 (2011) 3592 - 3602.

[7] M. Bouquerel, T. Duforestel, D. Baillis, G. Rusaouen, Heat transfer modeling in vacuum insulation panels containing nanoporous silicas-A review, Energy and Buildings 54 (2012) 320 - 336.

[8] H. Xiao, F. Yu, X. Zhang, Thermal conductivity measurement of materials based on a transient hot-plane method, Journal of University of Science and Technology Beijing 34 (2012) 1432 - 1436.

[9] F. Yu, X. Zhang, X. He, A review of the measurements of thermophysical properties of materials by transient method, Journal of Astronautic Metrology and Measuremen 26 (2006) 23 - 30.

[10] M. Reim, W. Korner, J. Manara, S. Korder, M. Arduini-Schuster, H. P. Ebert, J. Fricke Silica aerogel granulate material for thermal insulation and daylighting, Solar Energy 79 (2005) 131 - 139.

[11] J. Fricke, U. Heinemann, H. P. Ebert, Vacuum insulation panels-from research to market, Vacuum 82 (2008) 680 - 690.

[12] M. A. Aegerter, N. Leventis, M. M. Koebel, Aerogel Handbook, first ed., Springer-Verlag New York, LLC, New York, 2011.

Aging Performance of Glass Fiber-based and Chopped Strand-based Vacuum Insulation Panels: A Comparative Research

Huang Fengkang [a,b*], Li Manman[a], Zhu Jianguo[b], Xie Lixu [b], Wu Leyu[a], Wang Tangyu [a]

a. YinXing Electric Co., Ltd, Chuzhou, 239000, P. R. China

b. College of Materials Science & Engineering, SiChuan University, Chengdu, 610065, P. R. China

Abstract

Vacuum insulation panel (VIP) is a new high-performance thermal insulation material, which is widely used in buildings and refrigerators. However, it can never be appraised to be a promising heat insulation material of good market potential unless it can be used as long as possible to match the actual lifetime of partial insulation system or even the entire architecture, like a building. In this paper, VIPs use glass fiber and chopped strand as core materials were both treated in thermostatically controlled environment of four different temperatures, namely 20℃, 40℃, 60℃, 80℃, separately. A 90-days-long monitoring and continuous testing was carried out while a long term aging performance comparison of those two typical kinds of VIPs at different temperatures. It shows that chopped strand VIPs performed better than glass fiber VIPs in low temperatures conditions. But in higher temperature, performance of chopped strand VIPs was nearly as same as glass fiber VIPs. In addition, a special empirical formula for estimating the lifetime of VIP was referred to in the process of data analysis and conclusion.

Keywords vacuum insulation panel, lifetime, Aging performance, temperature, empirical formula

1. Introduction

Vacuum insulation panel (VIP) is a kind of thermal insulation material composed of porous insulation core materials, high gas and humidity barrier structure and gas adsorption material. The thermal conductivity of VIP can be as low as 0.004W/(m·K), nearly 1/7 of that of conventional thermal insulation material, even 1/10 [1]. VIP has been extensively developed and applied in the refrigerators, construction and other fields[2-3]. But according to the regulation of the United States ASTM C 1484—01 standard, the lifetime of VIP refers to the maintaining time that the thermal conductivity of the center of VIP plate meets the specified value of super thermal insulation material, and the specified value is 0.0115 W/(m·K). When the thermal conductivity of VIP is greater than 0.0115 W/(m·K), the VIP fails. So how to keep the thermal insulation performance of VIP has become top concern of manufacturers and users. The present study shows that the factors affecting the lifetime of the VIP including temperature, humidity, atmospheric pressures, etc. Temperature is the main cause leading to the malfunctioning of VIP.

Glass fiber is one of the most commonly used core material for vacuum insulated panels since its low thermal conductivity, and according to different production process they are divided into two different kinds: glass fiber and chopped strand [4]. At present there is much study of VIP lifetime, but mainly in single temperature condition. In this paper, the aging performance of glass fiber core VIP and chopped strand core VIP in thermostatically controlled environment of

* Corresponding author, Tel: 86-550-3075556 Fax: 86-550-3075556 E-mail: peter.huang@yxelectric.com

different temperatures were compared, and predicted the lifetime. The research results had great guiding significance to improve the level of production and usage of VIP.

2. Experimental Procedure

2.1 Experimental materials

In this paper, 20 pieces VIP made of glass fiber core and 20 pieces VIP made of chopped strand core materials were used. Dimension is 200mm×200mm×8mm. Parameters of glass fiber and chopped strand core material are shown in Tab. 1.

Tab. 1 Parameters of glass fiber and chopped strand core material

Chopped strand	Parameters	Glass fiber
Fiber diameter /μm	3.5	7
length of the fiber /mm	30	7
Core material layer	30	29
A single layer thickness /mm	0.5	0.4

2.2 Experimental method

(1) The initial K value of samples in 2.1 in the condition of 20℃, as the data of 0 days was measured.

(2) Place 5 pieces VIP made of glass fiber core and 20 pieces VIP made of chopped strand core materials and start aging in four different temperatures, namely 20℃, 40℃, 60℃ and 80℃.

(3) K value (in mW/(m·K)) of VIP after 14 days at 24℃ was measured, and then place them to their corresponding places at first.

(4) Steps (2) is repeated and complete test of 28 days, 60 days and 90 days.

3. Results and discussion

3.1 Analysis of aging result

K values of 0 day of VIP made of glass fiber core and chopped strand core materials are shown in Tab. 2.

Tab. 2 K values of 0 day of VIP made of glass fiber core and chopped strand core materials

Initial K value	Glass fiber	Chopped strand
K values of 0 day /(mW/(m·K))	1.750	2.225

Initial K value of glass fiber-based VIP was lower than that of chopped strand-based VIP.

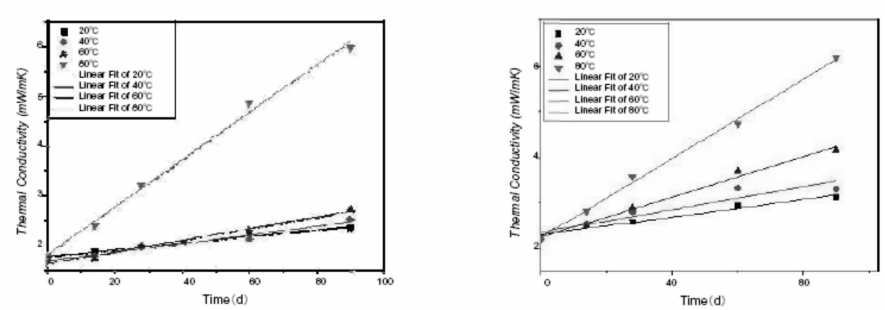

Fig. 1 VIP aging trend under different temperature

(a) chopped strand-based VIP, (b) glass fiber-based VIP

Aging trends of chopped strand-based and glass fiber-based VIP under different temperature (20℃, 40℃, 60℃, 80℃) are shown in Figure 1. As it can be seen, thermal conductivity of chopped strand-based and glass fiber-based VIP increased fast with increase in temperature. This was mainly due to as the aging environment becoming worse, adhesive layer between the layers of VIP barrier film was damaged seriously. Gas and oxygen permeability of VIP barrier film increased gradually. Vacuum degree within VIP rose rapidly, and eventually led to its heat insulation performance degradation.

Fitting equations of chopped strand-based and glass fiber-based VIP aging under different temperatures are shown in Tab. 3.

Tab. 3 Fitting equations of chopped strand-based and glass fiber-based VIP aging under different temperatures

Temperature / ℃	Glass fiber	Chopped strand
20	$y = 0.0068x + 1.7698$	$y = 0.0098x + 2.2945$
40	$y = 0.0088x + 1.6762$	$y = 0.0127x + 2.3454$
60	$y = 0.0117x + 1.6294$	$y = 0.0223x + 2.2345$
80	$y = 0.0478x + 1.8023$	$y = 0.0435x + 2.2$

According to equations in Tab. 3, under different temperature of 20℃, 40℃ and 60℃, life recession of chopped strand-based VIP was slower than glass fiber-based VIP. Because when aging under lower temperatures, on the premise that VIP barrier film was not lethal damaged, heat conduction path of chopped strand-based and glass fiber-based VIP was different. Fiber diameter of chopped stand was twice than glass fiber and fiber length was a quarter of that of glass fiber. So, chopped stand formed structure that fiber arrangement was perpendicular to heat transfer easily, and heat transfer within VIP plate was mainly horizontal heat transfer and radiation heat transfer between glass fibers. Glass fiber was thin and long. It was not easy to form disciplinary arrangement structure and distribution was disorderly. The heat transfer in the VIP plate was mainly longitudinal fiber heat transfer, boundary and the contact point heat transfer and radiation heat transfer [5]. It was greater than that of chopped strand-based VIP. So the thermal conductivity increase of glass fiber-based VIP was much faster than chopped strand-based VIP.

At high temperature of 80℃, which has already achieved or even surpassed the softening point of the adhesive between the layers of VIP's barrier film, force the layers of the film separated, and hence massively decrease the ability of the film to block the penetration of humidity and gas. The deterioration of the performance of the film plays a very important role in the increasing of thermal conductivity and lifetime decline of VIP under this circumstance. So that the lifetime decline of VIPs based on different core material, whatever glass fiber or chopped strand, are very similar at an ambient temperature of 80℃.

3.2 Lifetime prediction

The thermal conductivity of VIP will increase inevitably with the elapse of time. The lifetime prediction of VIP was very significant in production and application. According to tab. 3, we can figure out the annual lifetime growth value K of chopped strand based VIP and glass fiber based VIP in different ambient temperatures (Tab. 4. Employing K value as Y axis, ambient temperature T as X axis, we can get fig. 3 and fit formula 1 (chopped strand) and formula 2 (glass fiber).

Tab. 4 Annual lifetime growth value K of chopped stand based and glass fiber based VIPs

Temperature /℃	Chopped strand based VIP	Glass fiber based VIP
20	2.482	3.577
40	3.212	4.6355
60	4.2705	8.1395
80	17.447	15.8775

$$y = 1.0649e^{0.0307x} \quad (1)$$

$$y = 1.9328e^{0.0252x} \quad (2)$$

According to formula (1) and formula (2) we can figure out the thermal conductivity of chopped strand based and glass fiber based VIPs in different ambient temperature in one year's time. For instance, at 50℃, K value of chopped strand based is predicted to be 4.89 mW/(m·K) after one year.

Referring to the calculation methods above, using the samples mentioned in this article as examples, We can simulate the K value of chopped strand based VIP and glass fiber based VIP in different time at 24℃ (be approximated to the operating temperature of VIP), as shown in Tab. 5.

According to data, we can conclude that the prediction value has the same variation tendency of the actual value, while they are slightly different quantitatively.

4. Conclusions and outlook

At low temperature, chopped strand based VIPs aging performance is better than glass fiber based one; at a high temperature, their aging performance are similar. Through the aging experiment at different temperatures, a mathematical model of thermal conductivity and ambient temperature was established. The formula calculated results and actual measured

results of K value are well fitted in variation tendency and fitted at some aspects quantatively. There are some differences between the results of calculation method of the setup mathematical model and the actual results, despite the very limited factors that affect the lifetime of VIP, hence the model needs further calibration.

Tabble should go inside.

References

[1] Ankang Kan, et al. Chinese Journal of Vacuum Science and Technology 34(2014)665 - 670.

[2] Fricke J, et al. Vacuum 82(2008)680 - 690.

[3] Xiaobo Di, et al. Vacuum 97(2013)55 - 59.

[4] Ruben Baetens, et al. Energy and Buildings 42(2010) 147 -172.

[5] 11th International Vacuum Insulation Symposium. Wangping Wu, et al. (2013)33 - 34.

Tab. 5 The comparison of chopped strand based and glass fiber based VIP's predicted K value and actual K value in different time at 24℃

Time/y	0.08	0.16	0.24	0.49	1	2	3	5	10
Core material	Chopped strand								
Predicted value mW/(m·K)	1.781	1.834	1.888	2.047	2.374	3.021	3.667	4.961	8.193
Actual value mW/(m·K)	1.793	1.870	2.050	2.275	2.473	2.753	—	—	—
Core material	Glass fiber								
Predicted value mW/(m·K)	2.280	2.346	2.413	2.612	3.022	3.831	4.641	6.259	10.304
Actualvalue mW/(m·K)	2.490	2.570	2.942	3.128	3.323	—	—	—	

Assessing Long-term Thermal Resistance (LTTR) of Vacuum Insulation Panel (VIP) —Review of Challenges and Way Forward

Phalguni Mukhopadhyaya[a*], Anil Parekh[b]

a. Associate Professor, University of Victoria, Department of Mechanical Engineering, Victoria, BC, Canada

b. Senior Research Manager, Canmet ENERGY, Natural Resources Canada, Ottawa, ON, Canada

Abstract

Application of VIP in building envelope construction offers many advantages such as increased energy efficiency of exterior building envelope, thinner wall thickness, optimum space use, reduced material consumption etc. However, there are a number of issues that are being raised by the construction industry professionals and stakeholders and, undoubtedly, long-term thermal resistance (LTTR) of VIP is one of those issues. Various researchers from Asia, Europe and North America have tried to predict the LTTR of VIP through laboratory-based experimental data, field observations and numerical modelling of aging processes. This paper summarizes the known and unknown facts related to the LTTR of VIPs, and critically assess the inherent challenges faced by the researchers to predict the LTTR of VIP. The paper also presents a practical way forward to overcome these challenges.

Keywords vacuum insulation panels, long term thermal resistance (LTTR), accelerated aging, challenges

1. Introduction

Long-term performance of a thermal insulation is indicated by its ability to sustain thermal properties during the expected service life. Usually mentioned as LTTR (long term thermal resistance) value, it is a very important characteristic of an insulation material and used by the building envelope designers for energy calculations. Building envelope designers in North America became familiar with the LTTR concept while dealing with aging of closed-cell foam insulation with captive blowing agents [1,2].

Aging mechanisms of closed-cell foam (Fig. 1) and VIP (Fig. 2) have both similarities and differences. Diffusion of gas and/or vapour is the common phenomenon that governs aging and LTTR of both closed-cell foam and VIP. In closed-cell foam, the aging rate is relatively higher at the beginning (i. e. just after production and first few months afterwards) but thereafter aging rate reduces with time and eventually reaches to a steady state equilibrium with no further aging due to gas/vapour diffusion. However, for VIP, the aging rate seems to be about constant, at least for the first 5 to 10 years, and aging process appears to be a continuous process over a much longer duration of time [3,4]. Moreover, the relative impact of aging (i. e. percentage of initial thermal resistance) during its service life (25 years or more) is expected to be higher for VIP, compared to closed-cell foam insulation. It is to be noted, even with continuous aging, due to its extremely high initial R-value (measure of thermal resistance, as used in North America) VIP provides much higher thermal resistance than conventional thermal insulations (foam, fibre etc.) during its service life. Furthermore, even a totally failed (i. e. no more vacuum) VIP can have higher R-value than traditional insulations used for building envelope construction.

2. Challenges

Prediction of aging rate for VIP still remains a

* Corresponding author, Tel: 1-250-472-4546, E-mail: phalguni@uvic.ca

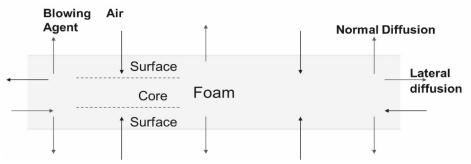

Fig. 1 Agingmechanism – closed cell foam insulation with captive blowing agent

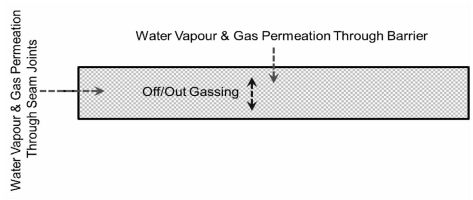

Fig. 2 Aging mechanism – vacuum insulation panel

challenging task. However, a significant amount of theoretical research had been carried out to develop fundamental understandings of the VIP aging mechanisms [5 – 7]. In general, theoretical aging models identify following primary mechanisms for VIP aging:

(1) Increased thermal conductivity due to gaseous diffusion and resulting internal pore pressure rise,

(2) Increased thermal conductivity due to vapour diffusion and resulting vapour pressure rise, and

(3) Increased thermal conductivity due to accumulated moisture content.

There exists absolutely no doubt on the fundamental physics of these aging models. But there remains a number of fundamental and practical challenges for the implementation of these theoretical aging principles into practical use and they are:

(1) Reliable and repeatable measurement techniques to establish the functional relationships between the thermal conductivity and aforementioned parameters [8].

(2) Changes in gas/vapour diffusion properties due to aging of the facer and seam joint, and

(3) Lack of reliable and controlled field performance data to validate the outputs of the theoretical aging model.

3. The way forward

In a way, the aforementioned challenges are not unforeseen in the history of building materials research. New materials when introduced in the building construction industry do not come with long term field performance data to back its performance claims. Moreover, chemical and physical compositions of many of these building materials keep on changing with the time. These are indeed formidable challenges. One way to address these issues is to conduct accelerated aging tests in the laboratory. By definition, these are short duration tests which can clearly demonstrate VIP's aging characteristics qualitatively and quantitatively. The only challenge with the results from accelerate aging tests is to establish the relationship between the accelerated aging test results and field performance data. This becomes even more complicated when one considers variation of climatic conditions at different geographical locations. However, sustained material research in the laboratory conducted by different research groups and availability of field performance data from various construction types and geographic locations can overcome aforementioned inherent limitation of the accelerated aging tests. The key factor that makes the difference here is the combination of research expertise, experience and power of diverse field performance data. This is a time tested approach that had worked in the construction industry for many novel construction materials [1,2,9]. Based on this approach, it is possible to develop a comprehensive accelerated aging test methodology for VIPs and predict the LTTR value of VIP within an acceptable margin of safety. However, it is to be noted that assessment of LTTR of VIP would remain an ongoing process as global VIP research community members gain more knowledge and generate more information.

4. Conclusions and outlook

This paper has provided a simple, brief and comprehensive review of the challenges associated with the prediction of long term thermal resistance (LTTR) of VIP for applications in building envelope construction. Development of LTTR prediction methodology based on accelerated aging test principles is recommended.

Acknowledgements

The authors would like to acknowledge their collaborations with NRC Construction, numerous VIP

manufacturers and informal discussion with fellow researchers for the information presented in this paper.

References

[1] ASTM C1303 / C1303M - 14, Standard Test Method for Predicting Long-Term Thermal Resistance of Closed-Cell Foam Insulation, ASTM International, West Conshohocken, PA, 2014, www.astm.org.

[2] CAN/ULC S770 - 15, Standard Test Method for Determination of Long-term Thermal Resistance of Closed-Cell Thermal Insulating Foams, Underwriters Laboratories of Canada, 02/17/2015.

[3] Mukhopadhyaya, P., Kumaran M. K., Sherrer G., van Reenen, D., An Investigation on Long-Term Thermal Performance of Vacuum Insulation Panels (VIPs)", Proc. of 10th Int. Vacuum Insulation Symp. (IVIS-X), pp. 10, 2011, Ottawa, ON, Canada.

[4] Mukhopadhyaya, P., Molleti, S., van Reenen, D., Vacuum Insulation Panel (VIP): An Historic Opportunity for the Building Construction Industry, RCI Interface, August 2014.

[5] Schwab H., U. Heinemann, A. Beck, H. P. Ebert, J. Fricke, Prediction of Service Life for Vacuum Insulation Panels with Fumed Silica Kernel and Foil Cover, J. of Thermal Env. & Bldg. Sci., 28 (4), 2005, 357 - 374.

[6] Simmler H., S. Brunner, Vacuum Insulation Panels for Building Application: Basic Properties, Aging Mechanisms and Service Life, Energy and Buildings, 37, 2005, 1122 -1131.

[7] Yrieix, B., Morel, B., Pons, E., VIP Service Life Assessment: Interactions between Barrier Laminates and Core Material, and Significance of Silica Core Aging, Energy and Buildings, Volume 85, Dec 2014, pp. 617 -630.

[8] Pons, E., Yrieix, B., Heymans, L., Dubelley, F., Planes, E., Permeation of Water Vapor Through High Performance Laminates for VIPs and Physical Characterization of Sorption and Diffusion Phenomena, Energy and Buildings, Volume 85, Dec 2014, pp. 604 -616.

[9] Chen, Y., Davalos, J. F., Ray, I., Kim, H - Y., Accelerated Aging Tests for Evaluations of Durability Performance of FRP Reinforcing Bars for Concrete Structures, Composite Structures, V. 78 (1), 2007, 101 -111.

Determination of the Thermal Conductivity of Vacuum Insulation Panels at Fire/Elevated Temperatures

Dimos A. Kontogeorgos[a*], Georgios K. Semitelos[a], Ioannis D. Mandilaras[a]
Roland Caps[b], Libor Kubina[b], Maria A. Founti[a]

a. National Technical University of Athens, School of Mechanical Engineering, Lab. Of Heterogeneous Mixtures and Combustion Systems, Heroon Polytechniou 9, 15780 Zografou, Greece
b. Va—Q—Tec AG, Karl Ferdinand Braunstrasse 7, 97080 Wurzburg, Germany

Abstract

In this study, a new method for the determination of the thermal conductivity of the VIP's core material (i. e. fumed silica) at elevated temperatures, up to 900℃, is proposed. An experimental set up, based on the heat flow meter apparatus method, is designed and realized. Two VIPs are joined together to form a specimen, which is subjected to fire conditions from one side, while the other side faces ambient conditions, simulating realistic fire conditions. The temperatures on both sides and the heat flux on the unexposed side are recorded and utilized for the determination of the thermal conductivity. The experimental data are coupled with a detailed numerical model, used for the determination of the VIP's core material thermal conductivity. An optimization technique is utilized in order to define the parameters of the model. The contribution of each heat transfer mechanism, i. e. gas conduction, solid conduction and radiation, of the detailed numerical model to the overall thermal conductivity is investigated.

Keywords vacuum insulation panels, thermal conductivity, modeling, fire

1. Introduction

In the last decade, VIPs were extensively investigated and introduced in the market for a variety of applications, such as aerospace, refrigerator, transport, container and building applications [1]. Research has mainly focused on the thermal behavior of VIPs under low and moderate temperatures (up to ca. 200℃) [2].

On the other hand, in building applications, and under the frame of the fire protection of buildings, the assessment of the materials when exposed to fire temperatures is essential. Especially, in recent years, where the implementation of "performance-based" fire codes is increasing, the need for accurate physical properties becomes even more important [3,4].

This work studies the effect of fire temperatures, up to 900℃, on the thermal conductivity of VIP's core material (i. e. fumed silica). Temperatures and heat flux measurements on the surfaces of a VIP are coupled with a detailed model in order to determine the thermal conductivity of the VIP. The detailed model takes into account all the significant heat transfer mechanisms occurring inside porous materials, i. e. gas conduction, solid conduction and radiation.

2. Experimental Methodology

In order to define the thermal conductivity of VIP's core at fire temperatures, an experimental set up, based on the heat flow meter apparatus method [5,6] was designed and realized. Two samples of the VIP's core were joined together to form the final test specimen. The specimen was equipped with two thermocouples and a heat flux sensor in order to record the temperature on both sides and the heat flux at the

* Corresponding author, Tel: 0030-210-7724002, Fax: 0030-210-7723527, E-mail dimkon@central. ntua. gr

unexposed side of the specimen. The specimen was placed between two steel plates and the total assembly was positioned in front of a Nabertherm® B180 radiation furnace, so as one surface of the specimen to be exposed to the furnace's thermal load and the other to be exposed to ambient conditions. Fig. 1 illustrates a schematic diagram of the experimental set up.

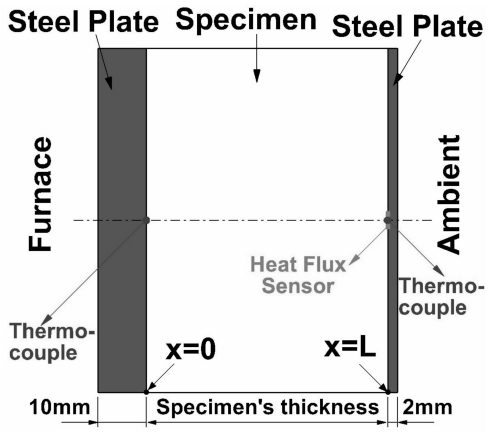

Fig. 1 Schematic diagram of the experimental set up

For the temperature and the heat flux measurements, an Agilent data acquisition unit with accuracy of ±2% was utilized, while the data were recorded and stored in intervals of 10s using the "LabVIEW" software. Two steel plates were used in order to ensure uniform temperature distribution on both surfaces of the specimen. The experimental set up was firstly calibrated, in order to take into consideration the lateral thermal losses, using a reference material (i. e. Kaowool 1260 paper).

The experimental methodology consisted of two main steps. Firstly, the temperature of the furnace was set to a desired level. Then, the temperature and the heat flux evolution were recorded until steady state conditions were reached. The temperature of the furnace ranged from 100℃ to 900℃ with an interval of 100℃ (i. e. 9 total furnace temperature levels). The steady state temperature and heat flux values at all temperature levels in the furnace were utilized for the definition of VIP's thermal conductivity.

3. Numerical Modeling

The equivalent thermal conductivity, λ_e, is considered to be the summation of different distinct heat transfer modes [2,7,8]:

$$\lambda_e = \lambda_s + \lambda_g + \lambda_c + \lambda_r \quad (1)$$

where λ_s is the solid conduction, λ_g is the gas conduction, λ_c is the gas convection and λ_r is the radiation. The solid conduction is usually assumed to be constant, while the gas convection is negligible for pore sizes smaller than 1μm [2].

The gas conduction in porous media can be written as [2,7,9]:

$$\lambda_g = \frac{\lambda_{g,0}(T)}{1 + \frac{2\beta k_B}{\sqrt{2}\pi d_g^2}\frac{T}{\delta P_g}} \quad (2)$$

Where $\lambda_{g,0}$ is the air's thermal conductivity [W/(m·K)], β is a constant varying between 1.5 and 2 characterizing the efficiency of energy transfer when gas molecules hit the solid structure of the material, k_B is the Boltzman constant (1.38066×10^{-23} J/K), d_g is the diameter of the gas molecules (3.53×10^{-10} m), T is the temperature [K], δ is the characteristic pore size [m] and P_g is the pressure [Pa]. It should be noted that at the examined temperatures, the VIP was considered to be at atmospheric pressure (i. e. P_g=101325Pa).

The radiation inside porous media can bewritten as [2,7,10]:

$$\lambda_r = \frac{16}{3}\frac{n^2\sigma T^3}{E} \quad (3)$$

Where n is the index of refraction, σ is the Stefan-Boltzman constant (5.67×10^{-8} W/(m^2·K^4)) and E is the extinction coefficient (m^{-1}).

Taking into account Eqs. (1) to (3) and considering one dimensional heat transfer through the thickness of the specimen, the steady state heat flux can be calculated as:

$$q_{calc} = -\lambda_e(T)\frac{dT}{dx} \rightarrow q_{calc} = -\frac{1}{L}\int_{T_0}^{T_L}\lambda_e(T)dT \quad (4)$$

Where L is the thickness of the examined specimen, while T_0 and T_L are the steady state temperatures in the positions x=0 and x=L (see Fig. 1), respectively.

The equivalent thermal conductivity was defined by minimizing the difference between the experimental, q_{exp}, and the calculated, q_{calc} (Eq. (4) values of the steady state heat flux for all the experimental data set (i. e. furnace temperature levels), according to Eq. (5):

$$e_q = \min_X \sum_{i=1}^{N_{exp}} (q_{exp,i} - q_{calc,i})^2 \quad (5)$$

Where e_q is the error to be minimized, N_{exp} is the number of the furnace's temperature levels ($N_{exp}=9$) and X is the vector of optimization parameters (independent variables) of the model of the thermal conductivity that minimizes the heat flux error.

In this study, the optimization parameters that were taken into consideration were the parameters β, λ_s and E, i. e. $X=\{\beta,\lambda_s, E\}$. Based on the values given in [2,7], the ranges for these parameters were set to be $1.0 \leqslant \beta \leqslant 3.0$, $1\text{mW/(m}\cdot\text{K)} \leqslant \lambda_s \leqslant 4\text{mW/(m}\cdot\text{K)}$ and $4000\text{m}^{-1} \leqslant E \leqslant 13000\text{m}^{-1}$. The mean pore size of the specimen was $\delta = 300\text{nm}$.

4. Results and discussions

Tab. 1 summarizes the steady state temperature and heat flux values recorded for all the temperature levels of the furnace. These values were utilized in the optimization process in order to determine the VIP's equivalent thermal conductivity. The optimization process (Eqs. (2) to (5)) was performed by utilizing the MATLAB's curve fitting tool and the optimization parameters were found to be $\beta = 2.0$, $\lambda_s = 2.1$ mW/(m·K) and $E = 9305\text{m}^{-1}$, respectively.

Tab. 1 Measured steady state temperatures and heat flux values for each temperature level of the furnace

Furnace Temperature /℃	Measured Temperatures		Measured Heat Flux
	T_0/℃	T_L/℃	$\frac{q_{exp}}{\text{W/m}^2}$
100	101.9	24.2	40.9
200	197.9	29.7	86.6
300	294.9	35.5	129.2
400	391.0	40.7	176.3
500	488.8	47.0	231.6
600	587.2	53.6	299.3
700	682.5	61.4	381.6
800	771.2	70.1	490.4
900	860.5	81.4	633.1

Fig. 2 shows the comparison between the steady state heat flux values calculated from Eq. (4), taking into account the optimization parameters reported above (i. e. $\beta = 2.0$, $\lambda_s = 2.1\text{mW/(m}\cdot\text{K)}$ and $E = 9305\text{m}^{-1}$), with the respective experimental values for all the temperature levels of the furnace. As it is shown, the obtained heat flux values are in sound agreement with the respective experimental (the predictions lie within the experimental error bars). The small discrepancies that are observed can be related to the fact that the optimization parameters, i. e. β, λ_s and E, were assumed to be temperature independent.

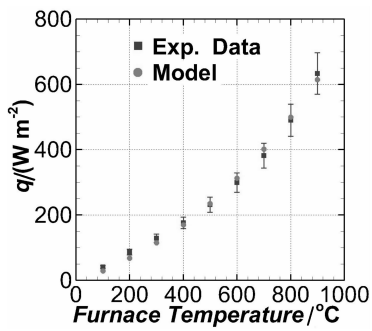

Fig. 2 Comparison between the predicted and the experimental steady state heat flux values for all the temperature levels of the furnace

Fig. 3 illustrates the contribution of each heat transfer mechanism, i. e. gas conduction, solid conduction and radiation, to the equivalent thermal conductivity. As it is shown, at temperatures up to 200～250℃ the main heat transfer mechanism is gas conduction. At higher temperatures, the role of radiation heat transfer mechanism increases significantly and above 500℃ prevails against the other heat transfer mechanisms.

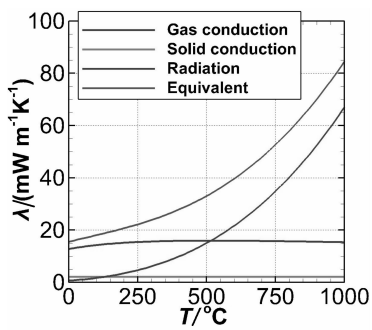

Fig. 3 Contribution of each heat transfer mechanism to the equivalent thermal conductivity

In order to further support the reliability of the VIP's core thermal conductivity defined in this work, the evacuated thermal conductivity, defined by Eq. (6), was compared with respective experimental data from ANNEX 39 [2]. Figure 4 shows the comparison of the

calculated evacuated thermal conductivity, with the experimental data. As it is shown, the defined evacuated thermal conductivity lies between the respective experimental data at temperatures up to 200℃. Hence, the defined thermal conductivity can be considered to be accurate and reliable within the total temperature range examined, i. e. 100℃ to 900℃.

$$\lambda_{evac} = \lambda_s + \lambda_r \quad (6)$$

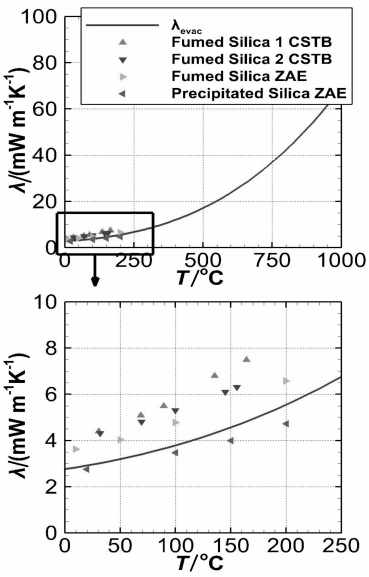

Fig. 4 Comparison of the evacuated thermal conductivity with experimental data from ANNEX 39 [2]

5. Conclusions and outlook

This study describes a method for the estimation of the thermal conductivity of VIP's core material (i. e. fumed silica) at fire temperatures. The method comprises two different steps. Firstly, temperature and heat flux measurements on the surfaces of a VIP, are recorded at several temperature levels. Next, the experimental values are compared with a detailed model, valid for the estimation of the thermal conductivity of porous materials. Finally, an optimization algorithm is utilized in order to define the optimum parameters of the model, which minimize the difference between the experimental and the model's values.

The proposed method was successfully employed for the determination of the thermal conductivity of a VIP at temperatures up to 900℃. The optimum parameters of the model were found to be $\beta = 2.0$, $\lambda_s = 2.1\text{mW/(m} \cdot \text{K)}$ and $E = 9305\text{m}^{-1}$, respectively. The thermal conductivity of the VIP varied between ca. 18mW/(m · K) and 85mW/(m · K) at ambient temperatures and at 900℃, respectively.

Acknowledgements

For the financial support the authors acknowledge the European Commission in the frame of FP7 NMP project "ELISSA".

References

[1] H. Simmler, S. Brunner. Energ. Buildings 37 (2005) 1122-1131.

[2] IEA Annex 39, Subtask A, H. Simmler et al. 2005.

[3] K. Ghazi Wakili et al., J. Fire Sci 25 (2007) 267-282.

[4] D. Kontogeorgos, M. Founti, Appl. Therm. Eng. 30 (2010) 1461-1469.

[5] ISO 8301: 1991, Thermal insulation - Determination of steady-state thermal resistance and related properties - Heat flow meter apparatus.

[6] ASTM C518 - 10, Standard Test Method for Steady-State Thermal Transmission Properties by Means of the Heat Flow Meter Apparatus, 2010.

[7] R. Baetens et al., Energ. Buildings 42 (2010) 147-172.

[8] W. Wu et al., 11th International Vacuum Insulation Symposium, September 19 - 20, 2013, Empa, Switzerland, 33.

[9] M. Grandcolas et al., 11th International Vacuum Insulation Symposium, September 19 - 20, 2013, Empa, Switzerland, 43.

[10] M. Alam, H. Singh. 11th International Vacuum Insulation Symposium, September 19 - 20, 2013, Empa, Switzerland, 45.